Spring 2013

Biomechanics of failure modalities in total hip arthroplasty

Jacob Matthias Elkins
University of Iowa

Recommended Citation

Elkins, Jacob Matthias. "Biomechanics of failure modalities in total hip arthroplasty." PhD (Doctor of Philosophy) thesis, University of Iowa, 2013.
https://doi.org/10.17077/etd.addybua3

BIOMECHANICS OF FAILURE MODALITIES IN TOTAL HIP ARTHROPLASTY

by

Jacob Matthias Elkins

An Abstract

Of a thesis submitted in partial fulfillment
of the requirements for the Doctor of
Philosophy degree in Biomedical Engineering
in the Graduate College of
The University of Iowa

May 2013

Thesis Supervisor: Professor Thomas D. Brown

ABSTRACT

Total hip arthroplasty (THA) is the treatment of choice to relieve joint pain and loss of mobility as a result of advanced stage osteoarthritis or other hip pathologies. Despite their general success, THAs do fail, with revision rates estimated near 5% per year. Instability, defined as the complete subluxation (dislocation) of the femoral head from the acetabular socket – which usually occurs due to implant impingement – has recently supplanted wear-induced osteolytic aseptic loosening as the leading cause of failure in THA. Soft tissue integrity has long been recognized as influencing joint stability, and therefore there has been great interest recently in improving soft tissue restoration following THA. However, there is little quantitative information related to the degree of soft tissue repair necessary to restore joint stability. Additionally, impingement events, besides their role in prelude to frank dislocation, hold potential to damage new-generation hard-on-hard bearings, due to the relatively unforgiving nature of the materials and designs. Despite the largely biomechanical nature of these impingement-related complications, they remain under-investigated relative to their burden of morbidity. In addition to impingement, failure modalities unique to hard-on-hard bearings merit careful biomechanical scrutiny. This includes investigation of catastrophic fracture in ceramic-on-ceramic bearings, as well as analysis of patient, implant and surgical variables associated with increased wear and adverse soft tissue engagement potential for metal-on-metal implants. Toward the goal of improving current biomechanical understanding of failure modalities in THA and to provide an objective basis for orthopaedic surgeons to choose the most favorable implants and to identify optimal intraoperative parameters which minimize failure propensity, a novel, anatomically-grounded finite element (FE) model with hip capsule soft tissue representation was developed. This FE model was used to investigate four principal modes of failure in THA, including dislocation, impingement, fracture mechanics of ceramic implants, and various issues related to failure mechanisms in metal-on-metal implants. The influence of soft tissue integrity and patient obesity on dislocation was investigated. The model demonstrated that (1) posteriorly directed capsule defects resulted in a substantial decrease in THA stability; (2) proper repair of these defects returned stability to near baseline levels; (3) repairs with too few sutures risked suture failure; (4) dislocation risk in obese patients increased for body mass index exceeding 40 kg/m^2; and (5) dislocation risk in obese patients could be reduced with the use of cups in lower degrees of inclination and with the use of an offset femoral neck. The FE model was also used to investigate potentially deleterious consequences of impingement in THA. It was determined that (1) egress site stresses exceeded impingement site stresses; and (2) stresses generated from bone-on-bone impingement were less severe than those from hardware impingement scenarios. Linear elastic fracture mechanics FE and eXtended FE (XFEM) models were also developed to investigate fracture risk in ceramic liners. Fracture risk was found to be increased (1) for malpositioned cups; (2) during stooping and squatting motions; (3) for cups with sharp edges; and (4) for instances of high body weight. The final section of the research involved various failure modes using metal-on-metal implants. Edge-loading is a particularly important consideration for metal-on-metal THA, and edge-loading severity was found to be highly sensitive to subtle changes in cup design. Additionally, a novel method of implant orientation optimization was developed, and allows for ideal acetabular cup positioning to be determined for any femoral head size and any patient-specific degree of femoral anteversion. Finally, wear potential at the trunnion interface for large diameter THA was found to increase dramatically for head diameters exceeding 40mm.

Abstract Approved: ______________________________
Thesis Supervisor

____
Title and Department

____
Date

BIOMECHANICS OF FAILURE MODALITIES IN TOTAL HIP ARTHROPLASTY

by

Jacob Matthias Elkins

A thesis submitted in partial fulfillment
of the requirements for the Doctor of
Philosophy degree in Biomedical Engineering
in the Graduate College of
The University of Iowa

May 2013

Thesis Supervisor: Professor Thomas D. Brown

Graduate College
The University of Iowa
Iowa City, Iowa

CERTIFICATE OF APPROVAL

PH.D. THESIS

This is to certify that the Ph.D. thesis of

Jacob Matthias Elkins

has been approved by the Examining Committee
for the thesis requirement for the Doctor of Philosophy
degree in Biomedical Engineering at the May 2013 graduation

Thesis Committee:

Thomas D. Brown, Thesis Supervisor

John J. Callaghan

Nicole M. Grosland

Douglas R. Pedersen

Madhavan L. Raghavan

ACKNOWLEDGMENTS

First, I would like to acknowledge the many funding sources for this work. At various times, I have been generously supported by grants from the NIH (AR46601 and AR53553) and the Veterans Administration, as well as the National Center for Resources (TL1RR024981) and the Iowa Medical Scientist Training Program.

This work would not have been possible without the unwavering support and encouragement from my advisor and mentor, Dr. Thomas Brown. It has been an honor and privilege to learn biomechanics from you.

I am also indebted to Dr. John Callaghan for years of enthusiasm, guidance and inspiration. It, too, has been an honor to learn orthopaedics from you.

From day one, I received an incredible amount of assistance from Dr. Doug Pedersen. Whether I needed a new $10,000 toy (or two!), or just to blow off some steam, his office was always the first stop. The importance of the provided computational resources cannot be overstated: without these, the amount of work completed could not have been finished this decade.

I would also like to thank many current and former members of the Orthopaedic Biomechanics Laboratory. Drs Don Anderson, Jim Rudert and Yuki Tochigi have always been quite willing to help with specific problems, no matter how inane they must have seemed. Substantial imaging, meshing and FE assistance was received from my former co-graduate students Drs Curt Goreham-Voss, Thad Thomas and Jess Goetz. And Tom Baer has been incredibly helpful, building and designing several “proof-of-concept” ideas. I owe a special debt of gratitude to Nick Stroud. Without his impressive work related to capsule physical validation, my graduate “career” might not have taken off like it did. Of course, sharing an office with a good friend was also nice.

Additionally, I was fortunate enough to receive a great deal of assistance from several people outside the lab. I greatly appreciate Dr Nicole Grosland and Dr. Madhavan

Raghavan for serving on my committee. Bhupinder Singh and Dr. John Yack provided helpful expertise regarding obesity and dislocation kinematics. Dr Jeff Weiss and Ben Weiss of the University of Utah were instrumental in helping me get the soft tissue FE model to (finally) run. And Dr. Tony Sanders, also at the University of Utah, graciously spent hours helping me through the analytical contact validation work, even though I was (almost) a total stranger.

Above all, I thank my family. My parents: your tireless support of my every ambition in life is inspiring. Maddie and Tessa: while your physical contribution to this work is questionable, your emotional and spiritual support is not.

And Jaymie: where and who I am is because of you.

ABSTRACT

Total hip arthroplasty (THA) is the treatment of choice to relieve joint pain and loss of mobility as a result of advanced stage osteoarthritis or other hip pathologies. Despite their general success, THAs do fail, with revision rates estimated near 5% per year. Instability, defined as the complete subluxation (dislocation) of the femoral head from the acetabular socket – which usually occurs due to implant impingement – has recently supplanted wear-induced osteolytic aseptic loosening as the leading cause of failure in THA. Soft tissue integrity has long been recognized as influencing joint stability, and therefore there has been great interest recently in improving soft tissue restoration following THA. However, there is little quantitative information related to the degree of soft tissue repair necessary to restore joint stability. Additionally, impingement events, besides their role in prelude to frank dislocation, hold potential to damage new-generation hard-on-hard bearings, due to the relatively unforgiving nature of the materials and designs. Despite the largely biomechanical nature of these impingement-related complications, they remain under-investigated relative to their burden of morbidity. In addition to impingement, failure modalities unique to hard-on-hard bearings merit careful biomechanical scrutiny. This includes investigation of catastrophic fracture in ceramic-on-ceramic bearings, as well as analysis of patient, implant and surgical variables associated with increased wear and adverse soft tissue engagement potential for metal-on-metal implants. Toward the goal of improving current biomechanical understanding of failure modalities in THA and to provide an objective basis for orthopaedic surgeons to choose the most favorable implants and to identify optimal intraoperative parameters which minimize failure propensity, a novel, anatomically-grounded finite element (FE) model with hip capsule soft tissue representation was developed. This FE model was used to investigate four principal modes of failure in THA, including dislocation, impingement, fracture mechanics of ceramic implants, and various issues related to failure mechanisms in metal-on-metal implants. The influence of soft tissue integrity and patient obesity on dislocation was investigated. The model demonstrated that (1) posteriorly directed capsule defects resulted in a substantial decrease in THA stability; (2) proper repair of these defects returned stability to near baseline levels; (3) repairs with too few sutures risked suture failure; (4) dislocation risk in obese patients increased for body mass index exceeding 40 kg/m^2; and (5) dislocation risk in obese patients could be reduced with the use of cups in lower degrees of inclination and with the use of an offset femoral neck. The FE model was also used to investigate potentially deleterious consequences of impingement in THA. It was determined that (1) egress site stresses exceeded impingement site stresses; and (2) stresses generated from bone-on-bone impingement were less severe than those from hardware impingement scenarios. Linear elastic fracture mechanics FE and eXtended FE (XFEM) models were also developed to investigate fracture risk in ceramic liners. Fracture risk was found to be increased (1) for malpositioned cups; (2) during stooping and squatting motions; (3) for cups with sharp edges; and (4) for instances of high body weight. The final section of the research involved various failure modes using metal-on-metal implants. Edge-loading is a particularly important consideration for metal-on-metal THA, and edge-loading severity was found to be highly sensitive to subtle changes in cup design. Additionally, a novel method of implant orientation optimization was developed, and allows for ideal acetabular cup positioning to be determined for any femoral head size and any patient-specific degree of femoral anteversion. Finally, wear potential at the trunnion interface for large diameter THA was found to increase dramatically for head diameters exceeding 40mm.

TABLE OF CONTENTS

LIST OF TABLES

LIST OF FIGURES

INTRODUCTION

> Surgeons are exposed very briefly to physics in school. They have no acquaintance whatever with the problems of stress mechanics and industrial design. Many of the problems of orthopaedic surgery lie in these fields, but the surgeon goes blithely on his way of doing things that an engineer would never dream of doing. I have done them; others have done them; and it never occurred to us that our complete disregard of mechanical principles made failure inevitable. Ignorance of the laws of mechanics does not preclude failure.
>
> Duncan C. McKeever, Biomechanics of Hip Prostheses [1]

Total hip arthroplasty (THA) is the treatment of choice to relieve joint pain and loss of mobility as a result of end-stage osteoarthritis or other severe hip pathologies, and is widely considered to be one of the most successful surgical interventions in all of medical history [2]. Currently, more than 250,000 cases are performed per year in the US, a figure which is expected to double in the next 20 years [3]. Over many decades of innovation, hip replacement has seen continual advances; however, the rates of failure, measured in terms of diagnoses requiring a revision surgery, have actually increased in recent years [4], underscoring the need to further our understanding of THA failure mechanisms. Historically, the most common cause of failure in conventional THA has been from loosening of the implant (osteolysis) due to immunological reaction to polyethylene wear. Efforts to reduce wear have led to a recent shift toward advanced low-wear bearing couples for THA. As a result, implant dislocation is now the most common cause of failure. While successful in reducing failure due to osteolysis, these advanced THA designs are susceptible to their own novel failure mechanisms. However, mechanistic information regarding these failure modalities are under-investigated relative to their burden of morbidity. Therefore, the objective of this body of work has been to improve the biomechanical understanding of failure mechanisms in contemporary THA. This thesis presents results from a series of novel FE models developed to explore THA failure mechanisms, and further technical details of model formulation and additional results are presented in a series of manuscripts and abstracts listed in the Appendix.

Failure in Hip Arthroplasty: Historical Perspectives

Arthroplasty is the surgical reconstruction of the articular surface of a joint. Anthony White of London is considered to have carried out the first successful arthroplasty of the hip in 1821, when he corrected a traumatic deformity of the hip in a nine-year-old patient by excising the head, neck and trochanters of the femur, resulting in the eventual formation of a fibrous pseudoarthrosis at the hip, permitting pain relief and "perfect" restoration of function in the previously bedridden patient [5].

Likely influenced by the pioneering work of American J. M. Carnochan beginning in 1840 [6], Auguste Verneuil and later Leopold Ollier of Paris, France began using foreign materials – including muscle, fat, and connective tissues – between contacting surfaces in the hip joint (so called "interpositional arthroplasty") to relieve pain and prevent permanent deformity for debilitating hip pathology beginning in 1860. However, lacking suitable fixation methods for the interpositional material to the articular surface of the joint, these early attempts generally resulted in poor clinical performance.

While experimentation with different interpositional arthroplasty materials continued for many years, it was German surgeon Themistocles (Thomas) Gluck who in 1891 attempted the first hip arthroplasty by physically replacing bone with a foreign material [7]. After trialing a variety of materials including wood, glass, and steel in animal studies, and perhaps influenced by German colonies in West Africa, Gluck settled on ivory as the ideal biomaterial for numerous orthopaedic applications, including joint replacement of the knee, ankle, wrist, elbow, shoulder, and hip (Figure 1). While "spectacularly successful" [8] short term, Gluck's ivory prostheses all ultimately succumbed to infection.

While Gluck's pioneering work was largely ostracized by the German medical community [8], work with ivory hip replacements continued to some degree in Britain. Surgeon Ernest Hey Groves developed an ivory femoral head prosthesis (Figure 2) to treat various hip ailments of both pediatric and adult patients [10]. Again, despite promising short-term results, ivory as a hip biomaterial failed to realize a viable path towards long-term success.

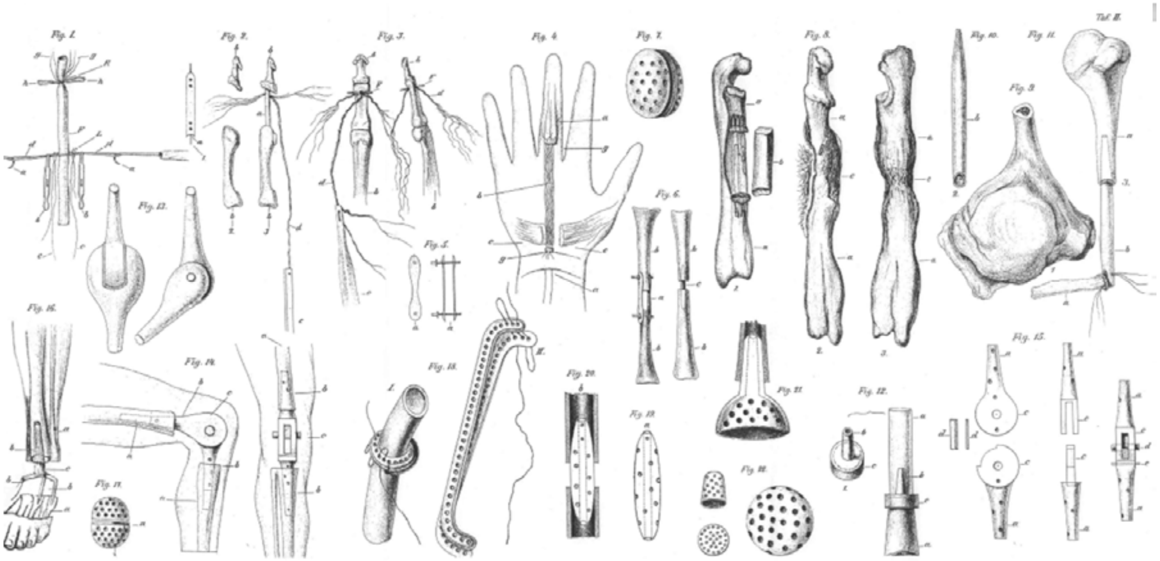

Figure 1: Various ivory implants developed by T. Gluck [9].

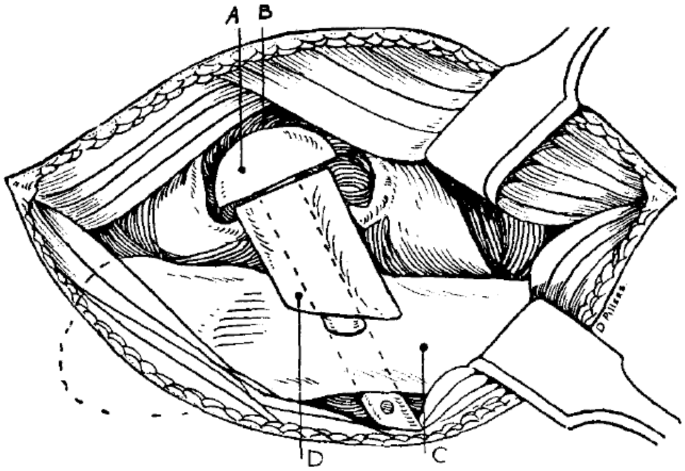

Figure 2: Diagram of ivory femoral head replacement developed by E.W.H. Groves [10]. A, Head of nail; B, Acetabulum; C, Shaft of femur; D, New neck made from the shaft of opposite femur.

A new era of hip treatment was ushered in by Norwegian-born surgeon Marius N. Smith-Petersen of Boston [11]. After observing the formation of a glistening smooth membrane surrounding a piece of glass removed from a patient's back after a year *in situ*, Smith-Petersen conceived the idea that a similarly inert material may act as a "mold" between the femoral head and acetabulum. Temporary implantation of this mold between the reshaped surfaces of the femoral head and acetabulum, he conjectured, would allow for the physiologic generation of smooth, repaired articular surfaces. Once the mold was subsequently removed, it was believed the incongruous surfaces of the joint would be healed and the procedure would permit the return of normal joint articulation and function. Smith-Petersen began implanting glass molds in patients in 1923 (Figure 3).

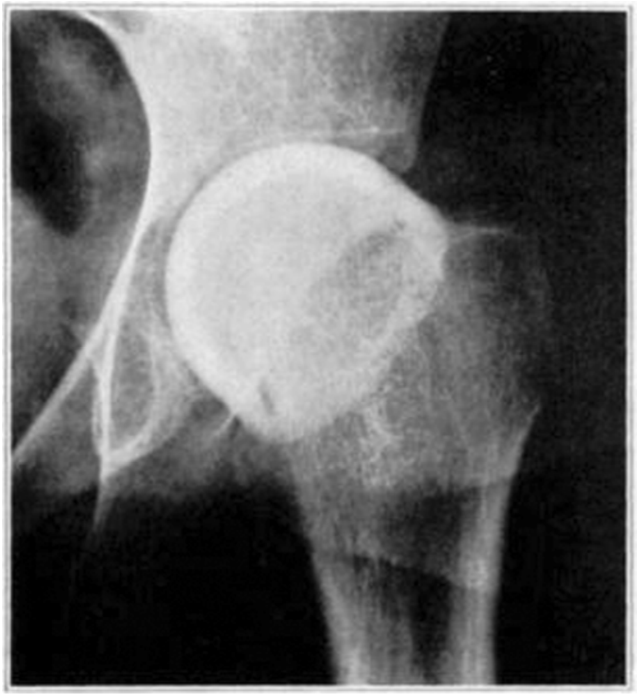

Figure 3. Smith-Petersen glass mold arthroplasty. One such device was implanted in a 19 year old female patient with ankylosis of this hip which occurred as a complication of scarlet fever at the age of three years. Roentgenogram taken after 20 months implantation of the mold [12].

While some of these earliest glass molds (predictably) fractured, Smith-Petersen was encouraged by the promising short- and intermediate-term results of the procedure. Realizing that glass was not the ideal material for mold arthroplasty, he investigated the use of several other candidate materials, including celluloid (Viscaloid), pyrex, and Bakelite. However, these materials were found to be too brittle (Pyrex) or to elicit too severe of a soft tissue reaction following material wear. Encouraged by his dentist, J.W. Cook, Smith-Petersen developed a mold crafted from ‘Vitallium’, an advanced alloy of cobalt-chrome which had recently come into use in dentistry. Smith-Petersen’s Vitallium cup was first implanted in 1938, and immediately resulted in improved clinical performance. With the introduction of Vitallium, mold arthroplasty soon became the treatment of choice for various hip disabilities, and continued so for many years.

While interpositional mold arthroplasty was becoming more widely adopted in the orthopaedic community, evidence surfaced suggesting this was not the robust treatment modality surgeons had hoped for. A rather large clinical study of 1000 mold arthroplasties [13] indicated a revision (failure) incidence approaching 25%, with only 20% of patients reporting their satisfaction following the procedure as “good” or “excellent”. Additionally, given the “many months of convalescence and economic loss” with the procedure [13], investigation continued for a better option for hip joint disability. Motivated by the successful femoral head replacement performed by Hey-Groves a decade earlier, and by the recent successes in the introduction of cobalt-chrome alloys for orthopaedic operations, Nebraska native Harold Ray Bohlman, collaborating with South Carolina surgeon Austin Moore, performed the first successful functional replacement of the femoral head and neck with a metallic (Vitallium) implant in 1940 [14]. Bohlman, who long displayed an enthusiasm for laboratory experimentation (which was quite rare at the time), verified the corrosion resistance of Vitallium by burying the implants at his farm prior to implanting the alloy in his patients.

The first metallic total (i.e., both the femoral head and acetabulum) hip arthroplasty is credited to Philip Wiles of London, in 1938 [15]. Using an assortment of screws, lags and bolts (Figure 4), Wiles replaced the femoral head and acetabulum in six patients crippled by Still's disease, using accurately ground stainless steel implants. Despite some clinical benefit for his patients, Wiles's THA eventually resulted in mechanical failure of the implant.

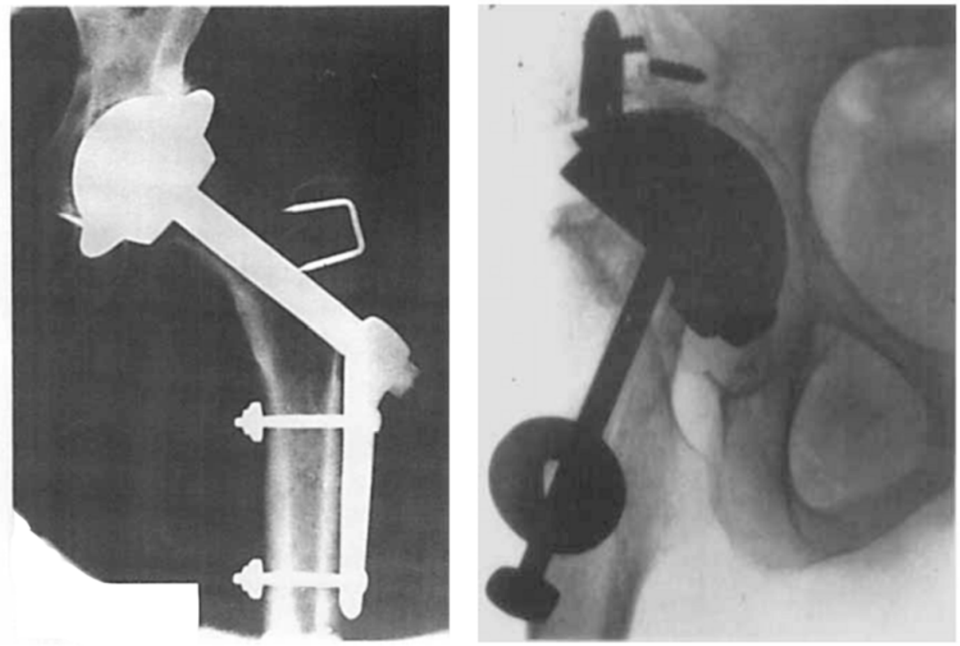

Figure 4: Philip Wiles's ball-and-cup arthroplasty developed in 1938. (Left) The cup was fixed to the acetabulum with two screws. Bolts passing through the femoral neck secured the femoral component. (Right) Radiograph of an implant after thirteen years. The lug and screws retaining the metal acetabulum have disintegreated, much of the neck of the femur has been absorbed, and the bolt has broken away from the head [15].

Further "advances" to femoral head replacement were developed by the Judet brothers (Robert and Jean) in France [16]. Seeking to treat patients with osteoarthritis, femoral neck fracture, joint ankylosis and dislocation, the Judets, beginning in 1946, developed a "resection-reconstruction" of the femoral head, using an acrylic hemispheric head implanted via a steel (or acrylic) rod inserted through the femoral shaft (Figure 5).

Following their widely-promoted contention that the polymethethacrylate resin used for their prosthesis displayed “perfect and astonishing tolerance” *in vivo*, the Judet prosthesis rapidly garnered wide-spread adoption. Despite early warning signs of severe biomechanical deficiencies, the Judet prostheses was widely copied and modified by others, and was rapidly pressed into clinical service. However, “enthusiasm outstripped judgment” [11], as many surgeons “succumbed to the temptation of trying replacement arthroplasty of the Judet type because of the brilliant early results” [15], and the Judet and similar prostheses soon demonstrated astonishingly poor biomechanics and even poorer biocompatibility.

Figure 5. The original Judet femoral prosthesis. The implant featured a hemispheric femoral head surrounding a steel pin to be inserted into the femoral neck (A). (B) Bilateral “resection-reconstruction” using the Judet prosthesis. [16]

Lessons learned from the widespread failure of Judet-type implants inspired rapid development of improved prosthesis designs. Beginning in 1950, Austin Moore [17], building upon earlier work with Bohlman in development of a Vitallium femoral head replacement, designed a series of Vitallium femoral implants (Figure 6A) whose stems passed into the femoral medullary canal. Later iterations of design featured fenestrated stems, allowing bone ingrowth and thereby stably anchoring the prosthesis within the intramedullary canal. Working in collaboration with Moore, Frederick R. Thompson [18] in 1951 designed another intramedullary Vitallium femoral prostheses (Figure 6B) which aimed to more closely resemble the native joint anatomy. Owing to vastly improved considerations as regards mechanics and biocompatibility, the Moore and Thompson prostheses represented the most successful treatment modalities for hip disability at the time.

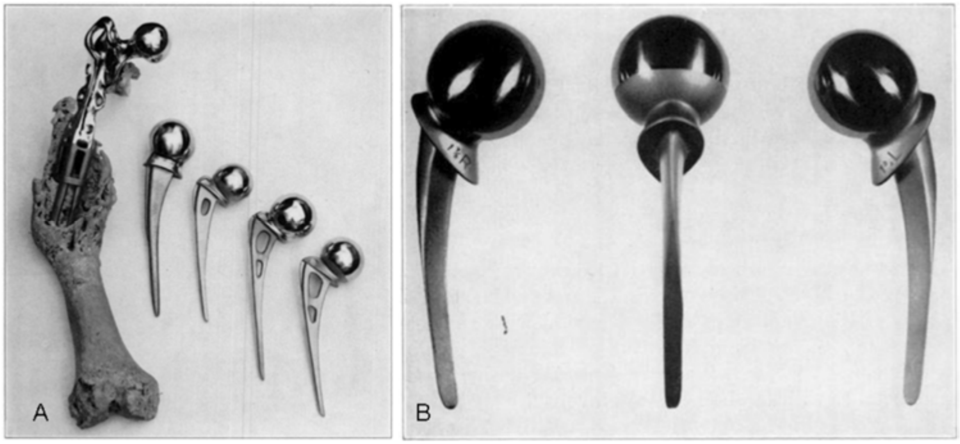

Figure 6: Early Vitallium intramedullary femoral components. (A) Development of the Austin Moore prostheses. At left is a femur with an early type of prostheses which was inserted in 1939 by Moore and Bohlman. Later developments featured fenestrations in the stem of the prostheses. (B) Vitallium femoral prostheses designed by Frederick Thompson demonstrating varying degrees of femoral anteversion. [17, 18]

Following the successes of the Moore and Thompson prostheses, there was a burst of renewed enthusiasm towards metallic total hip arthroplasty, and Kenneth McKee of Norwich, England, was instrumental in promoting its use and development. Working under the tutelage of Philip Wiles, McKee's first THA design in 1940 (Figure 7A) was only a "pipe dream" and never used clinically owing to perceived inadequacies with cup fixation [19]. McKee later devised a method of screw-fixation of the cup within the acetabulum, and a stainless steel device was used in three patients in 1950 (Figure 7B). Unfortunately, two of these three cases failed within the first year from cup loosening. However, motivated by the success of the third case, McKee traveled to the US and soon became acquainted with Thompson and his femoral prosthesis. Convinced that osteoarthritis equally afflicted both articular surfaces of the joint, McKee envisioned a Thompson-like femoral prosthesis mated with a clover-shaped Vitallium cup (Figure 7C). This early model was implanted in some 40 cases between 1956 and 1960, resulting in a success rate of approximately 50%. Analyses of the failed cases gave insight into possible biomechanical issues related to the failed design, specifically bone fixation, impingement and instability. McKee addressed these concerns with both the use of acrylic bone cement (as advised by John Charnley), and a redesigned femoral neck (credited to his pupil John Watson-Farrar) beginning in 1960 (Figure 7D). Further modifications to design occurred for several years, and by 1967, the McKee-Farrar THA had become a well-established treatment option for hip disabilities.

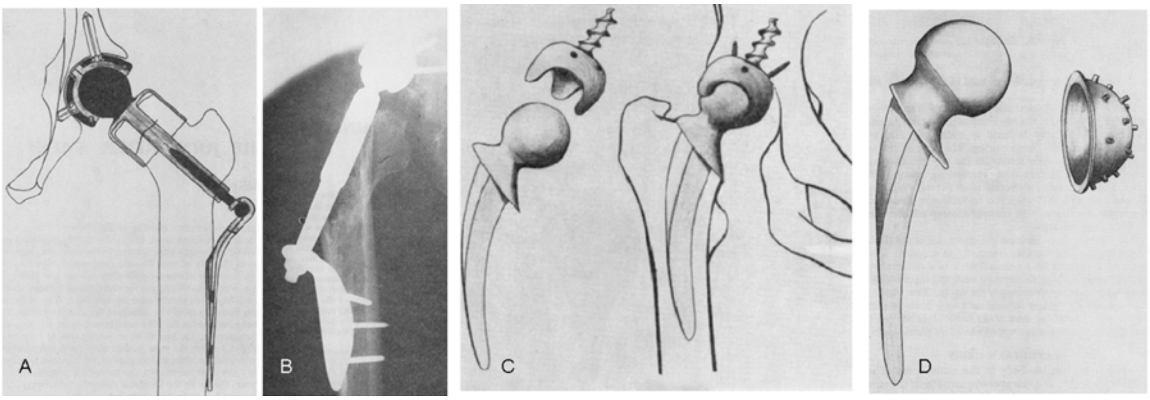

Figure 7: Stages and development of the McKee THA. (A) Conceptualized implant from 1940. (B) Modified THA implanted in 1950. (C) McKee implant using modified Thompson stem and Vitallium cup with screw-fixation to the acetabulum. (D) 1965 McKee-Farrar model with larger head, recessed neck and cup specially designed to key on to plastic cement. [19]

The rapid adoption of metal implants for arthroplasty, and a few emerging reports of early failure due to poor manufacturing or surgical deficiencies, led to backlash against the device by some in the orthopaedic community: “Metal replacement introduces a new and to me a frightening period of experimental surgery . . . I regret the reckless abandon with which prostheses have been utilized” [20]. While acrylics [16], polyethylene [21] and nylon [22] had all been previously used as a bearing surface, without exception these all failed due to adverse physiologic reactions to the wear particle debris. Yet, the contention remained by many that rigid bearing surfaces deviated too much from physiologic articulation to become a tenable solution for arthroplasty. After extensive observation with his animal studies of joint lubrication, John Charnley [23] was convinced that only a material with similar mechanical properties to articular cartilage would reproduce the physiologic low-friction and natural shock-absorption found in native joints. Charnley first investigated the use of polytetrafluorethylene (p.t.f.e, “Teflon”), and between 1959 and 1963, some 300 patients had received implants with some form of this bearing surface. However, despite encouraging laboratory wear properties, p.t.f.e. demonstrated extremely poor wear-resistance *in vivo* (Figure 8). Additional laboratory investigation identified wear rates of high molecular weight polyethylene, a polymer first synthesized at the Max Planck Institute in 1954, at least 500 times greater than that for p.t.f.e. cups [24]. Additionally, Charnley sought to overcome what he considered to be the greatest deficiency of the Moore-, Thompson- and McKee-type prostheses, i.e., their inability to resist torsional stresses. Building upon the prior demonstration of the feasibility and utility of acrylic (methylmethacrylate) in orthopaedic [25, 26] and neurosurgical [27] applications, Charnley adopted its use for the intramedullary fixation of the femoral stem. Charnley’s resulting “low friction arthroplasty” proved to be wildly successful and served as the yardstick against which all future devices were measured.

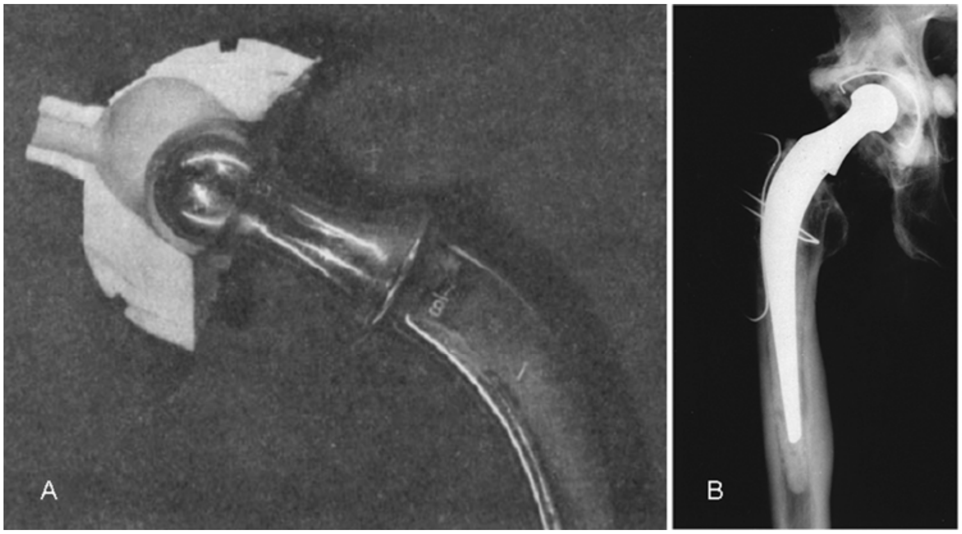

Figure 8. Development of the Charnley low friction arthroplasty. (A) Wear of the Teflon cup with a 22-mm femoral head prosthesis after three years in vivo. (B) Charnley's improved implant consisted of an acrylic-fixed stainless steel femoral component articulating against high molecular weight polyethylene [24].

By the mid 1970s, the rapid adoption of Charnley's low friction arthroplasty led to the general abandonment of metal-on-metal devices. This was in part due to five factors [28]: (1) early success of the low friction arthroplasty; (2) excessive frictional torque with large head metal-on-metal implants; (3) increased stress transfer to the peri-prosthetic bone; (4) increased concern regarding elevated carcinogenic potential of metal ions; and (5) hypersensitivity to metallic ions in some patients. The early success of Charnley's low friction arthroplasty has been partly credited to the careful training of orthopaedic surgeons, and to the initial restriction of the device only to those specifically trained for its use. This is in contrast to the McKee prostheses, which were widely available without restrictions. Frictional torque, long a chief concern of Charnley's, was hypothesized to be increased in McKee-type total hip arthroplasties, due to increased head size (thereby increasing the moment arm) and the increased friction of metal-on-metal articulation. Similarly, it was suggested that the relative stiffness of McKee-type implants would lead to fatigue stress failure of the trabecular bone adjacent to the implant. Concerns related to increased frictional torque on the implant manifested clinically as an increased propensity to loosen the bone-implant interface, precluding the possibility of a successful clinical outcome for the patient. Both the carcinogenic and hypersensitivity concerns related to the perceived increase in wear of the metal-on-metal implants, compared to Charnley's low friction prosthesis. This apparent increase in wear debris was related to several factors. The first was the lack of precision in early testing protocols, preventing accurate measurement of submicron-sized polyethylene particles. The second relates to manufacturing tolerances of early all-metal implants. While it has since been well established that wear from properly machined all-metal bearings is at least an order of magnitude less than that for metal-on-polyethylene, this is not true when manufacturing defects, specifically diameter mismatches, exist, and early McKee implants were especially prone to poor quality control. Whether justified or not, concerns regarding local and systemic effects of wear were quite sincere. While animal studies have identified increased carcinogenic potential from cobalt, nickel and chromium ions, epidemiologic investigations in humans had been (and remain) rather dubious. Similar uncertainty remains today regarding the role of metal hypersensitivity as a potentiator of failure [28].

The relative success of Charnley's low-friction model for THA directly led to this procedure being lauded as one of the most successful surgical interventions in history. However, despite its many accolades, the era of arthroplasty ushered in by Charnley was not without its own biomechanical limitations. Ideal candidates for THA were usually the elderly with severe osteoarthritis with substantial deficits in daily activities, and THA allowed these patients to regain some pain-free mobility. Post-operatively, patients were not encouraged or expected to partake in high-impact, high-stress activities. However, as THA became more successful, and thereby more accepted, the demographics of the typical THA patient changed. Patients receiving THA were younger, lived longer, were more active, typically weighed more, and in general, were less accepting of a low-activity lifestyle following hip replacement. These demographic changes resulted in biomechanical burdens on the implants exceeding their intended limit. Of prime concern in metal-on-polyethylene bearings is the generation of wear particles (debris) which accumulates during the millions of duty cycles throughout the lifespan of the device. These sub-micron sized particles are shed into the periarticular joint space and are phagocytized by macrophages. This elicits an immunologic foreign-body response thereby initiating an inflammatory cascade disrupting the delicate balance between osteoclasts and osteoblasts, resulting in increased bone resorption, osteolysis, and eventually implant failure. Osteolysis became the major limiting factor for THA longevity. While 10- and even 20-year survivorship of Charnley THAs has been generally excellent, diminished survivorship past 20 years, especially in the more active, younger patients, is rather sobering (Figure 9).

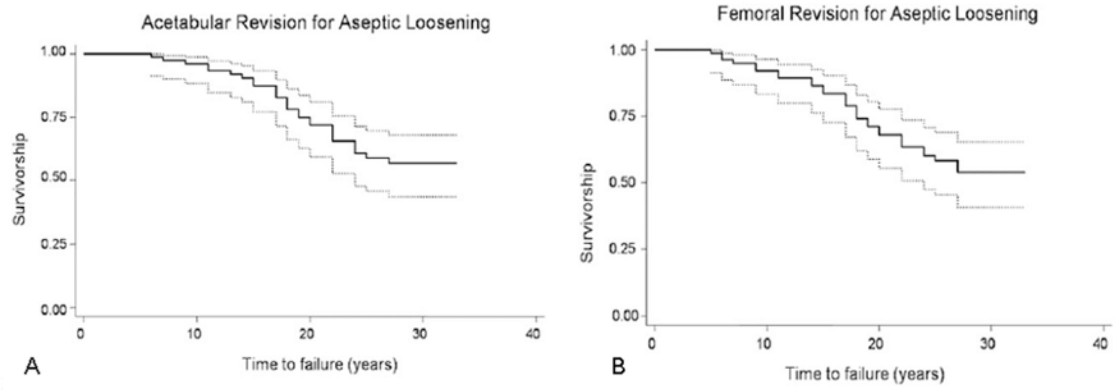

Figure 9: Survivorship curves for Charnley low friction arthroplasty for young patients, demonstrating revision for aseptic loosening for the acetabular component (A) and femoral component (B).[29]

Further analysis of Charnley-type prostheses identified other areas of concern. Charnley had used a small (22.225 mm) femoral head, to decrease the frictional torque at the bearing surface and to minimize polyethylene wear. However, small diameter femoral heads constituted a substantial risk factor for dislocation following THA, and the cumulative risk for dislocation following a Charnley-type THA was quite high [30]. Increasing the head size was presumed to lead to increased joint stability; albeit at the potential cost of increased osteolysis risk. These competing considerations led to (re)investigation into other bearing couples for THA. By the mid 1970s, polyethylene had nearly entirely displaced all-metal implants. However, it remains debatable if this dismissal may have been premature. A substantial number of early metal-on-metal implants survived thirty-plus years with excellent clinical performance [31] and with no indication of wear or adverse soft tissue reactions [32]. This seemingly peculiar contrast between the generally mediocre performance of most all-metal implants and the outstanding clinical performance of a few devices confused even Charnley himself [24]: “it is a surprising fact in the light of standard mechanical practice that chrome-cobalt alloy …appears to perform in an acceptable fashion.” Investigation into examples of successful early-era McKee implants identified that certain mechanical factors – including proper bearing clearance, surface smoothness, cup orientation and adequate fixation [28] – seemed to determine excellent vs. poor clinical outcomes. These observations led to the ‘rediscovery’ of all-metal bearings in the mid 1980s [33], where it was argued that proper selection of biomechanically-sound implants would naturally lead to vastly improved clinical performance compared to metal-on-poly or early-era all-metal THAs. In addition to the re-introduction of metal-on-metal THAs, other alternative bearings were introduced to combat the growing incidence of osteolysis. Ceramics had been tried as a bearing surface as early as 1970 in Europe [34], but the limited capacity for ceramic engineering and questionable quality control in the 1970s led to disastrous clinical performances. Yet, continuous advance in materials science during the last four decades has led to the development of vastly improved ceramics, suitable for long-term orthopaedic applications.

Rationale for Computational Investigation

The introduction (and re-introduction) of alternative bearings surfaces has had a significant impact on contemporary hip arthroplasty. Presently, metal-on-metal and ceramic-on-ceramic are in their 3rd or 4th generations of development, and represent a growing share of the THAs performed today. In the US, where adoption of alternative bearings has lagged behind Europe and Asia, metal-on-metal and ceramic-on-ceramic bearings recently accounted for over 50% of the market share [35]. The rapid and widespread adoption of advanced low-wear bearings perhaps represents a cure for the "man made worldwide disease" [36] of wear-induced osteolysis. Yet, the introduction of these advanced bearings has been accompanied by novel modes of failure. Of chief concern in ceramics is (catastrophic) fracture, requiring immediate revision surgery, and frequently re-revisions due to abrasive third-body debris remaining in periarticular space. For metal-on-metal, there is mounting concern regarding potentially adverse soft tissue reaction to metal debris. In rapidly adopting these THA advances, the orthopaedic community assumes the burden of responsibility to ensure the safety and efficacy of these devices for their patients.

Perhaps the most frequent tool used to guide clinical practice is the traditional retrospective clinical study. These investigations give insight into the apparent causality of outcomes in THA. However, inherent weaknesses of clinical studies, such as limited patient population and uncontrolled confounders, often result in ambiguities and occasionally in directly conflicting conclusions as regards implant-, surgical- or patient-specific risk factors for poor THA outcomes [37]. Many of the intrinsic weaknesses of clinical studies can be overcome by experimental biomechanical methods. However, conventional biomechanical investigation, whether by simulator or cadaveric studies, is greatly restricted by excessive resource demand (both time and cost). Additionally, laboratory benchtop studies must be sufficiently robust to parametrically address individual factors potentially related to adverse outcomes with the device, which is an exceedingly ambitious and often unattainable goal. An additional limitation of investigation into these new modes of failure is the frequent – and sometimes apparently arbitrary – design changes which occur when "improved" devices come to market, further compounding the resource burden of laboratory study. Computational models – specifically finite element (FE) analyses – by contrast share none of these severely limiting hindrances. FE investigation enables the generation of hundreds, or even thousands, of parametric simulations in minimal time or at minimal economic expense. Of course, the onus of model validation is the responsibility of the investigator. Generally, validation of an FE model occurs through physical (experimental) or analytical analysis of an idealized physical situation of sufficient complexity to reproduce the intricacies of the real-world condition being modeled, with the computational model being directly compared to this "gold standard" result. Hopefully, the computational model is shown to agree well with the idealized standard, allowing the investigator to rationally extend the model to all similar physical circumstances.

Brief Introduction to the Finite Element Method

The FE method is a numerical approximation tool to determine solutions to partial differential equations. In the area of continuum mechanics, these differential equations (i.e., governing equations) describe the mechanical response of a material to an applied load and/or other applied condition (i.e., "boundary conditions"). The FE method primarily evolved from mathematical techniques for structural analysis beginning in the mid 1940s [38]. However, the term "finite element method" was not used until 1960 [39]. In FE analysis, a structure is divided (discretized) into many smaller, simpler structures (elements). These elements are then connected to each other (equivalenced) at "nodes." The unknown variables (displacement for an elasticity problem) are solved for at each node in the model, simultaneously. Then, using simplified integration techniques (e.g. Gaussian quadrature), the response through the element (the field quantity) is then approximated over the element, usually as a polynomial function. The order of the polynomial is determined by the “order” of the element, which is determined by the element type (e.g. 4-vertex tetrahedral elements or 8-vertex hexahedral elements) and the number of nodes for each element (e.g. linear 8-noded hexahedra vs. quadratic 20-noded hexahedra).

It is important to recognize that results obtained from a FE model are highly user-dependent. Hence, the user bears the burden of responsibility to ensure model accuracy. In this regard, there are several important considerations during the generation of the FE mesh (preprocessing). The first such consideration is the element type used for the analysis. For complex three-dimensional geometries, manual mesh generation is frequently a prohibitive process due to the amount of manual labor required. However, mathematical algorithms have evolved to allow fully-automated meshing of complex structures using tetrahedral elements [40]. Unfortunately, for stress/displacement analyses, first-order tetrahedral elements allow only for uniform stress across the entire tetrahedron, therefore requiring prohibitively refined mesh densities. The uniform stress limitation can be overcome by the use of quadratic (or higher) order elements. However, this incurs substantial increases in model complexity, often resulting in computational intractability. On balance, hexahedral meshes are preferred. Unfortunately, generation of well-formed hexahedral meshes, especially for complex geometries, generally cannot be done fully automatically. Additionally, hexahedral elements, while representing considerable performance improvement over tetrahedral elements, are rather sensitive to initial element shape, and become much less accurate when initially distorted. These considerations therefore place a significant premium on user adeptness in manual mesh generation. In addition to element type, element mesh refinement (zoning density) is also of critical importance. Characteristically, increased mesh refinement provides more accurate results, albeit at the expense of increased computational cost. Typically, sensitivity (convergence) studies are therefore conducted to identify the point of diminishing returns as regard model accuracy versus computational tractability. In general, convergence is tested by increasing the element number (h-type) or by increasing the order of the elements (p-type). Since most commercially available FE platforms do not support element order beyond quadratic, most convergence studies are of the h-type.

In addition to efforts at the preprocessing stage, model complexity and accuracy can also be modified at the processing stage. In the FE method, there are two main approaches used to determine the unknown nodal variables: implicit and explicit. The implicit formulation is independent of time, and is thus frequently used in static or quasi-static analyses. By contrast, the explicit approach is time-dependent, and is most applicable for non-linear dynamic problems. The primary difference between these two approaches is in the consideration of acceleration and velocity within the problem. In FE, the equation relating the behavior (e.g. displacement for an elastic problem) to an input(e.g. applied force) is:

$$M\ddot{u} + C\dot{u} + Ku = F$$

where F is the applied force, u, $\dot{u}$, and $\ddot{u}$ are the nodal displacement, velocity and acceleration, respectively, and M, C, and K are matrices that relate to the mass, damping, and stiffness of the model. In the implicit approach, nodal displacement is taken as independent of time, with $\dot{u}$, and $\ddot{u}$ set to zero. Solution of the nodal unknown displacement in effect requires the computation of the inverse of the stiffness matrix K, i.e.,: $u = K^{-1}F$. For large, complex models, the calculation of the inverse matrix can require substantial computation time, and may involve numerical instabilities. By contrast to the implicit method, the explicit method stipulates nodal displacements as a function of time. Therefore, the explicit model also considers nodal velocities and accelerations. Rather than requiring the inverse of the stiffness matrix, the explicit method requires the inverse of the combined "lumped" mass matrix. However, because of the solution approach involved with the explicit method (known as central difference integration), the lumped mass matrix has nonzero values only on its diagonal, and therefore computation of its inverse is trivial. The explicit method is thus numerically stable (i.e., no convergence criteria are involved), and it is therefore extremely successful in modeling complex problems involving large material deformation, non-linear material properties, and contact – all important considerations for constructing an FE model of THA dynamics. However, the explicit method requires that forward progression of the solution be calculated by taking very small time increments. At physiologic time scales, the explicit method can require millions of increments, thus involving substantial computational cost. To ensure stability, the FE algorithm determines, at each iteration, the smallest stable increment size, based on a stability limit. This stability limit is defined as the smallest transit time of a dilatational wave across any one of the elements in the entire model. For linearly elastic materials, the stability limit can be approximated as:

$$\Delta t = \frac{L_{min}}{\sqrt{\dfrac{E(\nu - 1)}{\rho\left(2\nu^2 + \nu - 1\right)}}} \quad ,$$

where L_{min} is the smallest element dimension in the mesh, ρ is the material density, and E and ν are the elastic modulus and Poisson ratio, respectively. The total number of required time increments (n) will be approximately equal to the simulation time (T) divided by Δt. There are two approaches to reduce the computational cost associated with the explicit method. The first is to decrease the number of increments by artificially reducing the time period, T, of the simulation. If T is decreased by a factor f, then the number of increments required for the simulation will be correspondingly reduced: n`=n/f. However, if the simulation speed is increased too much, inertial effects in the simulation may become appreciable and may adversely affect the predicted response. The second approach is to artificially increase the material density ρ (a technique referred to as mass scaling). Increasing ρ by a factor f^2 reduces n to n/f, similar to speeding up the simulation. However, also like speeding up the simulations, inertial effects can become dominant if the mass scaling value is too large. It can be argued, therefore, that execution of explicit FE models can be even more analyst-sensitive than that with implicit modeling. Thus, careful generation of the FE mesh is a prerequisite for explicit FE modeling, as poorly constructed meshes can substantially increase run times (small L_{min}) or can serve as a source of inertial errors if run times or element masses are scaled. Therefore, in addition to demonstration of mesh convergence, the analyst also bears the responsibility to assure that significant inertial errors are not introduced when performing a quasi-static explicit FE simulation.

CHAPTER 1: STABILITY IN HIP ARTHROPLASTY

> If the intrinsic stability of the joint were to reside entirely in the contraction of the muscles, it is clear there would be a great danger of dislocation when the muscles are relaxed or off their guard. Surgical experience leads me to believe that the stability of an artificial hip joint resides entirely in the fibrous sleeve which develops to form the capsule round the joint.
>
> Sir John Charnley – Factors in the design of an artificial hip joint [24].

Owing to the rapid adoption of advanced low-wear bearings, dislocation – defined as the complete subluxation of the femoral head from the acetabular cup – is currently the number one cause of failure in primary THA [41]. Clinically, dislocation is usually classified as an early complication, with 23% of instances occurring in the first 3 months, and 66% within the first year [42]. The initial treatment of choice of a first-time dislocation is closed reduction, which has been shown to be successful in up to two-thirds of cases with optimal component orientation [43]. However, for recurrent dislocations, multiple attempts at closed reduction risk damaging the implant, and are frequently unsuccessful in terms of subsequent dislocation avoidance, [43], so revision is typically preferred. As a solution for recurrent instability, however, revision surgery is successful in only a minority of cases, with recurrent dislocation occurring in over 50% of cases, often resulting in re-revision surgery [44]. For these unfortunate patients, additional surgical options are limited. One fall-back is a constrained component, which can prevent subsequent dislocations in 71% of cases. A variant is a tripolar constrained component, successful preserving stability in 93% of hips [43]. However, these constrained devices have been shown to have increased wear [45] and to have decreased range of motion, thus predisposing to acetabular loosening and/or dissociation of components [43].

The risk factors for dislocation in THA are many and varied [44, 46-61]. Many of the hypothesized risk factors deal with geometrical design of the implant, along with surgical orientations of both the femoral and acetabular components. The use of larger femoral head sizes, or the use of implants with higher head-to-neck ratios (which similarly allow for increased range of motion before impingement) have been shown to significantly increase the stability of the prosthesis in most [44, 48, 60, 62] but not all [63] clinical studies. The theoretical benefits of impingement avoidance have also been demonstrated computationally [64, 65]. Additionally, positioning of the acetabular component within a so-called "safe zone" (approximately 40° of cup inclination and 15° acetabular anteversion) appears to provide at least a degree of protection against impingement and subsequent dislocation [46, 66, 67]. The overall effect of increasing acetabular cup inclination and anteversion serves to provide a greater range of motion for flexion-dominated kinetic challenges, similar to the use of large femoral heads or high head/neck ratios.

Nonetheless, despite decades of investigation and hundreds of studies, there is yet no clear consensus as to which patient-, surgical- or implant-specific risk factors truly predispose to instability following THA. However, one premise on which there is nearly unanimous [37] agreement is that disruption of the soft tissue integrity of the hip clearly predisposes the THA patient to hip instability.

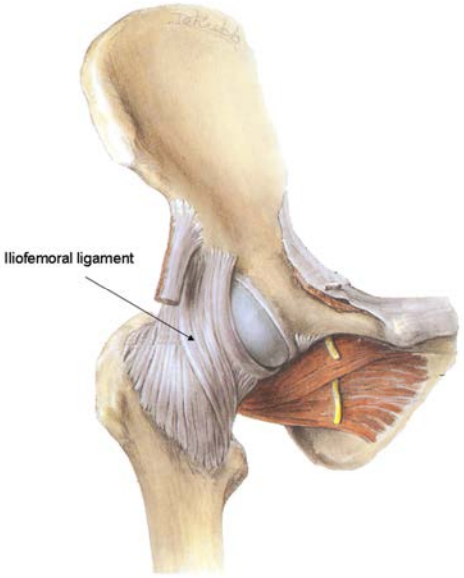

Figure 10: Hip joint capsule. The hip capsule stabilizes the hip joint by constraining subluxation between the femoral head and acetabulum. Modified from [69].

Stability and the Hip Capsule

The hip joint is surrounded by a strong, fibrous capsule, composed of the Y-shaped iliofemoral ligament anteriorly (which resists hyperextension of the joint), the pubofemoral ligament inferiorly (which prevents excessive hip abduction), and the ischiofemoral ligament, which limits hyper-flexion of the joint [68]. The hip joint is further restrained by several muscles and their attachments.

Stability, Dislocation and the Hip Capsule

Compromised soft tissue integrity has long been linked to decreased hip stability following THA. The preservation of the various soft tissue structures during THA is greatly dependent upon the surgical approach. The posterior approach, commonly employed due to its excellent exposure and its reduced operative time and blood loss, has long been associated with significantly greater dislocation rates [47], presumably due to damage to the posterior soft tissue structures. Because of these higher dislocation rates compared to more complicated surgical approaches, several surgeons have advocated for the preservation of soft tissue structures following a posterior surgery, either by meticulously repairing them or through modified surgical procedures that eliminate the need to incise them [50, 52, 54, 70, 71]. Careful repairs of soft tissue structures, or preservation of those structures through modified approaches, have been shown to dramatically reduce the incidence of dislocation otherwise associated with the posterior or posterolateral surgical approaches. It has been estimated that a posterior approach without soft tissue repair has an 8.21 times greater dislocation risk than that for soft tissue repair [61]. For example, a 1998 study [72] compared the stability of THA patients following a traditional posterior approach with capsulectomy and rotator muscle repair only, versus an "enhanced" repair of the posterior soft tissue sleeve, including robust repair of the posterior capsule, and of the short external rotators, quadratus femoris and gluteal attachments. For two separate surgeons, dislocation incidence decreased significantly, from 4% and 6.2% in the surgeons' respective control cohorts, to 0% and 0.8% in their enhanced repair groups. In a similarly designed study [52], incidence of dislocation following enhanced repair with a posterior approach decreased from 2.8% to 0.6%. Interestingly, of the 2.8% of dislocators in the control group (14 out of 500), 13 dislocated posteriorly and only one anteriorly. In the modified repair group, all three of the dislocators had an anterior dislocation. A separate study observing THA stability for capsulectomy versus complete repair [50] reported dislocation rates of 4.8% and 0.7%, for the non-repaired vs. repaired groups, respectively. Similar benefits have been reported by many other authors [54, 61, 71, 73]. While repair of the posterior periarticular structures appears to have a major beneficial impact in reducing dislocation, there have been many studies indicating propensity for mechanical failures of such repairs, either clinically [74-76] or in cadaveric studies [77]. While the dislocation rates following modified/enhanced soft tissue reconstruction with a posterior surgical approach are near the much lower dislocation rates historically occurring for lateral and anterior approaches [47, 78, 79], these other approaches have a steeper learning curve technically and are associated with higher intraoperative complication rates [80].

Soft Tissue-Enhanced Finite Element Model [81]

Because of the many confounding factors involved, clinical registries of dislocation have often been equivocal in terms of elucidating the relative importance of predisposing factors. However, one issue where there is near unanimity of opinion is that hips with mechanical compromise of the capsule are at heightened risk. Insufficiency of capsule function can be due to various factors (e.g., thickness anomaly, stiffening/scarring, substance tears, insertion detachment, and surgical incisions), most of which involve very different technical considerations intra-operatively. Moreover, since some of the causes of capsule deficit which are amenable to surgical repair unfortunately involve trade-offs (especially, additional exposure), intra-operative decision making would benefit from background quantitative information linking defect site/severity with dislocation propensity. To date, most biomechanical work involving the influence of capsule status on dislocation propensity has come from physical experiments, involving either cadaver preparations or mechanical surrogates. While both approaches have their attractions, neither one offers a platform conducive to systematic, clinically realistic study of multiple individual variables, due to limitations such as experimental unwieldiness, tissue deterioration, inter-specimen variability, etc. Therefore a three-dimensional finite element model of THA dislocation was developed using a biofidelic fiber-dominated anisotropic constitutive material model for the capsule (Figure 11).

Figure 11: The capsule FE model of THA. The model consisted of THA hardware, bony anatomy and the hip capsule.

A human cadaveric hemipelvis specimen was obtained, and was carefully dissected to remove all non-capsular tissue. Major families of fiber bundles were identified on the exposed, intact capsule, and were demarcated with nine aqueous barium contrast-(Isovue-370) filled silicone tubes (0.6 mm ID, 1.2 mm OD), which were attached to the intact capsule with 6-0 silk sutures. Marking tubes were directed along the limits of the capsule to span from the proximal to distal attachment sites on the acetabulum and femur respectively. To allow for air contrast during CT imaging, a hole was bored across the acetabulum into the intra-capsular space, and fitted with a brass inlet valve. The hemipelvis was positioned in full-extension, with the pelvis and femoral movements constrained by use of potting the components in PMMA and attaching distal boney regions with brass screws. The specimen was scanned in a 64-detector multi-detector CT scanner using bone and soft tissue (B60 and B31) reconstruction kernels at 0.3mm-0.5mm slice thicknesses, using 10.3kPa of injected room air as a contrast medium (Figure 12A). After the initial scan, the hemi-pelvis was again dissected, this time to remove all soft tissue from the joint. Marking tubes, as described previously, were again used to mark the capsular insertion regions (inner and outer attachments of the capsule) for both the acetabular and femoral attachments. The specimen was again scanned with the same scanning protocol. These two data sets were then segmented using Amira 5.2 software (Mercury Computer Systems, Chelmsford, MA) to obtain surfaces for the capsule (inner and outer), marking tubes and bony landmarks (Figure 12B). After segmentation, the two data sets were registered to each other so as to include both the major fiber orientations as well as the insertion regions.

The segmented and registered data set was further pre-processed in Mathcad (v 14.1). Because of ambiguity of capsular tissue identification (for example, vs. adipose tissue) on the outer surface of the image data set during segmentation, the outer capsule surface was not used directly. Instead, the inner surface was projected outward a uniform distance to form the outer surface. These capsule surfaces then underwent a series of rotations and translations to correctly orient the capsule with respect to a previously validated finite element THA model [82]. The segmented marking tubes were converted to three-dimensional curves, and were operated upon with the same series of translations and rotations. These surfaces and curves were imported into the TrueGrid (v 3.2. XYZ

Scientific Applications, Inc., Livermore, CA) mesh generator, and were meshed entirely with hexahedral continuum elements. The capsule mesh was parsed into eight surgically relevant sectors, allowing for simulated surgical capsule incisions, incision-repair, attachment releases, regional capsule compromise, etc. The fiber-direction curves were projected onto the inner and outer surfaces, forming the boundary for nine volume definitions within the capsule (Figure 13B). Each such volume definition was further divided into three sub-regions, thus forming a total of 27 regions, allowing for 27 individual material regions to be defined in the capsule. For each of the 27 distinct regions, the two boundary vectors defining that volume were averaged. Using the Abaqus keyword *orientation, a prevailing fiber direction in that volume was assigned (Figure 13C). Based on convergence studies (Figure 14), the mesh was structured to minimize aspect ratio globally, while achieving an average element volume of 4 mm^3, resulting in 9,744 brick elements and 13,440 nodes.

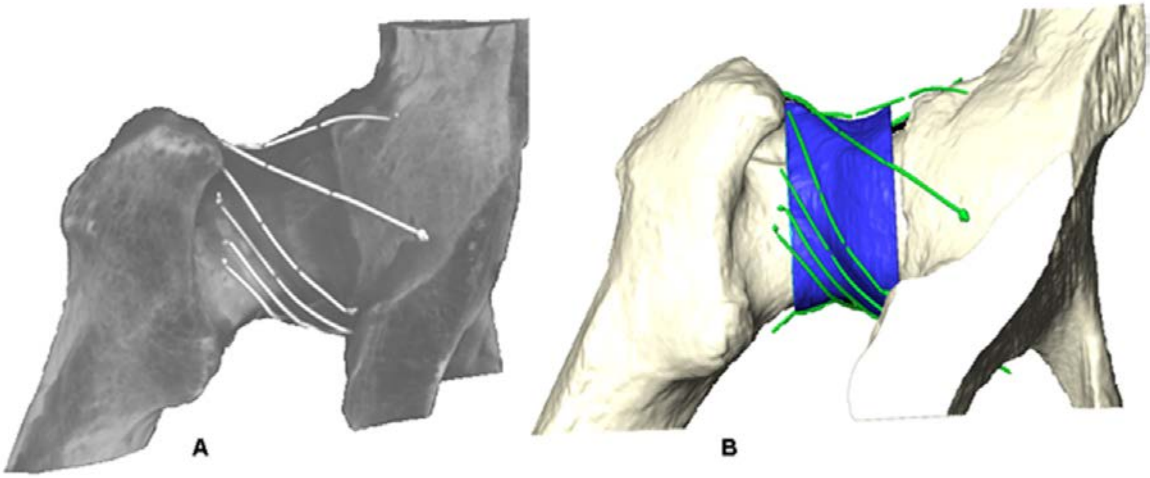

Figure 12: Capsule segmentation protocol. CT scans of the dissected hemipelves (A) were segmented (B) to include surface representation of bone (white), the hip capsule (blue) and principal fiber directions (green).

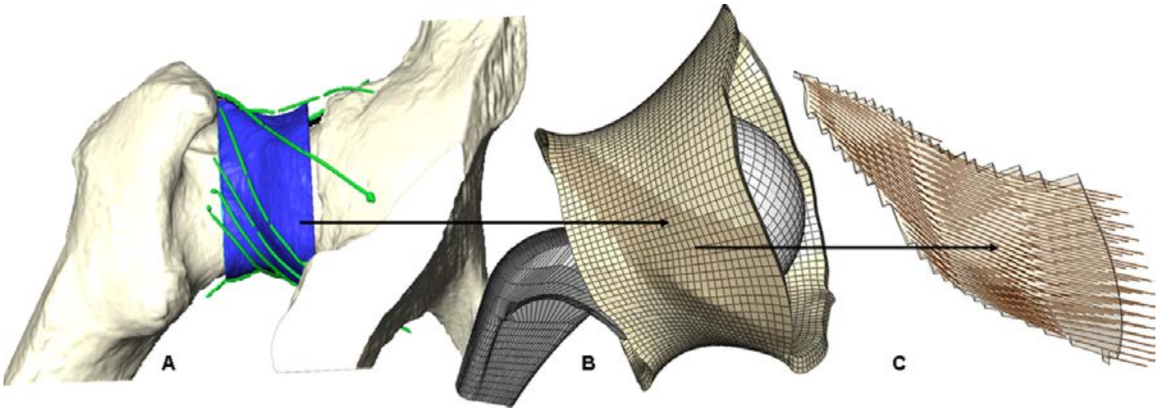

Figure 13: Capsule registration. The segmented CT dataset (A) was registered to the FE model of THA hardware using capsule insertion sites on bony landmarks. The FE capsule model consisted of 27 fiber-direction-specific sectors, three of which are shown shaded (B). Within each of these sectors, an averaged fiber direction was projected throughout each element (C).

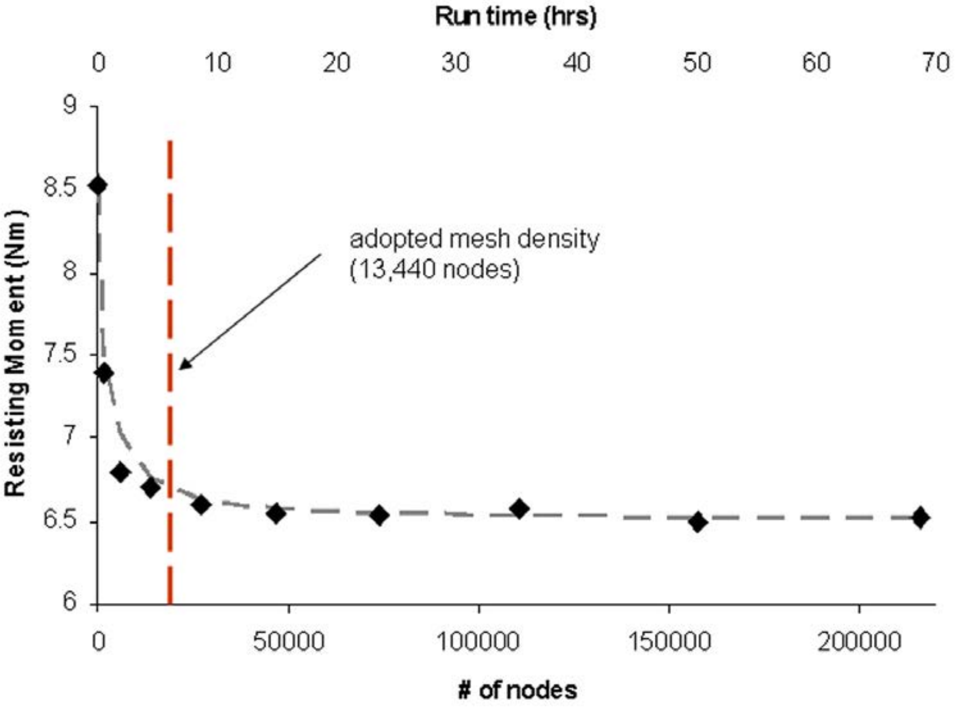

Figure 14: Mesh convergence study for the capsule. Results demonstrated convergence for a mesh density of approximately 13,000 nodes. A user routine was employed to create meshes with near-uniform aspect ratios for each individual element of the mesh.

Anisotropic representation of the capsule was realized using a micromechanically based hyperelastic material model proposed by Gasser, Holzapfel and Ogden [83], which had turn-key implementation in Abaqus 6.9. The strain energy potential (U) of the Holzapfel-Gasser-Ogden hyperelastic material as calculated in Abaqus takes the form:

$$U = C_{10}(\bar{I}_1 - 3) + \frac{1}{D}\left(\frac{(J^{el})^2 - 1}{2} - \ln J^{el}\right) + \frac{k_1}{2k_2}\sum_{\alpha=1}^{N}\left(e^{\left[k_2(\bar{E}_\alpha)^2\right]} - 1\right)$$

with $\bar{E}_\alpha \equiv \kappa(\bar{I}_1 - 3) + (1 - 3\kappa)(\bar{I}_{4(\alpha\alpha)} - 1)$

Here, $\bar{I}_1$ is the first strain invariant, $\bar{I}_{4\alpha\alpha}$ are pseudo-invariants of the deviatoric part of the right Cauchy-Green deformation tensor, J^{el} is the elastic volume ratio, and N is the number of fiber families. C_{10}, D, k_1, k_2 are material coefficients, and κ is a parameter quantifying the degree of heterogeneity in the distribution of fiber directions locally within the material.

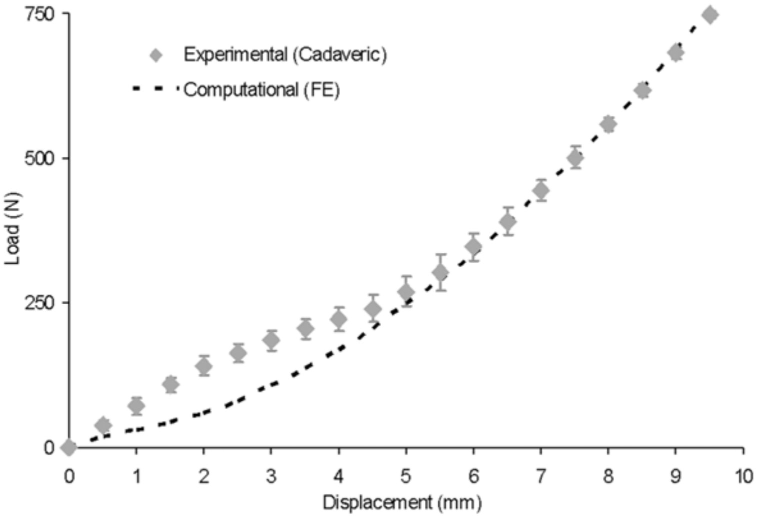

Figure 15: Comparison of load-displacement data measured experimentally in a cadaver specimen [84], versus that for the computational model. The specimen and the FE model were identically loaded, by distraction along the femoral neck.

Material coefficients for the capsule were optimized so that load-displacement data from a simulated distraction test using the model matched previously published experimental load-displacement data [84] for capsule distraction (Figure 15). The best-fit coefficients were as follows: C_{10}=0.004 MPa, D=0.10, k_1=11.0 MPa, k_2=17.33, and κ=0.1. The fibers were modeled as a unidirectional distribution within each of the 27 material sectors. For dynamic FE analysis, all soft tissue was assigned a density of 0.941 gm/cm^3.

Physical validation of the FE analysis was conducted using a novel "transpelvic implantation" [85] of THA-replicating specialty hardware into a cadaveric hemipelvis (Figure 16).

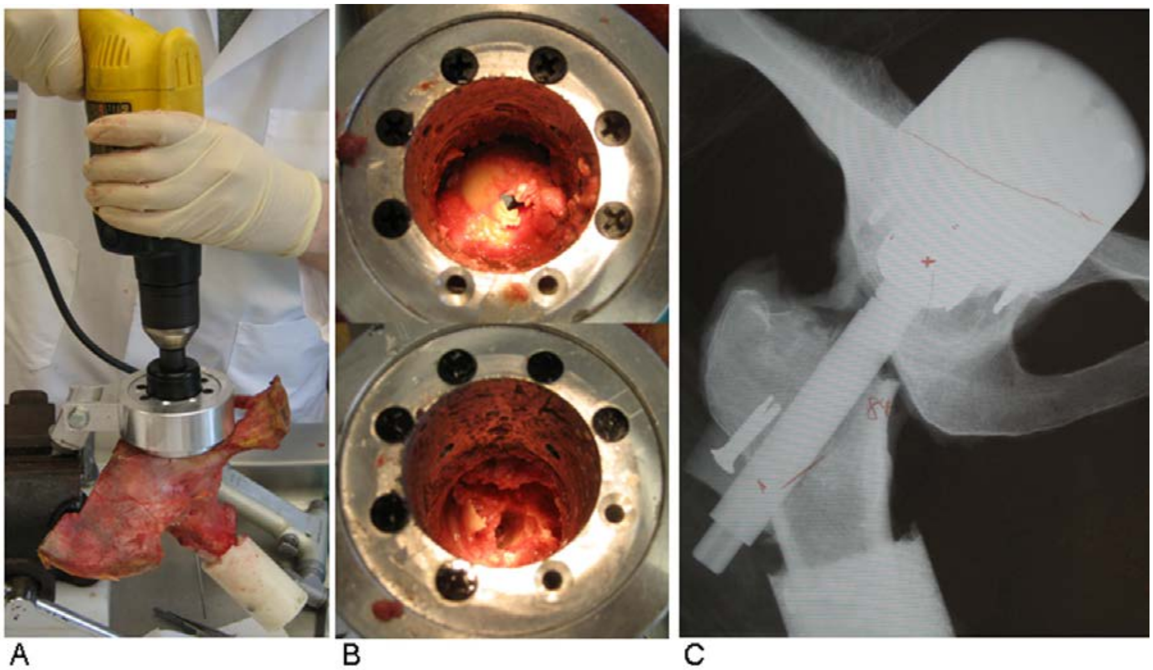

Figure 16: Transpelvic THA implantation. The transpelvic procedure allowed for implantation of THA-geometry-replicating hardware into a cadaveric hemipelvis without violating the capsular soft tissue integrity. (A): Access to the hip joint was gained by guiding a hole saw from the posterior pelvis. (B): The femoral head was exposed (top) and removed (bottom) through the access port. (C): THA-geometry-replicating hardware is implanted, and alignment is verified using a coronal radiograph.

The transpelvic procedure, in which the THA-replicating hardware was implanted via a posterior portal through the pelvis, allowed for investigation of the capsule's contribution to THA stability, beginning from a baseline condition where the capsule's normal anatomic integrity was fully preserved. A cadaveric hemipelvis implanted so as to replicate the THA's intra-articular geometry was affixed to a purpose-built [86] four degree-of-freedom servohydraulic hip simulator (Fig. 17). This simulator allowed for compound joint rotation (flex/extension, ab/adduction and endo/exorotation), along with axial loading. The moment resisting dislocation was recorded during sit-to-stand simulations. The measured resultant moment behavior compared very favorably with that from an FE analysis simulating identical loading and motion inputs (Fig. 18). Excellent computational vs. experimental agreement was also achieved regarding the spatial and temporal occurrence of impingement.

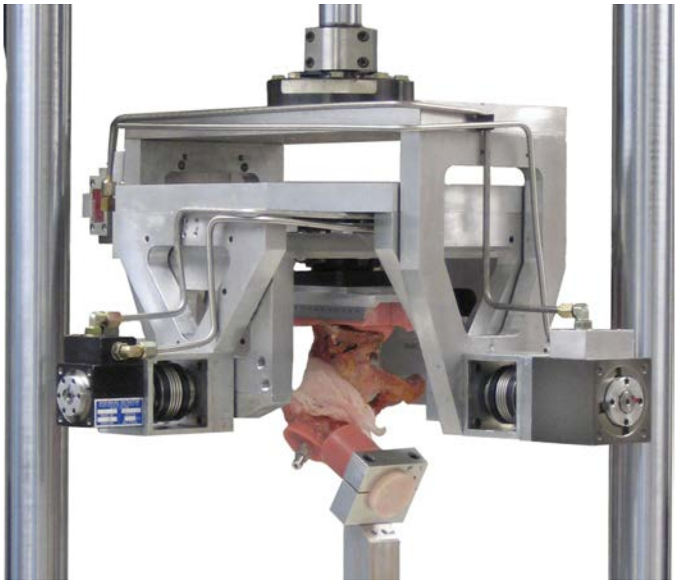

Figure 17: Four-degree-of-freedom servohydraulic hip simulator. This system independently prescribed flex/extension, endo/exorotation, ab/adduction, and joint loading magnitude.

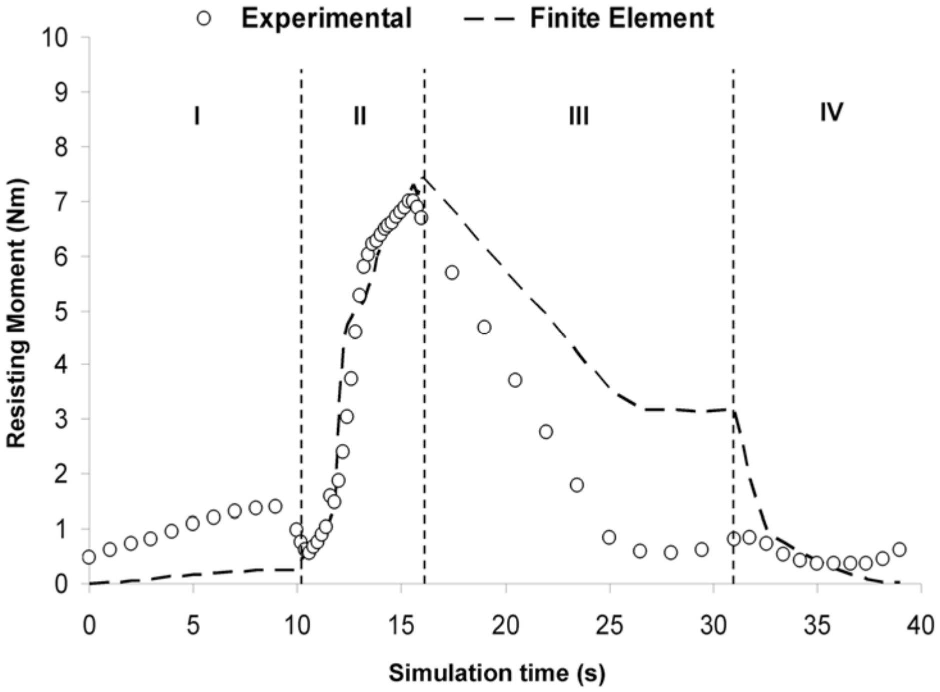

Figure 18: FE model validation. Finite element validation comparing results for a sit-to-stand dislocation challenge for a cadaveric specimen implanted with THA equivalent hardware, versus FE prediction using identical kinematic and kinetic profiles, for the case of uncompromised hip capsule.

Investigation of Capsular Defects and Repair

Obtaining and/or maintaining the best practicable level of capsule integrity is clearly a desirable surgical objective. Abnormality of capsule function can be due to various factors (e.g., thickness anomaly, stiffening/scarring, substance tears, insertion detachment, and surgical incisions), most of which involve very different technical considerations intra-operatively. Moreover, since some of the causes of capsule deficit which are amenable to surgical repair unfortunately involve trade-offs (especially, additional exposure), intra-operative decision making would benefit from background quantitative information linking defect site/severity with dislocation propensity. Because dislocation is fundamentally a biomechanical event, quantitative biomechanical data can aid in understanding which particular aspects of capsule compromise are most deleterious, and in understanding the degree of construct stability improvement attainable by respective repair alternatives. To determine the sensitivity to which dislocation resistance depended upon capsular defects, as well as repair of capsule defects, a parametric FE series using the hip capsule model was conducted.

Simulation of Capsular Defects and Repair Methods

Systematic parametric computational study of the joint capsule required a mesh-based framework to allow for rapid and repeatable capsular perturbations which deviate from the baseline configuration of a contiguous capsule with intact bony attachments. Surgical incisions were created using block boundary and sliding boundary interface definitions (in TrueGrid) between adjacent sectors of the capsule. Defining an incision involved creating an interface which prevented nodes from being merged across segments. Incision repairs were created by allowing specified nodes across a sliding boundary interface to become merged (i.e., equivalenced). Nodes were selected at equidistant locations using two, three or nine sutures across the transverse incision. Attachment releases were simulated by removing those nodes associated with the desired detachment region(s) in the boundary condition constraints, freeing up all translational degrees of freedom. Attachment release repairs were simulated by selecting various nodes across the thickness of the released section, and returning them to a boundary-condition constraint, again at equidistant locations across the defect. Regional atrophy was simulated by stripping away layers of elements in the desired anatomical region. Circumferential locations of the imposed capsule deficits were determined by fitting several elliptical curves to rows of nodes at various heights of the capsule, and assigning the corresponding polar elliptical coordinates to each node along a defect, which were then averaged to obtain a single location (Figure 19).

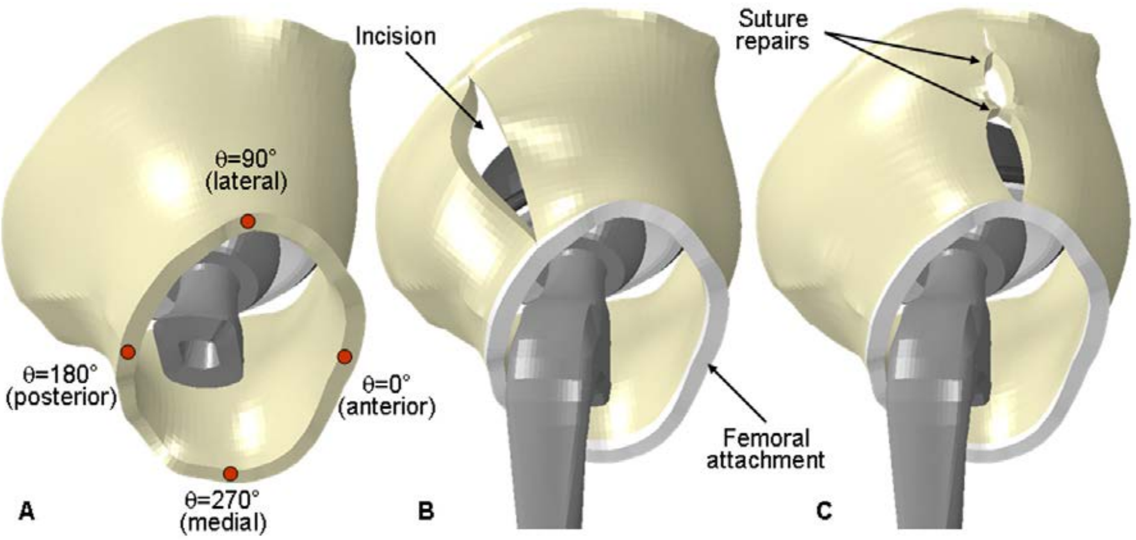

Figure 19: Coordinate conventions for specifying circumferential location. (A): The anterior-most aspect of the capsule was assigned a value of θ=0°, with θ increasing in a counter-clockwise fashion (for visual clarity, the femoral stem has been rendered transparent). (B): A single longitudinal incision is shown located at a posterolateral capsule position. (C): Repair of a separate lateral incision with two sutures. For clarity of visualization, the bony femur and acetabulum have been removed.

THA hardware for the FE model was developed from manufacturer-provided surface geometry files (IGES) and was pre-processed using TrueGrid. The femoral component (28 mm) was meshed with 9,784 hexahedral elements. The cup liner (28-46 mm) was meshed with 7,200 hexahedral elements, while the cup backing contained 1,690 elements. Mesh densities for the femoral component as well as the cup liner were determined from multiple convergence and sensitivity studies, to optimize the FE model for contact analysis while maintaining computational efficiency. Implant positioning was operator-specified, with 35° of tilt and 20° of anteversion for the acetabular component, and 0° of adduction and 0° of anteversion for the femoral component used. A metal-on-metal bearing couple was chosen, with the head, neck and liner modeled assuming linearly elastic behavior of cobalt chrome (CoCr, modulus 210 GPa, Poisson’s ratio 0.3). To further aid in reducing excessive computational run times, the cup backing and distal regions of the femoral component were assigned rigid body definitions. The acetabular and femoral insertion sites of the capsule were attached to rigid bony surfaces. These rigid bony regions also served as the implant anchorage references, allowing for capsule motion to be specified in terms of hip joint movement.

The dislocation kinematic challenge was computationally simulated for a sit-to-stand maneuver. The solutions were driven by a sequence of prescribed incremental rotations of the femoral head with correspondingly applied joint reaction forces [56]. The sit-to-stand kinematic challenge began at 30° extension, continues to 110° of hip flexion, and returns to full extension. Large deformations, highly non-linear material behavior, and multiple independent contact interfaces necessitated the use of the dynamic explicit integration capability within Abaqus. Contact was defined individually between the capsule and itself (self-contact), as well as between the capsule and each hardware component, using the Abaqus/Explicit General Contact algorithm. Additionally, kinematic contact algorithms were specified for hardware/hardware and hardware/bone contact engagements. In the case of capsule incisions, new surfaces created by the incisions were captured as face sets, and included in the general capsule surface definition. Ninety-five total FE models were completed, including the baseline intact capsule model and 94 unique parametrically compromised capsule models, each requiring approximately 60 processor-hours of computational time to complete on a dual quad-core Intel® Xeon platform configured with 24 GB of RAM.

Capsule Defect/Repair Results

For all FE runs, the resultant moment that developed to resist dislocation (designated as the resisting moment) was tracked throughout the entire kinematic input sequence. The development of resisting moment consisted of three distinct phases (Figure 20). First, there was an initial gradual increase, due to a progressive tautening of the capsule. Second, at the instant of component impingement, the discontinuous action of the femoral head starting to lever out of the cup, and the very large (near-line-loading) head/liner contact stresses that developed at the egress site, caused an abrupt increase in the resisting moment. Finally, depending on the specific situation of capsule thickness/defect/repair being considered, the femoral head subsequently either completely displaced out of the cup (frank dislocation) later during flexion, or if dislocation did not occur, the head slipped back into normal congruous articulation during the subsequent hip extension phase of the sit-to-stand maneuver. The area under the moment-rotation curve corresponds to the mechanical energy dissipated within the construct during the dislocation challenge. This energy value, determined for each parametric run by numerically integrating the area under spline curves fitted to each analysis' motion-rotation data, provided a useful comparative metric of overall resistance to dislocation.

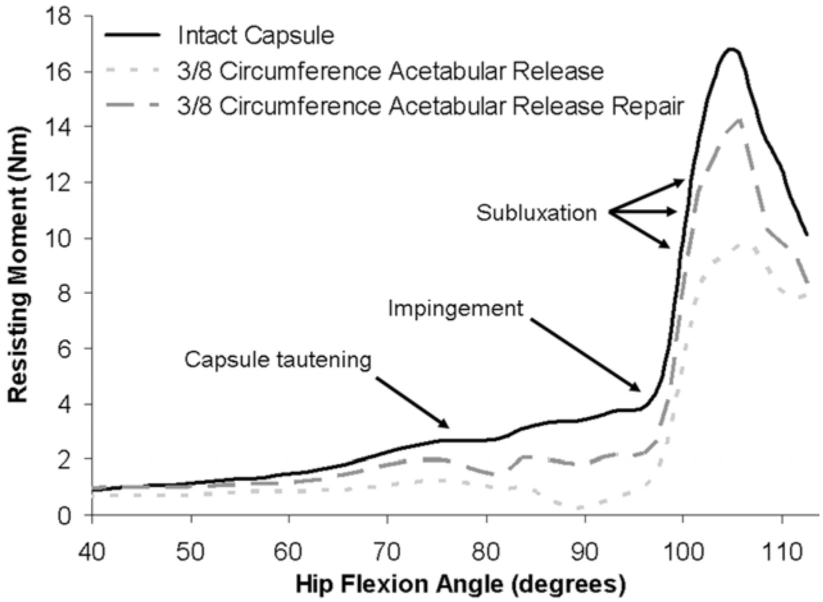

Figure 20: Resisting moment development for hip flexion during the sit-to-stand maneuver for the intact capsule, and for the most stability-compromising capsule defect (3/8 acetabular insertion release) and its repair. For this most compromising case, the capsule provided virtually no resistance to dislocation, and the resisting moment was attributable to hardware interactions only. Repair of this defect returned construct stability to near baseline levels.

Variations in capsule thickness had substantial effects on construct stability (Figure 21). For the thinnest capsule considered (1 mm), peak dislocation resistance reached only 53% of that for a (baseline) 3.5 mm capsule thickness, and reached only 31% of that for the thickest capsule modeled (6 mm). Population-wide, at the 25th percentile vs. 75th percentile of thickness for males and for females, the peak resisting moment values reached only 43% vs. 56% and 40% vs. 57%, respectively, of values for a 6 mm thick capsule.

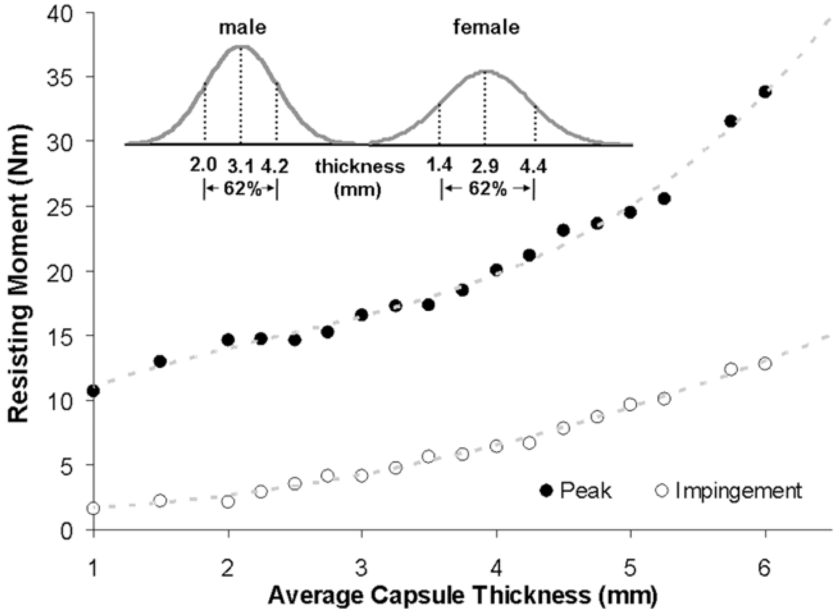

Figure 21: Resisting moment developed during hip flexion versus capsule thickness, across the population-wide range (inset) of capsule thicknesses. Moment values are reported both at incipient impingement, and at the instant of maximum resistance to dislocation. Insert curves are replotted from the data of Dihlmann et al [87].

The effects of localized capsule detachments/releases at the femoral and acetabular insertion sites showed similarly strong dependence on the location of the defect (Figure 22). Posterior- and posterolateral-aspect capsule insertion defects, along either the acetabular or femoral attachments, involved decreases in computed dislocation energy dissipation of more than 50% relative to intact-capsule levels. As might be appreciated conceptually from Figure 22, posterior attachment defects effectively removed substantial fractions of capsule substance from being able to contribute to opposing dislocation in flexion-dominated maneuvers. Repairs of such defects returned peak resisting moment values to within 10-20% of baseline levels.

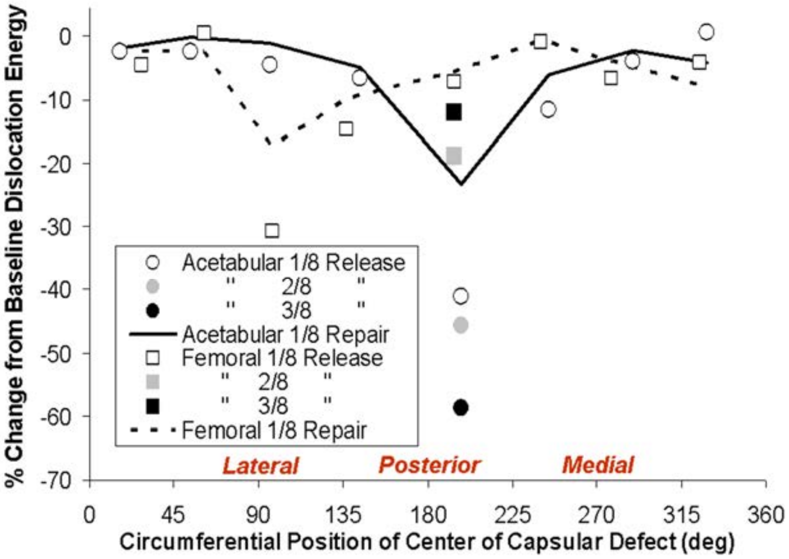

Figure 22: Relative (percent) change in computed dislocation-resistance energy expended during hip flexion, for simulated capsule insertion detachments as a function of circumferential position of detachment site. Note that construct stability compromise depended on both the site and extent of the detachment. In general, otherwise comparable-extent defects involved greater stability compromise for femoral attachment defects located on the medial aspect, and for acetabular attachment defects located on the lateral aspect. Construct stability was consistently returned appreciably toward intact levels for suture repair of the most compromising detachments (posterolaterally located), although for less compromising defects the benefits of repair tended to be equivocal.

Unrepaired full-length longitudinal capsule incisions likewise were found to substantially compromise construct stability (Figure 23), but again in a very site-dependent manner. The most deleterious positions for longitudinal incisions tended to be located somewhat more laterally than was the case for acetabular insertion site defects, and more medially than was the case for femoral insertion site defects, presumably a consequence of the obliquity of directional fiber architecture. Another distinction was that the most severe levels of stability compromise for longitudinal incisions (~50% reductions from intact baseline) were much less pronounced than those for extremum insertion defects (~60%), presumably because capsule material on either side of the incision could still participate in load transmission “in parallel”, whereas insertion defects represent “in series” disruptions of load transmission. Suture repairs of even worst-case longitudinal incisions successfully returned stability to within approximately 10% of baseline levels.

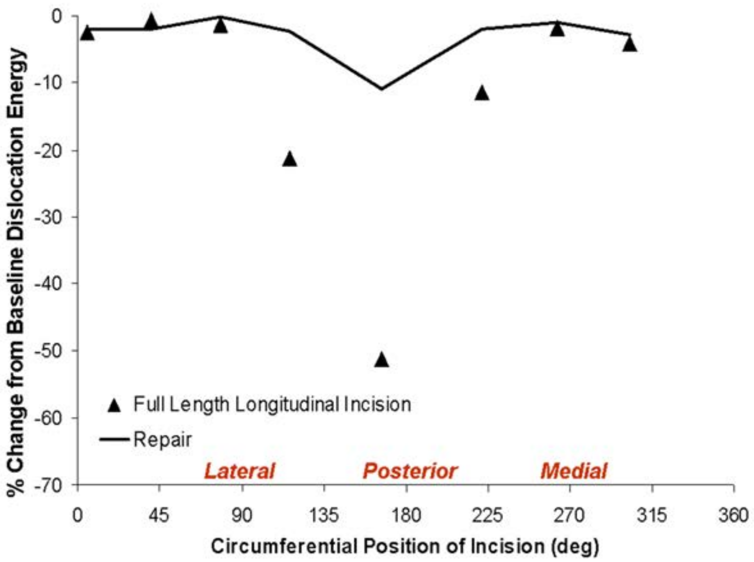

Figure 23: Relative (percent) change in computed dislocation-resistance energy developed during hip flexion, for unrepaired and repaired longitudinal capsular incisions located at selected stations circumferentially. Assuming that suture failure or pull-out did not occur, appreciably improved stability (although not to intact-capsule levels) was obtained for the more compromising posteriorly located incisions.

Successful restoration of construct stability to near-normal levels by means of suture repair of detachments and/or incisions of course depends on avoiding failure at the suture site(s). The use of computational node equivalencing to model suture sites holds the advantage, analytically, of allowing straightforward reporting of the internal nodal force needed to enforce that equivalencing, i.e., the effective pull-out tension at the posited suture site. Computed pull-out forces for individual sutures for various repair alternatives for various capsule defects are shown in Figures 24-26. It can be appreciated (shaded bands in Figures 24 & 26) that many repair arrangements that theoretically would restore near-normal construct stability for severe defects unfortunately involved the suture sites being at substantial risk of failure, either from suture material breakage [88] or from pull-out. By far the best strategy mechanically was multiplicity of sutures. However, it needs to be recognized that the safety factor improvements thus achieved are not in direct proportion to the numbers of sutures employed (Figure 26), because load allocation between individual sutures in a given suture row could be appreciably non-uniform, owing to the complex global load transmission patterns within the capsule.

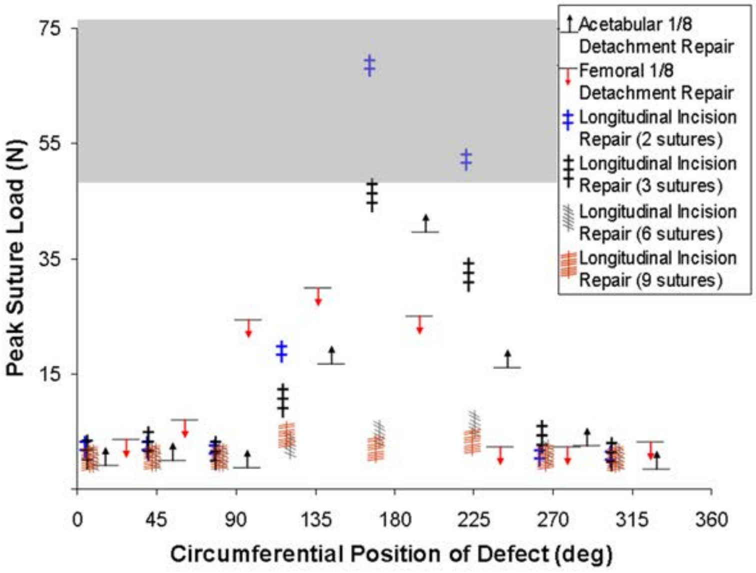

Figure 24: Peak tension developed at the suture site, for repairs of longitudinal slits with two, three, six, or nine sutures, and for single-site repairs of regional acetabular and femoral insertion detachments. For these model runs, it was assumed that suture material failure or suture pullout would not occur. For reference, the range of ultimate tensile strength for No. 1 and No. 2 suture materials reported in the literature [88] is shown in gray.

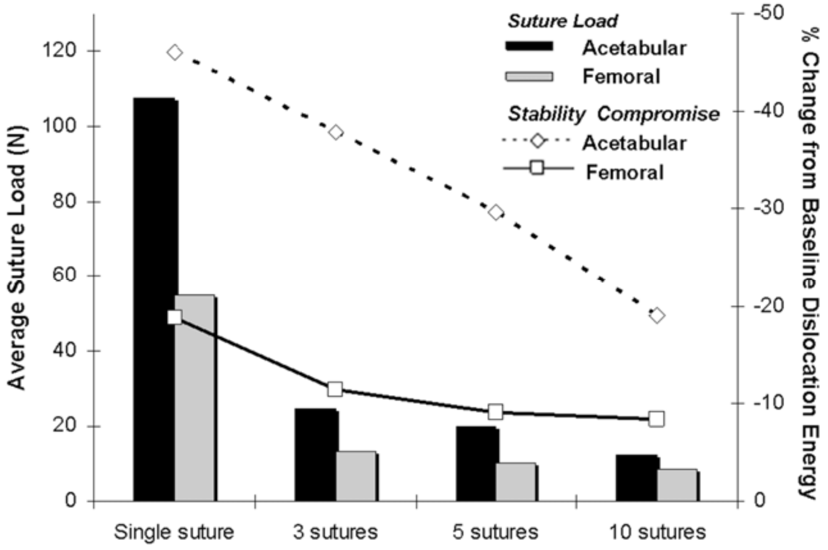

Figure 25: Per-suture tensile loads (bars) developed at simulated femoral and acetabular repair sites for a 3/8- circumference posteriorly centered capsule insertion release, for single-suture versus averages for 3-suture, 5-suture and 10-suture repairs spaced equally along the defect. Deviations from baseline dislocation dissipation energy are also shown (open symbols) for each repair.

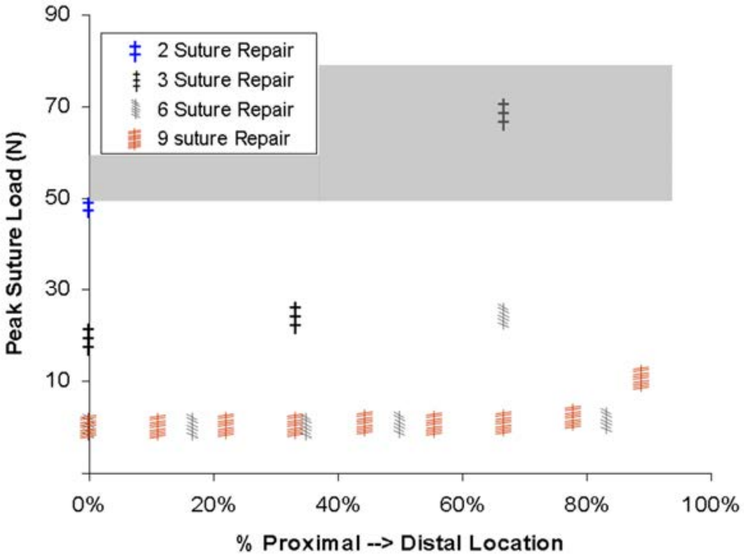

Figure 26: Peak suture tensile load for repair of a posterior longitudinal incision for 2-suture, 3-suture, 6-suture and 9-suture repairs, as a function of suture location along the proximal-distal length of the incision. In general, greater tensile load occurred at the distal aspect of the incision repair.

Capsule Defect/Repair Discussion

This apparent dominance of capsule compromise as a factor affecting instability arguably merits substantial further attention, particularly for identifying the most effective strategies for surgical repair of specific categories or locations of defects and deficiencies. The substantial stress concentrations computed adjacent to local detachment sites in the present model, and the high tensile stresses at some of the suture repair sites, are disconcertingly consistent with the very high incidence of early failures of certain posterior structure repair procedures [75, 76]. While suture failure in the present model is predicted based on ultimate tensile stress, this is certainly a conservative approach: surgical wound healing is a dynamic process and does not begin until the acute phase of resulting inflammation subsides [89]. Progressive subacute phase insertion-site tendon degeneration has been shown to persist for at least six weeks [90], suggesting that repair failure immediately post-op might be more likely to occur due to suture pullout, than due to suture breakage. While the present global-construct FE model was not an ideal formulation for addressing the detailed local mechanics of suture rupture/pull-out, these global results clearly show that some repairs are much more challenged than others. Localized FE models potentially could provide useful insights into the relative benefits of various technical repair alternatives. In summary, this series provided novel mechanistic information regarding the sometimes dramatic degree to which capsule compromise can contribute to THA instability. Since most THA dislocations occur for flexion-dominated motion challenges such as that modeled here, the present FE results help explain the lower dislocation rates documented in clinical series where the posterior capsular structures either have not been violated or have been robustly repaired. And, the present data reinforce the need to meticulously re-approximate and repair the posterior capsular structures to the greatest extent possible, both for primary and for revision surgery, in order to maximize THA construct stability.

Dislocation of Morbidly Obese Total Hip Patients

The dislocation mechanism addressed thus far, i.e., extremes in range of motion leading to mechanical impingement and subsequent subluxation of the femoral head, is that supported by the overwhelming majority of clinical investigation. However, there are a limited number of situations which do not neatly follow this paradigm, and which merit focused biomechanical investigation. Of these, the recognition of increased dislocation risk in morbidly obese THA patients is of paramount importance.

The Obesity Epidemic

National obesity rates, after being relatively stable for several decades [91], increased to epidemic proportions some 30 years ago. Obesity prevalence doubled in US adults between 1980 and 2002, while nearly tripling in adolescents in this same time period [92]. Current obesity prevalence in the US is staggering: 68.3% of US adults are classified as overweight (body mass index, BMI, greater than 25 kg/m2), of which 33.9% are classified as being obese (BMI>30 kg/m2) [93]. When stratified at higher categories of obesity, the rates are equally alarming: 14.3% of US adults are at a BMI level of at least 35, and 5.7% are at a BMI level of at least 40, implying that at least 10 million American adults have body weight at least twice their ideal. The obese population encounters more severe medical problems [94, 95] and thus present a very difficult challenge to the healthcare system. Unfortunately, the trends of the morbidly obese (often defined as BMI>40) do not simply parallel those for the overweight or mildly obese. Between 2000 and 2005, the prevalence of obesity (BMI>30) increased by 24%, while the prevalence of BMI over 40 increased by 50%. This disparity is even greater at the higher extremes of obesity – this same time period saw a 66.4% increase in prevalence for those with BMI > 45, and a 75% increase in those with BMI>50 [96]. The prevalence of obesity is even higher in certain medical subpopulations. In a cross-sectional analysis of 1,710,032 veterans receiving care at Veteran’s Affairs medical centers in 2000 [97], 73% of all men were shown to be at least overweight (BMI>25), with 32.9% classified as obese (BMI>30) and 3.3% as morbidly obese (BMI>40). The peak obesity prevalence was seen in those aged 50-59, with 39.9% classified as being obese. In the same study, 68.4% of women were at least overweight, with 37.4% and 6.0% in the obese and morbidly obese classifications. These prevalence rates were seen to be greater than the national rates for the same year.

Obesity, given its long-established role as a risk factor for several chronic diseases, is thus a serious global healthcare issue. It has been estimated [98] that the risk of the moderately obese for hypertension is 2-fold higher than those of non-obese peers. Similarly, the risks for other chronic health conditions are also elevated for moderate obesity: A three-fold increase is expected for type-2 diabetes mellitus, a 25% increase in the risk for hypercholesterolemia, and a nearly 20% increase in the risk of coronary heart disease. This health disparity is even more exaggerated at higher levels of obesity. Data from the National Health and Nutrition Examination Studies [95] estimated that the mortality associated with obesity (BMI>30) was associated with 111,909 excess deaths relative to normal weight peers. The excess mortality was seen to be higher for greater degrees of obesity, but interestingly was not elevated for those in the overweight category (BMI between 25 and 30).

In addition to its role in predisposition to chronic medical conditions, obesity also places a wide-reaching burden on the musculoskeletal system. A plethora of data exist linking obesity with osteoarthritis (OA), not only in the weight-bearing joints (especially of the knee but to a lesser extent the hip), but also in joints of upper extremity [99]. While the link between obesity and OA is deemed to be a complex interplay of multi-factorial effects, the increased axial force due to body mass, often compounded with joint malalignment, is seen to be a causative factor for knee OA [100]. The anatomical geometry of the hip, in contrast to the knee, possibly affords a slight protective role due to increased stability from additional soft tissue support and geometrical conformity, perhaps explaining the degree of disparity between load-induced OA in the knee versus in the hip [101]. Given the causative effects of OA and resulting joint arthroplasty, it is not surprising that obesity has been directly linked to increased odds for requiring knee or hip arthroplasty. Several studies [102-104] have demonstrated BMI as constituting the greatest relative patient risk for knee (RR>8) and hip (RR>2.5) arthroplasty. Expectedly, the degree of obesity has been shown to correlate strongly with the need for joint replacement. A power-law relationship was shown to exist between BMI and the requirement for either knee or hip replacement [104]. Compared to normal-weight patients, overweight (BMI 25-30) patients had a 3.2- and 1.9-fold higher risk for total knee arthroplasty (TKA) and total hip arthroplasty (THA), respectively. The risk increases substantially for those with BMI 30-35, with an 8.5- and 3.4-fold risk increase for TKA or THA. The relative risks jump even higher for those in the 35-40 classification: 18.7 (TKA) and 5.2 (THA), while those in the greatest obesity classification (BMI>40) were demonstrated to be at a 32.7-fold increased risk for TKA and an 8.6-fold increased risk for THA. It has also been shown that obesity affects the age at which joint replacement is required. In a study of 1,369 patients having total joint replacement [105], morbidly obese patients were shown to require knee replacement at 13 years younger age than non-overweight patients. For hip joints, morbidly obese patients required hip replacement 10 years earlier. Given the large-scale shift towards increased prevalence of obesity in the United States, and the increased requirement for total joint replacement in a younger and more obese population, the demographics of the total joint patient have changed as well. In a 15 year prospective review of patients with joint arthroplasty [106], the proportion of obese patients increased significantly, from 30.4% in 1990 to 52.1% in 2005. In step with population-wide trends, the TJA rates for the morbidly obese increased even more: 5.2% in 1990 compared to 12.8% in 2005. These prevalence rates were much higher than the national obesity prevalence rates for the same years.

Post-arthroplasty obese patients also differ substantially from their non-obese peers in terms of peri- and post-operative complications and outcome measures.

Management of the obese arthroplasty patient has proven to be difficult. In a study of 1,343 THA patients [107] those with BMI > 35 were 2.3 times more likely to have a hospital stay exceed 5 days and were 2.6 times more likely to be discharged to skilled nursing inpatient rehabilitation. Also, periprosthetic infection has frequently been cited to occur at higher levels in the obese population [108-114]. Like many other obesity-related complications, there appears to be an association between level of obesity, and risk stratification: a retrospective review of 6,108 total joint patients [109] revealed an odds ratio of 3.2 for deep infection for patients with a BMI>40 vs BMI<40, whereas those with BMI>50 had an 18.3 times odds ratio of infection vs. those with BMI<50. While it has been suggested that the longer operating time required for obese patients undergoing arthroplasty [115] may be responsible for the increased risk for periprosthetic infections, several studies have shown the increased propensity for infections to be independent of operating time [110, 111].

Other post-operative complications have been shown to increase in the obese orthopaedic patient population. One study [116] reported a greater than 2.5-fold increase in total complication rate post-THA for morbidly obese patients relative to normal weight subjects, including greater than a 4.7-fold increase in all orthopaedic complications one year post-operatively. In the same population, a nearly 2-fold increase was seen in patients reporting difficultly descending or ascending stairs. The outcomes were much more affected by obesity compared to those at one-year for TKA patients. Another study, using a 15-year follow-up period [117], observed a near perfect dose-effect decrease in ambulation with BMI during the entire 15-year follow-up period. Statistically significant reductions were seen for walking time without support, stair-climbing performance, hip flexion and shoe-tying ability. In another study [118], obese patients were observed to have a significantly reduced Harris Hip Score in all parts except pain, when compared to non-obese controls. Andrew et al. [115] reported significantly reduced Oxford Hip Scores, with a dose-effect relationship to degree of obesity. In another prospective study of revision

THA patients [119], obesity was seen to be a profound predictor in several outcome measures. Statistically significant associations were determined between obesity and pain, use of NSAID medication, and moderate-severe activity limitations including walking-aid dependency, in the obese subjects compared to the non-overweight cohort, after both 2- and 5-year follow-up. The effect of degree of obesity in this study was shown to be most profound for the activity-limitation prediction.

The costs associated with obesity, in terms of both individual and global health burdens, are sobering. It has been estimated [98] that the expected lifetime medical care costs for the moderately obese patient are about 50% higher than those for the normal weight patient, while the increase for those with higher levels of obesity is even greater, with a predicted 84% increase for those with a BMI of 37.5. The cost of treating obesity and associated comorbidities is estimated to be 117 billion per year [106], rivaling the costs attributed to cigarette smoking [98]. Owing to the disproportionate share of medical complications accrued by the obese population, the healthcare cost-burden for the obese is greater than normal-weight patients. A study analyzing 8 million inpatient medical records of US hospitals [120] found cost-of-illness was 6.1% higher for obese patients, and 18.7% higher for the morbidly obese, compared to the non-obese, independent of hospital stay or comorbidities. Given the alarming increase in obesity prevalence in the US, the cost-burden, both individually and on the healthcare system as a whole, is certain to increase in the foreseeable future.

Obesity and Instability following Total Hip Arthroplasty

Obese patients, owing to various anatomic and biomechanical factors, present with varying degrees of structural and functional limitations. These limitations place diverse restraints on ambulation and motions required for daily living. In a study of 20,553 primary THA patients [117], hip flexion in the obese patient was seen to be significantly less than that for the non-obese cohort at 3 and 6 years follow-up, with only

73.1% of obese patients able to flex > 90°, compared to 80.9% of non-obese subjects. Jackson et al. [118] observed in a study of over 2,000 THA patients after 6 years of follow-up that those with BMI > 30 had significantly reduced range of motion. Hip motion was significantly reduced in terms of flexion (113° vs 122.5°), adduction (23.2° vs 25.2°), and internal rotation (11.2° vs 14°) versus non-obese subjects. It is well understood that, while highly complex and multi-factorial, dislocation in THA is very much a biomechanically dominated phenomenon [121]. It has been shown convincingly in computational models [56] that dislocation risk increases with extremes in the range of motion. Given these factors, it is therefore somewhat intuitive that obesity, because of restricted ranges of motion, would provide some degree of stability protection, or at the very least would not be associated with increased dislocation risk, from a purely biomechanical view of the dislocation sequence. Thus, it is not surprising that this result has been reported clinically [49, 122, 123]. However, there is a growing collection of evidence that obesity, especially morbid obesity, is a significant independent risk factor for dislocation for both primary and revision THA.

In a study of 2,106 Swedish male primary THA patients [124], there were dislocations in 1.2% of the normal BMI group (BMI 18.5-25), compared to 2.8% of overweight patients (BMI 25-30) and 4% in those with BMI>30. When adjusted for age, the overweight and obese had significantly increased risk, with odds ratios of 2.4 and 3.6, respectively. In another large study [114], dislocation rates were assessed for the obese (BMI > 30) vs non-obese (BMI < 30) for 2,495 primary THA patients. The dislocation rates for the obese patients (3.7%) were significantly higher than those of the non-obese (1.6%). Interestingly, while the total incidence rate for dislocation was nearly twice as high for men versus for women, the relative rates in the obese group were significantly higher in women than men (RR 3.0 vs 1.8). A large, multi-center study [115] stratified instability rates in 1,421 primary THAs into three groups: non-obese (BMI<30), obese (BMI 30-40) and severely obese (BMI>40). The obese groups had dislocation rates of

2.7% and 5.6%, compared to 1.3% in the non-obese group, resulting in odds ratios of 2.1 and 4.3, for the obese and severely obese groups, respectively. In a separate study of obese Veterans Affairs Medical Center male veterans [112], morbidly obese patients were seen to have a significant 5-fold increase in dislocations when compared to those with BMI < 40, resulting in an adjusted odds ratio of 3.5 for the most obese group.

While the clinical studies listed above report an average relative risk 3.7 for the most-obese vs. non-obese groups, the discrepancy due to body weight reported for revision THAs is even higher. Compared to primary THA, revision THA is associated with significantly longer operation times, more extensive tissue/bone damage. Revisions are associated with higher total dislocation rates, and are linked to a different set of risk factors[44] for instability. In a study of 204 revision THAs over a ten year period [113], dislocation was observed in 10 (19.2%) obese patients versus 10 (6.6%) in non-obese patients, with an adjusted odds ratio of 3.5. In this same study, the rate of all adverse events in obese subjects (33%) was significantly higher than those in the non-obese group (9%). Recently, a study by Kim et al. [125] of age-, gender-, and procedure-type matched revision THA in 93 patients, dislocation rates were stratified into two levels: morbid obesity (BMI>35) and non-obese (BMI<30). The morbidly obese patients were found to have dislocation rates greater than six-times those for non-obese controls (19% vs 3%). In the same morbidly obese patient cohort, seven patients required re-revision surgery, six of whom required further surgical intervention to treat the instability.

The majority of studies examining stability following THA support the positive association of body mass index and post-operative instability, both for primary and revision surgeries. The studies reporting no statistical association between obesity and dislocation rates [49, 122, 123] tended to be smaller studies compared to the much larger studies described above reporting a significant association.

In addition to its linkage to a wide-reaching collection of chronic medical conditions, obesity, independent of other concomitant medical conditions, has been shown to have detrimental effects on soft tissue structures. Adipose tissue, long thought of being simply a static energy reserve, is rapidly gaining recognition as a potent endocrine organ, modulating potent effects on inflammation and the on the immune system through the release of soluble mediating factors [126]. These include a group of adipose-tissue specific “adipocytokines” including adiponectin and leptin, as well as several systemic proinflammatory cytokines such as tumor necrosis factor α (TNF_{α}), and interleukin-6 [126, 127]. Leptin has been directly linked to deleterious affects on cartilage [128], providing a possible metabolic link between obesity and development of osteoarthritis. The notion of obesity causing a chronic, inflammatory condition is supported in part by a strong correlation between obesity and development of rheumatoid arthritis [99, 129]. However, direct linkage in the literature between obesity and other musculoskeletal-specific soft tissue detriments is more tenuous, and is mostly based on clinical observation. Obesity has been associated with plantar fasciitis (OR = 5.6), and was seen as a greater risk factor for that condition than manual workers reporting spending most of the day standing on their feet. In a large case-controlled study of 849 patients [130], a significant dose-effect increase in rotator cuff tendonitis was seen for various levels of obesity, with an adjusted odds ratio of 3.13 for males and 3.51 for females. In another study of 501 workers [131], obesity was seen to be a significant risk factor for development of upper extremity tendonitis. Additionally, obesity has been recognized as a risk factor for quadriceps tendon rupture [132]. And, obesity has been described as an independent risk factor for the development of degenerative disc disease and back pain [127].

While clinical evidence supports an association between obesity and development of various soft tissue disorders, there is reason to believe that this is an under-reported linkage, especially for collagenous structures. In a radiographic study of lean tissue properties of the thigh [133], investigators reported a noteworthy decrease in lean-tissue density. Other investigators, using a hypothalamic-induced mouse obesity model, have shown that obese mice have significant deficiencies of soft tissue structures, including decreased levels of mucopolysaccharides, glycoproteins, elastin and collagen [134]. Obesity has also been postulated as a primary cause of vascular dysfunction: cutaneous microvascular function was found to be significantly impaired in obese women compared to normal weight controls [135]. These vascular alterations, including deficiencies in capillary recruitment and endothelium-dependent vasodilation, were postulated to be responsible for obesity-related developments of microangiopathy, hypertension and insulin resistance.

Additionally, obesity has been strongly associated with altered collagen organization and disrupted matrix properties. In a study characterizing skin properties in bariatric surgery patients [136], histologic analysis of skin samples demonstrated a significant deviation towards poorly organized collagen organization, with several inclusions of non-staining amorphous regions being noted. The collagen matrix of these patients was described as degraded and diffuse, and distinctly acellular. Elastin fibers, found in lower numbers than in non-obese controls, were identified as displaying significant disintegration and fragmentation. Collagen bundles demonstrated a marked decrease in thickness, with visually apparent "pockets" of resorption. The overall assessment of tissue was similar to that seen in chronic inflammation. Differential scanning calorimetry was used to quantify additional skin properties through assessment of collagen denaturation. This can give insight into the degree of crosslinking and thus mechanical integrity, and showed that skin from the obese group had measurably poorer characteristics. This mechanical strength incongruity has been explored in animal models: Enser et al. [137] had previously reported weaker mechanical strength of skin in obese vs. lean mice.

Possibly mediated through the same mechanisms of decreased vascularity against the backdrop of a chronic inflammatory state, a strong association exists between obesity and poor wound healing [138]. Hypoxia, or conditions favoring hypoxia, is often observed in the obese patient. Given the significantly larger body mass, obese patients are thought to place excessive demands on the heart and cardiovascular system, leading to poor tissue oxygenation and subsequent ischemia in the tissue, causing undue tissue necrosis susceptibility and other tissue compromise. These conditions are further worsened by the respiratory burden seen in the obese: excessive adipose tissue in the abdomen and chest can restrict proper thoracic inflation during inhalation, impairing respiratory vital capacity, and leading to hyperventilation [139], further compromising tissue oxygen tension and adversely affecting wound healing functions. Many of the steps in the wound healing process are oxygen-dependent. Fibroblast maturation, leukocytosis and phagocytosis, and the proliferation and migration of cells to areas of tissue damage might also be impeded in the obese patient. Additionally, many of the proinflammatory cytokines related to the chronic inflammatory state of the obese patient have been shown to have detrimental effects in the wound healing process [140].

Functional limitations in the obese patient tend to reduce the extremes of motion shown to cause dislocation [56]. It is during these extremes of motion that the effect of soft tissue integrity on THA construct stability is expected to be greatest. While there is strong evidence linking soft tissue compromise and dislocation propensity in THA patients, and while there is a linkage between obesity and compromised soft tissue function and repair, it is doubtful that soft tissue deficiency alone explains the increased incidence of THA dislocation in the obese patient population. Of the various risk factors associated with dislocation, many involve biomechanical abnormality in routine execution of normal daily activities, abnormalities which are known to be greater in the obese. A 1999 study by Woolson et al. [49] evaluated potential risk factors in the first three months following primary THA. Only a condition they called "cerebral dysfunction" (a known history of excessive ethanol abuse or mental confusion) was statistically significant. Interestingly, while obesity was not seen to be a significant risk, all primary surgeries were performed with complete capsulectomy following a posterior THA. A separate study [123] also indicated heavy alcohol consumption as an independent risk factor for THA instability, showing a dislocation rate of 23% in excessive drinkers compared to 5% in abstainers. While the strength of correlation between excessive ethanol consumption and obesity is controversial, there does appear to be at least some linkage between consumption and obesity risk [141]. However, the more plausible relationship exists between obesity, alcohol, and postural stability. Alcohol has both acute and chronic detrimental effects on balance, leading to postural instability and possible aberrant movements and falls. Irrespective of the casual linkage between obesity and alcoholism, individuals with higher BMIs have been shown to have substantially impaired posture and balance [142-145], possibly defining a mechanism for the decreased THA stability in the obese. Other authors have suggested decreased lower extremity peripheral muscle strength as a risk factor for THA dislocation [44, 112, 113], especially for obese patients, in whom muscle strength has been shown to be decreased for both women [146] and men [147].

However, perhaps the most likely explanation for the increased dislocation rate seen in the obese is caused by the same anatomic functional limitations that seemingly should protect them from instability. Recent work by our group [148] has shown that extra-articular soft tissue impingement can reduce stability for patients undergoing high flexion (Figure 27).

Such impingement, termed “panniculus impingement”, creates an eccentric force potentiating subluxation, analogous to what happens with hardware impingement; it has been commented upon in the clinical literature [118]. The occurrence of panniculus impingement creates an additional force near the mid-thigh region. This additional force can be significant, in some instances approaching 20% of body weight [148]. It may substantially alter the kinematics of high-flexion motions, and increase the dislocation risk by decreasing joint contact force during impingement, facilitating subluxation of the femoral head from the acetabular cup.

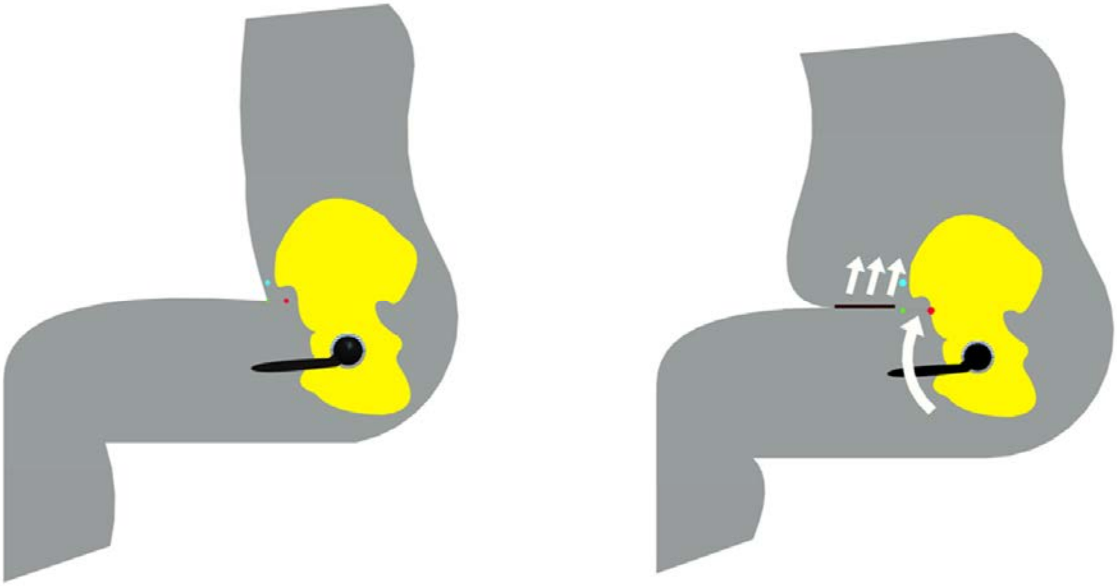

Figure 27: Possible soft tissue impingement leading to decreased stability post-THA for obese patients. Left: Sagittal plane schematic at the instant of maximum flexion prior to lift-off of the buttocks during a sit-to-stand maneuver. Right: Adverse kinetics involved in the obese sit-to-stand, demonstrating panniculus impingement, which creates an additional abdominal force and subsequent torque tending to cause subluxation of the hip joint.

A somewhat analogous relationship between extra-articular soft tissue impingement and subsequent dislocation was recently observed by Kim et al. [125]. In that study, a higher dislocation rate observed in obese patients following revision THA was attributed to extraarticular soft tissue impingement during hip adduction and flexion (Figure 28), with hip adduction noted as typically causing instability. Given the gender differences in adipose tissue deposition [149], with females predominately depositing fat in the hip and thigh area compared to a more abdominal distribution for males, the idea of increased dislocation risk from increased thigh adipose tissue content is given additional credence due to the higher dislocation rates observed in obese females compared to obese males [114].

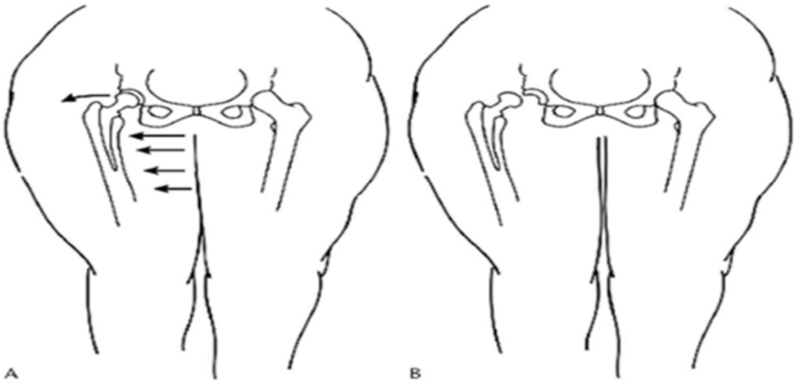

Figure 28: Possible mechanisms for dislocation in obese THA patients. (A) Thigh impingement during adduction creates a laterally directed force on the femoral component. (B) Thigh impingement is relieved if dislocation occurs. Modified from [125].

These observations highlight the point that the kinetics and kinematics of locomotion in obese patients, differ from those of normal weight subjects. This has been studied most extensively in gait, with observed differences as a function of BMI [142, 150-152]. Similar decreased motion strategies have been observed in goal-directed upper-extremity movement [153] and in jumping [154, 155]. Unfortunately, however, there is a paucity of data reporting functional differences between obese and normal weight individuals undergoing motions associated with increased risk of hip dislocation. Studies in obese individuals performing a sit-to-stand maneuver [156, 157] show that obese subjects tend to utilize a strategy which limits trunk flexion, in order to minimize momentum of the lower back, compared to normal-weight subjects whose strategy was characterized by fully forward trunk flexion. Obese subjects therefore had higher knee torque and decreased hip torque production compared with normal weight controls. Interestingly, it was seen that with repeated trials, obese subjects changed their rising strategy by increasing trunk flexion, possibly leading to yet higher panniculus impingement forces and altered hip joint kinetics. The kinematics of obese subjects undergoing other dislocation-prone kinetics, however, is currently unknown.

To move beyond conjecture as regards a potentially under-appreciated mechanism for THA instability, the previously physically-validated FE model of total hip dislocation was augmented to include the biomechanical effects of external soft tissue (thigh-thigh) impingement. Toward the goal of providing quantitative data to help guide surgical management regarding hip replacement in the morbidly obese, this FE model was utilized to determine whether thigh soft tissue impingement could substantially decrease THA stability, and if so, at what level of body mass index this effect would become significant. Additionally, factors under the surgeon's control (implant head size, neck offset, cup geometry and cup abduction) were investigated, to determined these factors' influence on THA stability in the obese patient.

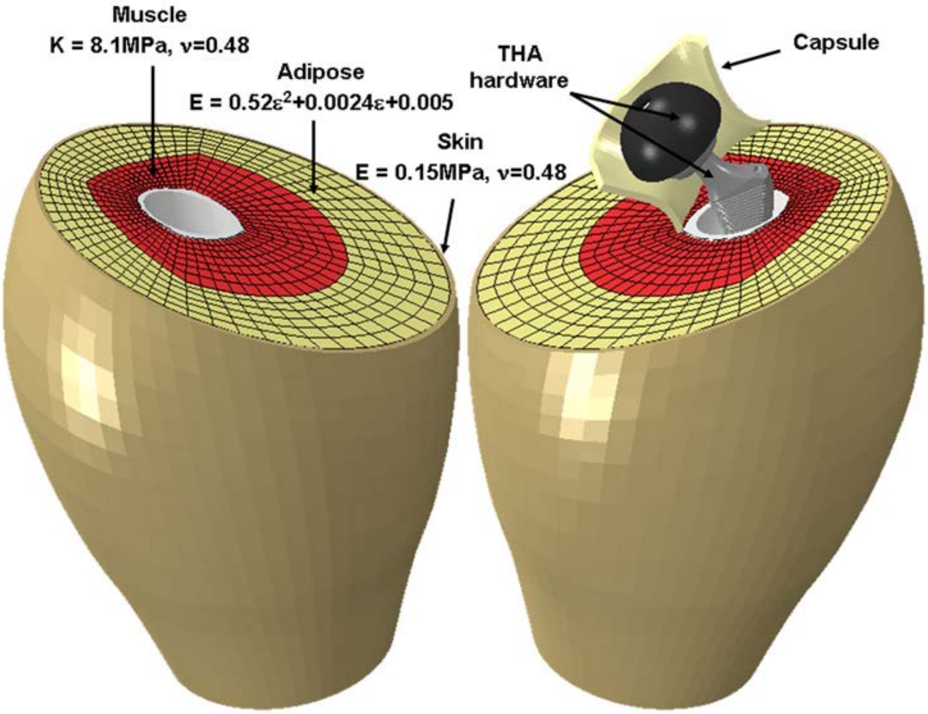

Figure 29: The FE model of extra-articular soft tissue impingement and subsequent THA instability consisted of (1) implanted THA hardware; (2) hip capsule (posterior half of the capsule rendered transparent for clarity); and (3) extra-articular soft tissue including muscle, adipose tissue, and skin, surrounding a rigid femoral canal. The model assumes right-left anatomic symmetry. E=Young's modulus, K=Bulk modulus, ε=nominal strain, ν=Poisson's ratio.

Methodology for the Obesity-Related Dislocation FE Model

The obesity THA dislocation FE model consisted of three parts (Figure 29): (1) THA hardware, (2) hip capsule, and (3) mirrored left and right thighs. Left and right thighs were composed of a femoral shaft (assumed rigid), muscle, adipose tissue and skin. The bulk material of adipose tissue in compression was modeled as a neo-Hookian hyperelastic solid [158]. Using a small strain assumption, skin and (passive) muscle were modeled as linearly elastic [158, 159].

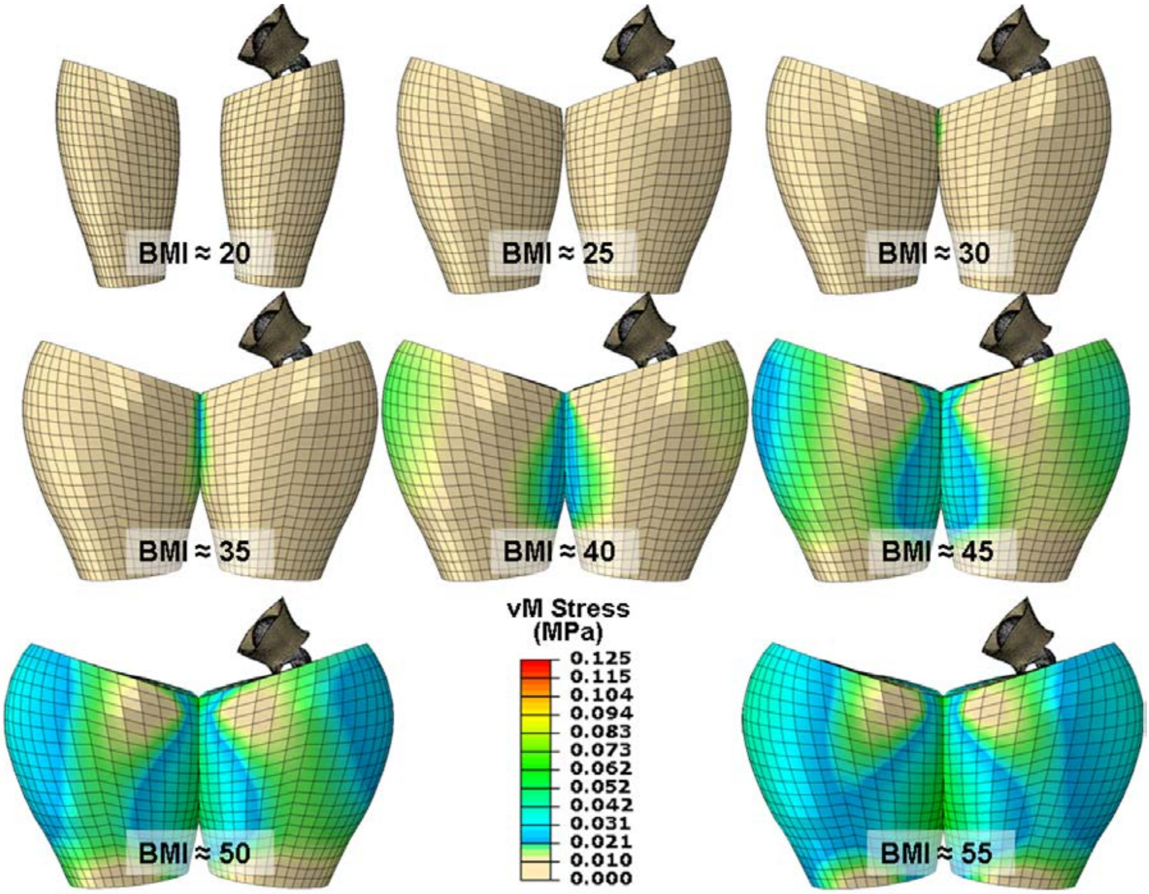

Figure 30: Eight graded levels of BMI were used in the dislocation FE series. Anatomic shape parameters where used for the baseline case (BMI=20), which were then scaled using anthropometric data to assume thigh geometry for an overweight patient (BMI=25) and six grades of obesity. An initial analysis step brings the thighs into appropriate apposition (as shown) for the beginning of the analysis, resulting in contact occurring between the thighs in all six obese FE models.

Thigh morphology was based on anatomical geometric shape functions. Using anthropometric data [160], these shape functions were scaled for eight separate graded levels of BMI (Figure 30). It was assumed that the skin thickness and muscle mass would remain constant across all levels of BMI, with the girth increase across the models being attributable solely to increase in adipose tissue.

Two separate THA implants were modeled. The first incorporated a 28-mm head. The second was a contemporary modular large-head (36mm) implant with a standard or high-offset (8mm) neck. Fifteen separate acetabular cup orientations were generated by varying cup abduction from 30° to 65° in 2.5° increments, with constant 10° of cup anteversion.

A sit-to-stand maneuver was used as the dislocation challenge. Input kinematics and kinetics were obtained from motion data previously collected for 10 subjects performing this motion [56]. The input data were modified to reduce peak flexion during the motion sequence, to simulate the reduced flexion of obese subjects performing a sit-to-stand [157]. (This same obese sit-to-stand input sequence was used for all BMIs addressed in the FE series, to remove the potentially confounding influence of the joint angulation range utilized.) Right-left motion symmetry was assumed during the maneuver, i.e., each leg was driven by mirrored kinematics. Joint contact forces were scaled for each model's simulated body weight. Based on cadaveric measurements, a constant initial distance between femoral head centers (200mm) was assumed.

All mesh zonings for the model were pre-processed with TrueGrid. A separate FE model was generated at each of the 15 cup orientations for all eight graded levels of BMI, for each of the three implant combinations, resulting in a total of 360 individual FE simulations. For each simulation, the (assumed rigid) metal backing was rigidly fixed in space (i.e., anchored to the bony pelvis) by constraining its control point's nodal rotation and translation. The acetabular liner was held within the shell through frictional interactions. The femoral stem was orientated at 5 degrees of anteversion for all cases.

All rotations and loads associated with each dislocation motion sequence were prescribed at the center of the femoral head. Because of the non-linear behavior of both capsule and adipose tissue, all analyses were executed using Abaqus/Explicit. For computational economy, the THA hardware was assumed rigid. For each FE simulation, the components of the femoral head displacement were tracked throughout the entire input sequence.

Physical corroboration of the thigh-impingement FE model was conducting using a calibrated interface pressure mat (CONFORMat, Tekscan, Inc.), allowing for real-time analysis of contact pressures and for integration of the total loads registered between the thighs of obese subjects during a sit-to-stand kinematic challenge (Figure 31). Real-time Tekscan pressure acquisition was performed on a 41-BMI female subject during a sit-to-stand sequence. Peak thigh-thigh contact load was reached at the terminal phase of the sit-to-stand. The maximum thigh circumference of the subject fell between the simulated thigh circumference of the 35- and 40- BMI FE models. Registering the mat's sensing area to the finite element mesh, agreement of the physically measured versus computed thigh-thigh contact force was within 16%, for the 35- BMI case (Figure 31).

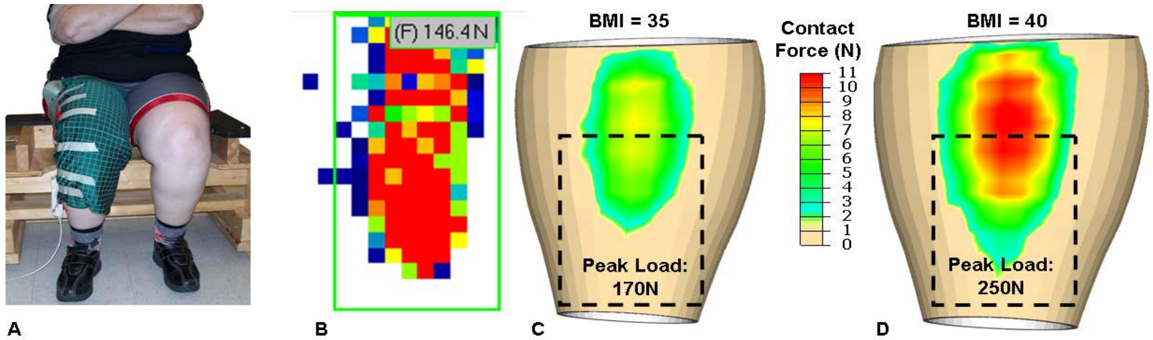

Figure 31: Physical corroboration of thigh-thigh impingement computation was performed using an interface pressure mat applied between the thighs of an obese (non-THA) subject performing a sit-to-stand maneuver (A). Spatial integration of the Tekscan mat contact stress measured during thigh impingement resulted in 146.4N of peak lateral load (B). Physical representation of the placement of the pressure mat (A) is demonstrated for the 35 BMI FE model (C) and 40 BMI model (D). The peak thigh circumference of the patient fell between these two simulated cases. Peak computed load within the approximate area covered by the sensing mat (dashed boxes in C and D) was 170N for the 35 BMI case.

Results of Obesity FE Study

The thigh-thigh impingement was found to deliver a substantial impetus for dislocation in the obese patient models, independent of implant hardware impingement and/or bony or intra-articular soft tissue impingement. Peak thigh-thigh impingement loads were developed during the terminal phase of the maneuver, when the hip adduction was greatest. Those force magnitudes exceeded 1000N for the highest BMI cases (Figure 32), leading toward joint instability (Figure 33). However, femoral head displacement (instability) did not become appreciable until BMI reached approximately 40 (Figure 34A-B). Beyond that threshold, for higher values of BMI, there was a monotonic increase in femoral head subluxation, often resulting in frank dislocation.

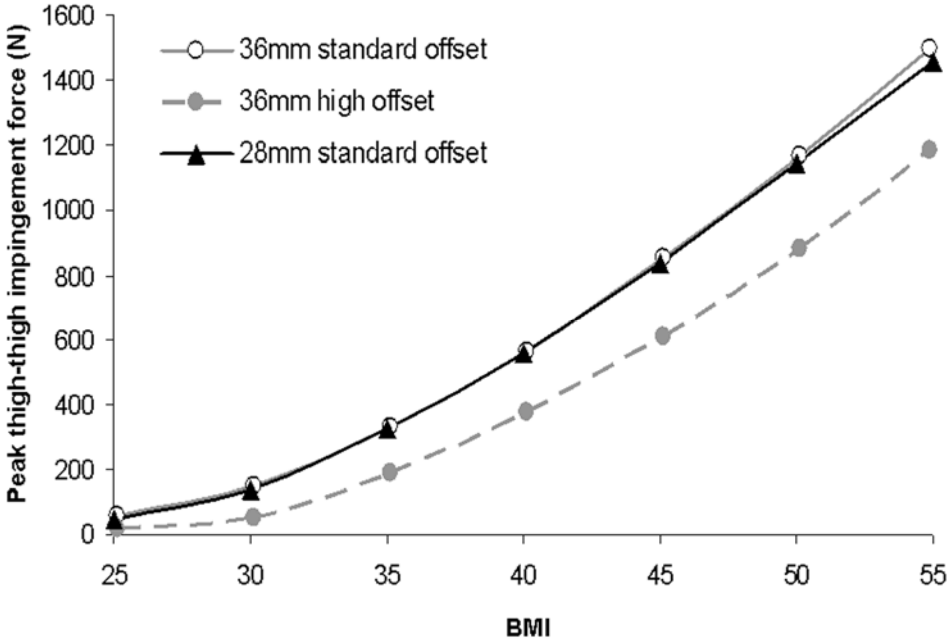

Figure 32: Peak thigh-thigh impingement forces were developed during hip adduction in the terminal phase of the sit-to-stand maneuver. Thigh-thigh impingement forces exceeded 1000N for both the 36mm and 28mm standard neck models at an approximate BMI of 50, but were significantly reduced for all BMI levels with the use of an offset stem.

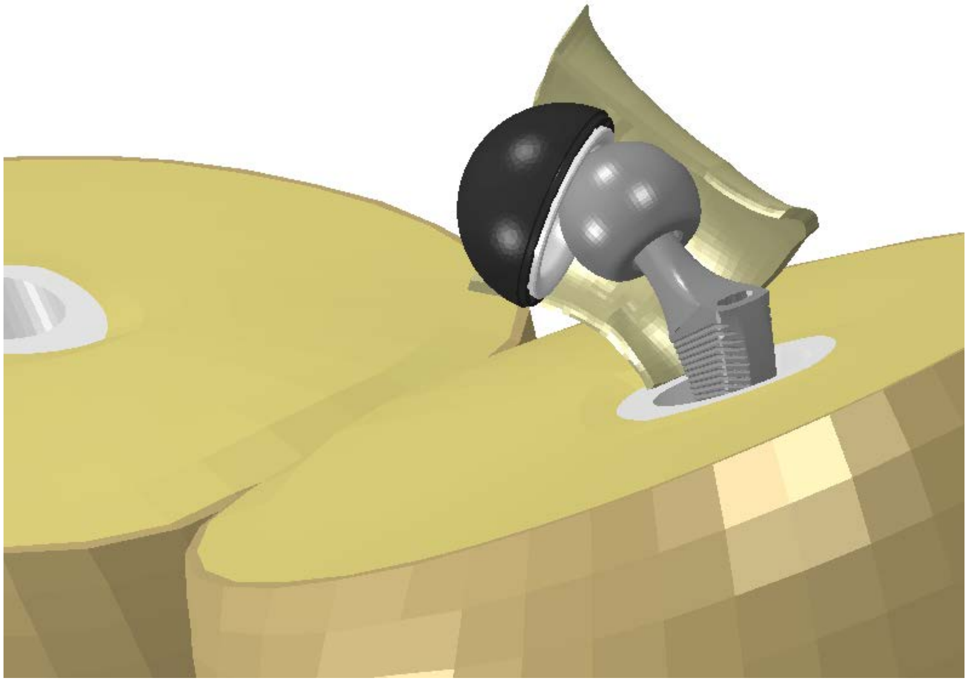

Figure 33: Instability (quantified in terms of femoral head subluxation) in the simulated obese THA models occurred during hip adduction at the terminal stage of the sit-to-stand kinematic challenge. Impingement between the thighs, the intensity of which increased during hip adduction, developed a laterally-directed force whose magnitude was sufficient to alter joint kinematics, leading to frank dislocation in the highest-BMI models.

Dislocation propensity was shown to be highly sensitive to cup abduction, with cups at high abduction demonstrating substantial decreases in stability. Increased head diameter demonstrated slight improvements in joint stability, especially for less abducted cup orientations (Figure 34B). Dislocation propensity decreased substantially with the use of the 8mm high offset neck, which effectively increased the problematic BMI threshold from 40 for the standard offset to 50 for the high-offset cases. While simulations of the highest BMI and the largest cup abduction resulted in joint subluxation (4mm), frank dislocation (i.e., joint subluxation numerically greater than the head radius) did not occur for any FE simulation incorporating the high-offset stem (Figure 34C).

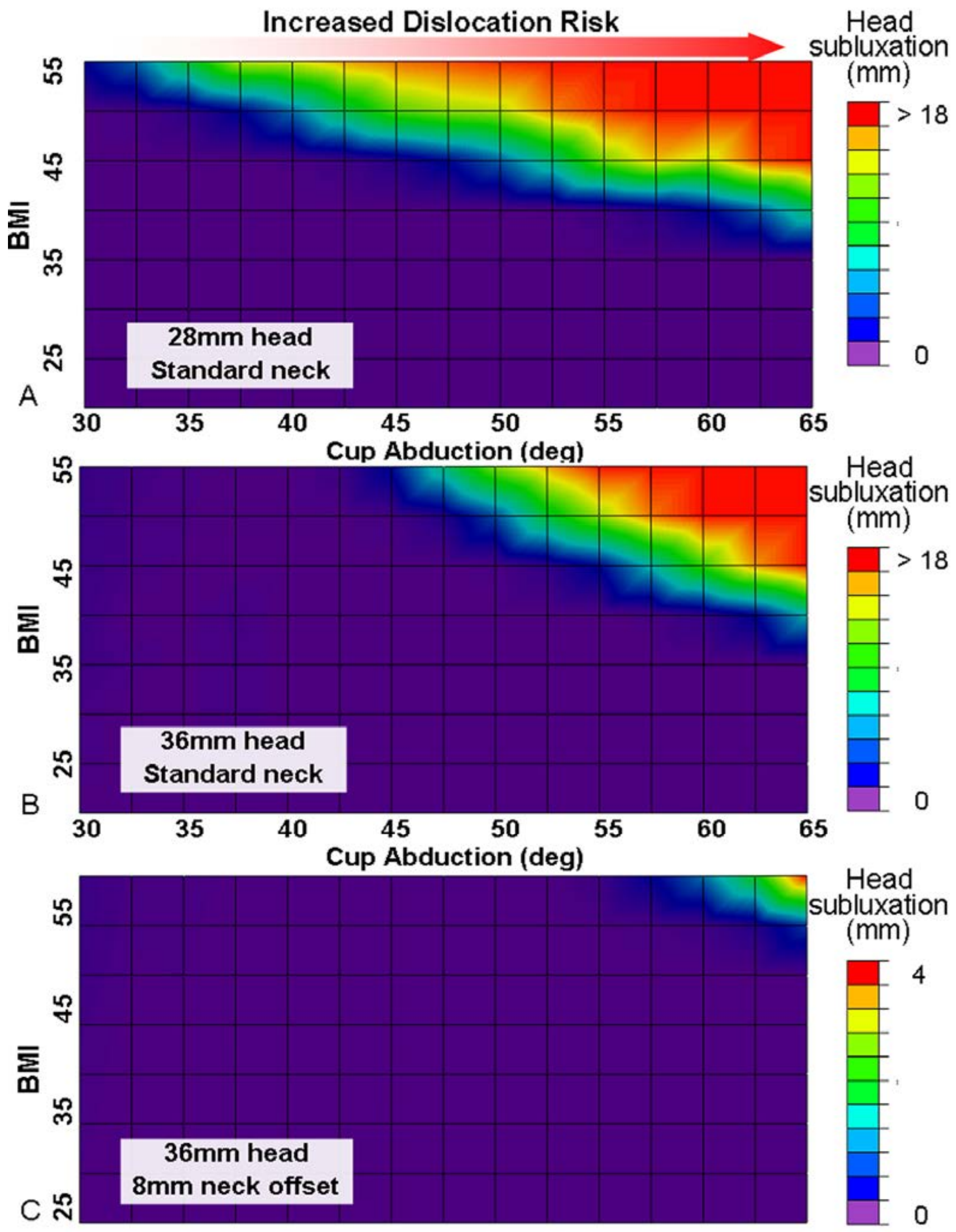

Figure 34: Dislocation risk was found to be highly sensitive to both BMI and cup abduction for the 28mm head (A), although instability (quantified in terms of femoral head subluxation) did not occur for simulated BMIs of 35 or less. Increased cup abduction also led to elevated dislocation risk. A similar BMI-versus-cup-inclination relationship was shown for the standard offset 36mm cup (B), where instability was most pronounced at higher cup abduction angles. Dislocation risk was substantially reduced when a high offset (8mm) neck was used with the 36mm cup (C).

Discussion of Obesity FE Study

This model corroborates clinical observation that thigh-thigh impingement in the obese THA patient can predispose to hip instability. The model demonstrated a dose-effect relationship between BMI level and THA instability, with an apparent BMI threshold of 40 above which obesity effects became appreciable. An effect onset threshold in this range has been noted clinically when dislocation rates have been stratified for higher grades of obesity [112, 115]. Additionally, the present work suggests that thigh circumference, rather than BMI *per se*, is what directly acts to decrease joint stability. (This is as opposed to most other obesity-related health problems, which strongly correlate to central obesity.) A corroboration clinically is that when normalized to BMI, THA dislocation rates in obese females have been shown to be higher than in obese males [114]. Because of the gender differences in adipose tissue deposition [149] – females predominately depositing fat in the hip and thigh area compared to a more abdominal distribution for males – the paradigm of elevated dislocation risk being due to increased thigh adiposity is given additional credence.

Cups positioned in more vertical orientations are typically thought to improve joint stability, as the overall effect of increasing acetabular cup inclination and anteversion is to provide a greater range of motion prior to neck-on-liner impingement for flexion-dominated kinetic challenges, similar to the rationale for the use of large femoral heads or high head/neck ratios. However, this study suggests that these classic range-of-motion-increasing considerations might not be as helpful for the morbidly obese patient. Rather than impingement “lever-out”, the instability encountered in the present series occurred due to “slide-out” or “shear-out”, the mechanics of which are completely independent of any hardware or bony impingement. While this slide-out mode of dislocation has been demonstrated both experimentally [161] and computationally [56, 65], design strategies to afford protection against it are not so well evolved as for impingement-preceded dislocation. Only modest benefit was seen when using a 36mm head compared to a 28mm head, regardless of the theoretical improvements in range of motion prior to neck-on-cup impingement. As regards slide-out, these two implants differ in that the 28mm cup provides a full hemisphere (180°) of femoral head coverage, compared to only 163° for the 36mm head construct. Additionally, the rounded chamfer of the 36mm cup would tend to allow for easier slide-out head egress than does the sharp edged/flat chamfer design of the 28mm cup, due to decreased shearing of the head as it slides over a rounded lip (Figure 35). Such considerations suggest that cup shape/geometry (especially the extent of head coverage), rather than simply head diameter, more strongly influence stability in the morbidly obese patient.

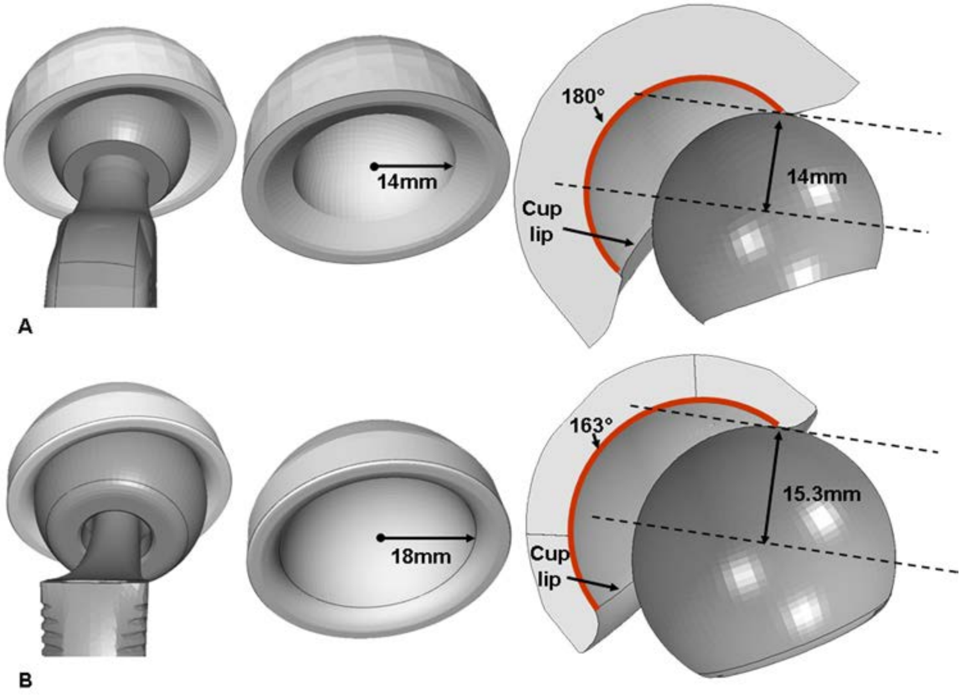

Figure 35: Jump distance with larger heads and rounded cup edges. The 28mm THA hardware (A) consisted of a standard offset neck with a 5° anteverted stem (left), and a 28mm cup diameter cup (middle) with a flat lip and chamfer (right) and 180° of head articular coverage, resulting in 14mm of "jump distance" required for dislocation. The 36mm THA hardware (B) also consisted of a standard offset neck anteverted to 5° (left). The cup diameter was 36mm (middle), but the rounded lip/chamfer of the cup (right) resulted in only 163° of articular coverage, decreasing the "jump distance" from a full head diameter (18mm) to only 15.3mm.

To more fully investigate the role of cup lip geometry on instability tendency, several permutations of cup design were considered (Figure 36). There was a nearly linear inverse relationship between cup lip fillet radius and the load required to subluxate the head.

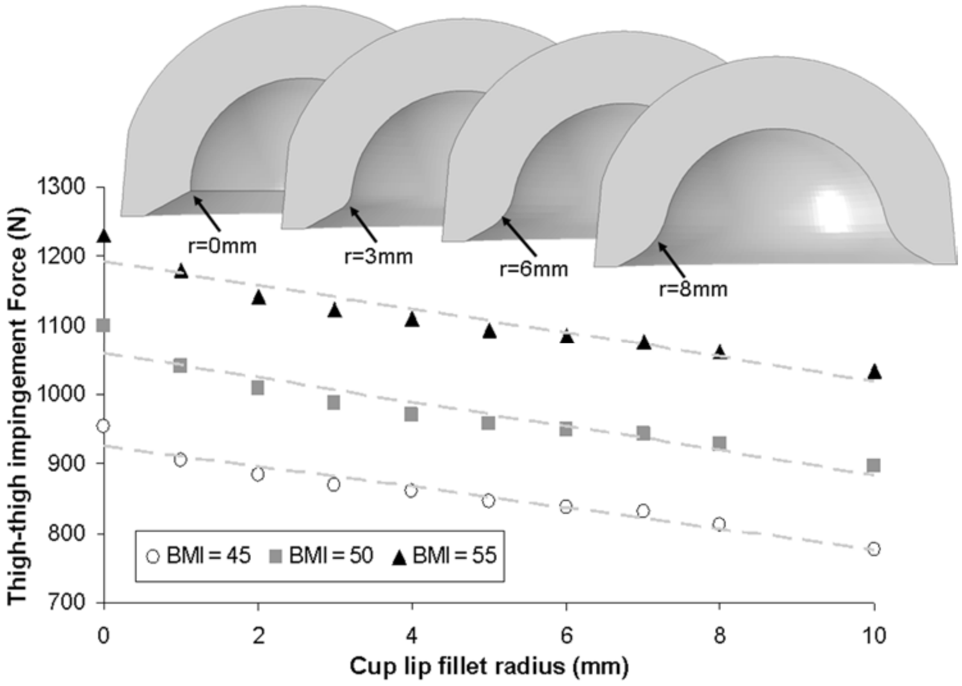

Figure 36: Thigh-thigh impingement force. Peak loads required to initiate subluxation of the femoral head were strongly sensitive to cup lip design, with cups with larger lip fillet radii (and therefore less articular head coverage) requiring less laterally-directed thigh-thigh contact force to become unstable. Cups were in 50° of abduction.

Increased neck offset, possibly due to increasing peri-articular soft tissue tension, has also been associated with improved stability following THA [57]. The use of an 8mm neck offset in the present model yielded substantial improvement in joint stability. However, as opposed to simply the theoretical advantage of increased soft tissue tension, another contributing mechanism may have been the corresponding increase of the distance between the two femurs, effectively reducing the intensity of the thigh-thigh impingement. Therefore, usage of offset necks might be especially helpful to mitigate THA dislocation propensity in the morbidly obese. Finally, the present data suggest that, in light of functional hip angulation utilized by the morbidly obese patient, cups with higher inclination angles will have elevated dislocation risk. While avoiding vertical cup inclination is challenging intraoperatively in the obese due to the difficult surgical exposure and retraction [162], these data suggest that every effort should be made toward that end.

CHAPTER 2: IMPINGEMENT *PER SE* IN TOTAL HIPS

> In physical science the first essential step in the direction of learning any subject is to find principles of numerical reckoning and practicable methods for measuring some quality connected with it. I often say that when you can measure what you are speaking about, and express it in numbers, you know something about it; but when you cannot measure it, when you cannot express it in numbers, your knowledge is of a meagre and unsatisfactory kind; it may be the beginning of knowledge, but you have scarcely in your thoughts advanced to the state of *science*, whatever the matter may be.
>
> Sir William Thomson 1st Baron Kelvin, Popular Lectures and Addresses Vol. 1

The majority of THA dislocations ensue from mechanical impingement [121], where the femoral component comes into contact with bone, soft tissue, or the acetabular component of the implant, creating a fulcrum causing levering-out of the femoral head from the cup, in turn leading to instability and often to frank dislocation. Impingement of the femoral neck on the acetabular cup liner is the most frequent such engagement mechanism. The risk factors for impingement generally mirror those for dislocation. Specifically, implant geometry (particularly head:neck ratio) and component orientation have been addressed extensively. Of these, the effect of component orientation has had the greatest recognition. For surgical implantation for THA, various terms are used to describe the orientation of the acetabular cup, including inclination, anteversion, cover, abduction, tilt, opening and flexion. Inclination and anteversion are the most commonly used, but these terms historically have had imprecise definitions [163]. Component orientation can be assessed anatomically, radiographically or by direct observation during surgery (Figure 37). The angles determined from these three different methods differ due to their different spatial definitions of rotational axes. Therefore, there are three separate definitions of inclination and anteversion, which is often a source of confusion when comparing investigations of cup orientation across multiple studies.

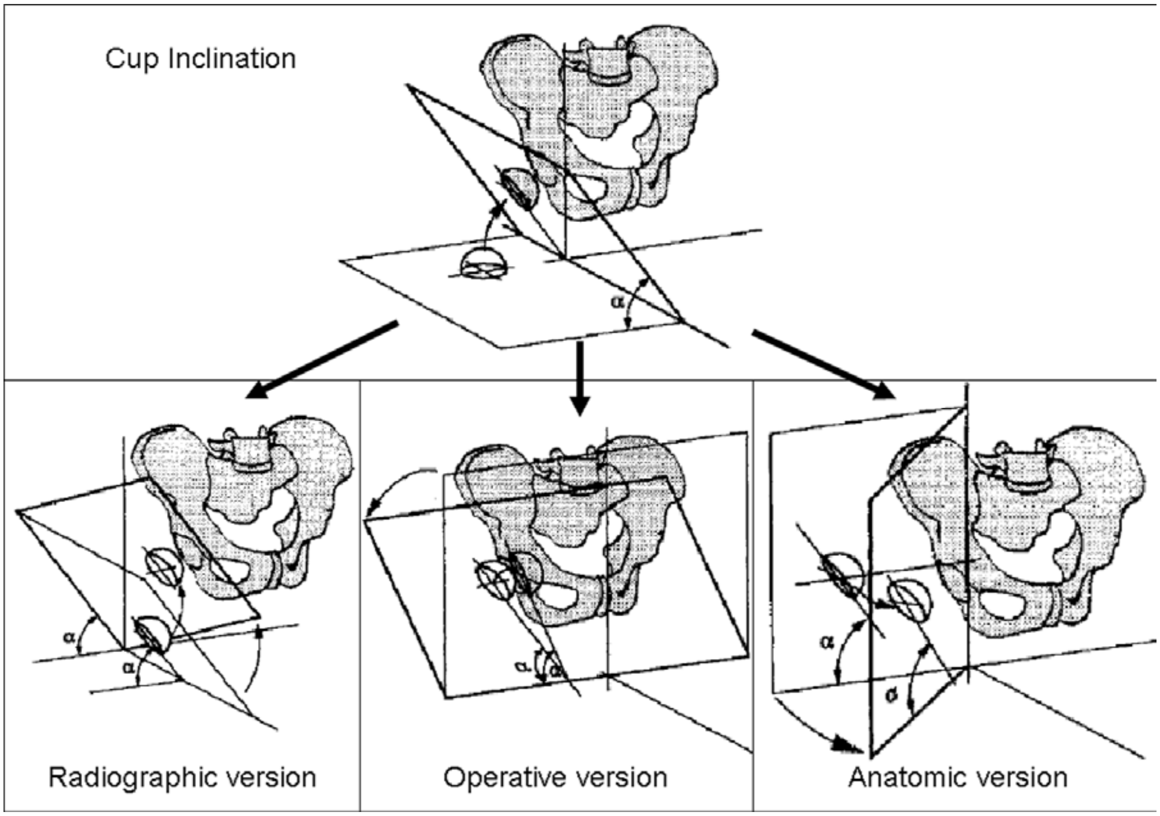

Figure 37: Commonly used acetabular cup orientation measurements. Each orientation method defines cup inclination identically, while version is based upon different reference planes and rotational axes. Modified from [164].

Contact Mechanics of Impingement [165]

Introduction

Although concerns regarding impingement generally focus on its role in leading to instability, impingement *per se* also merits attention due to propensity for damage to the implant components themselves. Neck-on-liner impingement is a common complication of THA, with evidence of impingement damage being reported in a majority of explanted THAs [62, 63, 166]. Concerns associated with impingement-related bearing damage in conventional metal-on-polyethylene (MoP) constructs are usually associated with increased osteolytic potential with accelerated wear [167]. However, the recent (and rapid) adoption of advanced low-wear bearings brings new considerations to the fore regarding impingement-related bearing damage. Impingement in hard-on-hard bearings (including metal-on-metal, MoM, and ceramic-on-ceramic, CoC), given the relatively unyielding nature of the “hard” surfaces, is presumptively more detrimental than impingement with conventional MoP implants.

For conventional MoP implants, the stress concentrations following impingement have been previously investigated using finite element analysis [58, 168]. However, for hard bearings, computing the contact stresses arising from impingement events involves additional computational difficulties. Owing to their generally unyielding material behavior compared to conventional polyethylene, contact with hard bearings results in highly localized contact zones at the site of neck impingement on the liner and at the liner edge during head subluxation and subsequent egress edge-loading, resulting in severe spatial gradients of stress concentration. Element mesh zoning sufficiently refined to capture the spatial stress gradients associated with contact at the impingement and egress sites are logistically prohibitive, owing to excessive computational resource requirements. To overcome this limitation, a multi-stage FE formulation was utilized. The first stage involved whole-construct level analysis of global impingement dynamics. Subsequent stages involved progressively refined “sub-models” of stress concentration sites, to capture the stress concentrations associated with impingement in hard bearings. This formulation allowed for investigation into the extent to which the severity of localized stress concentrations challenges the (bulk) material limits of hard-on-hard bearings. Additionally, such refinement of the contact stress zones enabled the calculation of propensity for debris generation (“scraping wear”) during impingement events in HoH bearings.

Impingement Contact Mechanics FE Methods

Physically-realistic analysis of impingement and subsequent femoral head dislocation requires modeling at the whole-construct level. These considerations include accounting for soft tissue (capsular) deformation, joint contact loads, and modeling the large sliding distances encountered during joint angulation for the normally contacting surfaces of the bearing, as well as the abnormally contacting surfaces during an impingement/subluxation sequence (Figure 38).

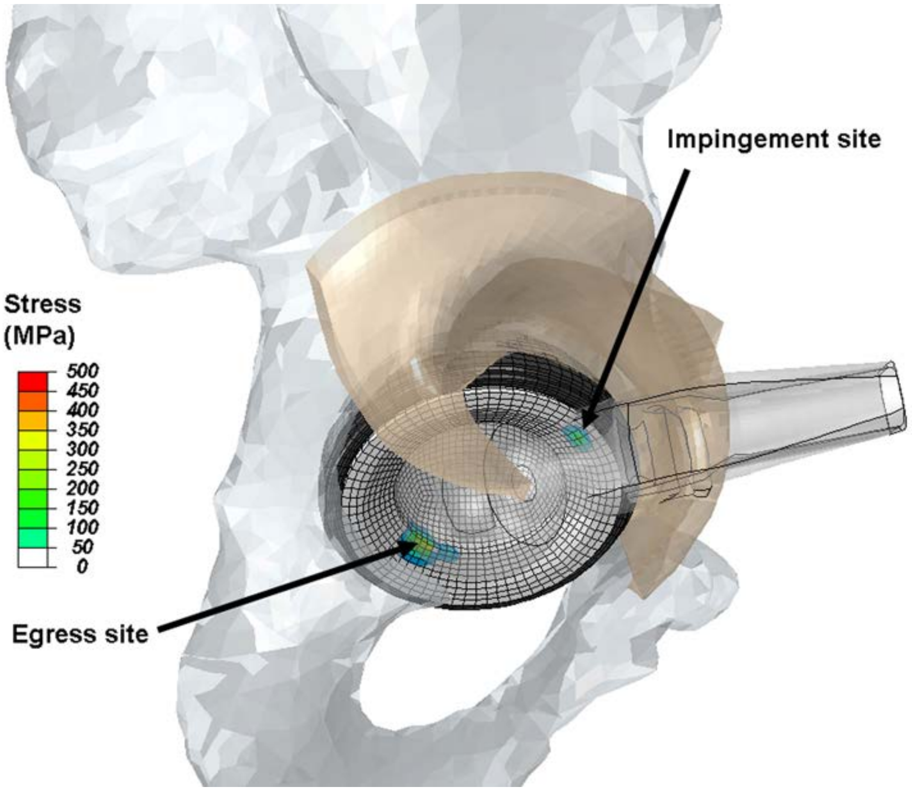

Figure 38: Contour plot of liner von Mises stresses developed during impingement/subluxation of a right hip at high flexion. Stress concentrations occur at two distinct regions of the cup: the impingement site (anteriorly) and the egress site (posteriorly). For visualization clarity, the bony femur is removed, the femoral component is rendered translucent, and only the anterior half of the capsule is shown.

However, accurately quantifying the localized contact mechanics during implant impingement necessitates an alternative FE modeling approach: very high mesh refinement at specific locations that can only be known *a-posteriori* from a global analysis. Therefore, to simultaneously address both these concerns, a multi-tiered approach was used. Given the model complexities associated with large soft tissue deformation during hip flexion, and multiple contact engagement sites, an explicit FE scheme was used for the global analysis. Output metrics of the global solutions included impingement-free range-of-motion (ROM), ROM to frank dislocation, and surface von Mises stress. For those analyses which resulted in frank dislocation, the computational simulation was truncated after 4 mm of femoral head subluxation. Mesh convergence studies were conducted to identify the level of mesh refinement appropriate for the global analysis. However, mesh refinement appropriate for this purpose is far too coarse for appropriate resolution at the sites of stress-concentration arising from component impingement. Convergence studies, as well as comparisons with analytical Hertzian [169] contact solutions, aided in the identification of appropriate mesh refinement for those localized analyses (Figures 39-40).

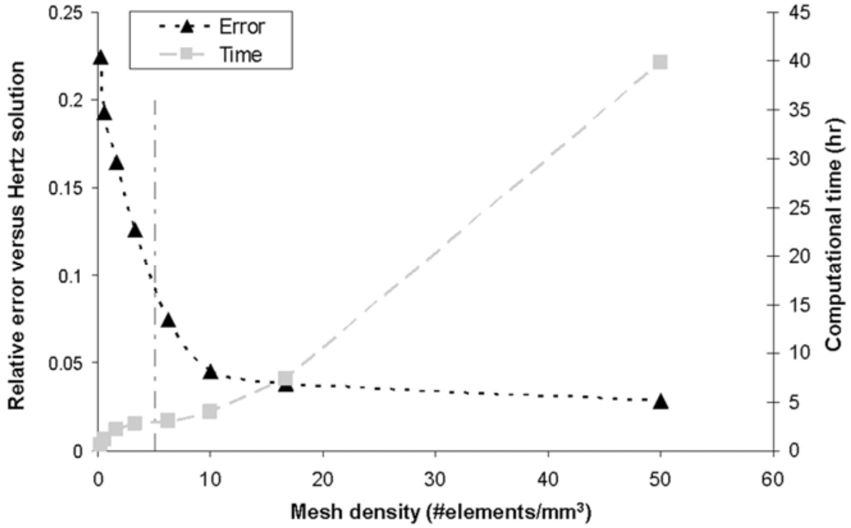

Figure 39: Contact analysis convergence study for neck impingement. Mean relative errors for FE-predicted contact pressure, compared to a Hertzian analytical solution for a surrogate contact analysis for eight different mesh densities. Model run times for each simulation are also shown (right axis). A target global mesh density of 5 elements/mm^3 yielded an appropriate trade-off between accuracy and computational economy.

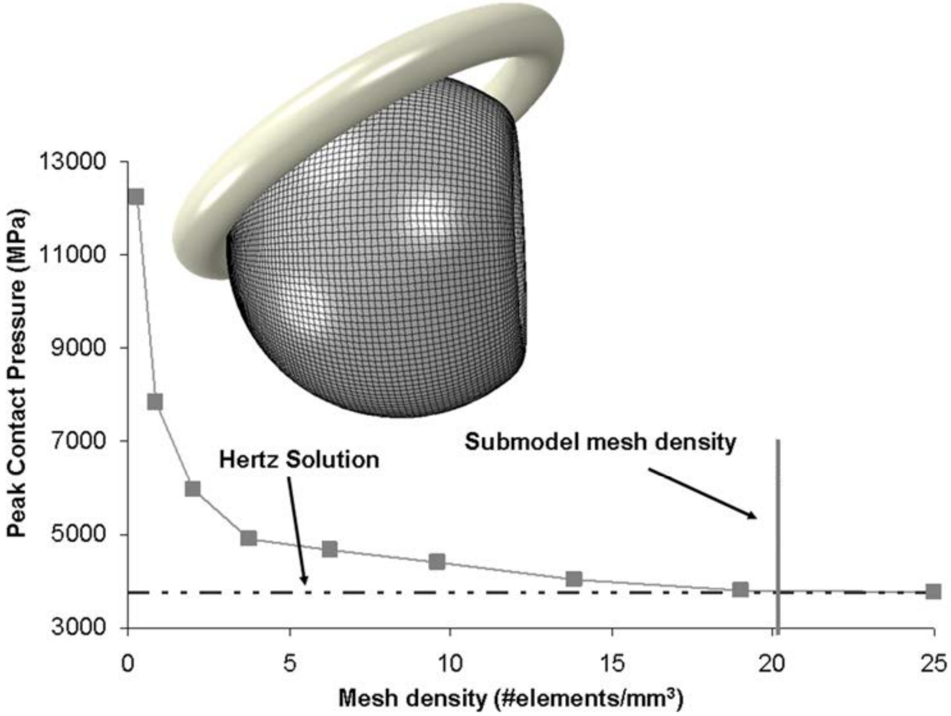

Figure 40: Peak contact pressure vs. mesh density for submodeling. The gold standard was an analytical Hertzian solution for contact of a partially nested sphere-in-torus, simulating the geometry of egress-site edge-loading during femoral head subluxation. Convergence was attained at an approximate mesh density of 20 elements/mm^3.

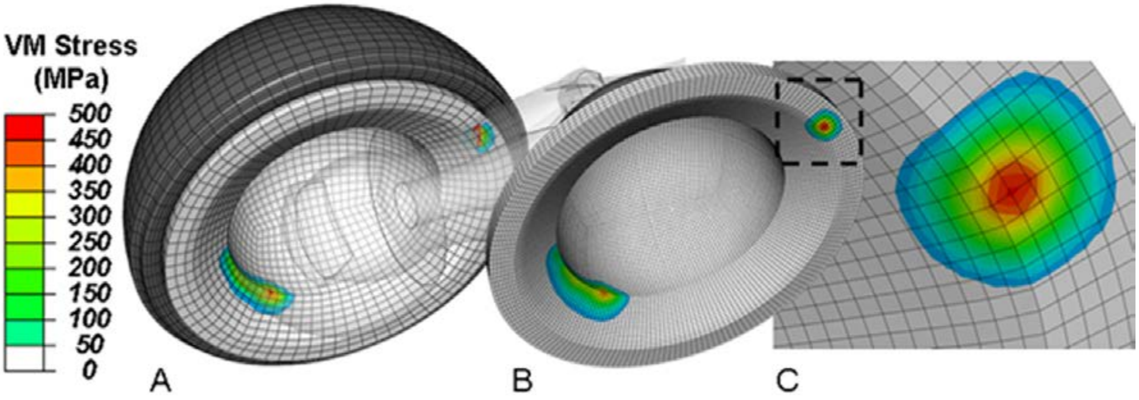

Figure 41: (A) Global model for a 40°-tilt, 20° anteversion cup during neck-on-liner impingement. For visualization clarity, the hip capsule has been removed and the femoral component rendered translucent. (B) Associated second-stage submodel for the liner, demonstrating substantial improvement in resolution of the contact stress contours as compared to the global model. (C) Close-up view of the impingement-site for the submodel shown in (B).

Attempting to run the global analysis with such refined element zonings would have resulted in runtimes measured in months for each simulation, wholly intractable for considering several parametric permutations of cup positioning. For this reason, a multi-staged modeling approach was performed using a submodeling approach (Figure 41). The use of this formulation allowed for high mesh-density stress computations to be driven by boundary-conditions passed from solutions of the large-scale global model.

The global model (Figure 38) consisted of THA hardware (28mm head, 28-46 mm acetabular cup, and metal shell), the hip capsule and bony anatomy. Each global model of THA impingement/subluxation was accompanied by two separate submodels, each with progressively increased mesh density. Preprocessing of the THA hardware was performed using Truegrid. The MoM implants were modeled as linearly-elastic CoCr ($E = 210$ GPa, $\nu = 0.3$, $\rho = 9.2$ gm/cc), with 0.029 mm of radial clearance and with a friction coefficient of 0.1 [170]. The ceramic portions of the CoC constructs were also assigned linear elastic material coefficients (alumina, $E = 380$ GPa, $\nu = 0.23$, $\rho = 3.98$ gm/cc), the radial clearance was 0.034 mm, and the friction coefficient was 0.04 [170]. All analyses were run with the femoral component in 5 degrees of femoral anteversion. Two separate dislocation-prone motions were investigated: (1) a sit-to-stand from a normal chair height and (2) a stooping motion [56].

In addition to quantifying the localized stress concentration arising due to component impingement, the propensity for localized liberation of particulate debris due to component "scraping" was also determined. This scraping wear was viewed as being dependent upon the interaction of the local mechanical stress, local sliding distance, and mutual tribologic abrasiveness of the two contacting surfaces. A methodology for quantifying the local wear rate $\dot{w}$ from such interaction is provided by the Archard-Lancaster formulation: $\dot{w} = \sigma * \dot{s} * k$ where σ is the local mechanical stress, $\dot{s}$ is the local relative sliding speed of the two contact surfaces, and k is a wear factor that reflects contacting surface abrasiveness [171]. Scraping wear then was assessed by temporospatially integrating this instantaneous local wear over all acetabular liner elements that experienced either neck contact (impingement sites) or edge-contact from the femoral head during subluxation (egress site).

One hundred forty-eight distinct global FE simulations were run using an explicit FE scheme, each one followed by two separate submodel analyses executed using Abaqus/standard (implicit). Fifty-four separate cup positions were investigated, with cup tilt (inclination) and anteversion defined in the anatomic reference frame (Figure 37). Each global FE simulation required approximately 120 processor-hours of computation time. Subsequent submodels required less than 2 processor-hours of computation time.

Results of Contact Mechanics FE Study

Impingement-free ROM increased approximately linearly with increased cup anteversion and inclination (Figure 42). ROM prior to component impingement was consistently greater for the sit-to-stand challenges than for stooping (111° vs. 105°). The kinematics for the stooping challenge, while also flexion-dominated, involved significantly more internal rotation and abduction than did the sit-to-stand motions, thus tending to reduce the flexion ROM.

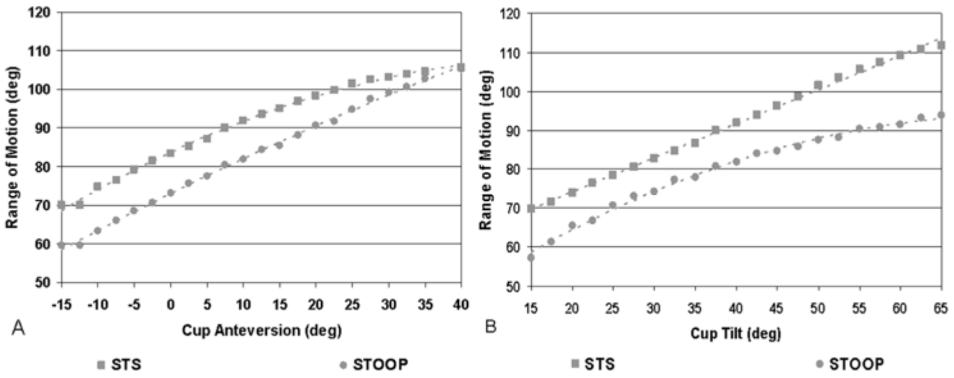

Figure 42: Range-of-motion at incipient impingement for sit-to-stand (STS) and stooping dislocation challenges for (A) 40° of cup tilt as a function of cup anteversion and (B) for 10° of cup anteversion as a function of cup tilt.

Values for peak surface effective vM stresses at the egress and impingement sites were seen to increase also approximately linearly with tilt and anteversion, over most of the range of cup orientations modeled (Figure 43). However, at some extreme conditions of cup orientation, impingement onset either occurred relatively late in the motion challenge, or even failed to occur. In such circumstances, appreciable egress-site stresses did not develop (Figure 44). Egress-site stress, because of the highly localized nature of rim line-loading, involved stress concentrations that were generally higher than those at the impingement site (Figures 43 and 45). Peak stresses developed for the stoop dislocation challenge were consistently higher than those for the sit-to-stand challenge, for any given cup orientation. For the ceramic bearing, peak stresses at both the impingement site and the egress site were consistently greater than those for the MoM bearing, owing to the higher modulus for the ceramic versus metal liner (Figures 44-45).

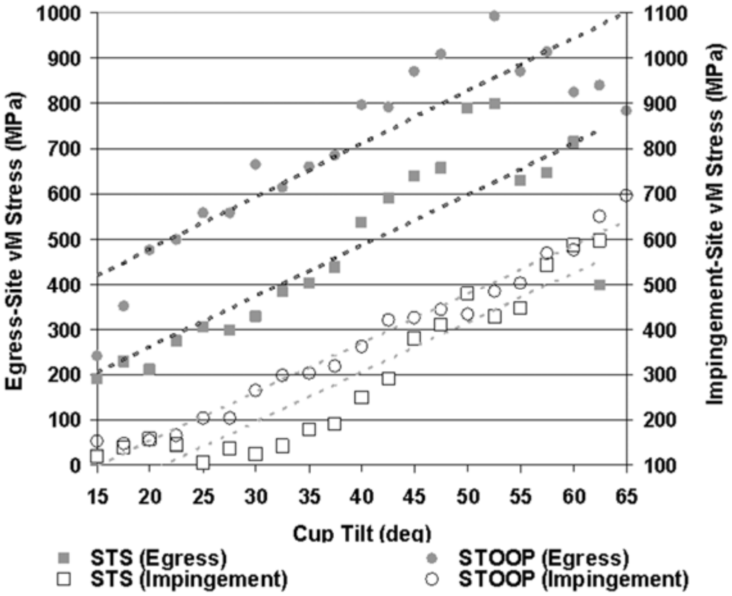

Figure 43: von Mises stress for egress-site and impingement-site regions for both sit-to-stand and stoop challenges, as a function of tilt for a 10° anteverted cup. The relationships were approximately linear (dashed lines are linear regressions).

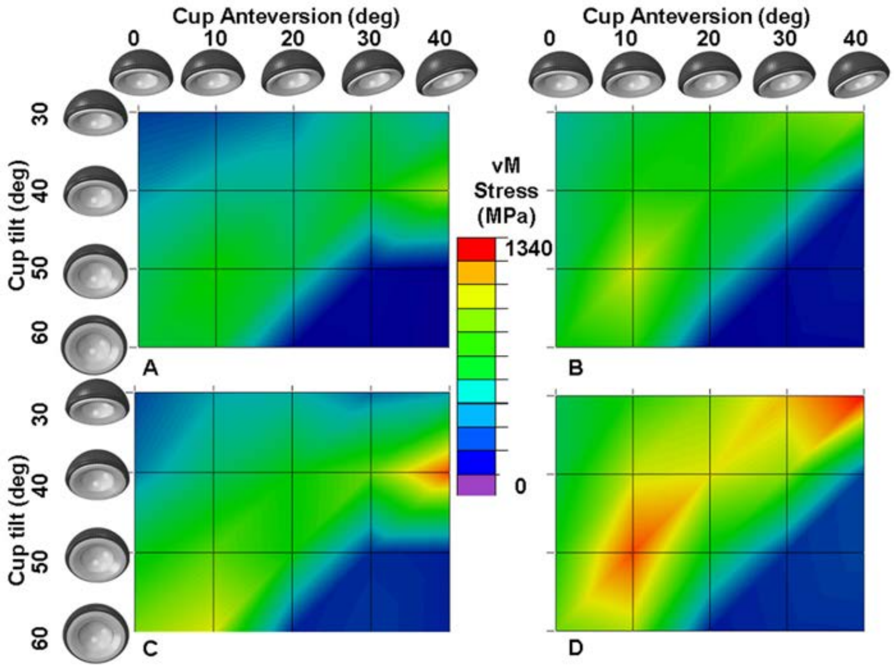

Figure 44: Egress-site peak vM stresses. (A) MoM sit-to-stand; (B) MoM stoop; (C) CoC sit-to-stand and (D) CoC stoop.

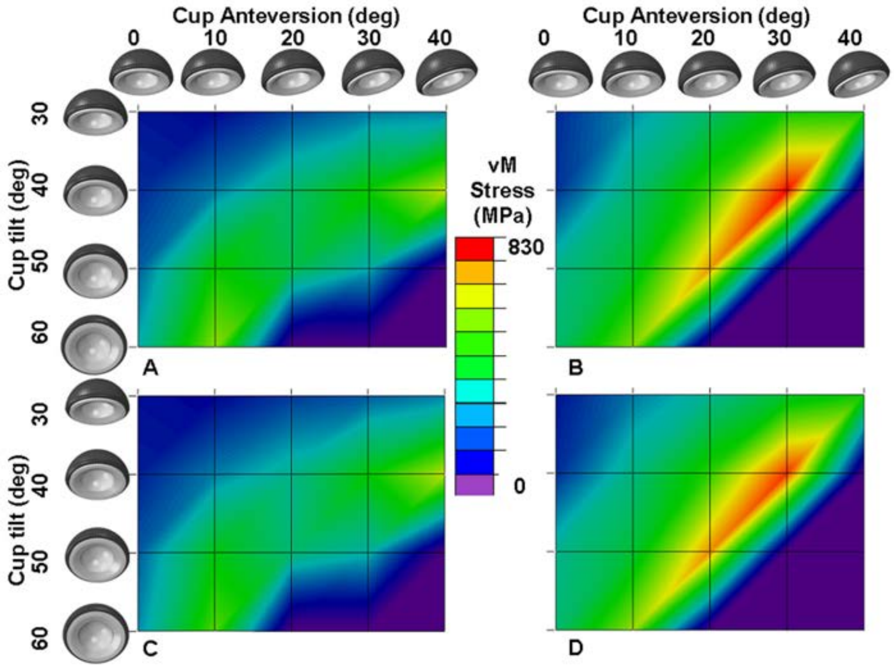

Figure 45: Impingement-site peak vM stresses. (A) MoM sit-to-stand; (B) MoM stoop; (C) CoC sit-to-stand and (D) CoC stoop.

Table 1: Summary of cup-orientation-dependent damage severity assessment.
* denotes impingement did not occur; # denotes frank dislocation did not occur

Sit-to-Stand MoM				**Stoop MoM**				**Sit-to-Stand CoC**		**Stoop CoC**	
Cup Orientation		Damage Severity		Cup Orientation		Damage Severity		Cup Orientation		Cup Orientation	
Tilt	**Ante-version**	**vM Mpa**	**Vol. Wear 10^{-6} mm^3**	**Tilt**	**Ante-version**	**vM Mpa**	**Vol. Wear 10^{-6} mm^3**	**Tilt**	**Ante-version**	**Tilt**	**Ante-version**
15	10	188	6.53	15	10	240	4.72	30	0	30	0
17.5	10	226	5.53	17.5	10	351	11.57	30	10	30	10
20	10	210	4.76	20	10	476	10.88	30	20	30	20
22.5	10	274	4.32	22.5	10	500	10.40	30	30	30	30
25	10	303	4.46	25	10	558	9.08	# 30	40	# 30	40
27.5	10	297	4.01	27.5	10	558	12.44	40	0	40	0
30	0	290	7.07	30	0	500	46.69	40	10	40	10
30	10	326	4.88	30	10	666	15.84	40	20	# 40	20
30	20	400	5.38	30	20	759	31.82	40	30	# 40	30
30	30	617	8.41	30	30	904	39.10	# 40	40	*# 40	40
# 30	40	485	5.96	# 30	40	973	64.86	50	0	50	0
32.5	10	384	7.05	32.5	10	614	26.36	50	10	# 50	10
35	10	402	18.02	35	10	661	27.18	# 50	20	# 50	20
37.5	10	438	12.43	37.5	10	686	39.09	# 50	30	*# 50	30
40	-15	244	8.27	40	-15	334	6.71	*# 50	40	*# 50	40
40	-12.5	234	8.20	40	-12.5	328	6.68	60	0	60	0
40	-10	244	4.68	40	-10	394	10.30	# 60	10	# 60	10
40	-7.5	289	7.19	40	-7.5	336	7.17	*# 60	20	*# 60	20
40	-5	290	8.98	40	-5	515	12.43	*# 60	30	*# 60	30
40	-2.5	335	7.50	40	-2.5	534	21.42	*# 60	40	*# 60	40
40	0	427	10.19	40	0	592	19.56				
40	2.5	391	13.38	40	2.5	625	28.87				
40	5	483	15.71	40	5	687	33.70				
40	7.5	572	19.64	40	7.5	666	27.10				
40	10	537	20.88	40	10	795	49.02				
40	12.5	506	18.74	40	12.5	918	53.91				
40	15	561	21.01	# 40	15	837	64.10				
40	17.5	510	18.88	# 40	17.5	873	72.43				
40	20	558	20.12	# 40	20	783	64.63				
40	22.5	608	22.05	# 40	22.5	786	38.09				
40	25	661	22.08	# 40	25	748	33.71				
40	27.5	718	22.14	# 40	27.5	798	25.04				
40	30	748	22.70	# 40	30	825	10.47				
# 40	32.5	689	31.25	# 40	32.5	724	2.91				
# 40	35	715	30.09	# 40	35	704	0.55				
# 40	40	986	39.42	*# 40	40	214	N/A				
42.5	10	590	23.28	42.5	10	789	62.62				
45	10	640	29.85	45	10	870	66.84				
47.5	10	656	32.41	# 47.5	10	907	68.65				
50	0	606	22.50	50	0	609	33.25				
# 50	10	789	39.62	# 50	10	1040	111.97				
# 50	20	647	9.02	# 50	20	645	12.16				
# 50	30	204	0.30	*# 50	30	202	N/A				
*# 50	40	166	N/A	*# 50	40	227	N/A				
52.5	10	797	50.42	# 52.5	10	992	86.94				
# 55	10	629	40.39	# 55	10	870	75.81				
# 57.5	10	648	30.15	# 57.5	10	913	53.14				
60	0	676	44.94	60	0	741	43.88				
60	10	714	6.57	# 60	10	824	41.20				
*# 60	20	180	N/A	*# 60	20	172	N/A				
*# 60	30	187	N/A	*# 60	30	195	N/A				
*# 60	40	164	N/A	*# 60	40	199	N/A				
# 62.5	10	397	2.30	# 62.5	10	838	33.73				
*# 65	10	157	0.07	# 65	10	782	22.54				

Computed values for volumetric "wear" from the scraping events for the MoM impingement simulations are reported in Table 1, along with corresponding values for metal-surface vM stresses. It can be appreciated that these two distinct aspects of implant damage propensity were highly coupled (concordance coefficient = 0.833) as regards their respective cup orientation dependencies. Computed scraping wear at the egress site generally exceeded that at the impingement site (Figure 46). Across the range of tilt-abduction combinations studied, the egress sites accounted for 57 % of the overall amount of computed volumetric scraping wear.

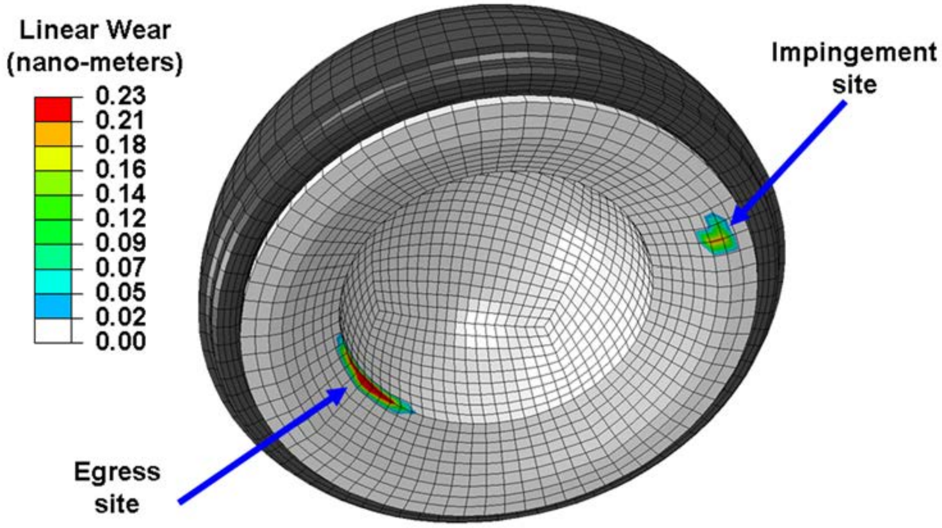

Figure 46: Contour plot of cumulative linear "scraping" wear at both the egress site and impingement site for a 40°-tilt, 20°-anteversion cup developed during the stoop challenge.

Discussion of Impingement Contact Mechanics

The extremely high stress levels here computed at hard-on-hard THA impingement/egress sites represent among the most severe mechanical environments yet quantified in the orthopaedic literature. For many cup orientations in this series, peak computed von Mises stress approached or in some cases even reached the GPa range.

Situations of high anteversion were particularly predisposed. In the case of metal-on-metal, the material failure modality of primary concern is that the yield strength of the CoCrMo alloy would be exceeded, leading to localized permanent (plastic) deformation. The yield strengths for cast versus wrought Co28Cr6Mo alloy are 450 MPa and 827 MPa, respectively (ISO 5832).

For ceramic bearings, the concern of course is not ductile (yield) failure, but rather catastrophic fracture. The mechanical considerations bearing upon crack nucleation and crack propagation in brittle solids such as ceramics are much more complex than those for yield failure in ductile materials such as metals. Taken as a whole, however, there seems good cause for concern that impingement events - if and when they should occur - pose a significant threat to the refined engineering integrity of hard-on-hard contemporary THA bearings.

Creation of particulate debris at impingement and egress sites is a second concern. Such particles would have only a very short path to migrate in order to enter the bearing surface and become third bodies, thus compromising otherwise excellent wear performance. Additionally, such debris would constitute direct particulate burden in the peri-articular tissue bed, and/or in distant organs. In the case of metal particles, the surface-to-volume ratio is enormously higher than for the bulk implant members, favoring dramatic acceleration of the metal ion release rate, possibly leading to soft tissue adverse reaction to metal debris or other immunologic reactions. At present, information regarding debris creation due to impingement is largely lacking. The present quantification of such debris in terms of “scraping” wear via the Archard formula is obviously a substantial simplification of what are undoubtedly very complex local tribological interactions at these sites. Moreover, the specific k factor utilized in this analysis was inferred from articulation of fluid-film-lubricated polished CoCr surfaces [172], and therefore probably substantially underestimates the abrasiveness of non-lubricated, non-polished contacting metal surfaces. For these reasons, the values of computed volumetric scraping wear need to be interpreted as relative rather than absolute. Nevertheless, the present parametric results convincingly demonstrate that (1) some impingement events are far more deleterious than others in terms of propensity to generate scraping wear debris, (2) that the egress site is a substantially greater cause of concern in that regard than is the impingement site, and (3) that cup orientations that are especially problematic in terms of bulk-level implant material failure generally correspond to the cup orientations that are especially problematic in terms of scraping wear.

Bone-on-Bone versus Hardware Impingement

Introduction to Bone vs. Component Impingement

In an implanted hip replacement, several forms of impingement are possible. Impingement can occur between the femur (femoral implant or native bone) and either the cup liner, the shell backing, the bony pelvis, or peri-articular soft tissues. In conventional THA, impingement typically occurs between components of the THA implant (as previously described). Therefore, in the vast majority of experimental studies of THA impingement and range-of-motion have used THA hardware tested in isolation. In these and other studies, it has been observed that increased femoral head diameter (a feature permissible with advanced hard bearings) increases the range of motion prior to occurrence of impingement, thereby increasing the implant’s safe range-of-motion. However, it has been suggested that with large femoral heads, bone-on-bone will be the most common impingement modality, implying that a point of diminishing returns exists for larger head sizes. Using a cadaveric model, Bartz et al. [161] determined that hardware impingement occurred with a frequency of 50% for 28mm femoral heads, and 30% with 32mm head diameters, versus osseous impingement. However, that study was limited in terms of motions analyzed (hip flexion simulating chair rising) as well as using only a single (neutral) cup position. Observation of a similar transition between prosthetic impingement and osseous impingement with increased head sizes were found in an early (and even more experimentally-limited) cadaveric study [173]. Using a mathematical model of hip range-of-motion for THAs with 28, 32, 36 and 38mm heads, Cinotti et al. [174] determined that osseous impingement is more common than prosthetic impingement for 36mm and 38mm implants versus smaller femoral heads. However, while this latter work analyzed impingement events for multiple cup orientations, again, simplified joint kinematics were used.

These cited studies represent the bulk of in-depth investigations in the orthopaedic literature on the topic of impingement-site variance in THA. However, owing to the many limitations, multiple questions regarding the kinematics and mechanics of impingement-site variability remain. Presently, little or nothing is known regarding differences in contact mechanics and joint stability for different modalities of impingement. To narrow this knowledge gap, the previously developed FE model of THA hardware impingement was modified to also address the issue of osseous impingement in THA with increased head sizes. In contrast to the studies previously addressed, this study investigated the impingement-type (bone-on-bone, component-on-component, or hybrid), impingement-associated bearing contact stresses, and intrinsic joint stability for several physiologically-realistic dislocation-prone challenge events.

Methods for FE Model of Osseous Impingement

The FE model was generated from manufacturer-provided engineering CAD files of a widely used contemporary THA implant (Summit stem, 36mm M-spec head, 36mm x 56mm Pinnacle cup, DePuy Orthopaedics, Warsaw, IN) which were pre-processed using TrueGrid and Mathcad software. Seven distinct femoral head diameters (32mm to 44mm in 2mm increments) were considered (Figure 47), by projecting the outer surface of the femoral head mesh onto scaled surfaces. Mesh densities for each were determined from prior convergence studies. Bony anatomy of the pelvis and femur were determined by manual segmentation of the Visible Human (NLM, Bethesda, MD). The bony anatomy was registered to the pelvic reference frame of the FE model, and virtual femoral osteotomy and pelvic reaming were performed using Geomagic Studio. The acetabular components were positioned in 40° inclination and 15° acetabular anteversion (anatomic reference frame)

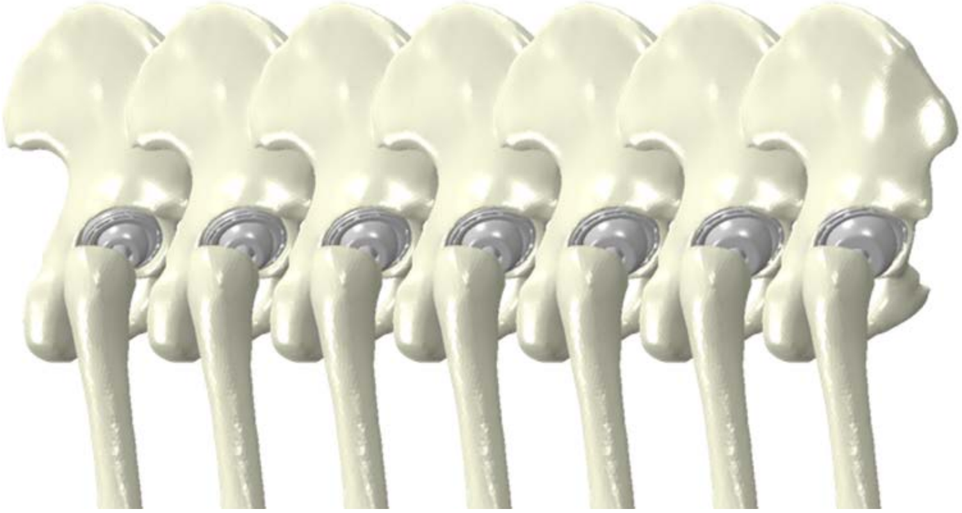

Figure 47: The THA FE models used in the bone impingement study. From left to right: 32, 34, 36, 38, 40, 42, and 44mm. The acetabular component was positioned neutrally within the pelvis (40° inclination, 15° acetabular anteversion)

Candidate impingement challenge motions were determined from five posterior-direction dislocation maneuvers (low sit-to-stand, normal sit-to-stand, sitting cross-leg, leaning, stooping, and squatting) and two anterior dislocation challenges: rolling over in bed and lateral foot pivoting [56] (Figure 48). For a neutrally-oriented cup (40° cup inclination, 15° anteversion) (Figure 49), of these candidate challenges, no component-on-component impingement occurred, and only squatting resulted in bone-bone impingement

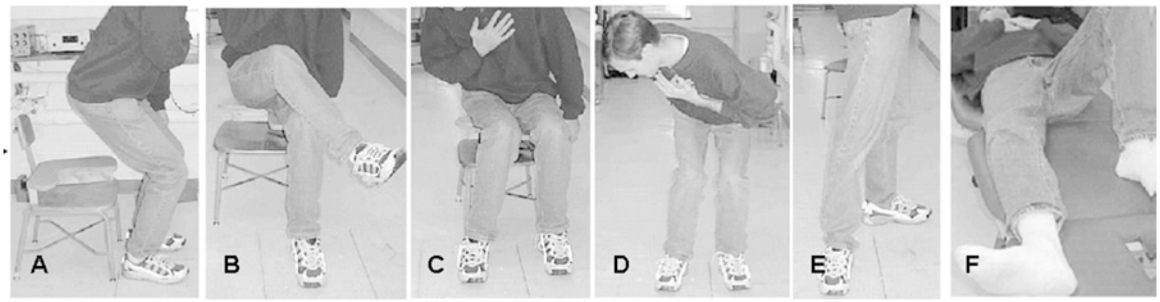

Figure 48: THA impingement challenges. A) sit-to-stand from a low and a normal-height seat, (B) leg crossing, (C) leaning, and (D) stooping. There were also two anteriorly-directed challenges: (E) standing while pivoting the upper body and (F) rolling over while supine. Squatting is not shown.

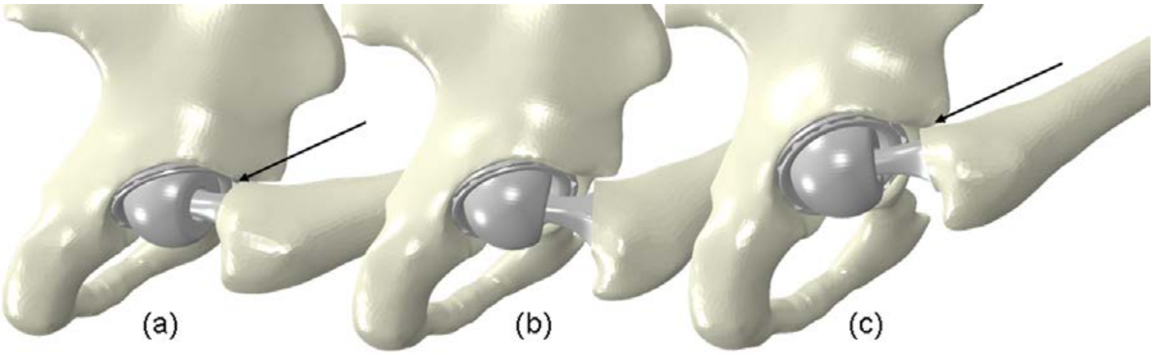

Figure 49: Site of osseous impingement. Pure flexion (a) resulted in impingement between the femur and the anterior inferior iliac spine, at approximately 100° of flexion. By contrast, even with 105° of flexion, stooping (b) did not result in impingement. Squatting, however, resulted in impingement on the acetabular rim at 108° of flexion (c). Illustration is for 38mm femoral head diameters

In addition to these seven FE models of bone impingement (referred to as “bone-40”) , seven additional FE models were generated with a more horizontal cup orientation (approximately 30°, “cup-30”), resulting in neck-on-cup impingement for the squatting challenge. To eliminate cup orientation as a confounding factor, seven additional FE models were generated at the 30° cup position, but with numerical contact removed between the neck and cup, thus forcing the contact instead to be bone-to-bone (“bone-30”).

For these 21 resulting FE simulations, peak bearing vM stress, as well as the dislocation resisting moment were recorded during the squat impingement challenge.

Results of Bone vs. Hardware Impingement Investigation

The component-on-component impingement events generated significantly higher contact and surface stresses compared to the two bone impingement events (Figure 50a). The two separate bone impingement models had similar stresses. Stresses for all three impingement situations decreased with increased head diameter, the effect being most pronounced for the cup impingement events. Peak resisting moment for the two bone impingement scenarios were, on average, 5.5- and 2.6-fold higher than for hardware impingement (Figure 50b).

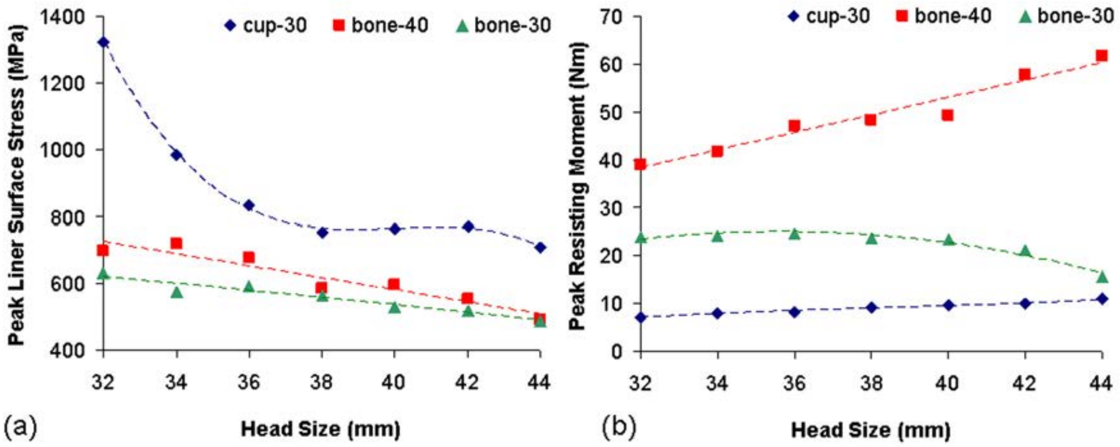

Figure 50: Peak surface (von Mises) stress (a) and peak resisting moment (b) for the 21 distinct FE models. Component-on-component impingement demonstrated substantially greater edge-loading stress compared to the two bone-on-bone impingement variants, but dislocation resistance for component impingement was significantly reduced.

Discussion of Bone vs. Hardware Impingement

To the author’s knowledge, this study represents the first investigation of the variance in mechanisms and consequences between implant-on-implant vs. bone-on-bone impingement events. While all impingement events are detrimental, these data corroborate previous investigations in terms of some impingement events being much more detrimental than others. Bone-on-bone impingement, which has been postulated to occur with greater frequency in larger head THAs, was shown to involve substantially greater resistance to dislocation, and considerably less bearing surface contact stress, than hardware impingement scenarios. For all but the largest implants investigated, generated surface stresses approached or exceeded the yield strength of cobalt-chrome alloy. Together, this suggests that, should impingement occur, impingement between the neck and cup is (1) more likely to progress to dislocation, and (2) more prone to cause damage of the bearing surface.

Additionally, while it is often suggested (based on a very limited number of experimental investigations) that osseous impingement in large-diameter THAs is the limiting factor for joint range of motion, this investigation has shown that hardware-only impingement is still possible (and indeed more likely) for multiple physiologically-realistic dislocation-prone motions.

Should impingement occur, contact between the bony femur and pelvis is substantially less detrimental than that between the implant neck and cup. Larger femoral heads, regardless of impingement location, result in less edge-stress and greater dislocation resistance.

CHAPTER 3: FAILURE OF CERAMIC BEARINGS

> Designing structures to avoid fracture is not a new idea. The fact that many structures commissioned by the Pharaohs of ancient Egypt and the Caesars of Rome are still standing is a testimony to the ability of early architects and engineers . . . since mankind's knowledge of mechanics was limited, workable designs were probably achieved largely by trial and error. The Romans supposedly tested each new bridge by requiring the design engineer to stand underneath while chariots drove over it. Such a practice would not only provide an incentive for developing good designs, but would also result in a Darwinian natural selection, where the worst engineers are removed from the profession.
>
> T.L. Anderson. Fracture Mechanics: Fundamentals and Applications 2nd ed.

Linear Elastic Fracture Mechanics [175]

Alumina ceramics for THA were introduced nearly four decades ago, to address concerns over polyethylene-particle-induced osteolysis and to improve long-term results in younger and more active patients [34, 176]. Ceramic-on-ceramic bearings offer several advantages over contemporary metal-on-polyethylene or metal-on-metal constructs. However, due to the brittle nature of ceramic materials, concerns persist regarding implant failure due to catastrophic fracture. Microscopic-level imperfections in a brittle material act as stress risers when load is applied. In linear elastic fracture mechanics (LEFM) theory, the Stress Intensity Factor (K) is a measure of the severity to which otherwise-present mechanical stress is amplified by the presence of a flaw. The magnitude of K depends on several factors, such as macroscopic geometry of the part, the geometry of the flaw, and the magnitude of the applied stress [177] (Figure 51).

Similar stress-magnification relationships exist for shearing mode fracture (K_{II}) and for out-of-plane shearing (tearing) mode fracture (K_{III}). For complex loading situations, all three modes can contribute to material failure, a circumstance known as mixed-mode fracture (Figure 52).

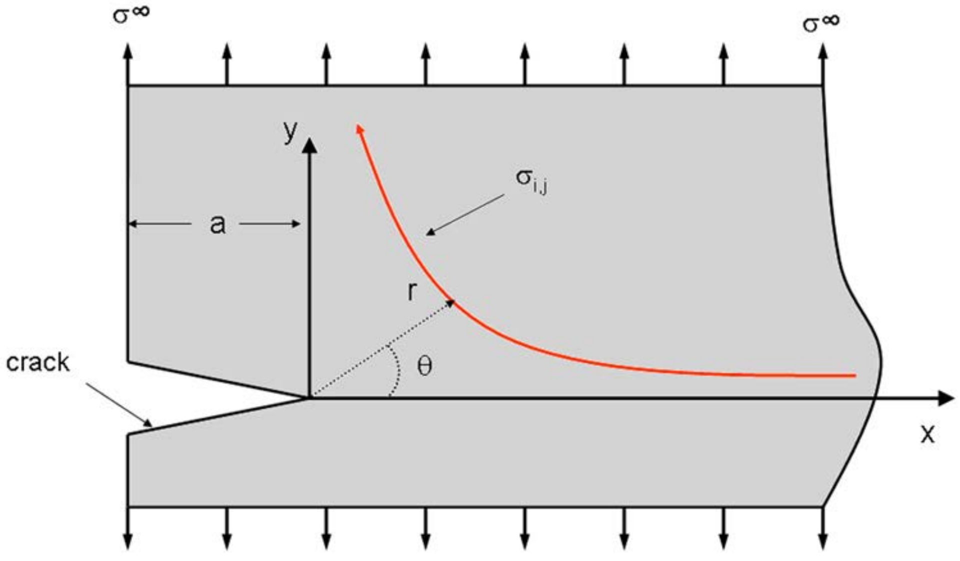

$$\sigma_{i,j} = \frac{\sigma^{\infty}\sqrt{a}}{\sqrt{2r}} f_{i,j}(\theta) = \frac{K_I}{\sqrt{2\pi r}} f_{i,j}(\theta)$$

Figure 51: Linear elastic fracture mechanics for mode-I fracture. The flaw-magnified stress tensor, σ_{ij} is determined from the far-field stress (σ^{∞}), the crack length (a), the distance from the crack tip (r), the angle of crack orientation (θ) and the mode-I stress intensity factor (K_I).

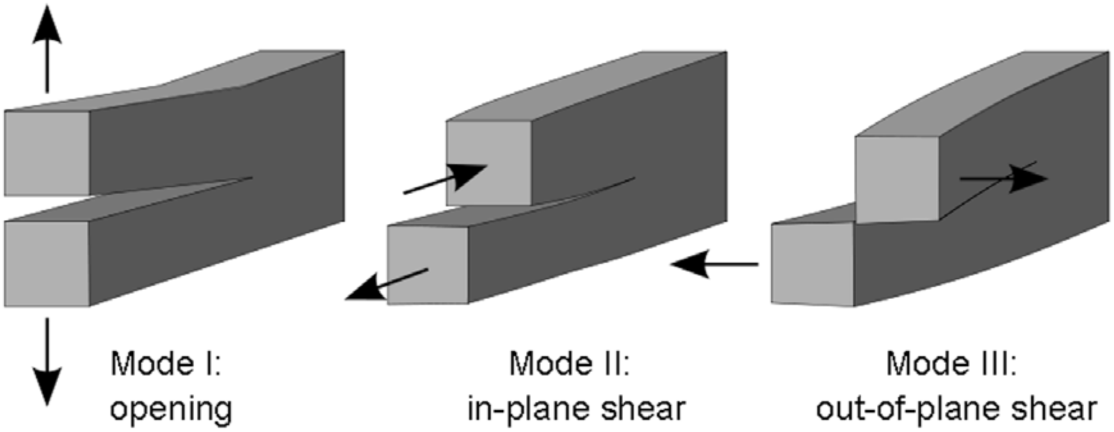

Figure 52: Different modes of fracture. Mode-I describes opening (tensile) at the crack tip. Mode-II describes sliding (in-plane) shear, while mode-III describes tearing (out-of-plane) shear. In real-world situations, typically all three modes contribute to material failure, a condition termed "mixed mode" failure.

Fracture of brittle materials can be considered as encompassing two phases: subcritical crack growth, and catastrophic fracture [178]. Small material flaws and imperfections, which are ubiquitous in sintered materials [178, 179], propagate subcritically if K exceeds a limiting threshold factor, K_0. When the value of K exceeds a critical stress intensity (e.g. K_{IC} for tensile-mode failure), uncontrolled crack growth and catastrophic fracture occur. Fracture of ceramic femoral heads has been a well recognized problem historically [178, 180]. Impact loading of the ceramic head onto the metal trunnion ("Morse" taper) of the femoral neck creates regions of high circumferential hoop stress, which sometimes tended to cause crack propagation and ultimately critical fracture (Figure 53). However, extensive investigation into the design of this ceramic-metal interface, by experimental [180-182], analytical [183] and finite element [184, 185] techniques, identified critical design factors responsible for increased fracture propensity. This led to optimization of design parameters such as component size, shape, taper angle, surface roughness and neck length. Those design modifications, along with improvements in materials engineering and in proof testing, decreased femoral head fracture rates from 13% for first-generation alumina heads [186], to rates in the range of 0.004% [187] for contemporary heads.

In contrast, ceramic liners have had a significantly less extensive body of work in systematic analysis regarding fracture risk mitigation. Recently reported fracture rates for contemporary liners are in the range of 3.5% [188] , 1.12% [189] and 0.22% [190], values which far exceed the rates for (alumina) head fracture. Furthermore, it has been suggested that, due to diagnostic difficulties, ceramic liner fracture is likely an "underestimated" issue. [190]. Various predisposing factors for ceramic liner fracture have been cited, including microseparation [191], trauma [192] and obesity [193]. But, liner fractures apparently due to component impingement far outnumber all other causes [188-190, 194, 195] (Figure 54). Given the brittle nature of ceramic materials, the high stresses which occur during impingement can give rise to elevated fracture risk. Optimal component positioning is thus arguably even more important for CoC constructs than for other bearing alternatives [196]. However, the strength of influence of the various surgical positioning factors as regards ceramic liner fracture propensity currently is purely conjectural. Therefore, need exists to systematically investigate the relationship between ceramic fracture risk and surgical cup positioning, for different variations in kinematic impingement challenges.

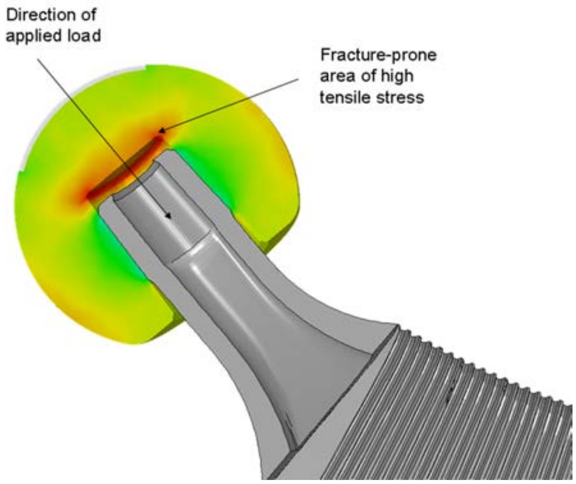

Figure 53: Fracture of the femoral head typically occurs during the impaction of the femoral head onto the neck, creating areas of high tensile stress.

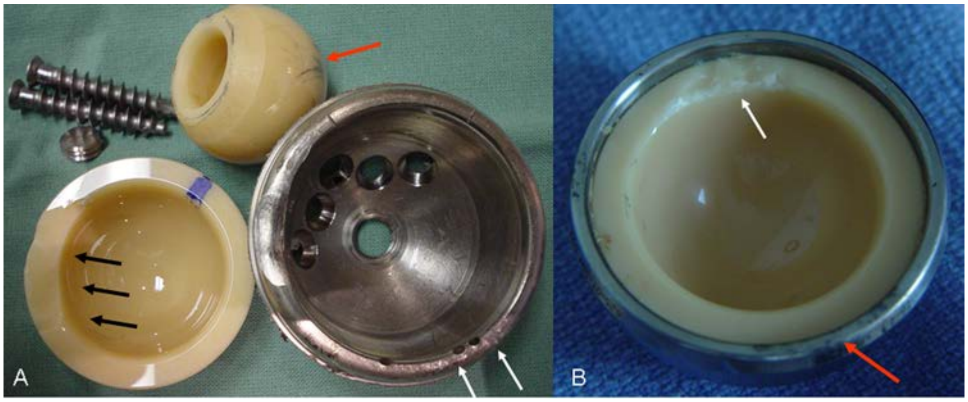

Figure 54: Retrieved ceramic liners from failed CoC THAs. (A), impingement damage is observed on the acetabular shell (white arrows), resulting in head subluxation and edge loading (stripe wear on head, red arrow). Edge-loading is thought to cause fracture of the ceramic liner (black arrows). Similar mechanisms are observed in (B), with impingement damage (red arrow) leading to liner edge fracture (white arrow).

Development of the LEFM FE Model

The ceramic liner LEFM FE model consisted of four distinct developmental and analysis stages (Figure 55).

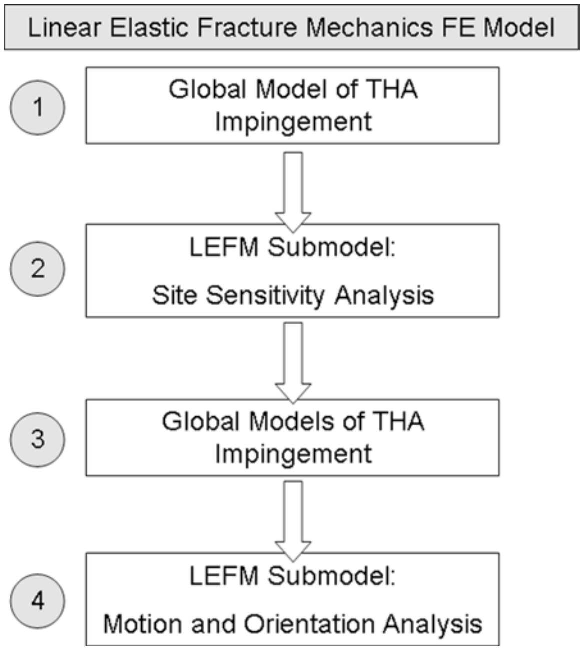

Figure 55: LEFM algorithm. The ceramic liner LEFM FE model consisted of several parts. (1) Impingement- and egress-site stresses in the ceramic liner occurring due to component impingement from a sit-to-stand challenge are determined from the global model of THA impingement (explicit solution scheme). These stresses are then passed as boundary conditions to the first LEFM submodel (2). In this first LEFM series, the position-dependency on sub-critical flaw propagation was determined. The worst-case site scenario was then identified. A second global THA FE series (3) was conducted, investigating multiple impingement/dislocation challenges, as well as parametric investigation of fracture propagation dependency on global cup orientation. These solutions were then passed to the second LEFM submodel series (4), where stress intensity factors were calculated as a function of motion challenge and acetabular cup position.

The LEFM global model (stages 1&3, Figure 55) consisted of the hip capsule, and THA hardware (Figure 56). Data for implant hardware were imported from manufacturer-provided IGES files, and pre-processed using TrueGrid. The femoral component (28 mm) was meshed with 15,856 8-noded hexahedral elements. The liner was meshed with 7,200 8-noded hexahedral elements. The backing was comprised of 1,690 hexahedral elements, with global mesh densities for the femoral component and liner determined from numerical convergence and sensitivity studies (Figures 39-40). Implant positioning for the site-sensitivity analysis was held constant at 35° of tilt and 20° anteversion for the acetabular component, and at 10° of femoral anteversion for the femoral component. For the bearing, the components were modeled as linearly elastic third-generation alumina ($E = 380$ GPa, $\nu = 0.23$, $\rho = 3.98$ gm/cm^3), with radial clearance of 0.034 mm and friction coefficient of 0.04. The femoral neck was modeled as linearly elastic CoCr ($E=210$GPa, $\nu=0.3$, $\rho=9.2$gm/cm^3). For computational economy, the metal backing of the liner, as well as distal regions of the femoral stem were assumed rigid.

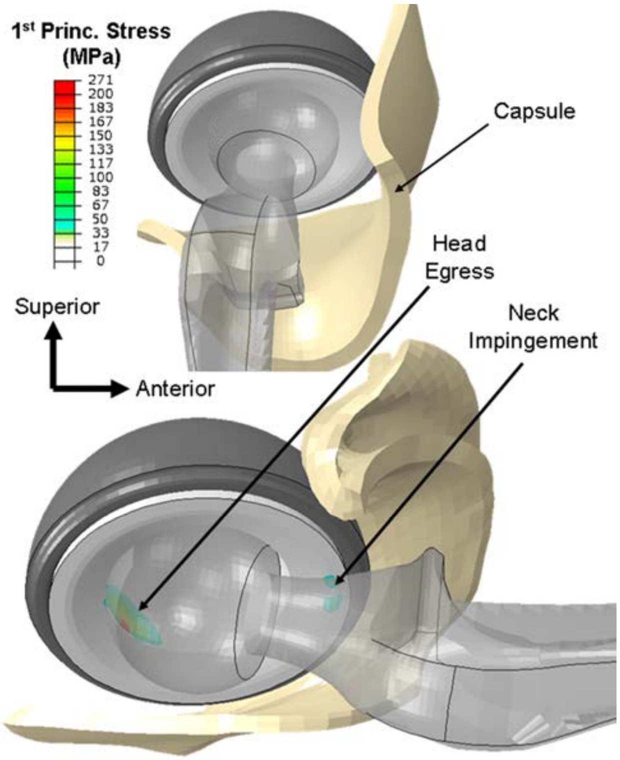

Figure 56: THA impingement FE model. Kinematic challenges begin in full extension (top), and progressed through hip flexion resulting in impingement (bottom), resulting in stress concentrations at both the site of neck-liner contact, and at the posterior region.

Developing the initial crack (sub-critical flaw) model posed several challenges. The crack was modeled to extend from the crack tip to the inferior surface of the liner (Figure 57).

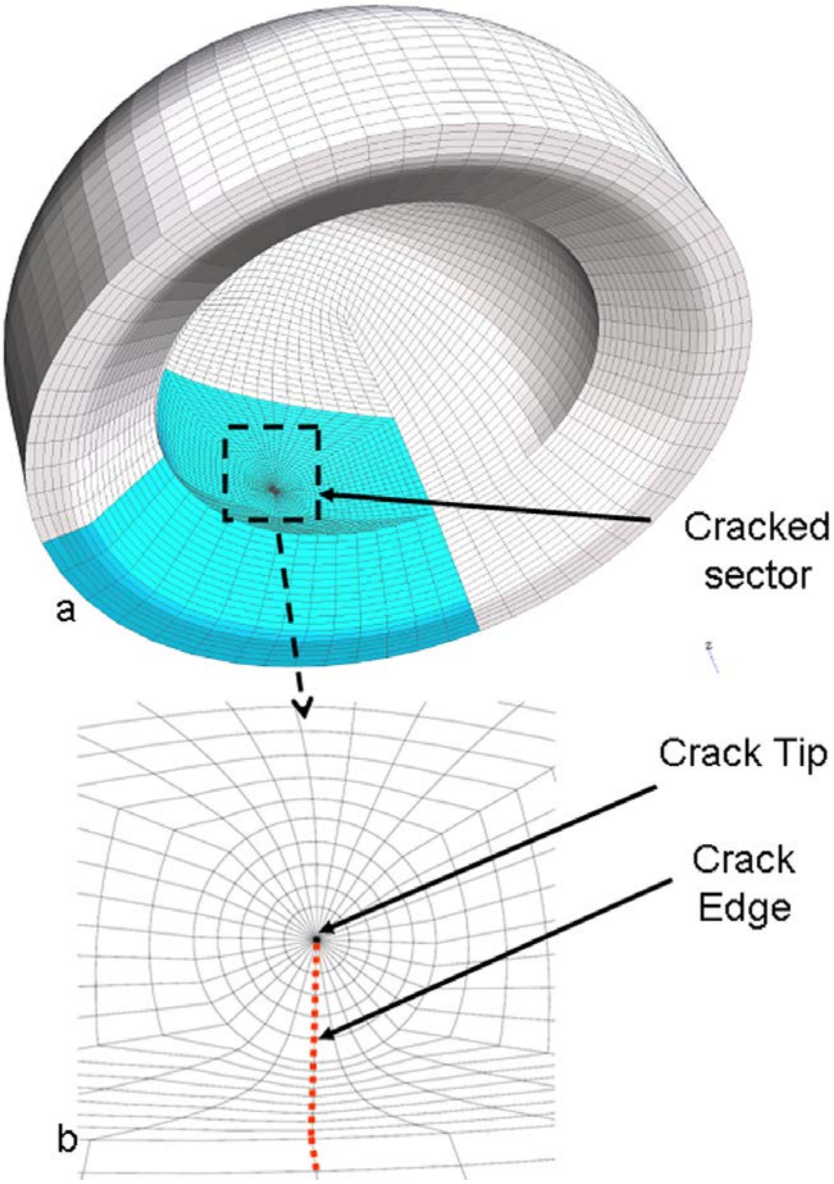

Figure 57: Cracked ceramic liner. (a) An affected sector of the liner. The crack tip (b) is composed of special fracture elements, surrounded by refined rosettes facilitating computation of stress intensity factors.

Creating the crack began by first meshing a single sector of the ceramic liner with 20-node hexahedral elements. The crack tip consisted of 10 rows of 32 elements forming the crack front (Figure 58). One edge of each of the 32 elements forming each row of the crack was attached to a single line, in effect collapsing a single edge of each crack-element, allowing crack-tip elements to take on the shape of a wedge. The crack front was given an arbitrary form, with the crack-tip elements forming the shape of a cone, with the crack faces approximately planar. Five rows of regular hexahedral elements formed the rosettes from which J-integral calculations were performed during FE analysis. The outer regions of these mesh blocks were then attached to curves and surfaces from the original manufacture-provided IGES files. Additional regions of the liner were meshed with 20-node brick elements, following the previously described procedure of edge and surface projections. Sliding interfaces were defined for the entire crack tip region (310 elements), as well as at the crack face (Figure 58). These sliding interfaces prevented merger (i.e., computational equivalencing) of the nodes, retaining the form of 20-node collapsed bricks at the crack front (instead of 15-node wedge elements), while maintaining the crack. Alternative definitions of the sliding interface would allow for the current through-crack to be modeled as a buried crack, or a crack which does not go through the entire thickness of the liner. Additionally, the variables used in the meshing of the crack are entirely parameterized, allowing for complete analyst control and rapid-remeshing of several crack properties, such as crack shape (eg. curved in lieu of planar), crack location (e.g., near the surface), crack face morphology (notched instead of a hairline crack, etc.). Also, mesh densities and the number of highly-refined rosettes could also be specified, allowing for sensitivity studies pertaining to the affect of mesh structure on outcome metrics. The resulting mesh, consisting of entirely 20 node brick elements, was written to an output file. The TrueGrid output format is structured as an Abaqus input file, reporting nodal coordinates, element connectivities, node and element sets, and surface definitions.

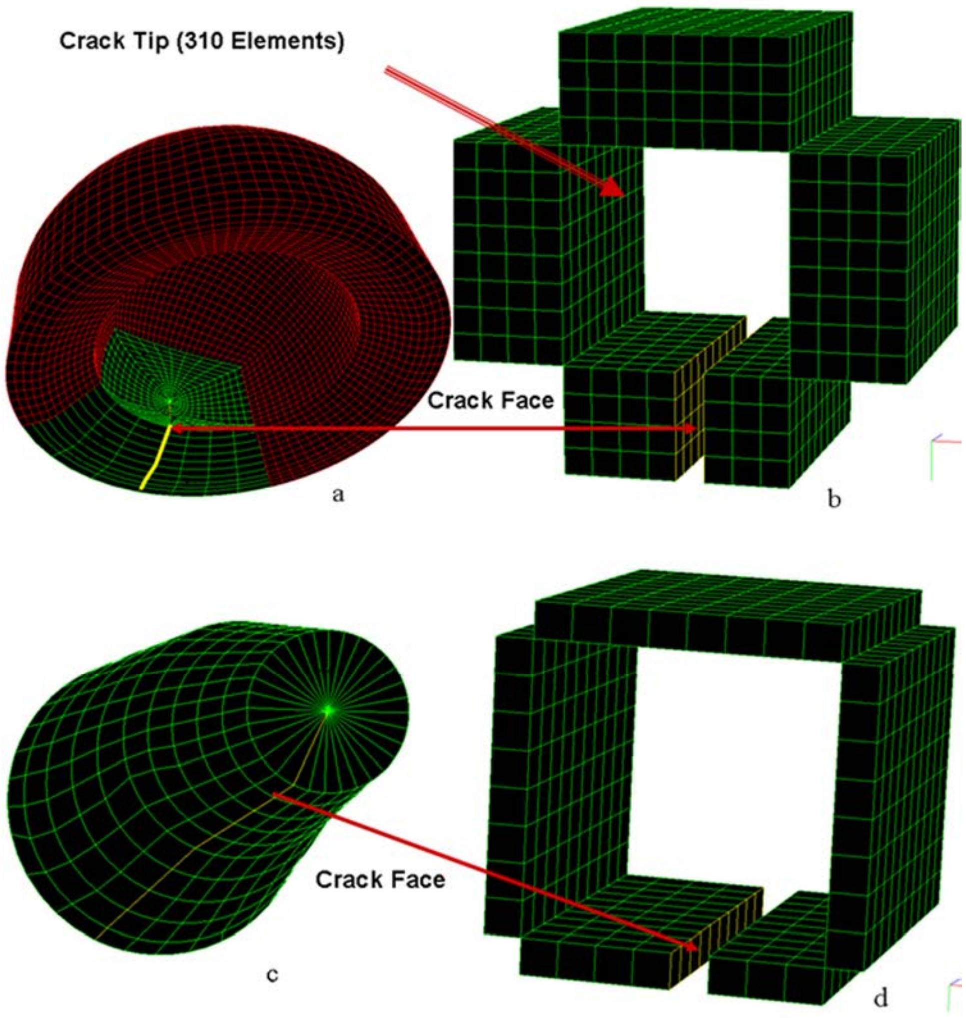

Figure 58: TrueGrid crack meshing scheme. (a) Physical mesh of a cracked sector of the liner. (b) Corresponding computational-space mesh of the cracked sector. The crack tip is composed of nodes from 310 elements. (c) Close-up view of the elements forming the crack-front, and corresponding computational window of crack front (d). The nodes on the crack face are constrained to be planar. The wedge-shaped elements seen in (c) were actually collapsed 20-noded hexahedral elements. However, there exist 31 crack-tips, instead of the desired single crack tip independent node set. Merging of these crack-tip nodes occurs during mesh-postprocessing in Mathcad.

The resulting mesh needed modifications to allow for J-integral calculations. The crack tip, as defined in the output file, consists of the nodes from 310 elements (10 rows of 31 elements, Figure 58). Since sliding-interfaces were defined by preventing the merging of all nodes, this resulted in 930 nodes (310*3) defining the crack tip. In this form, all nodes of the crack tip were allowed to move independently from each other. Post-processing was required to effectively merge these 930 nodes into only 21 independent nodes. Additionally, the mid-side node on the element sides radiating away from the crack tip needed to be moved to the quarter-point location, enabling singular treatment of the stress field near the crack tip, appropriate for the linear-elastic treatment of the brittle alumina components (Figure 59). These modifications, which allowed for the $/\sqrt{2r}$ singularity to be considered, were conducted in Mathcad, using numerous node and element sets defined in TrueGrid. Twelve such submodels (Figure 60) were generated using the TrueGrid/Mathcad processing scheme, with the location of the crack tip rotated in 30° increments circumferentially around the liner.

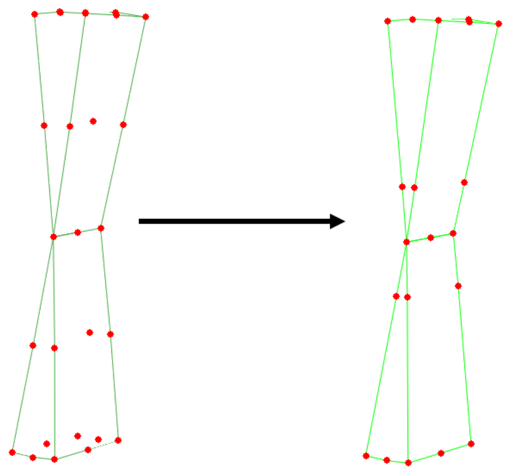

20-node brick
20 non-constrained nodes
Mid-side node at mid-point

20-node brick
15 independent nodes
Mid-side node at quarter point

Figure 59: Mesh post-processing. Left figure represents two elements from a single row of elements on the crack front for the un-processed TrueGrid output. Each element consists of 20 independent nodes, with the mid-side note located at the 50% station. The two elements depicted contain 40 individual nodes. Right: after mesh post-processing in Mathcad. The crack-tip has been merged, with a single set of 21 total nodes comprising the entire crack tip. Thus, for the two elements seen in the figure, 32 nodes were present. Also, the mid-side node has been moved to the quarter-point position.

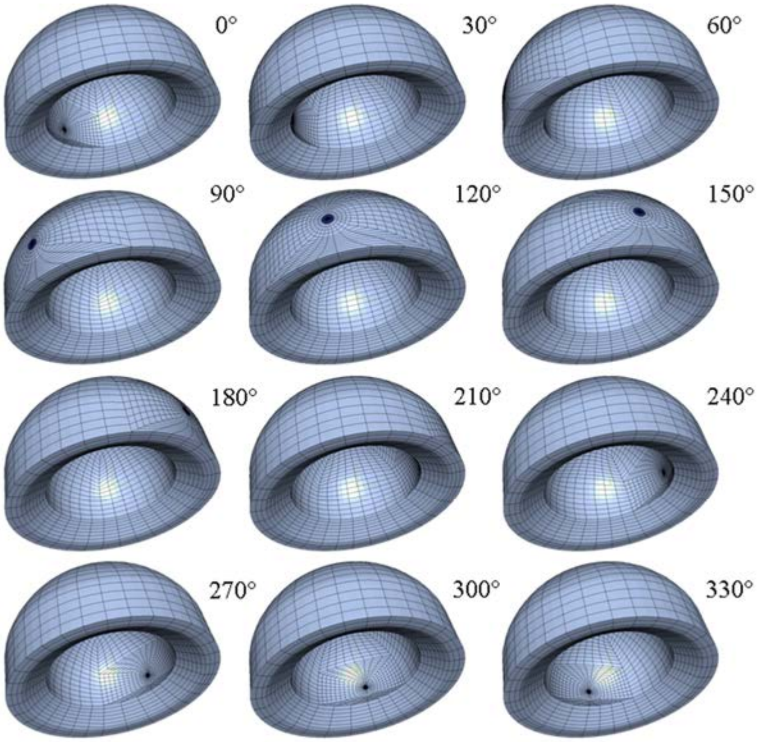

Figure 60: LEFM crack locations. Crack tip rotated circumferentially around the cup pole in 30° increments to create the twelve submodels used in this investigation. The 0° position was assumed to align with the egress-site stress concentration seen in Figure 56.

The global impingement model was solved using the explicit scheme to handle the highly non-linear behavior of the hip capsule. The particular dislocation challenge considered for the global model was a sit-to-stand maneuver from a low chair height. The sit-to-stand kinematic challenge began in full extension, continuing (unless dislocation occurred) to 105° of hip flexion, and then returned to full extension.

The twelve submodels (stage 2, Figure 55) were run using Abaqus' submodeling abstraction (as previously described), allowing for the nodal displacements reported in the explicit global solution to drive candidate nodes as applied boundary conditions in the static submodel solutions using Abaqus/Standard. Contour integral output was requested for the 5-layers of rosette elements in the liner submodel mesh, specifying both J-integral and K-factor output. Virtual crack extensions, required for J-contour integral calculations, were estimated by determining direction cosines for each node on the crack tip to the adjacent node across the crack front. J-integral and K-factor (mixed mode K_I, K_{II} and K_{III}) output from each of the submodels were collected and post-processed in Mathcad.

The values of J-integral and K-factors were seen to be highest at the same approximate location of the egress-site stress concentration (Figure 61). Peak values for K_I-K_{III} were reported to be approximately 30 MPa*mm$^{1/2}$.

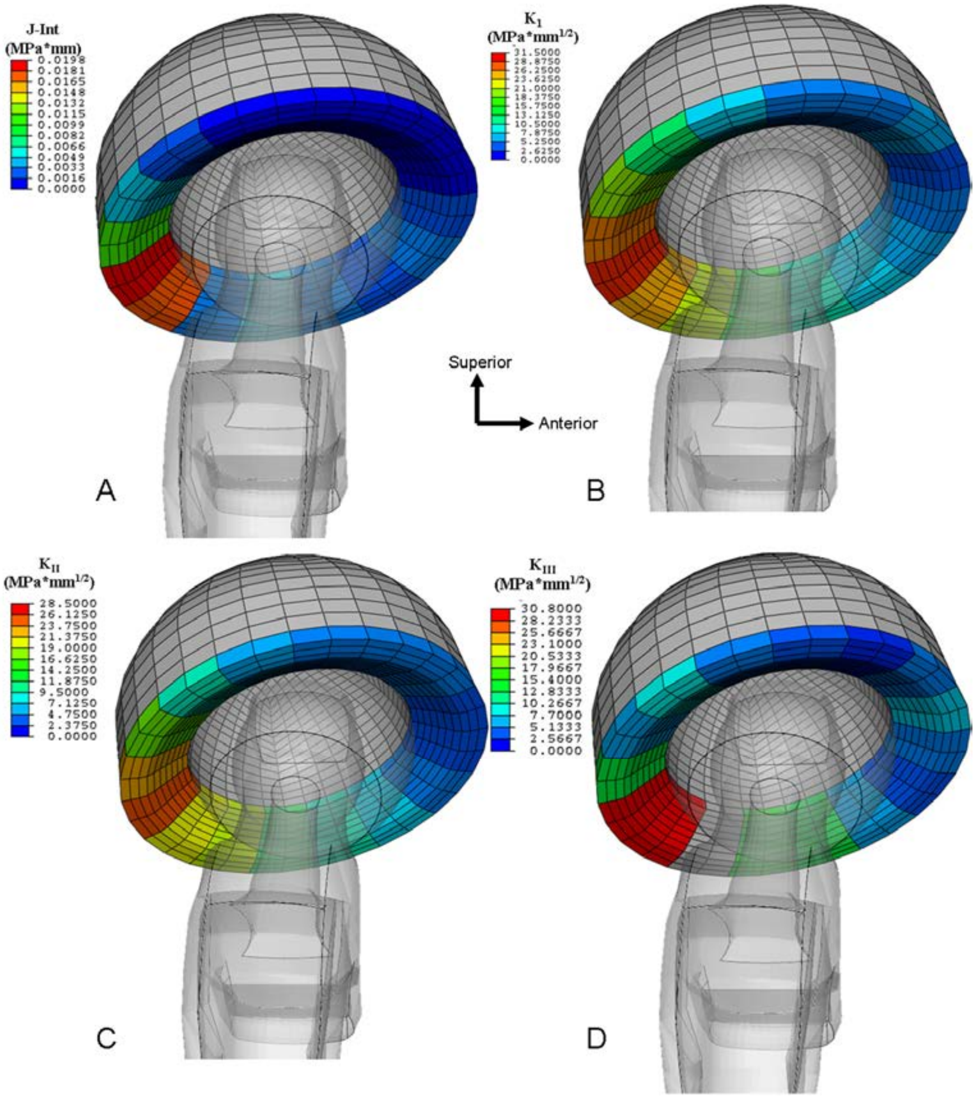

Figure 61: Flaw propagation was predicted by assessing regions of the liner which had the highest numerical values of J-integral (A), K_I (B), K_{II} (C) and K_{III} (D). Flaws positioned at the egress region resulted in computed values of K_I in excess of K_{I0}.

Following the determination of the worst-case initial flaw position, a second global FE series (Stage 3, Figure 55) was conducted. For this analysis, 54 separate FE models were generated to study effects of surgical cup positioning, by varying cup inclination (15° to 65°, in 2.5° increments) and/or cup anteversion (10° retroversion to 40° anteversion, in 10° increments). In addition, seven distinct impingement-prone challenge maneuvers were considered [56]: sit-to-stand from a normal chair height (SSN), sit-to-stand from a low chair (SSL), stooping, squatting, leaning shoe-tie, rolling over in bed, and seated leg-crossing (SXLG).

Impingement -and egress-site stresses developed during this series, which corresponded to the σ^{∞} parameter in Figure 51, were stored for later usage, to drive the quasi-static ceramic fracture submodel analyses (stage 4, Figure 55).

Results of Ceramic Liner LEFM FE Study

Predicted values of K were highly influenced by surgical cup orientation. For both the sit-to-stand and stoop motion challenge, K_I was monotonically correlated with increased cup inclination (Figure 62). Except for the most extreme cup orientations (where impingement either did not occur or was brief in duration), the K_{Ic} (4 MPa $m^{1/2}$) was not exceeded. However, stress intensity values developed during the stoop impingement challenge were consistently higher than those for the sit-to-stand for all orientations, with predicted values of K_I exceeding K_{Ic} for over half of the simulations considered. In addition to increased cup tilt, increasing cup anteversion also caused elevated values of K (Figure 63). There was no selectivity sensitivity over either cup inclination or anteversion, i.e., a unit increase in liner inclination increased computed values of K_I similarly to a unit increase in anteversion.

Mixed-mode stress intensity factors for a neutral positioned cup varied significantly between different motion challenges (Figure 64). The value of K_I for three of the kinematic challenges – stooping, squatting and shoe-tying – was shown to again exceed the K_{IC}. Trends for shear (K_{II}) and tearing (K_{III}) generally followed those for KI, with the primary exception of the shoe-tie.

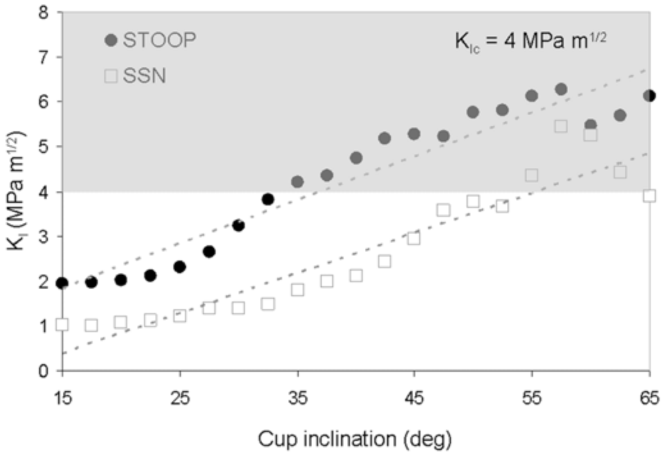

Figure 62: Orientation dependency of K_I on cup inclination angle for both sit-to-stand from a normal chair height (SSN) and stooping for a neutral (10°) anteverted cup. The K_{IC} (gray bar) was exceeded for malpositioned orientations for the SSN, and for several orientations of the stoop motion sequence. Computed values of K_I were monotonically correlated to cup position for both kinematics (dashed lines).

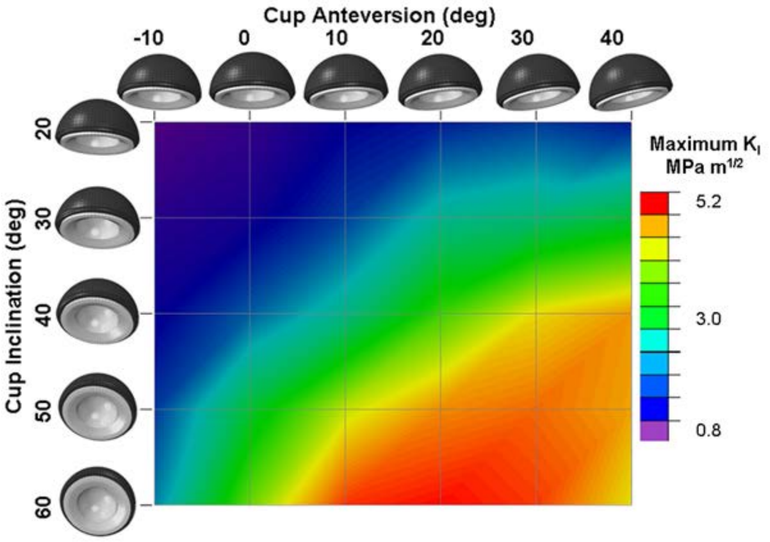

Figure 63: Computed values (continuously interpolated from 30 discrete samplings) for a stoop fracture challenge, demonstrating fracture sensitivity to both cup inclination and anteversion.

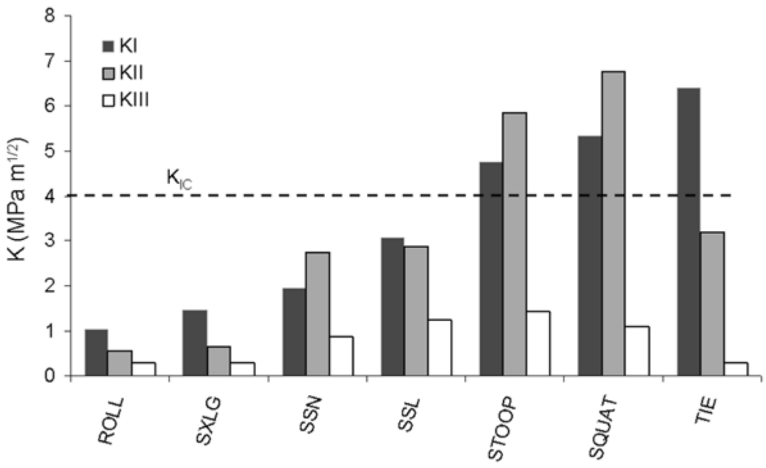

Figure 64: Mixed-mode stress intensity factors for seven impingement-prone motion challenges. Three kinematic sequences demonstrated K_I in excess of the K_{IC}, suggesting a high probability of critical fracture. Values of mode-II (shear) and mode-III (tearing) demonstrate similar trends to those for K_I.

Discussion of Ceramic Liner LEFM FE Study

While liner fracture is a well recognized issue surrounding the use of ceramic THA bearing couples, the mechanism of ceramic fracture, or clinical associations of causative factors, are still largely unknown. In contrast to femoral head fracture, where a specific mechanism of fracture stimulated wide-reaching investigation, followed by significant improvement in design, and consequently by substantially reduced fracture rates, much is left to discern regarding liner fracture. The rationale for the present investigation – which to the author's knowledge represents the first formal LEFM analysis of ceramic liner fracture – was to lay groundwork to understand which specific factors (patient and surgical) influence fracture propensity during impingement-subluxation. Parametric model variations addressed (1) to what extent ceramic liners demonstrated sensitivity to component malpositioning and (2) which impingement-prone maneuvers present the greatest fracture risk, other factors being equal.

Fracture risk during impingement-subluxation was found to be highly sensitive to cup orientation. Higher implant inclination and higher anteversion angles gave rise to the highest predicted values of K; similar dependency of implant angle and contact stress has also been reported [165]. Interestingly, even for cup orientations where impingement did not occur (e.g. 65° inclination – 10° anteversion), fracture risk was still significantly higher than for orientations where impingement occurred at lower flexion angles (e.g. 30° inclination, 10° anteversion). This suggests that, while impingement plays a clear role in fracture initiation/propagation for ceramic liners [188-190, 194, 195], impingement *per se* is not the singular causative factor. Toward reducing the incidence of impingement-associated liner chipping or fracture, many contemporary designs use a recessed ceramic liner, to ensure that any neck impingement that might occur involves the backing rather than the liner. The present data suggest, however, that this strategy may do little to avoid brittle fractures originating at the opposite (egress) side of the cup.

Besides simply whether or not impingement occurs, the present results show that the "quality" of impingement-subluxation also greatly influences ceramic failure propensity. When observing the joint contact forces computed from an inverse dynamics solution of a 47-muscle optimization model [56] (Figure 65), the three motion patterns with the highest fracture risk also demonstrated the highest joint load.

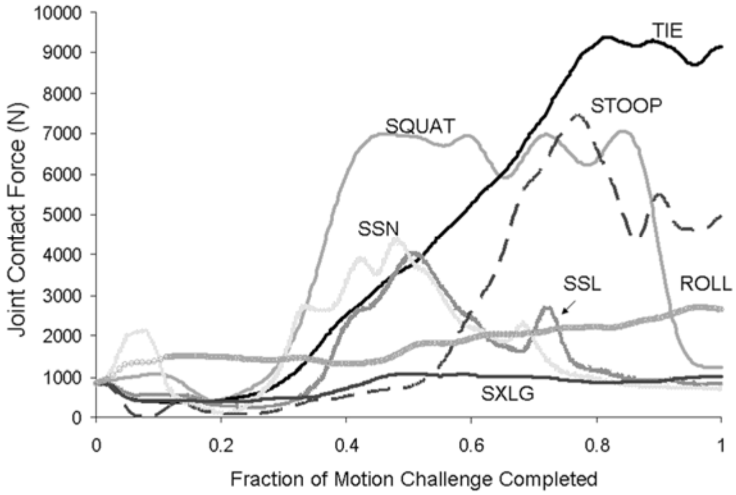

Figure 65: Computed reaction force (joint contact force) for the seven motion challenges. The three highest-risk motions (shoe-tie, squat and stoop) demonstrated the highest joint force.

Stooping and leaning (as done when tying shoes) involves a large upper-body offset from the hip joint center, leading to high joint reaction forces. These two motions, along with squatting, also result in sustained peak joint loads experienced at high flexion (i.e., when impingement is expected to occur), suggesting that the greatest risk of ceramic fracture occurs when high joint contact forces occur under conditions of impingement. Similar motions, especially squatting, have been clinically linked to liner failure [188, 195]. While the effect(s) of loading variations on ceramic fracture have not been experimentally investigated, Maher et al [197] identified a cut-off joint load of 12kN as being sufficient to cause liner fracture for simulated impingement impact conditions. While not quite exceeding that threshold, the presently computed contact forces for the three highest-risk maneuvers certainly approached that level. Owing to Newtonian force equilibrium, situations of excess body weight could plausibly push joint contact forces even higher, perhaps explaining the increased fracture rate in obese THA patients [193]. Further investigation into the association of fracture risk with loading conditions certainly deserve further attention.

Although the present LEFM computational formulation represents a substantial step forward in quantitative analysis of fracture in ceramic hip bearings, this study has several simplifications and limitations. First, while the spatial location of the initial "flaw" in the subcritical fracture series was posited at various positions circumferentially around the liner, the flaw in all instances was assumed to be located on the bearing surface of the liner. Whether sub-surface flaws and/or deep flaws would exhibit similar location-sensitivity circumferentially as do surface flaws is an open question. However, high local stress concentrations at the bearing surface [165] are associated with repetitive microtrauma (i.e. microseparation) [189], so surface cracks are especially of interest. Second, while seven distinct impingement-prone challenge maneuvers were investigated, in the interest of computational economy, the vast majority of computational analysis assessing the role of cup orientation on fracture focused on only two of these: sit-to-stand

and stooping. The effect of cup orientation upon fracture propensity for other challenges (such as seated leg-crossing) is also an open question, and an inviting topic for additional investigation. Third, the particular shape of the crack used in this analysis undoubtedly would have affected the K magnitudes computed. Analysis of crack propagation in FE models, while well grounded theoretically and while being relatively straightforward to implement in 2D, poses major challenges in 3D. Recent advances in computational analysis (as described later) hold promise to further facilitate the investigation of ceramic crack propagation in THA bearings. Finally, given the normally highly comminuted nature of ceramic liner fracture, accurate *post-facto* identification of the initial fracture location is probably impossible, and therefore direct clinical correlation with the fractures modeled in the present study are not available. Clinical collaboration, ideally, would strengthen the utility of the present study, but the fracture paradigm modeled here – impingement leading to subluxation, edge loading and eventually to fracture at the liner egress-site – has been proposed by multiple authors [188-190] following examination of explanted fractured ceramic liners. One very inviting topic for further study is to directly replicate such cracks in a bench physical model, which would provide direct physical corroboration not feasible *post-facto* clinically.

While fracture rates for ceramic components have dramatically improved, such fractures as do occur are devastating to the patient. Ceramic failures always require revision surgery, which is often complicated by the need to revise all components of the primary construct. When revision is delayed, or if debridement of fragment particulates is incomplete, severe third body wear and/or destruction to bone and surrounding soft tissue often occurs, leading to early failure of the revision [192, 196, 198, 199]. The work reported here introduces a novel computational framework within which systematic analysis of ceramic liner fracture can be conducted. Specifically, egress site (edge or near-edge) loading arising from neck-on-cup impingement was identified as leading to elevated fracture propensity, a mechanism which is well-corroborated clinically [188-190].

The flexibility of the current formulation allows for other potential fracture mechanisms to be similarly systematically explored. Fracture risk was found to be highly site-specific, highly sensitive to component positioning, and highly sensitive to specific challenge maneuvers.

Advanced FE Modeling of Ceramic Liner Fracture [200]

Currently, one in every seven hip replacements in the US is a ceramic-on-ceramic bearing [35]. Owing to continued efforts to reduce the incidence of wear-associated osteolysis, and to numerous recent reports of unacceptably high failure rates for some metal-on-metal devices, ceramics are expected to gain an even larger THA bearing market share [35]. However, as evidenced by very recent reports of ceramic liner fractures [201, 202], catastrophic failure of ceramic liners will remain a major concern with this bearing couple in the foreseeable future. Therefore, the ability to quantitatively analyze fracture risk, as well as the capability to investigate patient-, implant- and surgical-specific factors which may mitigate fracture risk, is a priority objective. Our initial efforts at fracture modeling of THA liners used a classic LEFM FE modeling approach (as previously described). However, the utility of this approach was restricted by several modeling limitations. First, a crack location (initialization) had to be assumed *a priori*, and it required significant effort to generate the 3D mesh and assign specialized fracture element properties. Second, fracture propagation required prohibitively laborious remeshing routines, and therefore was not attempted in the initial fracture FE study. However, recent FE model capability advancements, specifically eXtended Finite Element Modeling (XFEM) hold attraction for rapid parametric analysis of design and surgical influence over fracture initiation and propagation in THA ceramic liners. As a proof-of-concept, an XFEM fracture model was developed to parametrically investigate the effect of acetabular cup edge profile geometry and patient body weight on fracture risk.

Introduction to the eXtended Finite Element Method

XFEM, also known as the partition of unity method, is a numerical technique using “enrichment” of model geometry to allow for solution of differential equations in regions with discontinuous functions.

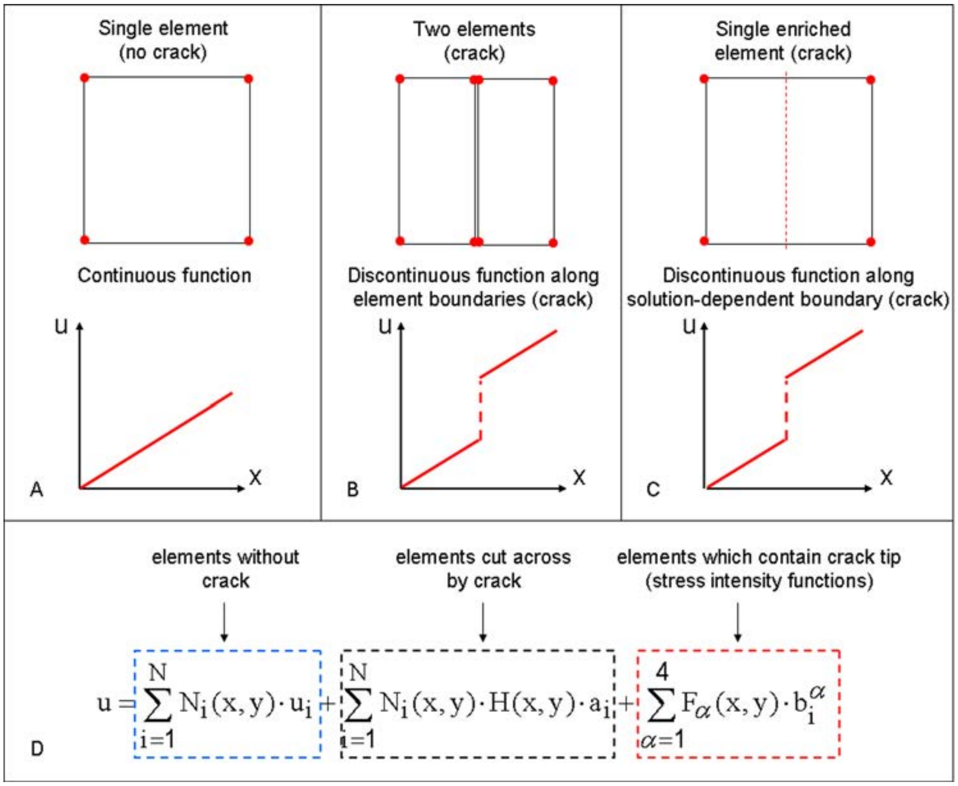

Figure 66: XFEM theory. In standard FE modeling, the displacement field is a continuous function across the element (A). To model a discontinuity across the element, the model mesh must be structured such that the discontinuity lies across the element boundaries (B). However, XFEM allows for mesh-independent modeling of discontinuities (C) by incorporating enrichment features to the standard displacement approximation. The element enrichment incorporates discontinuities (D) which cut across the entire element, as well as the crack-tip asymptotic fields (see Figure 51). u_i is the usual nodal displacement vector, $N_i(x,y)$ are the usual nodal shape functions, a_i and b_i are enriched degree-of-freedom vectors, $H(x,y)$ is the Heaviside step function, and $F_\alpha(x,y)$ are crack tip functions.

The XFEM method was initially developed in 1999 to alleviate shortcomings associated with conventional treatment of solution discontinuities, such as material cracks

[203]. In XFEM, standard displacement fields are enriched near a crack tip by including both discontinuous fields and crack-tip asymptotic fields (Figure 66). The greatest advantage to XFEM is the ability to model fracture initiation, and fracture propagation, without requiring model remeshing.

Ceramic Liner XFEM Study Methods

The XFEM study used similar methodology to the LEFM study (Figure 55), i.e., global solutions from an explicit analysis of THA impingement/subluxation were passed as boundary conditions for an implicit submodel. However, whereas the LEFM study involved extensive meshing considerations for the initial fracture location, the XFEM model was simply partitioned into two distinct enriched regions. For each enriched region, exactly one crack is allowed to initiate and propagate within the enriched zone. One enrichment region corresponds to the region of the cup associated with head subluxation and edge-loading stress concentrations, while the second is associated with neck-on-cup impingement (Figure 67).

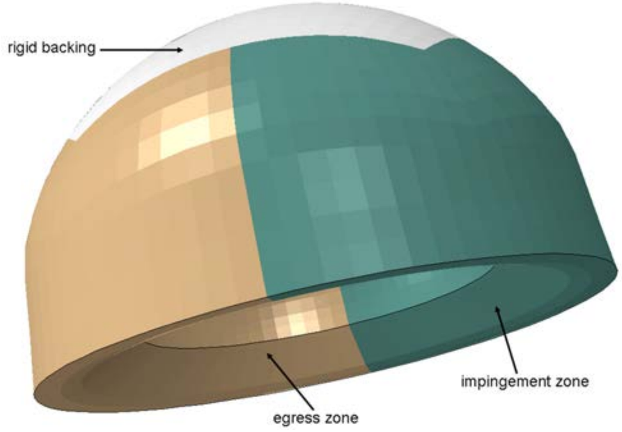

Figure 67: For each enriched region in an XFEM analysis, only a single crack is allowed to initiate and propagate. To model cracks associated with THA impingement, two such enrichment zones are required: One for the region associated with head egress, and the second corresponding to the region of potential neck-on-cup impingement.

For purposes of proof-of-concept establishment, two separate XFEM series were undertaken. The first assessed the effect of cup edge geometry on fracture propensity during chair rising, for 28mm bearings. Four distinct cups with varying cup edge fillet radii (0, 1, 2 and 4mm) were investigated (Figure 68). All cups were positioned in 40° of inclination and 10° of anteversion

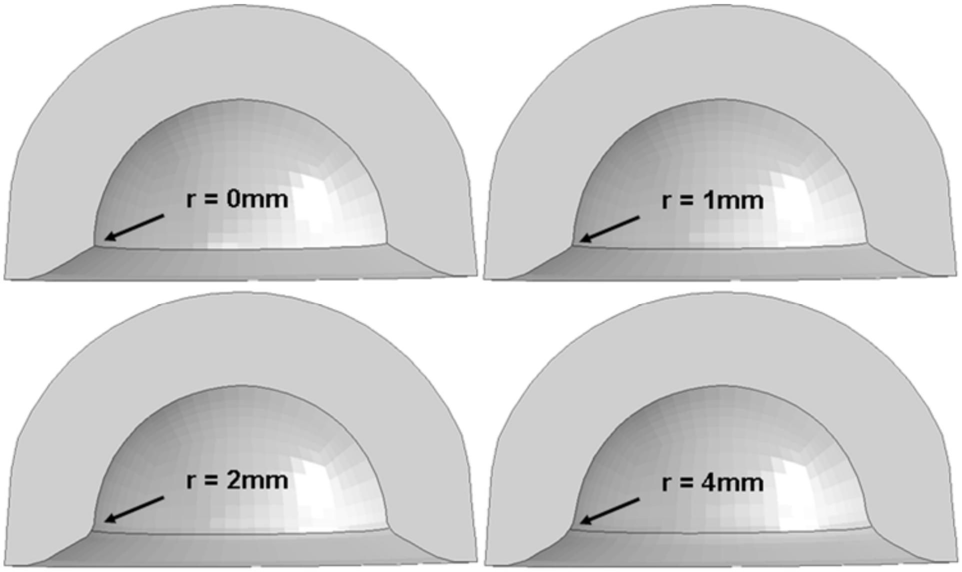

Figure 68: The influence of cup edge design on fracture risk was investigated by considering four distinct values of cup edge fillet radius.

The second XFEM series was performed to investigate fracture initiation and propagation in 36mm CoC bearings, for two additional fracture-prone challenges (squatting and stooping) for 25 variations in cup orientation (45° ± 15° inclination, 15° ± 15° anteversion). Since obesity has been identified as a risk factor for liner fracture [193], two distinct BMIs were considered: normal (25) and morbidly obese (50).

Since microscopic imperfections (which are ubiquitous in sintered ceramic materials) decrease the tensile stresses necessary for fracture, material properties of alumina were varied to simulate conditions of being both with and without micro-imperfections, for both XFEM series. Alumina without imperfections was modeled as having a damage initiation criterion (flexural strength) of 500 MPa (maximum principal stress), while the flexural strength of alumina with micro-imperfections was assumed to be 150 MPa [204]. For both analyses, alumina was modeled as linearly elastic (E = 380 GPa, ν = 0.23), with a strain energy release rate (defined as the change in potential energy with crack area) of 42 J/m^2.

Ceramic Liner XFEM Study Results

For the 28mm CoC bearings, fracture preferentially occurred at the head egress region (Figure 69).

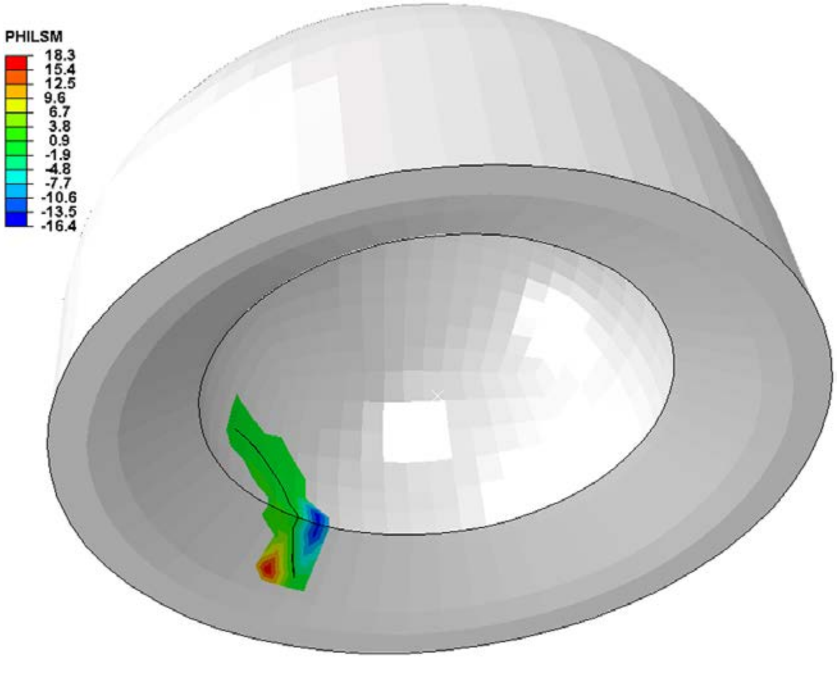

Figure 69: Contour plot of signed distance magnitude (PHILSM) following fracture of the 28 mm ceramic liner. Impingement during the sit-to-stand simulation led to egress-site stresses exceeding the fracture initiation criterion, resulting in fracture initiation at the cup edge (r = 0 mm). During subsequent steps, stresses exceeding the mixed-mode energy release rate resulted in fracture propagation.

For this series, the only fractures that initiated were at the egress site, and for the 0mm-lipped cup (Table 2). No fractures occurred at the impingement site for this series. When the fracture initiation criterion was reduced to reflect micro-flaw presence, considerably more fractures were encountered (Table 3).

Table 2. Cup radius XFEM series fracture initiation (micro-flaw-free material properties)

Radius (mm)	Egress-site fracture	Impingement-site fracture
0	yes	no
1	no	no
2	no	no
4	no	no

Table 3. Cup radius XFEM series fracture initiation (micro-flaw-present properties)

Radius (mm)	Egress-site fracture	Impingement-site fracture
0	yes	no
1	yes	yes
2	yes	yes
4	no	no

For the 36mm XFEM series, fracture initiation and propagation occurred following impingement during the stooping and squatting fracture challenges (Figure 70). In the normal-BMI simulations, 17 of the 50 alumina bearings with micro-imperfections experienced fracture. Spatially, cracks occurred at a location intermediate (Figure 71) between the liner edge and pole, at the inner edge, at the outer edge, and at the impingement site, in 41%, 41%, 18% and 6% of these fracture instances, respectively. No fractures occurred in the absence of alumina imperfections. In the high-BMI group, fracture occurred in 39 of the 50 simulations with micro-imperfections, with fracture initiating in nearly 87% of these instances at an intermediate location, and only 13% at the cup edge. Fracture occurred in three simulations without imperfections, with cracks initiating at the cup edge in all three, and all of which were cups positioned in 0° of anteversion.

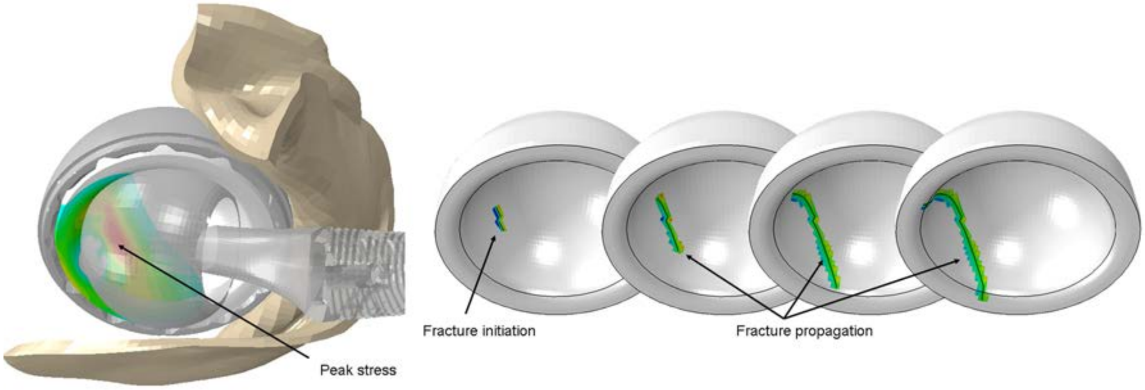

Figure 70: Deep flexion during squatting led to near-edge loading and development of high stress at an intermediate location between the cup edge and cup pole. These stresses were passed to the XFEM submodel, which allowed for both fracture initiation and crack propagation to occur.

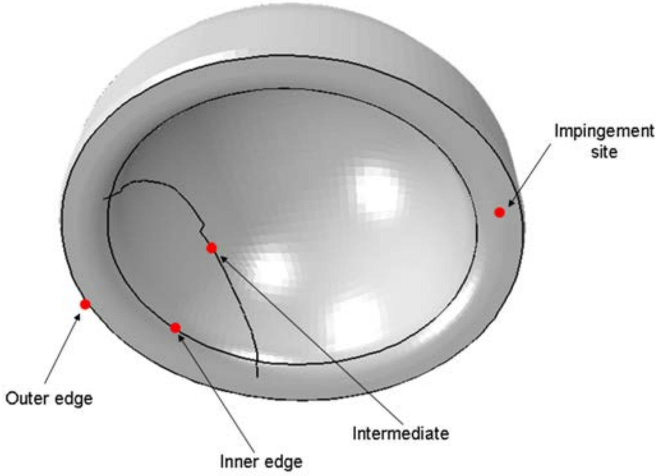

Figure 71: Fracture in the 36mm cup occurred primarily at one (or more) specific sites.

Discussion of Ceramic Liner XFEM Study

Although recent advances in material science and quality control have significantly improved long-term survival of ceramic bearings, fractures remain a clinical concern. Catastrophic failure of a ceramic hip has devastating consequences for the patient, substantially worse than other modes of THA implant failure. While fracture rates of ceramic heads have been reduced to 1/25,000 hips, rates for fracture of alumina liners are several orders of magnitude higher. Ceramic liners, unlike ceramic femoral heads, have no well-recognized fracture mechanism or causative factor. Therefore, mitigation of fracture risk requires greater scrutiny of specific factors, whether design, patient or surgical, which influence fracture propensity during impingement. The rationale for the present work was to identify a computational platform conducive to rapid parametric investigation of these factors. This work, to the author's knowledge, is the first application of extended finite element analysis to the field of joint arthroplasty research. Furthermore, to date, there is not a single peer-reviewed publication utilizing XFEM for any orthopaedic application. In fact, a current PubMed search on "XFEM" or "extended finite element" returns only five hits. Given the ease of use with XFEM compared to traditional LEFM fracture analyses, and the relatively high fracture burden in orthopaedics (bone, implants, bone-implant interface, etc.), in all likelihood, use of XFEM for orthopaedic applications will greatly expand in the foreseeable future.

Surgical cup orientation was found to influence fracture initiation, with greater fracture risk seen for cups positioned at higher inclination and at extremes of cup anteversion. Similar trends with elevated cup orientations have been reported clinically for wear of ceramic couples [205]. While "optimal" cup orientations have been identified as regards impingement avoidance, contact stresses sufficient to challenge implant failure strengths can occur even in the absence of component impingement [165]. Additionally, with current clinical practice trending toward larger head sizes so as to reduce dislocation risk, added safeguards against fracture, beyond simple impingement avoidance, need to be identified. In every analysis reported here, stress at the egress site exceeded that experienced at the impingement site, owing to the occurrence of edge-loading between the head and cup lip. As the radial diameter of the cup contact surface increased, contact area, and therefore contact force during this engagement decreased. Therefore, the reduction in fracture incidence when larger cup lip fillet radii are used is not surprising. However, as the cup lip becomes more rounded, joint stability decreases, since the displacement required for the head to dislocate (the "jump distance") is reduced.

CHAPTER 4: FAILURE OF METAL-ON-METAL BEARINGS

> Today, as never before, the power of advertising, rather than a scientific report, may cause a surgeon to select one prosthesis in favor of another. The insidious nature of marketing methods and overcommercialization is obvious … orthopaedic surgeons have thereby become consumers, and selection of prosthesis systems must be made with an awareness of the choices and compromises.
>
> John N. Insall, 1988 Presidential Address to the Knee Society

The orthopaedic industry is big. A recent report [206] projected that the global orthopaedic implant market will grow to $41.8 billion by 2016, with an annual growth rate of nearly 8% for the arthroplasty device industry. With this rapid growth, continued emergence of new or modified implants can be expected, especially those employing “new”, “alternative”, or “improved” technologies, materials, and/or designs. Experience has amply taught that potentially adverse phenomena in “new” THA designs merit proactive scrutiny; therefore ongoing advancements in hip implant design must be equally met with ongoing biomechanical surveillance. This charge is perhaps best exemplified with the recent renewed interest in metal-on-metal bearings for THA, which recently (2009) accounted for 35% of the THAs implanted annually in the US [35].

From an engineering standpoint, MoM bearings offer several advantages over conventional implants, including a reduction in bearing surface wear and improved joint stability, both such benefits ensuing from the larger head diameters enabled. These assets are reflected in the impressive intermediate-term clinical results of current-generation MoM bearings [207, 208]. However, there is rapidly mounting concern over wear-associated adverse soft tissue reactions following some MoM hip replacements. These reactions, variably referred to as metallosis [209], aseptic lymphocytic vasculitis-associated lesions (ALVAL [210]), pseudotumors [211] and adverse reaction to metal debris (ARMD [212]), have been implicated in unacceptably high short-term failure rates for some MoM devices [212-216]. The exact mechanism(s) for failure of these devices are incompletely understood.

Implant orientation [217, 218], cup geometry [219, 220] and head size [212] have all been suggested as contributing factors. Therefore, multiple large FE investigations were undertaken to identify potential sources and/or contributing factors for failure in MoM THA.

Role of Acetabular Geometry in Edge-Loading [220]

Introduction in Edge Loading

Of particular concern in hard bearings is the occurrence of edge loading, where near line-contact between the femoral component head and the acetabular cup lip results in a very narrow crescent-shaped region of contact, and therefore highly concentrated stress. This deleterious engagement situation interferes with the precise articulation conditions necessary for fluid-film lubrication of hard bearings [221], resulting in increased friction and accelerated wear [222]. Cup orientation is perhaps the most commonly cited surgical factor influencing edge loading in hard bearings [212, 217-219, 223, 224]. The influences of femoral head size [212, 224, 225] and soft tissue laxity in predisposing to "micro-separation" [226-228] are also recognized. Recently, however, the role of cup design – specifically, the role of head coverage (the cup's "articular arc") [219, 229] and of geometry of the cup edge [230] – has drawn increased attention for edge loading conditions. To systematically explore those relationships, a study was designed to test the hypothesis that there is a trade-off, in terms of increased head coverage versus more abrupt curvature sharpness of the cup edge, influencing the adverse mechanical stress concentrations developed during a subluxation event.

Methodology of Edge Loading FE Model

FE analysis was used to parametrically assess the independent influences of cup edge radius and of cup inclination and anteversion as factors influencing edge-loading during subluxation. Dependent variables of primary interest were the range of motion, the resistance to dislocation, contact stress on the cup lip, and propensity for debris generation due to scraping. The FE model consisted of the hip capsule and a widely used contemporary implant (Summit stem, 36mm M-spec head, 36mmx56mm Pinnacle cup, DePuy Orthopaedics, Warsaw, IN). Manufacturer-provided surface geometry CAD files were pre-processed using TrueGrid. The cup lip radius for the manufacturer's CAD file was 3.8 mm, and the articular arc of coverage was approximately 161° (Figure 72). For systematic investigation, the inner surfaces of the manufacturer-provided CAD surfaces were re-parameterized as simple axisymmetric curves, which could then be modified to allow for any desired lip radius (and obligate arc of coverage) to be substituted. Seven cup profiles were considered, corresponding to cup lip radii of 0, 1, 2, 3, 4, 5, or 6mm (Figure 72). Appropriate mesh zoning densities were determined from mesh sensitivity convergence trials. Mesh zoning of the liner was structured to concentrate high refinement near the edge of the cup (Figure 73), in the interest of computational economy.

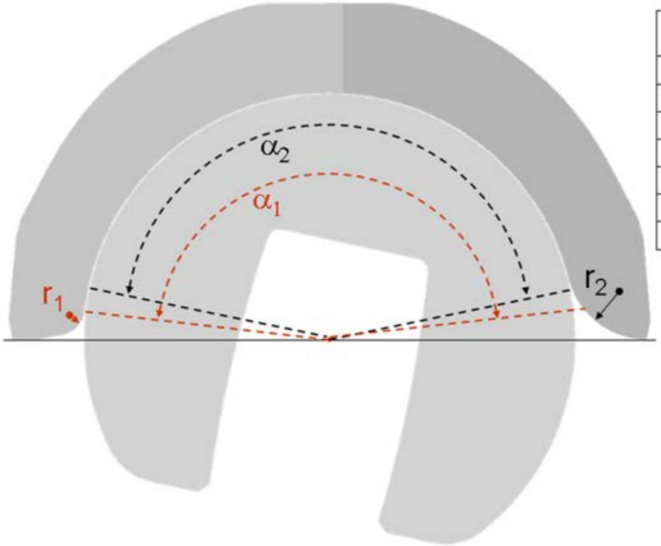

lip radius (mm)	arc (deg)
0	176.0
1	172.5
2	168.0
3	164.0
4	160.0
5	157.0
6	153.5

Figure 72: The articular coverage arc (α) of the liner is a function of the cup lip radius (r). Increasing the cup lip radius decreased articular coverage. The articular arcs corresponding to the seven cup lip radii considered were as tabulated.

Because the focus of interest was upon contact stress concentrations near the cup edge during subluxation, a key metric for model validation was the ability to approximate severe stress concentrations for a geometrically similar situation where gold-standard data were available. A Hertzian analytical solution for general elliptical contact (Figure 73) [169], for which sphere-on-torus (head-on-radiused rim lip) contact represents a special case, provides that standard. Good agreement was achieved for all six variants of non-zero cup edge radius (Figure 74), with a mean relative error of 8.8%.

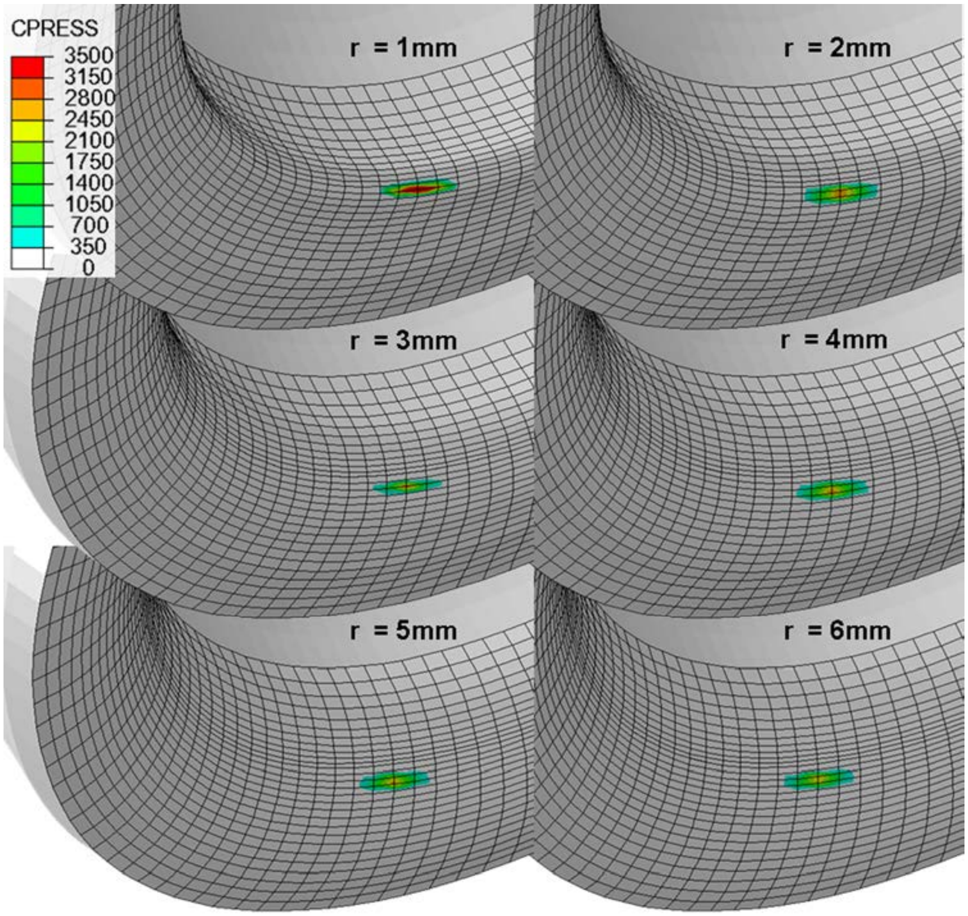

Figure 73: Contact pressures (CPRESS, MPa) are shown for the six non-zero cup radii used in the validation series. Contact simulations were highly sensitive to mesh resolution near the engagement site. Therefore, mesh zoning resolution, which was determined from mesh sensitivity convergence studies, was approximately equal for the entire contact region (shown here as the outlined elements near the edge of the cup).

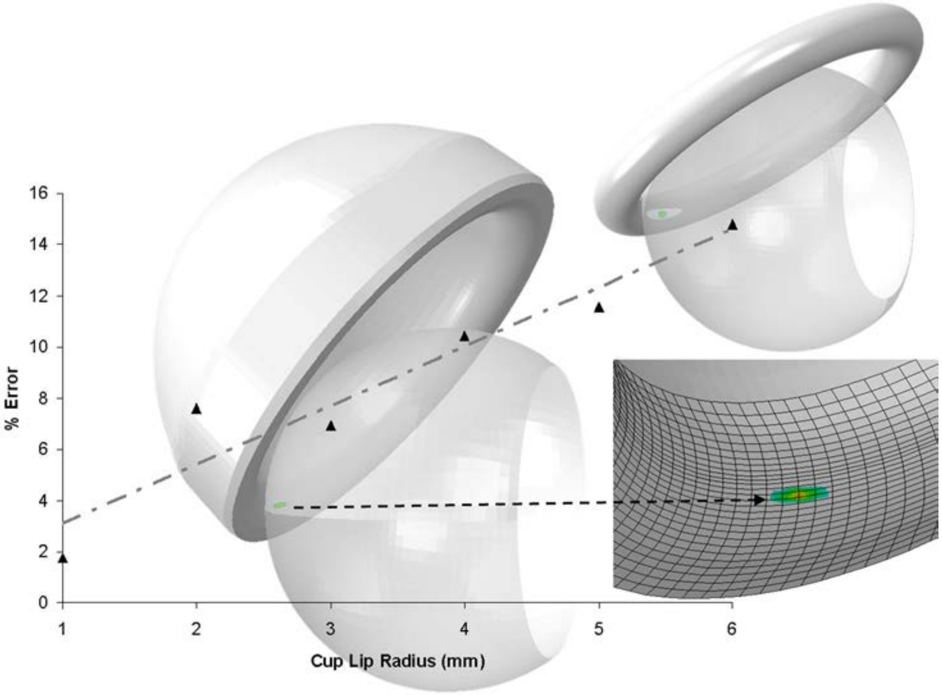

Figure 74: Validation of the FE simulations was conducted by comparing the computed contact pressures for edge-loading with corresponding Hertzian exact solutions for Hertzian elliptical (sphere-on-torus) contact. The specific cases used were a cup in 40° of inclination and 10° of anteversion (background image), at six values of cup lip radius. (The condition of 0 mm cup lip radius did not meet the predicate analytical solution conditions for elliptical contact.) The mean error in peak stress was 8.8%.

Cup inclination (abduction) effects were investigated by considering eleven distinct orientations, with tilt (radiographic definition [163]) varying between 20° to 70°, in 5° increments. For these eleven inclination variants, the cup was held in a constant 10° of anteversion. Similarly, cup version was also investigated by generating ten additional orientations, with (radiographic) cup version between -6.5° and 25°, in 3.15° increments, at a constant 40° of inclination. For all FE simulations, the femoral stem was oriented in 10° of anteversion. The MoM bearing components were modeled as linearly elastic CoCr.

The edge loading challenge investigated was a trunk leaning maneuver, such as when tying shoes [67].The motion and loading inputs were determined from kinematic and inverse dynamic data from human-subject optoelectronic motion capture[56], and were applied as boundary conditions to the center of the femoral head. The simulation began with the hip in full extension, and progressed (unless dislocation occurred) to approximately 103° of flexion, 22° of adduction and 7° of internal rotation.

The femoral head displacement and rotation and the moment resisting dislocation were tracked throughout the entire motion sequence. To avoid disparate situations with very different component appositions due to full or nearly-full dislocation, all comparisons were limited to poses having 2.0 mm or less of femoral head subluxation. Work done to displace the femoral head [81] was utilized as a comparative metric of resistance to dislocation. Additionally, the (von Mises) contact stress, contact pressure, and local relative slippages of head vs. cup nodes were registered. Estimates for scraping wear [165] were also computed, using an Archard-Lancaster approach [171].

A total of 147 separate cases were run, using Abaqus/Explicit 6.9.3. Each individual simulation required approximately 30 processor-hours of computer time.

Results of Edge Loading FE Model

The angular range-of-motion (ROM) showed strong dependencies upon both cup orientation and lip geometry (Figures 75-76). For any given lip radius, as cup inclination increased, the ROM increased (Figure 75). This effect was most pronounced at larger lip radii. At 6 mm of lip radius, each 5° increase in inclination resulted in approximately 1° of increased ROM; for 0 mm lip radius, each 5° inclination increase resulted in only 0.03° of ROM improvement. Similarly, for any given cup orientation, as lip radius increased, ROM decreased. Decreases of 1.65° and 0.02° per mm increase in lip radius were observed for cups with 20° and 70° of inclination, respectively. Similar relationships were observed between anteversion, lip radius and ROM (Figure 76). However, ROM reductions from increased cup lip radius became negligible for cups positioned in at least 10° of anteversion.

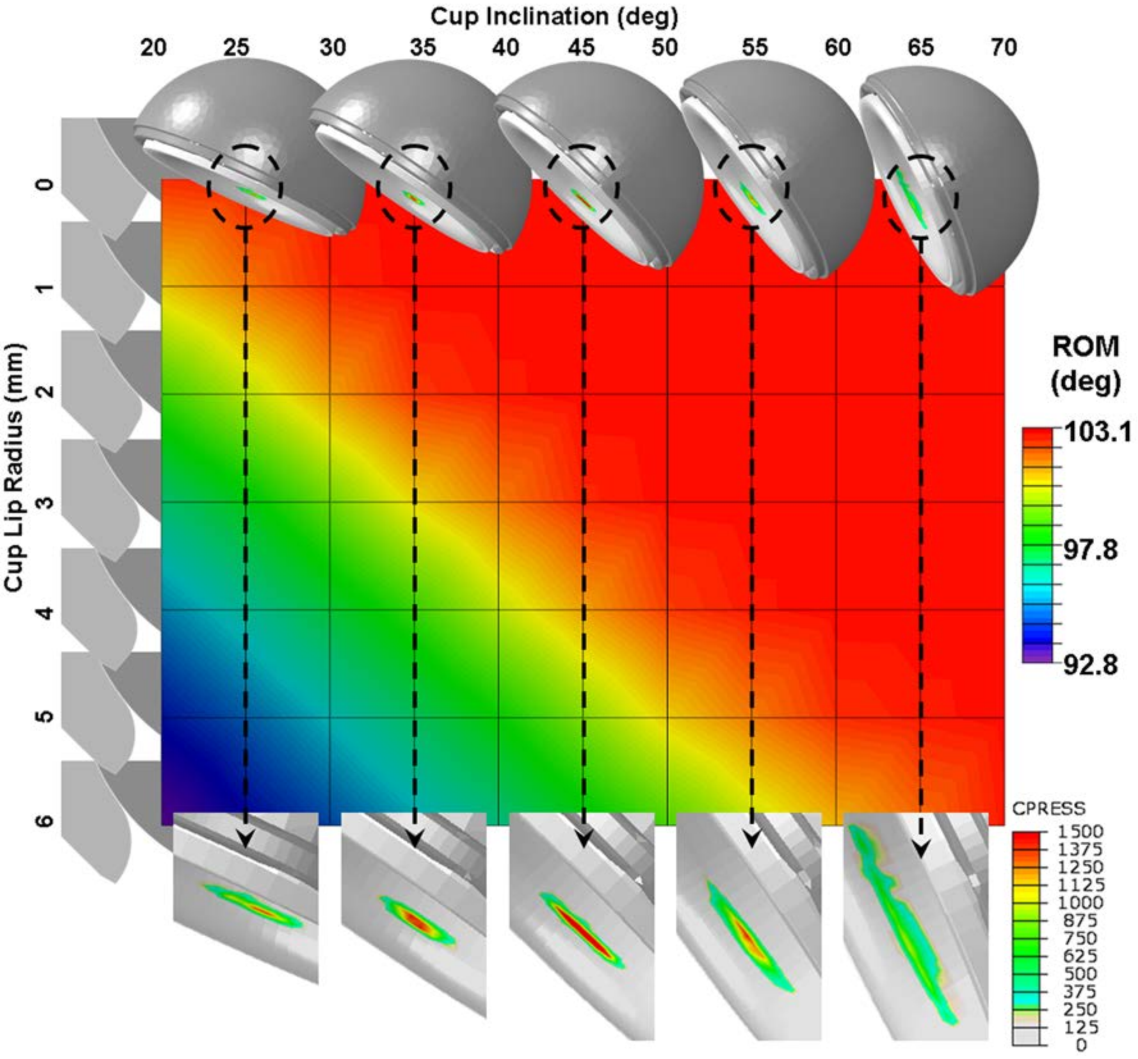

Figure 75: Subluxation-free range of motion (ROM) for 77 separate permutations of cup lip radius and cup inclination. In general, ROM was reduced for increased values of cup lip radius and decreased cup inclination. The reduction effect on ROM due to cup lip profile design was most pronounced for the more horizontally oriented cups, where a 10° decrease in ROM was demonstrated for cups positioned in 30° or less of inclination. Contact pressure (MPa) contours for the 5-mm lip radius cases are shown in the lower insets.

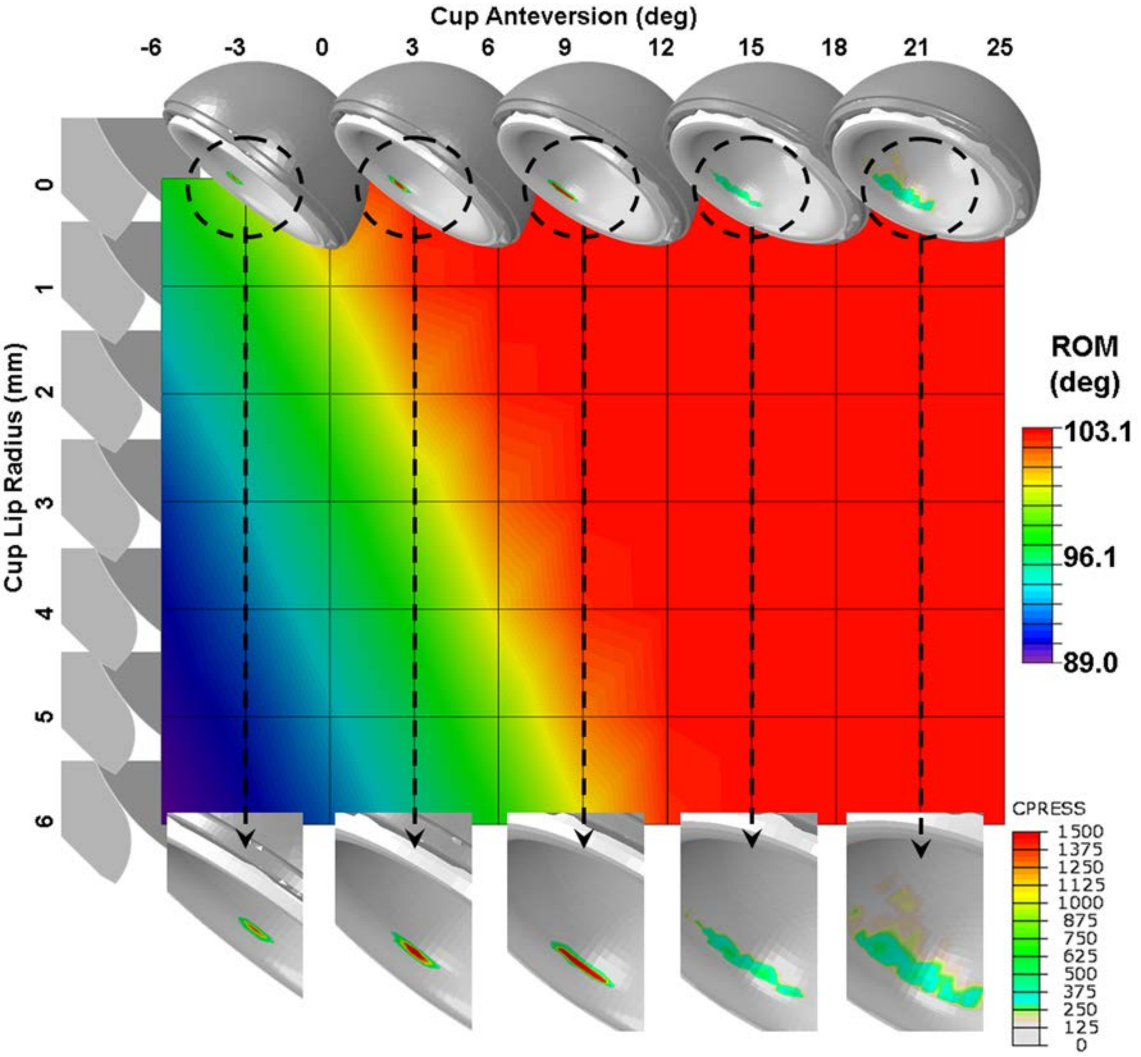

Figure 76: Subluxation-free range of motion (ROM) for 77 permutations of cup lip radius and cup anteversion. Similar to the inclination series (Figure 75), ROM was decreased for both increased values of cup lip radius and decreased cup anteversion. However, ROM at higher anteversion angles was less sensitive to cup lip radius. Contact pressure (MPa) contours for the 5-mm lip radius cases are shown in the lower insets

Head displacement work similarly depended upon cup design and orientation (Figures 77-78). In general, displacement work increased for increased cup inclination, for increased cup anteversion, and for decreased lip radius. For cups at 20° of inclination (Figure 77), each 1 mm of incremental increase in lip radius resulted in 0.30 J decrease of displacement work. This stability reduction diminished as tilt increased: cups at 40°, 50°, 60° and 70° demonstrated per-mm displacement work decreases of 0.23 J, 0.17 J, 0.13 J and 0.08 J, respectively. This effect was similar for cups at varying degrees of anteversion (Figure 78), with per-mm decreases of 0.38 J, 0.28 J, and 0.05 J for cups in -3°, 3° and 9° of anteversion. However, there was only minimal dependency of displacement work on lip radius for cups anteverted to 9° or more.

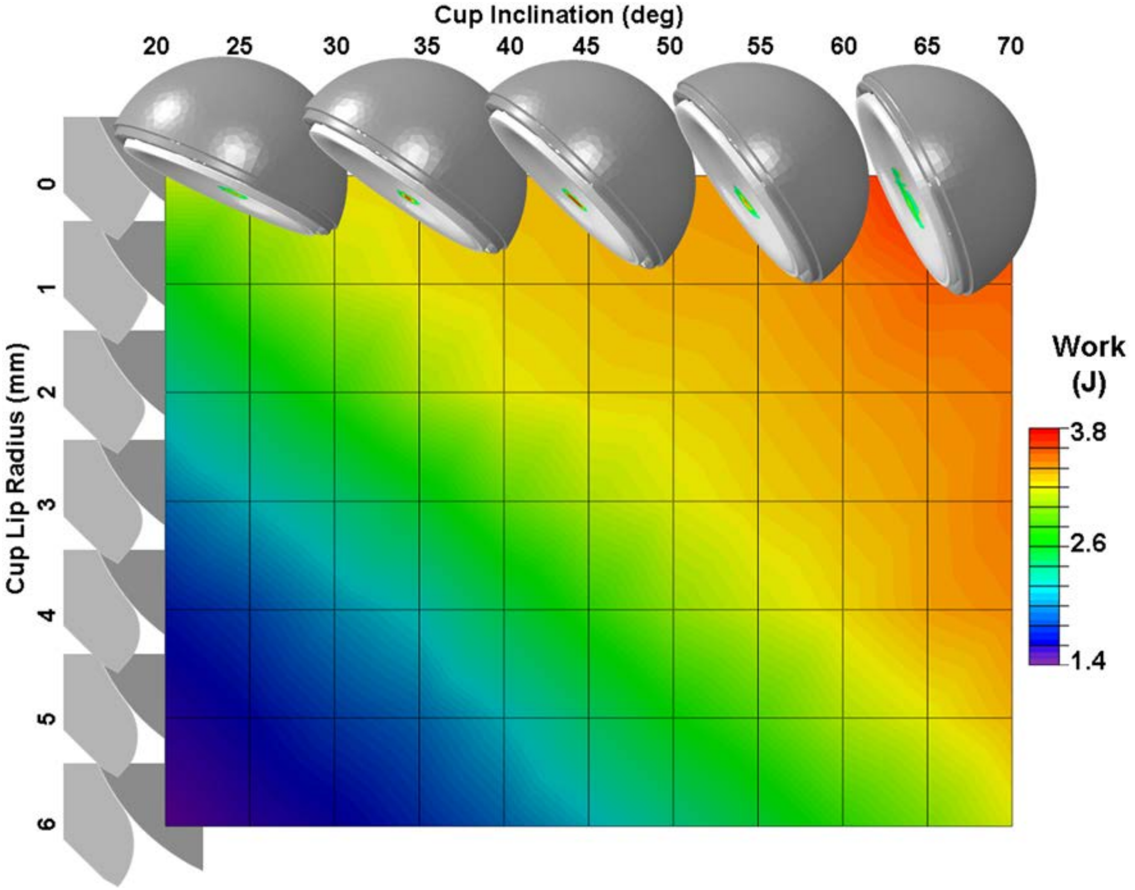

Figure 77: Dislocation resistance work for 77 separate permutations of cup lip radius and cup inclination. Resistance energy was greatest for cups with the smallest lip radius at higher cup orientations. The effect of cup lip radius was most pronounced at more horizontal orientations, where increasing the cup edge radius from 0mm (3.3J) to 6mm (1.4J) for a cup in 20° of inclination resulted in a 60% reduction in dislocation resistance energy

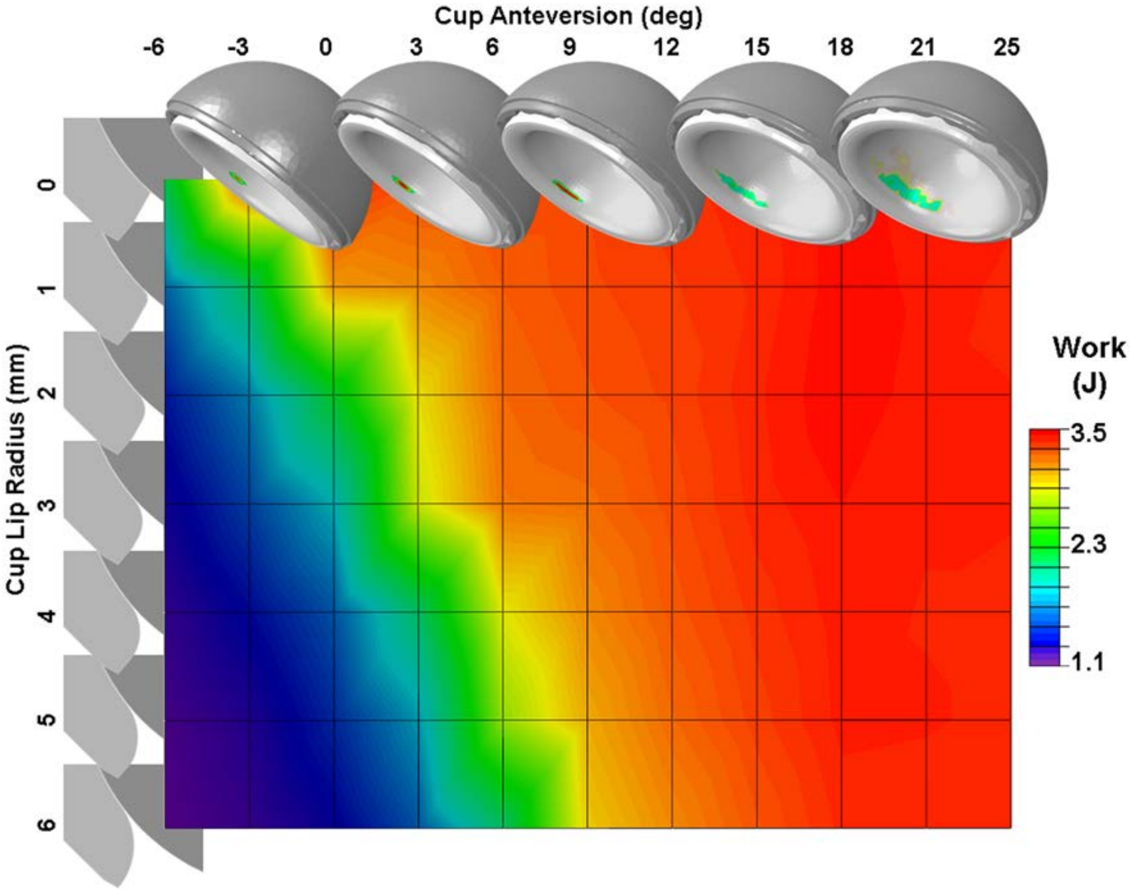

Figure 78: Dislocation resistance work for 77 separate permutations of cup lip radii and cup anteversion. In general, dislocation resistance increased for decreased values of cup lip radius and increased cup anteversion. However, cup edge design demonstrated little effect for cups anteverted at least 15°.

More than half the permutations of cup orientation and lip radius (Figure 79) had peak von Mises stresses that exceeded the yield strength of wrought CoCr alloy [231]. A few situations of cup version also exceeded the material yield strength, but this happened only for cups positioned in less than 12° of anteversion (Figure 80).

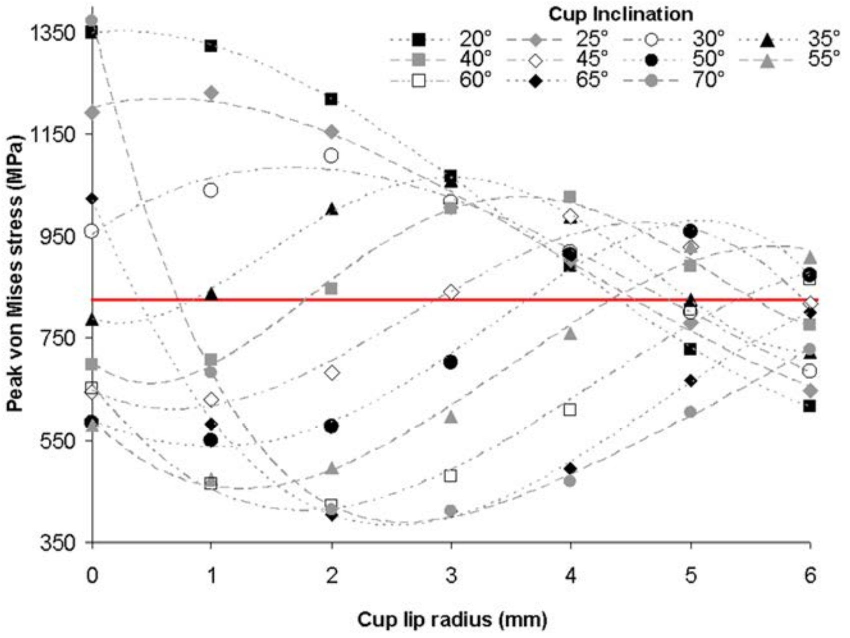

Figure 79: Computed peak values of surface (contact) von Mises stress versus cup lip radius for the eleven cup inclinations. For the higher cup inclinations (60°, 65° and 70°), polynomial regression trends (broken lines) demonstrate a distinct intermediate cup radius (~1.7 – 2.6 mm) for which peak contact pressure is predicted to be minimal. By contrast, trends for lower cup inclinations (20°-40°) all demonstrated a distinct radius for which peak contact stress is maximized. Intermediate cup inclinations (45°, 50° and 55°) demonstrated lip radii having both local minima and maxima of peak contact stress. Many of the permutations of cup lip radius and cup inclination demonstrated surface stresses in excess of the yield strength of wrought Co-Cr alloy (827 MPa, horizontal solid line), indicating a likelihood of permanent material deformation at the cup edge.

Computed scraping wear (Figure 81), when polynomial-regressed, tended to demonstrate similar dependency upon lip radius and cup inclination as was observed for peak stresses, with (worst-case) local maxima identifiable for each inclination investigated. The geometry and magnitude of computed scraping wear was consistent with head damage patterns seen in posteriorly dislocated femoral head retrievals (Figure 82).

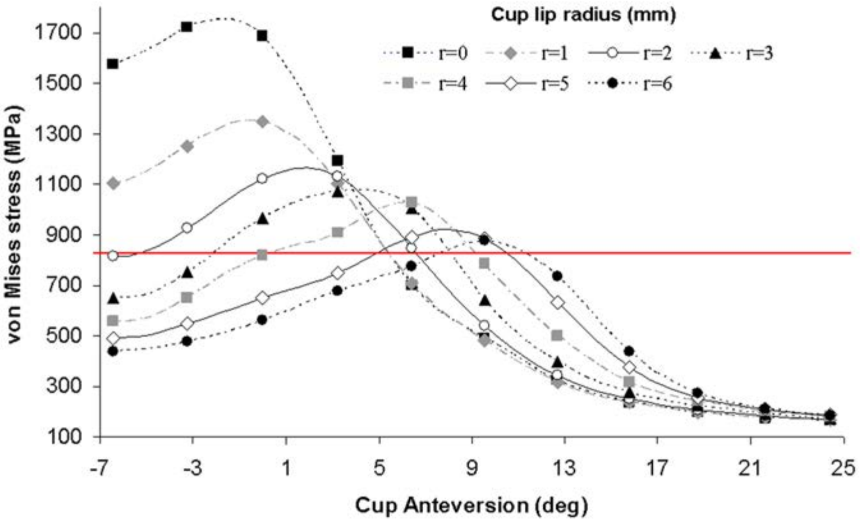

Figure 80: Peak surface von Mises stress versus cup version, for the seven cup lip radii. Variations in surface stress were greatest for lower values of cup anteversion, but demonstrated minimal variation for cups in 9° or more of anteversion. Many permutations of cup lip radius and cup orientation demonstrated surface stresses in excess of the yield strength of wrought Co-Cr alloy (horizontal solid line), indicating high likelihood of permanent deformation at the cup edge.

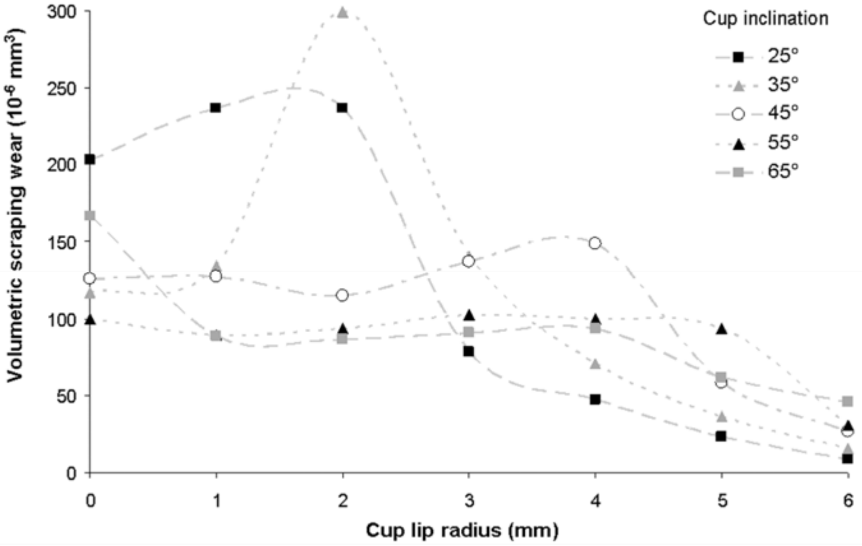

Figure 81: Computed values of volumetric scraping wear versus cup chamfer radius for various cup inclinations at 6° of anteversion. Scraping wear tended to decrease with increasing lip radius, especially for radii above 2mm, but there were several instances of heightened scraping for conditions of low inclination and small lip radius.

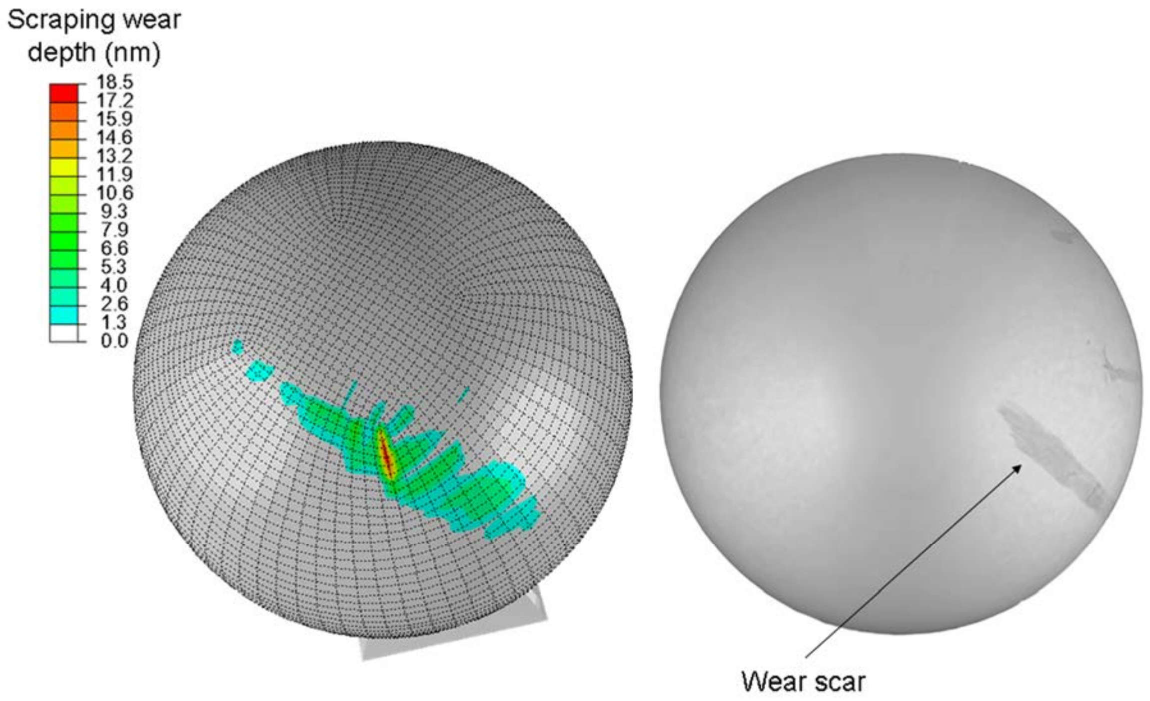

Figure 82: Scraping wear scar computed on the femoral head for a 40° inclined, 6° anteverted cup with a 3 mm radius. A similar damage feature is apparent on a femoral component head (similar trunnion taper axis orientation) from an implant that was revised at 2 months due to dislocation.

Discussion of Cup Design and Edge Loading Series

The precisely engineered elastohydrodynamic lubrication conditions in hard bearings afford excellent wear properties during normal conformative articulation, but these conditions no longer exist during edge loading. Rather, for edge loading situations, there is greatly accelerated bearing surface wear, and possible scraping wear from head engagement with the cup lip. The effect of cup orientation on bearing surface wear of hard bearings has been extensively investigated. Although most clinical retrieval and simulator studies have identified increased bearing surface wear for high inclination [217-219, 223], some have not [224, 232]. Similarly, controversy exists regarding acetabular anteversion effects, with both increased [212, 224] and decreased [222] wear having been measured. This inconsistency may be due in part the substantial differences of articular arcs among cup designs: 151.8° - 165.8° in one recent retrieval series [229]. (Interestingly, at 151.8°, the implant in that particular series (ASR, DePuy, Warsaw, IN) had even less coverage than the lowest-covering implant in the present study (153.5°, Figure 72)). Additionally, predilection to different challenge activities by individual patients might also explain some of the high variability in orientation-vs.-wear relationships.

Edge loading is associated with soft tissue laxity and with ensuing micro-separation during gait [226-228]. For gait-associated micro-separation, the most severe stresses occur near the superiolateral rim of the cup [228], an effect that tends to be worsened by increased cup inclination [226]. By distinction, this study addressed the more severe (albeit less frequently occurring) posterior lip edge loading arising from high hip flexion [222, 233] associated with leaning-type maneuvers. Leaning can progress to frank posterior dislocation for certain combinations of cup design and orientation even without impingement, whether of neck-on-liner/shell or of bone-on-bone [168].

Corroborated by Hertzian contact analysis [234] it is intuitive that a reduction in contact stress with increased lip radius would occur for micro-separation loading conditions [228, 230]. However, these data suggest that micro-separation perhaps should not be viewed as an entirely “independent” variable for hard-on-hard wear simulations. Rather, design-dependent differences in cup lip geometry unavoidably influence subluxation dynamics, and therefore micro-separation severity, at the whole-construct level.

Computed contact stresses and edge scraping wear demonstrated complex relationships with lip geometry and cup orientation (Figures 79-81). Four separate factors interacted to influence the lip stress concentrations: (1) the subluxation resistance afforded by cup orientation; (2) the subluxation resistance afforded by lip geometry; (3) the onset of edge loading, influenced in turn by cup orientation and geometry, and (4) nominal head-cup engagement due to the articulation arc span. For any given cup lip radius, increasing inclination (Figure 77) and increasing anteversion (Figure 78) increased the work required to subluxate the head. Conversely, for any given cup orientation, increased lip radius involved decreased subluxation work. Consider for example a cup with 35° inclination (Figure 79): At a lip radius of 0 mm, edge loading was minimal due to maximal cup coverage of the head (i.e., no subluxation, Figure 75). As the lip radius was increased to 3 mm, the articular arc necessarily decreased, and contact stress was necessarily elevated due to the associated subluxation and edge loading. For lip radii greater than 3 mm, however, although edge contact occurred earlier, edge loading intensity was reduced due to the lower subluxation resistance, and therefore contact stress was reduced. This same relationship held true for scraping wear (Figure 81).

For all but the lowest values of lip radius, the best-case cup orientation fell outside the accepted "safe zone" for dislocation avoidance [46] (Figure 83). That is to say, avoidance of dislocation and avoidance of near-edge stress concentration are divergent goals. Larger lip radii tended to avoid high edge-loading stresses, but their reduced articular coverage is detrimental to stability. Similar observations have been recently made regarding MoM resurfacing prostheses [212, 219, 229], where "cover appeared to be the most important factor explaining wear" [219].

This study is subject to a number of limitations. First, only a single challenge maneuver was considered. There potentially are an indeterminate number of patient-specific challenge maneuvers, and data presently are lacking as to how many and what type of such events occur. However, the particular challenge here considered was useful in isolating the effect of cup design and orientation on near-edge loading. Second, while the present study investigated a total of 147 distinct variants of cup design and orientation, only a single-sized (36mm) implant was considered. Since the increased jumping distance afforded by large heads [235] helps protect against dislocation [236], it would be expected that larger heads would influence the tendency for scraping wear. The effect of head size on posterior edge-loading wear is an inviting subject for future studies.

In conclusion, these data demonstrate complex relationships between cup lip geometry, cup orientation and edge loading-associated scraping wear. Under subluxation conditions, more radiused cup edges can unintentionally lead to elevated contact pressures, higher risk of material yield, and/or more severe scraping wear. And, importantly, even small changes in bearing surface design can dramatically influence these THA performance parameters.

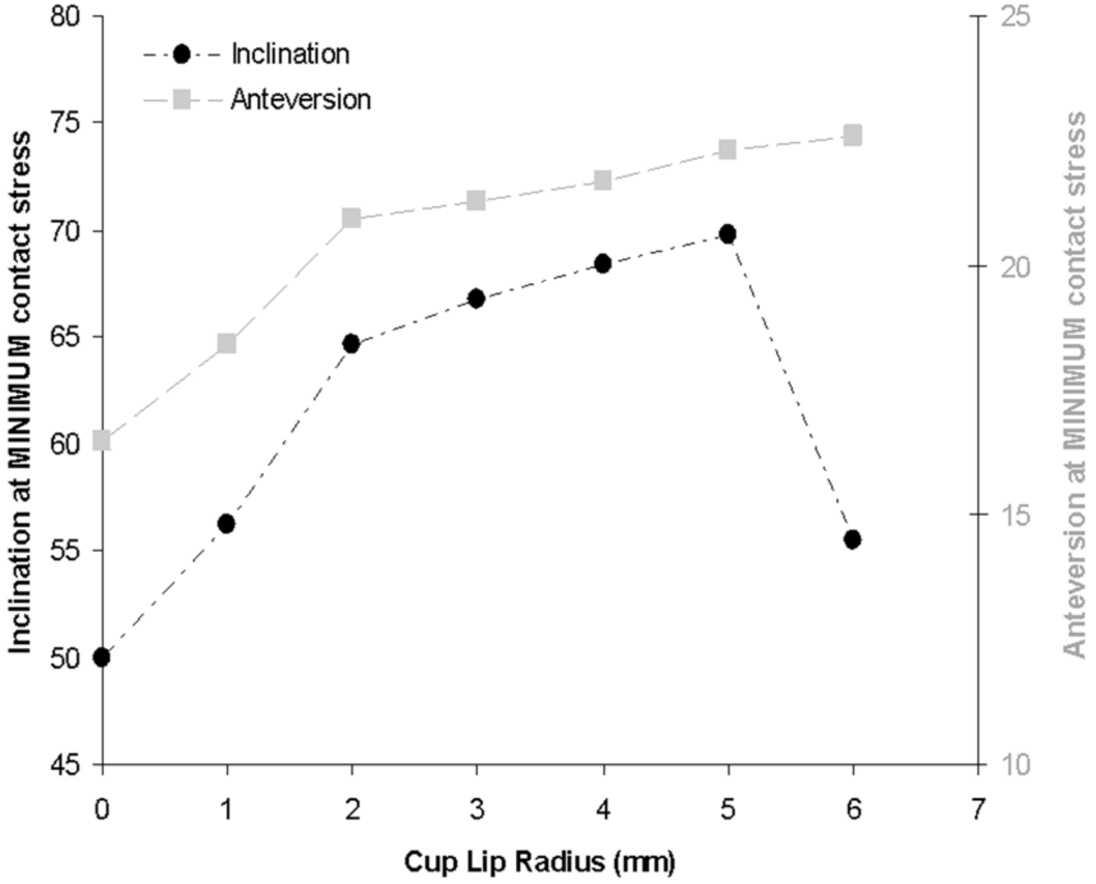

Figure 83: As a function of lip radius, values for inclination angle (left axis, circle symbols) and anteversion (right axis, square symbols) having the minimal peak surface stress. For cups with a lip radius greater than 1 mm, these “best-case” cup orientations lie outside the generally accepted “safe zone” for THA implantation. Therefore, it is suggested that the best possible cup edge design as regards wear minimization and implant stability is one with an edge radius as small as possible.

Trunnionosis Wear from Large Modular Heads

Introduction to Large Heads and Trunnionosis

Recently, there has been attention focused on increased failure rates associated with the large-diameter femoral heads commonly used in MoM THA [212, 213, 215, 216, 237]. There is increasing evidence that tissue reaction to wear at head/neck interface ("trunnionosis", Figure 84), as opposed reaction to wear at the bearing surface, may play a significant role in failure of large-diameter MoM THAs [215, 216, 238]. Trunnion wear increase for larger diameter heads plausibly might arise due to micromotion accompanying increased offset between the head center and the trunnion interface center of pressure (Figure 85).

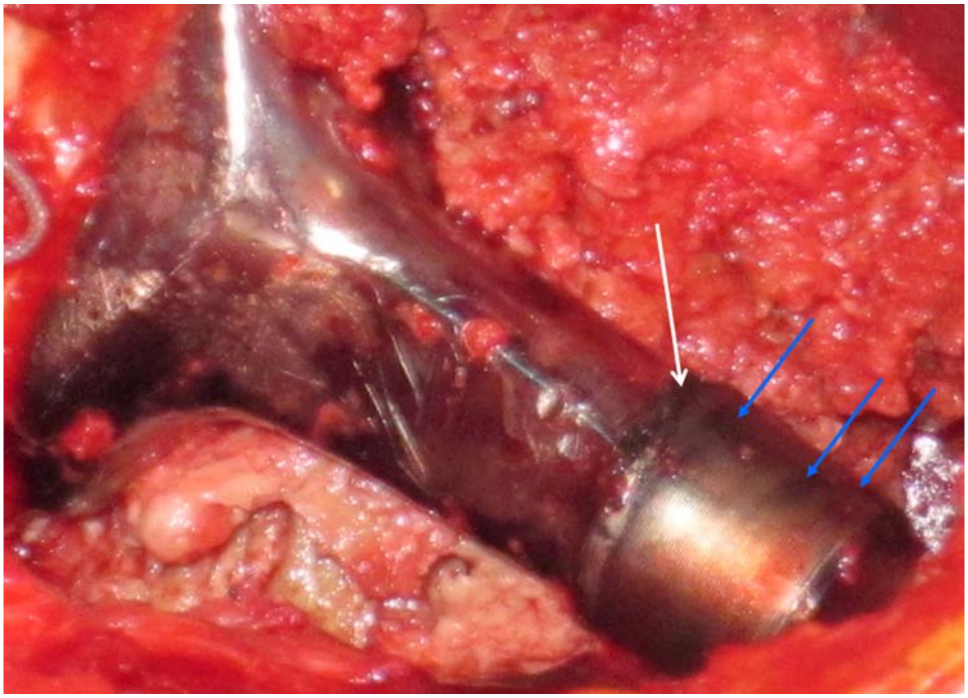

Figure 84: Intraoperative image of an MoM implant trunnion during revision THA, from a patient with pain and elevated metallic ions three years post-operatively. Visually extensive corrosion (white arrow) was identified along the distal aspect of the trunnion. Gross macroscopic wear was identified on the trunnion surface, especially at the leading and trailing edges (blue arrows). Histology confirmed tissue reaction to metal debris.

Femoral head size is a critical consideration for MoM bearings. Tribologic theory dictates improved fluid film lubrication – and therefore reduced bearing surface wear – for increased head sizes [239], a relationship that has been well confirmed by wear simulator testing [240]. Impingement avoidance, facilitated by the increased range of motion accompanying increased head diameter, is even more critical for MoM bearings than for conventional implants, due to impingement-associated accelerated wear potential [165, 241]. However, especially for large head diameters, the exact relationship between head size and joint stability remains unclear. Despite various clinical [161, 242-244], experimental [161, 245] and computational [246, 247] reports, there is no clear agreement as to whether there exists a practical limit as regards to improved stability with head size. Putative femoral diameter cutoffs have been identified at 28mm [161], 32mm [174] and 38mm [245] beyond which increased head diameter no longer improves stability. Additionally, there is conflicting evidence whether the stability afforded by the use of large heads is [174] or is not [248] maintained when there is cup malpositioning. An important limitation to several of these studies of instability has been the use of simplified joint motions or limited ranges of cup orientations.

In consideration of recent observations related to trunnionosis-associated wear from large-diameter THAs, we sought to determine if there was a point beyond which additional gains in stability might begin to be out-weighed by increases in trunnion wear propensity. Using an advanced computational model, we addressed the extent to which large femoral head size influences stability in THA for realistic dislocation-prone motions and (2) the relationships existing between trunnion wear propensity versus head size, cup orientation , hip joint motion, and assembly/impaction load.

Methods for FE Model of Trunnionosis

The FE model consisted of bony anatomy (National Library of Medicine Visible Male Project), the hip capsule, and THA hardware (Figure 85). Manufacturer-provided engineering CAD files of a widely used contemporary THA implant (Summit stem, 36mm M-spec head, 36mm x 56mm Pinnacle cup, DePuy Orthopaedics, Warsaw, IN) were pre-processed using TrueGrid and Mathcad software. Seven distinct femoral head diameters were generated, by projecting the outer surface of the femoral head mesh onto scaled surfaces. The surface geometry of the femoral head bore and its surrounding elements remained identical for each head diameter. The femoral neck, head, and cup liner were modeled as linearly elastic CoCr. Friction coefficients applied to the bearing and trunnion interfaces were 0.1 [170] and 0.15 [249], respectively. In the interest of computational economy, the bony anatomy, shell liner, distal neck and femoral stem were modeled with rigid shell elements.

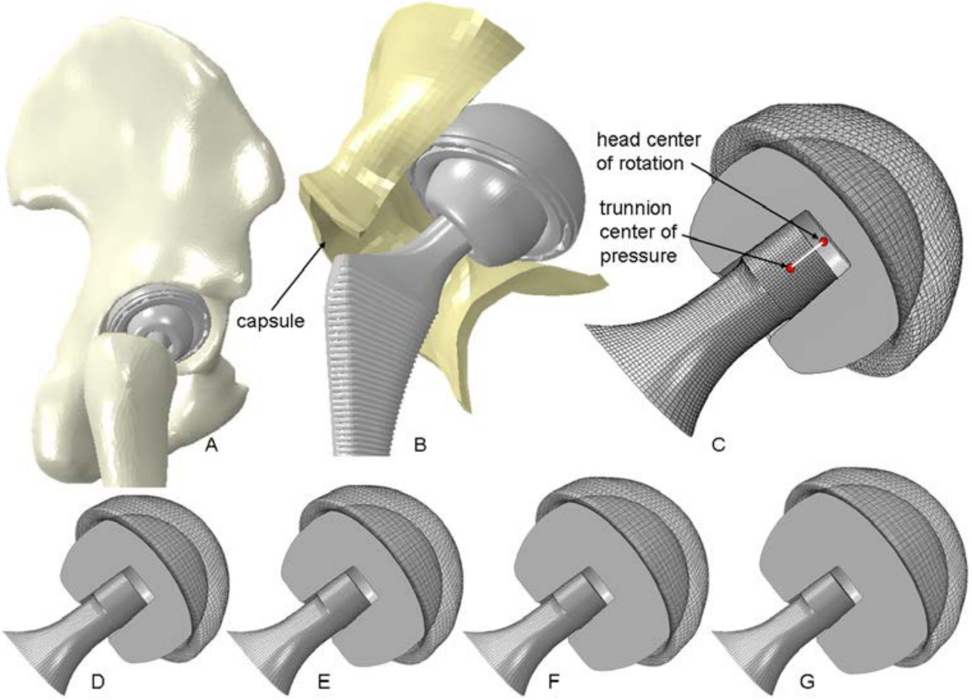

Figure 85: The FE model consisted of THA hardware, bony anatomy (A) and the hip capsule (B). When appropriately seated on the tapered trunnion of the neck, a moment arm exists between the center of rotation of the head and the center of pressure on the trunnion (C). Femoral head diameters used in this study included 32mm (A), 36mm (B), 40mm (C), 44mm (D), 48mm (E), 52mm (F) and 56mm (G). The trunnion/bore geometry was identical for all neck/head assemblies.

The femoral head was assembled ("taper-locked") onto the trunnion of the neck by applying an impaction load having an impulse duration of 20 ms. Impaction loads considered ranged from 1 to 17 kN, applied to the reference node of the head in the direction of the neck axis (Figure 86). Appropriate mesh densities for the trunnion and head bore were determined from a convergence study (Figure 87), where a final mesh density of 10 elements/mm^3 at the interface was determined to provide compromise between solution precision and computational economy.

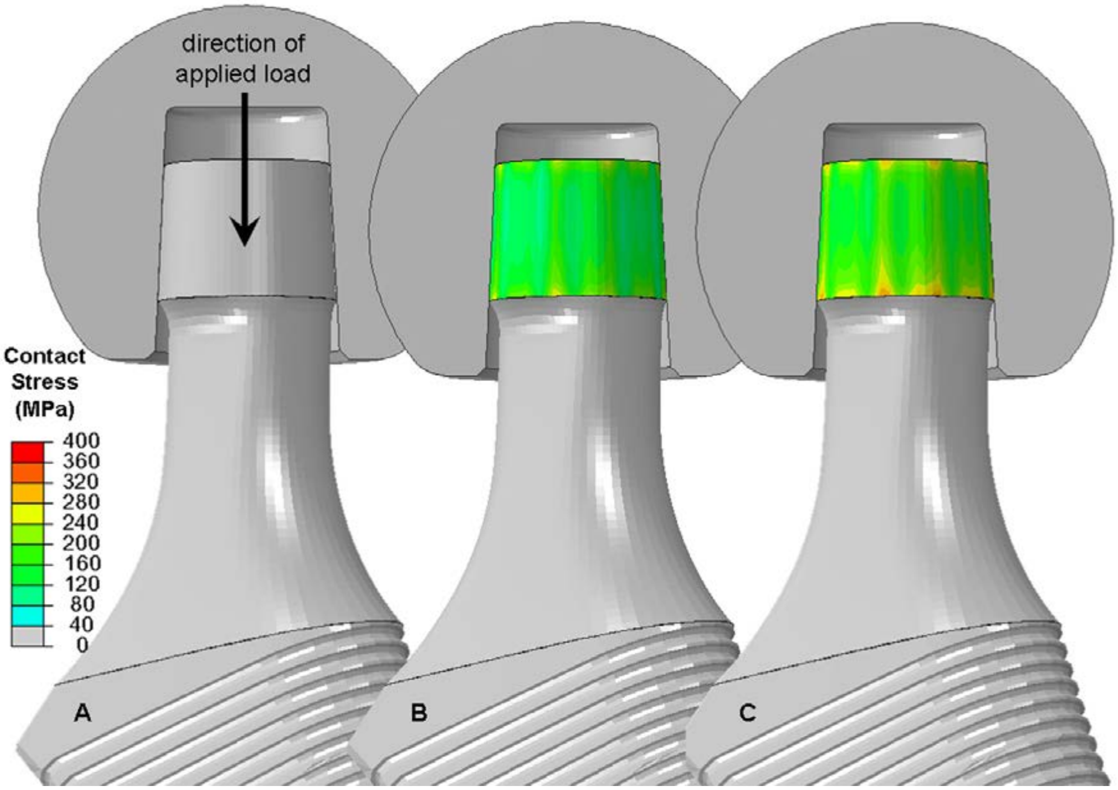

Figure 86: Impaction seating of the trunnion/head interface was performed by simulating a single impulsive (20 ms) load to the femoral head, in a direction parallel to the axis of the trunnion (A), resulting in initial contact between the trunnion and head bore (B). The head was firmly seated at the end of the impaction impulse (C). Loads of 5 kN (baseline), 1 kN and 17 kN were considered [250, 251].

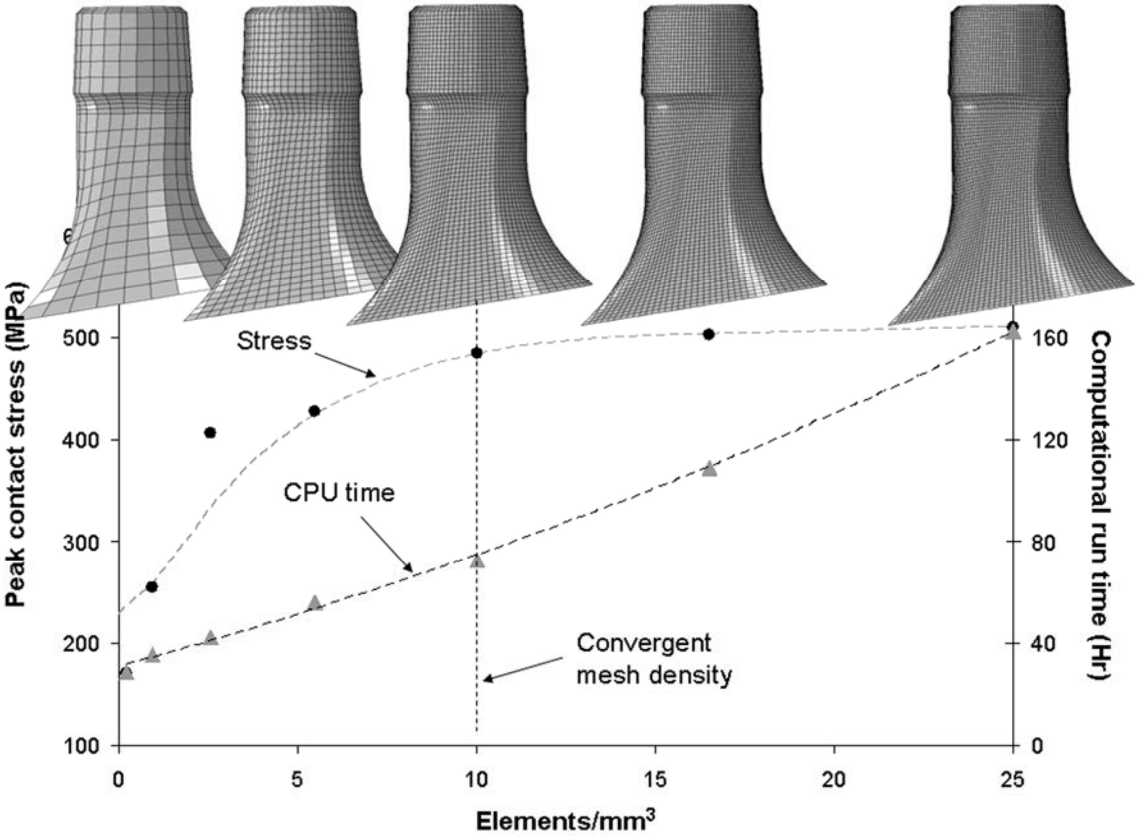

Figure 87: Convergence study for trunnion mesh FE study. A contact analysis convergence study was used to determine the appropriate mesh density used for the trunnion/bore assembly. Peak values of contact stress at the interface were recorded during the head seating analysis step. A nominal mesh density of 10 elements/mm^3 was deemed to provide suitably accurate solutions, consistent with reasonable computational economy.

Head diameter effects on stability were addressed by considering 36 separate cup orientations: six values of acetabular abduction (anatomic definition [163]) (25° - 75°, in 10° increments) and six values of acetabular anteversion (0° to 50°, in 10° increments). Five distinct dislocation-prone challenges [56] were used as kinematic and kinetic inputs for the simulations. This involved four separate posterior-dislocation-prone challenges (stooping, squatting, sit-to-stand from a low chair, and sit-to-stand from a normal height) and one anterior-dislocation-prone maneuver (lateral foot pivoting). This ratio of posterior:anterior dislocation challenges is similar to the posterior:anterior incidence observed clinically [252]. Five distinct values of femoral head size were used in this part of the study: 32mm, 36mm, 40mm, 44mm and 48mm, resulting in a total of 900 distinct FE instability simulations. In all instances, femoral component anteversion was held constant at 10°. The kinematic and loading inputs were applied to a rigid body reference node located at the center of the femoral head. Frictional interaction held the cup liner within the acetabular cup backing, which in turn was rigidly fixed to the bony bed. Because the primary objective of these first 900 simulations was to investigate joint stability rather than trunnion wear, the entire femoral neck was assumed to be a rigid monobloc in order to economize computer run time. For each simulation, femoral head subluxation was tracked through the entire input sequence, as an index of stability.

A second series of 65 FE simulations was undertaken to address the potential for wear debris generation at the trunnion/bore interface. For this series, three cup orientations (radiographic definition) were considered, including horizontally- (25° abduction, 0° anteversion), neutrally- (40° abduction, 15° anteversion) and vertically- (55° abduction, 30° anteversion) positioned cups. Seven distinct femoral head diameters were investigated: from 32mm to 56mm, in 4mm increments. To investigate the effect of activity maneuver on trunnion wear potential, three distinct patient motions were considered: gait, stooping, and sit-to-stand from a normal chair height. For each simulation, contact loads and contact stresses occurring at both the bearing surface and trunnion interface were recorded. To investigate the relationship between trunnion wear propensity and taper seating load, three distinct impaction loads were considered: a standard value of 5 kN [250], a low value of 1 kN, and a high value [251] of 17 kN. Linear and volumetric wear at the trunnion interface was modeled using the Archard-Lancaster formulation [171]. For these trunnion-wear simulations, a wear factor of 1.13×10^{-8} mm^3 $N^{-1}m^{-1}$ was used [172].

Results of Trunnionosis FE Model

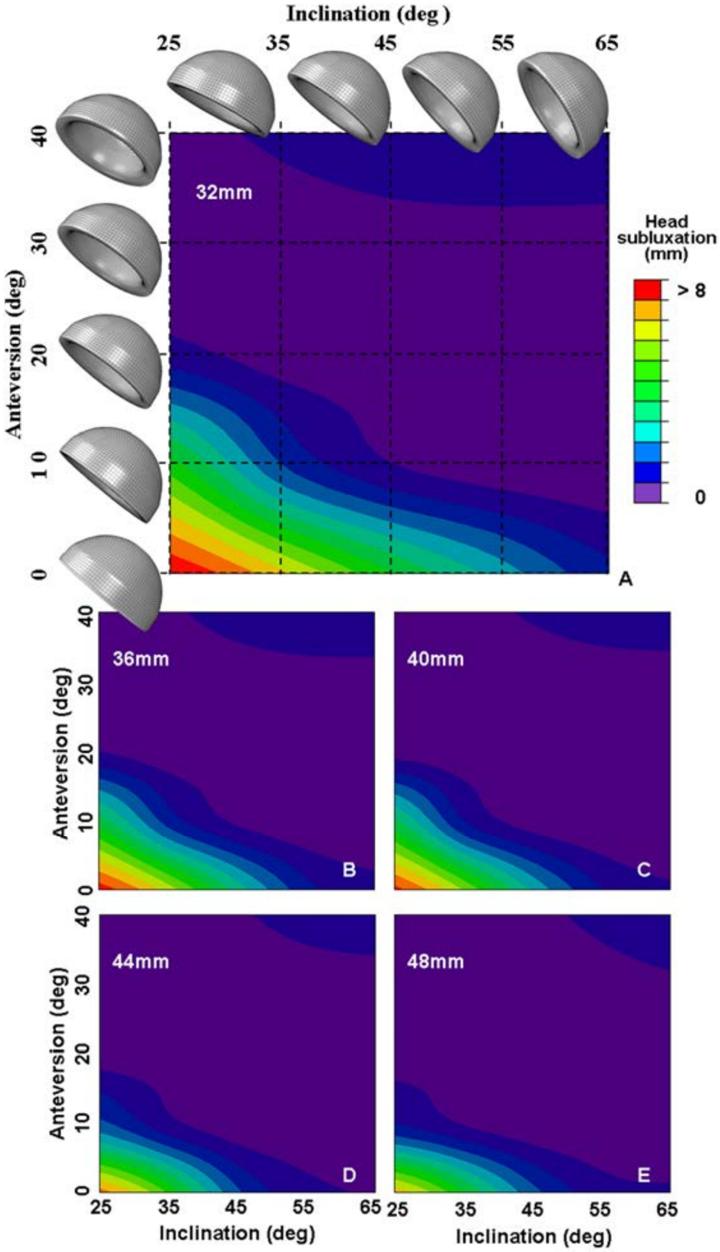

Figure 88: Femoral head subluxation. Subluxation was tracked during the entire kinematic sequence for each simulation. Subluxation distance during the five dislocation challenges were averaged for each of the 36 separate cup orientations (radiographic orientation) for a femoral stem in 10° of anteversion. For the 32mm head diameter (A), average femoral head subluxation was greatest for cups positioned in low values of acetabular anteversion and inclination as well as for cups positioned in high anteversion. Subluxation was similarly influenced for head diameters of 36mm (B), 40mm (C), 44mm (D) and 48mm (E).

Femoral head subluxation propensity was found to be strongly dependent upon both cup orientation and femoral head diameter (Figure 88). Femoral head subluxation propensity was greatest at low values of cup inclination and low values of cup anteversion (for posterior instability challenges), and at high values of cup anteversion (for anterior instability). Increasing femoral head diameter had a more pronounced effect on reducing subluxation for the posterior instability challenges than for the anterior challenge. Instability was preceded by (component-on-component) impingement for most cases, although some situations of foot pivoting with larger heads resulted in spontaneous (slide out [220]) dislocation. Using femoral head subluxation of less than 1mm as a definition of stability (Figure 89), substantial improvement in stability occurred when femoral head size was increased from 32mm to 36mm. However, further gains in stability with increased head size were progressively less evident at higher values of head diameter.

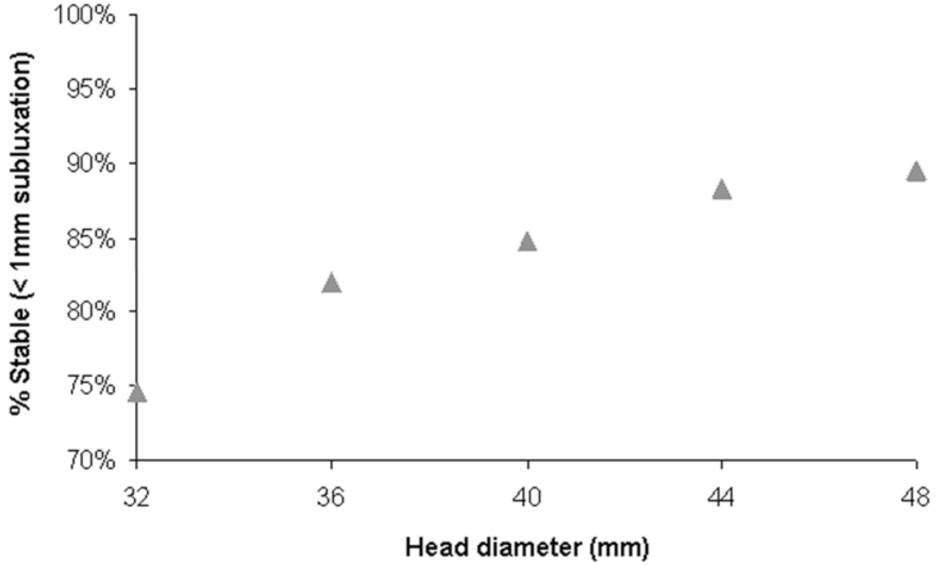

Figure 89: The percent of orientations yielding a stable articulation (defined as having a maximum femoral head subluxation <1mm) was shown to increase as a function of femoral head diameter. The effect of increasing head size was greatest when moving from 32mm to 36mm, while there was progressively diminishing improvement in stability with the further increases of head diameter.

At the bearing surface, the peak (von Mises) contact stress decreased appreciably when head diameter increased from 32mm to 40mm, for gait, for stooping and for sit-to-stand for neutrally- and vertically-positioned cups (Figure 90). For horizontally-oriented cups, impingement and the resulting subluxation and edge-loading caused substantially increased peak stress.

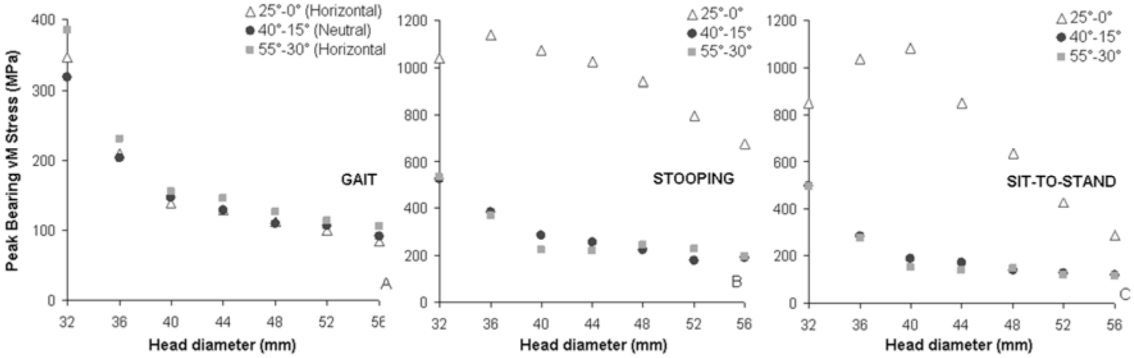

Figure 90: Peak values of surface von Mises (vM) stress occurring at the articular surface were determined for each simulation. For gait (A), bearing surface stress decreased precipitously when head diameter was increased from 32mm to 36mm, for all three cup orientations. Progressively more modest decrements in bearing surface stress with increased head diameter were observed for head increases beyond 36mm. Similar relationships were observed for stooping (B) and sit-to-stand (C) for the neutrally and vertically positioned cups. For both of these latter dislocation challenges, surface stress was greatly increased for horizontal cups, due to impingement, subluxation, and significant edge loading.

By contrast with the bearing surface, peak stress developed at the trunnion interface (Figure 91) demonstrated unabated (or in some cases even progressively increasing) sensitivity to femoral head diameter. For gait (Figure 91A), increasing the head diameter from 32mm to 40mm increased peak stress on the trunnion by only approximately 3.5%. Further increasing head size to 44mm increased peak trunnion stress by 9.5% relative to that for 32mm. However, increasing head size to 48, 52 and 56mm resulted in stress increases (compared to 32mm) of 24%, 40% and 51%, respectively. Similar trends were observed for the sit-to-stand simulations (Figure 91B). For stooping

(Figure 91C), a comparable dependency of trunnion stress on femoral head size was observed for neutrally- and vertically-oriented cups. For horizontal cups, the decreased trunnion stress compared to the two other cup orientations was due to frank dislocation occurring for the lower values of head size (32-40mm), prior to attainment of peak joint contact loads. For head sizes >40mm, subluxation and eccentric loading of the head caused higher stresses to develop at the trunnion than occurred for neutral or vertical cup orientations.

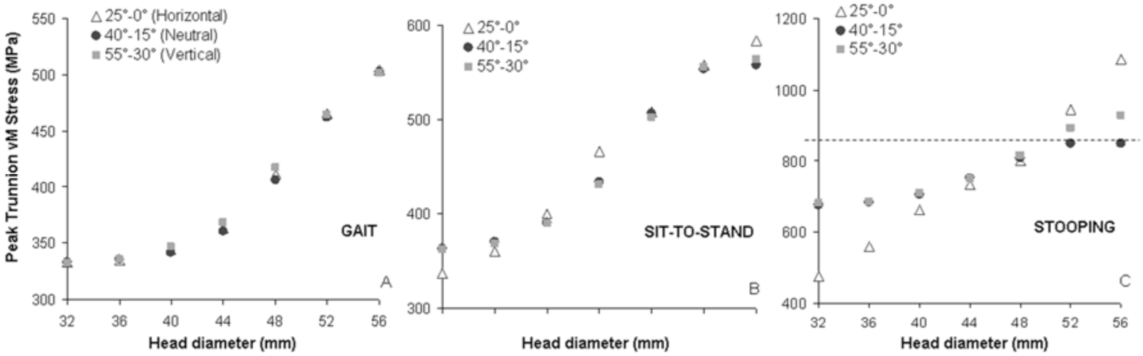

Figure 91: Peak values of von Mises (vM) stress occurring at the trunnion were found to increase with increased femoral head diameter for all three cup orientations during the gait motion challenge (A). The influence of head diameter on trunnion stress was progressively more pronounced for higher head diameters. A similar dependency of head diameter on trunnion stress was also observed for the sit-to-stand (B) and stooping (C) challenges. (Stooping simulations with horizontally positioned cups at lower values of head diameter resulted in frank dislocation before maximum joint contact stresses could be developed, resulting in lower values of trunnion stress.) For stooping, stresses at higher values of head diameter were found to approach or exceed the yield stress of CoCr (broken horizontal line), indicating increased potential for plastic yield on the trunnion surface for larger head diameters.

Micromotion (nodal slip) at the trunnion/bore interface varied according to the kinetics and kinematics of the patient motion cycle (Figure 92). Assembly/impaction seating of the head onto the trunnion resulted in slip aligned with the long axis of the interface. Increased frictional torque at the bearing surface resulted in rotational slip along the neck axis, while increased joint forces produced slip again predominantly parallel to the neck.

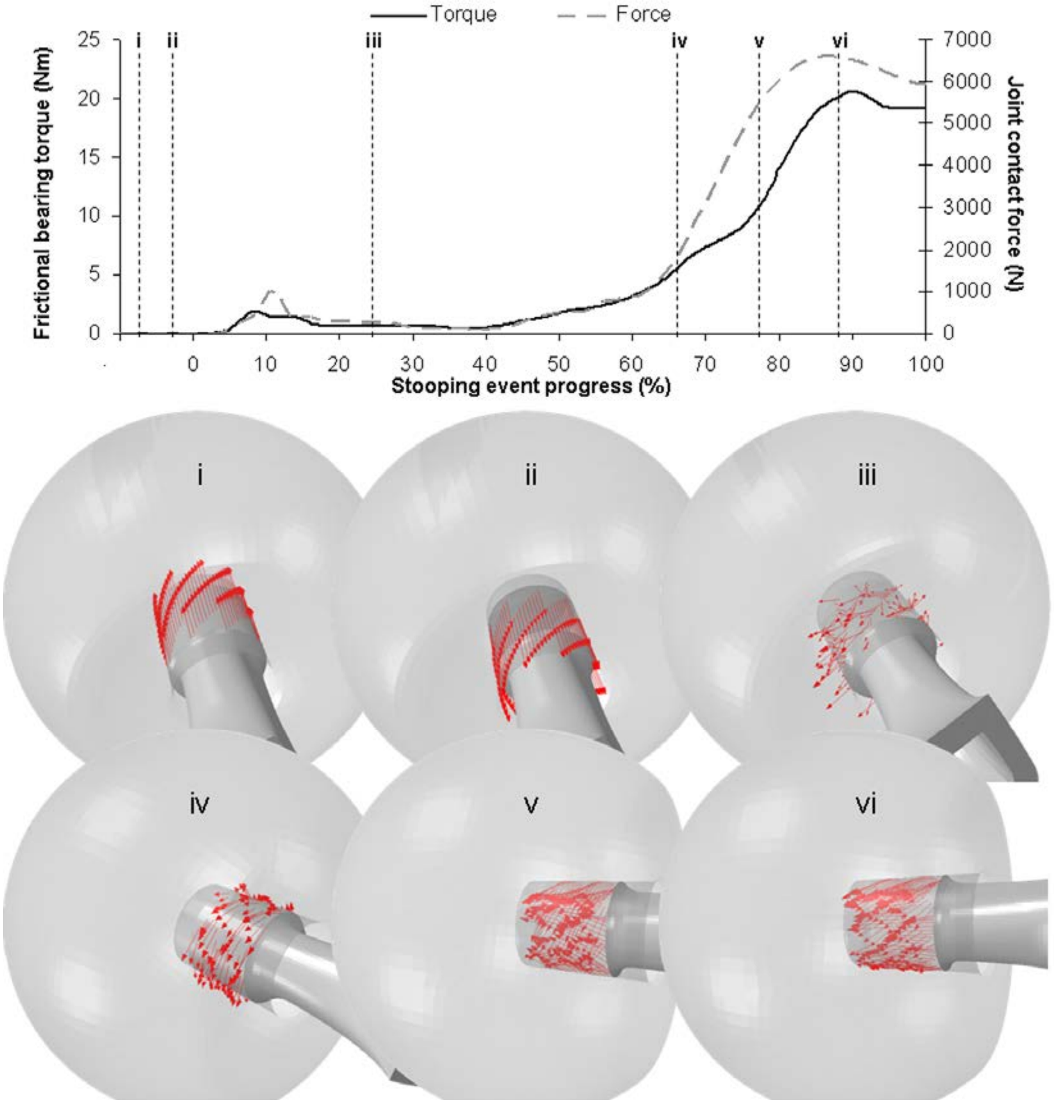

Figure 92: Relative nodal slippage (micromotion) during the input assembly/motion simulations occured in six distinct modes. Trunnion assembly during impaction resulted in vertical slip of interface nodes (i). After the impaction load, elastic recoil in the trunnion/bore interface resulted in relaxation of the assembly, and slip in the opposite direction (ii). During the motion sequence, node slip was minimal during low values of joint contact load and bearing surface frictional torque (iii). For intermediate values of both bearing surface frictional torque and joint contact force, net slipping was primarily rotational (iv). Further increasing both bearing surface frictional torque and joint contact loads resulted in a mixed rotational/translation slip (v). At peak values of joint contact load, slip was primarily parallel to the axis of the trunnion/bore (vi).

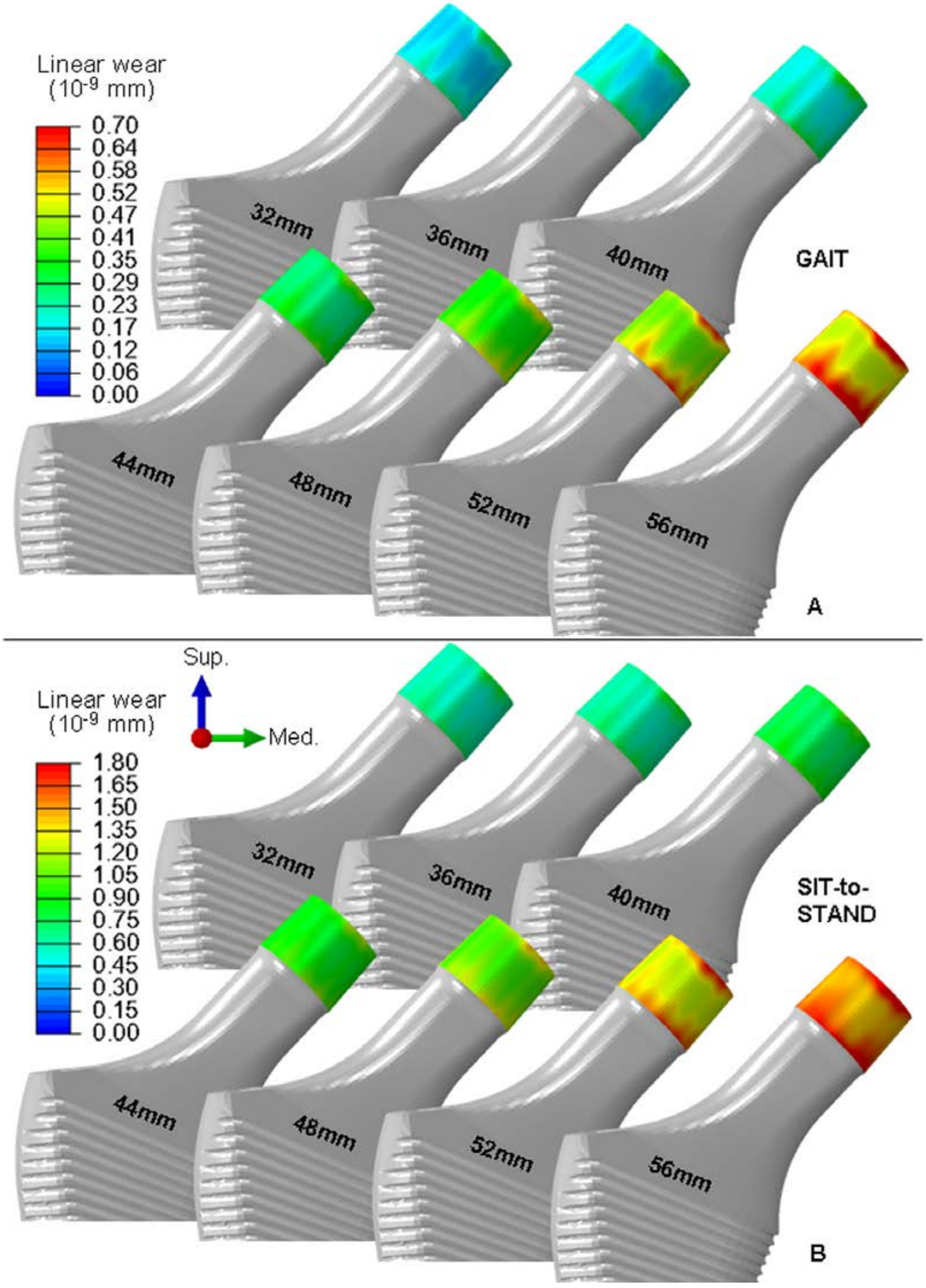

Figure 93: Micromotion of the trunnion relative to the head bore resulted in the generation of linear wear on the interface surfaces. Total cumulative linear wear for gait at the end of the motion cycle (A) was approximately half that occurring for the sit-to-stand (B). For all motions, linear wear increased with increased femoral head diameter.

Head-diameter-dependent trends for (Archard) computed linear wear (Figure 93) generally followed those for contact stress. Trunnion linear wear demonstrated a predilection to be most severe near the leading and trailing edges of the trunnion, similar to the trunnion wear scars observed during revision (Figure 84). Trunnion volumetric wear (Figure 94) demonstrated similar trends. Volumetric wear during gait (Figure 94A) was slightly elevated for vertically-positioned cups.

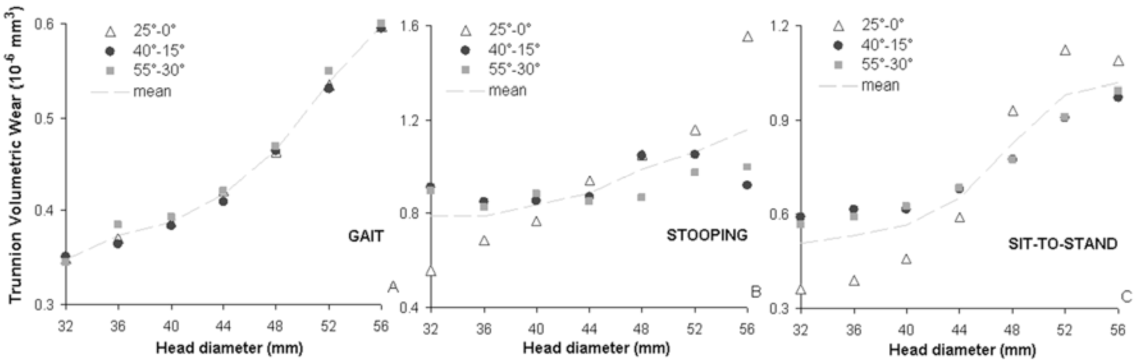

Figure 94: Volumetric wear at the trunnion demonstrated strong dependence upon head size for gait (A), stooping (B) and chair rising (C). This dependency of head size was most pronounced at higher values of head diameter.

The magnitude of impaction load used to seat the femoral head substantially influenced trunnion contact pressure (Figure 95), trunnion micromotion (Figure 96), and trunnion volumetric wear (Figure 97). As would be expected intuitively, increased impaction force resulted in increased trunnion stress, and therefore more trunnion interfacial frictional stress to resist micromotion. However, wear depends upon both contact stress (increased for stronger impaction) and on micromotion (decreased for stronger impaction). Therefore the overall effect of increased impaction force on trunnion interface wear was much less pronounced than on either contact stress or micromotion alone, and indeed, was almost negligible (Figure 97). This is very different than the effect of increasing head diameter, where both trunnion contact stress and micromotion unremittingly increased, therefore greatly increasing computed interface wear.

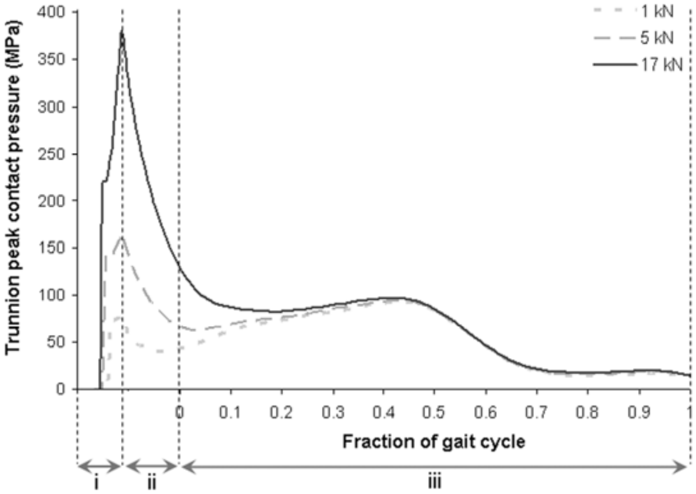

Figure 95: The FE simulation consisted of three distinct phases. The femoral head was impacted onto the trunnion (i) resulting in the rapid development of contact pressure at the interface. After the impulse loading, the trunnion/bore interface underwent elastic recoil (ii) until static equilibrium was reached. Then the motion cycle was run (iii) (gait in this example). While the use of higher impaction loads resulted in substantially greater initial contact pressure, all three simulations converged towards similar values of pressure during the simulation.

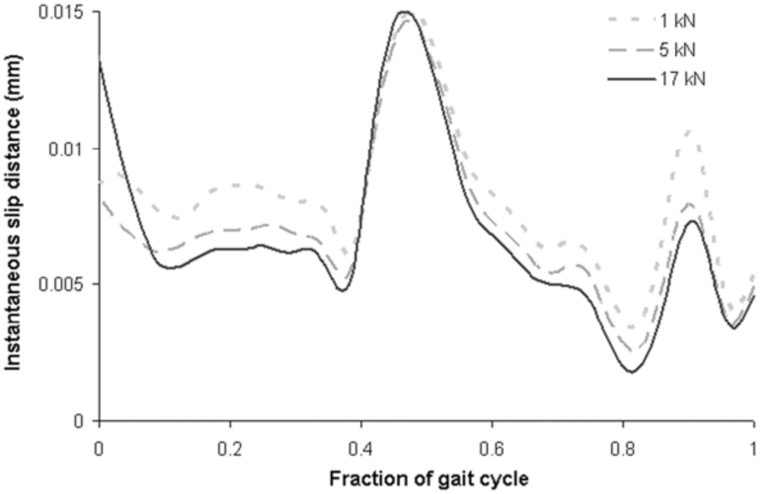

Figure 96: Increased interface motion, measured in terms of instantaneous slip distance between nodes at the interface, was seen for the simulation with a low (1 kN) impaction load, versus normal (5 kN) or increased (17 kN) loads.

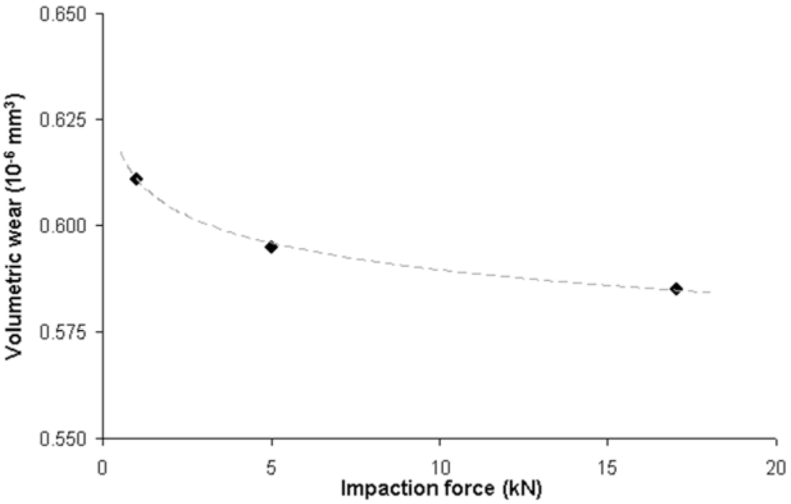

Figure 97: Increasing the value of impaction force decreased the volumetric wear occurring at the trunnion interface. This relationship exhibited exponential-type decay (inverse power law regression)

Discussion of Large Diameter Heads and Trunnionosis

While the theoretical advantages of large diameter MoM bearings hold attraction, actual clinical utility is currently an open question. Using an FE formation coupled with physiologically-realistic input motions and loads, parametric series were designed to address the interplay between (1) THA stability and (2) the propensity for increased trunnion interface wear, for large head MoM THA.

Historically, clinical issues arising from wear at the trunnion interface had been a well-recognized concern [253-255], even prior to the present era of large-sized heads. Various factors affecting wear had been empirically identified, including implantation time [255, 256], alloy composition (especially regarding galvanic corrosion effects) [256-258], joint load magnitude [259], numbers of loading cycles [255], moment arm [256, 260], and frictional torque at the bearing surface [261]. However, many of these factors were related to design inadequacies and/or inappropriate manufacturing tolerances for earlier-generation devices [262]. Indications of relatively low corrosion at the trunnion/head interface [263], and excellent intermediate-term survival [208] for (modest diameter) modern MoM implants, suggest that the trunnion interface is not necessarily the weakest link for all MoM implants. However, the emerging clinical picture for large-diameter modular THA is not so clear. Given the recent reports of high rates of trunnionosis-associated failure [215, 216, 238], along with increased incidence of pseudotumors [207] during comparatively short follow-up [237, 243] with large diameter implants, the use of large diameter MoM implants warrants further biomechanical and clinical scrutiny, especially in light of disturbingly-elevated revision rates for large-diameter THA in the most recent registry data [264].

The utilization of large heads in modular THA is an archetypical example of the "choices and compromises" [265] inherent in design of successful orthopaedic implants. It is well recognized that increasing head diameter reduces impingement, improves stability, and enhances the elastohydrodynamics of joint lubrication. However, it is unclear whether a practical head size limit exists as regards improved overall construct performance, given the potentially adverse effects at the trunnion interface. The present study sought to determine if such a limit could be indentified for large-diameter MoM bearings. Instability continues to be a major clinical concern in THA [41], with impingement avoidance being a particularly significant consideration for MoM bearings. The present data indicate diminishing further improvement of intrinsic joint stability for head diameters beyond 40mm (Figure 89). However, stress at the trunnion interface (Figure 91) continued to increase unabatedly for head diameters larger than 40mm for normal-function scenarios where impingement-associated edge-loading did not occur. Correspondingly, a tendency for increased wear at the trunnion interface continued, similarly unabated, for head sizes greater than 40mm (Figure 94).

Additional choices and compromises undoubtedly apply also to design of the trunnion. While it has been well established that increased trunnion diameter significantly reduces wear potential at this interface [256], implant manufacturers place high emphasis on keeping neck diameters low, in order to maintain favorable head:neck ratios. From a biomechanical viewpoint, it is plausible that a point of diminishing returns similarly exists between reduced taper diameter and improved impingement/stability. Quantification of the choices and compromises of using larger trunnions is another attractive avenue for further parametric investigation.

In summary, these parametric results corroborate recent clinical evidence that large-diameter heads for MoM THA have a tendency to cause deleterious wear generation at the head/neck interface. The propensity for trunnionosis-inducing wear increased substantially for head diameters greater than 40mm, and for malpositioned cups that underwent impingement. The tendency for trunnion wear could be only weakly influenced by higher impaction assembly/loading on the neck.

Optimizing Metal-on-Metal THA

Mounting concerns with MoM hip implants over approximately the last two years have resulted in the issuance of a UK Medical Device Alert (U.K. MHRA MDA/2010/033), and in the voluntary recall of all DePuy ASR THA and hip resurfacing prostheses. National joint registries [264, 266] have indicated disturbingly high failure rates for some MoM devices, with revision rates as high as 29% after 6 years for some implants [266]. Despite nearly seven decades of development and use, these recent events perhaps foreshadow the impending dismissal of MoM THA (again). However, a call for the total abandonment of MoM THAs may not be justified. Several reports of contemporary second-generation MoM THAs have demonstrated survival rates greater than 95% at up to ten years postoperatively, rates which are better than those for contemporary metal-on-polyethylene THA [267-282]. Additionally, excellent survivals at 30+ years postoperatively have been observed with McKee-Farrar MoM, with minimal wear and soft tissue engagement [31, 32]. And, as mentioned previously, MoM implants hold advantages – particularly the possibility to use larger femoral heads – not available with other bearing surfaces. How then might one explain the distinct incongruity between the majority of MoM THAs (which demonstrate excellent clinical results) versus that of a smaller subset with poor outcomes? As discussed and analyzed in the preceding two sections, (often subtle) implant design considerations can have pronounced effects on THA biomechanical performance. However, factors directly within the surgeon's control may influence outcome to a similar or perhaps even greater degree. The purpose of this final investigation was to indentify and analyze surgeon-controlled factors, and to quantify the extent to which those factors affect both short- and long-term outcome predictions in THA.

Surgical Factors Influencing Metal-on-Metal THA

The orientation of the cup in the pelvis has a direct influence on hip range of motion prior to impingement. Implantation of the cup at a position that is too vertical (high inclination and version) allows for high flexion, and offers protection against posterior dislocation, but involves increased risk for posteriorly-directed impingement and thus anterior dislocation [283]. Conversely, THAs that dislocate posteriorly often have more horizontal inclination and lower anteversion angles. Historically, a "safe-zone" of cup orientation was described by Lewinnek et al. in 1978 as being 40° ± 10° of inclination and 15° ± 10° of anteversion (radiographic definition). Outside of this safe zone, Lewinnek et al. noted a four-fold increase in dislocation risk (Figure 98).

Analogous safe-zone definitions have been reported from other clinical series [252, 284]. Other investigators have advocated for increased [285] or decreased [286] cup inclination. Owing to the complexity associated with intraoperative or postoperative orientation assessment, various investigators have proposed other methods of identifying optimal cup orientation. Barrack et al. [287], using a rigid-body computational approach, defined optimal acetabular cup positioning as 45°±10° inclination and 20°±10° cup anteversion. Using a mathematical model, Widmer and Zurfluh [288] described optimal placement as inclination of 40° to 45° and acetabular anteversion of 20° to 28°. Other computational [67] and analytical [289] models have identified generally similar, although not identical, definitions of optimal cup placement.

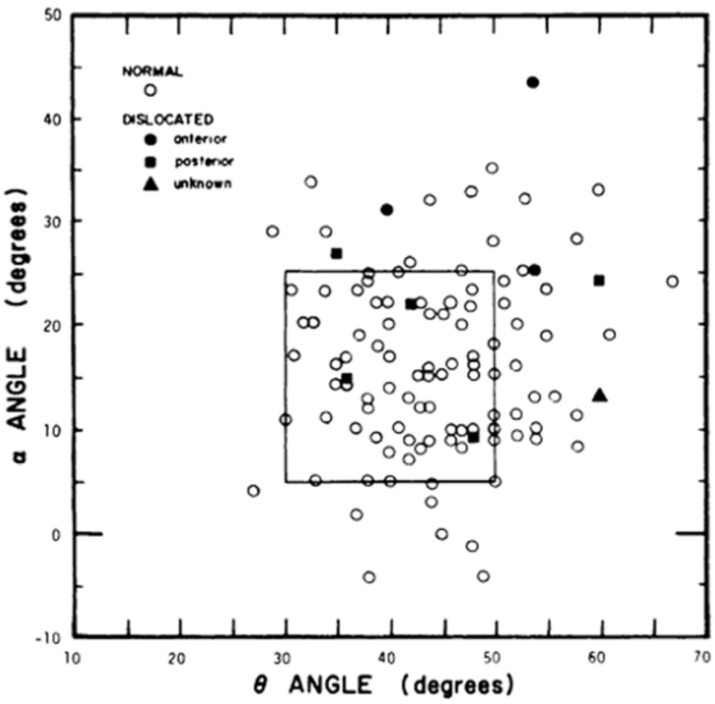

Figure 98: "Safe zone" as defined by Lewinnek et al. [46]. Optimal implantation was determined to be 40° inclination (θ) and 15° acetabular anteversion (α). A four-fold higher risk for dislocation was observed for THAs positioned outside this region.

The preponderance of implant orientation investigation has focused on acetabular cup positioning, with conspicuously less attention being directed toward the effect of femoral stem version. Usually 15° of femoral anteversion is recommended [66]. One study [290] recommended a combined (cup and stem) anteversion of 20° to 30° in males, and 45° in females. Another determined that dislocation risk was 6.9 times higher if combined anteversion was not between 40° and 60° [291]. Using a mathematical model of THA impingement, Widmer et al. [288] suggested that the anteversion of the cup plus 0.7 times the anteversion of the stem should equal 37°. Recently, a similar mathematical study identified a similar regression, independent of head size [292]. Historically, femoral anteversion has been a common source of malpositioning: Fackler and Poss [293] determined excessive femoral anteversion as the most common form of implant malposition, with the stem being outside the accepted range in 44% of patients who dislocated but only in 6% of those without dislocation. However, given the constraints of press-fit stems in most modern implants [294], the stem will necessarily be anteverted to the same degree as the femoral canal.

The design of the implant has been shown to have a dramatic effect on THA stability. The most widely investigated factor has been the use of large heads (or a concomitant increase in the head:neck ratio). Large diameter heads have been introduced to reduce the incidence of impingement and dislocation, by increasing the range of motion. Berry et al. [236] reported dislocation rates of 12.1%, 6.9% and 3.8% when using 22-, 28- and 32-mm femoral head diameters. Several other clinical studies have demonstrated similar relationships [44, 245, 295, 296]. However, the association between increased head size and increased stability has not been shown in all clinical studies. In their review of over 10,000 THAs, Woo and Morrey [47] found that the difference in dislocation rates between 22mm versus 32mm implants (2.9% and 3.3%, respectively) was not significant. In a study comparing 3,200 22mm Charnley stems with 2,900 32mm implants [297], dislocation rates were again similar (2.4% vs. 2.5%) after one year. This differing experience may be related to other factors, such as the head-neck ratio or surgical approach [57].

Therefore, there has been interest in investigating head size and head:neck ratio as modifiers of range of motion, and thus of stability, from a more biomechanical perspective. Using Sawbone-implanted pelves, Burroughs et al. [245] investigated the advantages of 28-, 32-, 38- and 44-mm heads for cups in neutral inclination and in 10°, 30° and 45° of anteversion. The use of a 38mm non-skirted implant increased range of motion (flexion) by 12° compared to a 28mm skirted prostheses. Similar increase in flexion (7°) was seen comparing the 32mm skirted device to a non-skirted 44mm implant. However, when a non-skirted neck was used for each implant, the range of motion in pure flexion was similar for each head size. Bartz et al. [161], using a cadaveric model, demonstrated an improvement in range of motion (flexion at dislocation) when moving from a 22mm head to a 28mm head. However no benefit was seen when comparing a 28mm head to a 32mm head. Using a three-dimensional computational model, D'Lima et al. [246] assessed the range of motion prior to impingement of implants with head ratios between 22 and 32 mm for cups placed within the safe-zone. They concluded that the improvement in range of motion was sensitive to the acetabular cup placement, with cups positioned in higher inclination demonstrating the most improvement when using larger necks.

These laboratory studies, however, have addressed only cup orientations within the conventional safe-zone of cup implantation. Only a single computational study [174] has specifically addressed large heads for malpositioned cups. That investigation corroborated other studies in terms of demonstrating an improvement in range of motion using 38mm heads compared to 28mm heads, with the improvements being greater for instances of cup malpositioning. However, the difference between 32mm heads versus either 36mm or 38mm heads was insignificant, with osseous impingement limiting additional rotational improvement for pure flexion/extension motions.

The overwhelming majority of computational studies which address either cup orientation, femoral head size, or both, use only range of motion as their assessment metric. Impingement and instability involve a complex kinematic and kinetic interaction with significant interplay; assessing only range of motion severely limits the utility of these studies in terms of translation to the clinical environment. Additional variables, such as dislocation resistance and (non-conforming) surface contact stresses are undoubtedly influenced by implant geometric design. To date, only a few computational studies [65, 247] have addressed these additional parameters, rather than just range of motion. Scifert et al. [247], using a physically validated FE model, demonstrated an increase in resisting moment both for increased head:neck ratios and for increased femoral head sizes at constant head:neck ratios, for metal-on-polyethylene constructs. Range of motion at impingement and at dislocation was also shown to be dependent on head:neck ratio (but not on head size *per se*). However, while reported as an output metric for variations in cup orientation, surface stresses were not regressed to head size. Although validated experimentally, their model did not include the effect of periarticular soft tissue, and it used only simplified (planar) motion kinetics.

More recently, Kluess et al.[65] assessed the effects of range of motion, resisting moment and polyethylene contact stress for four separate femoral head diameters, using an experimentally validated FE model. This corroborated the findings from Scifert et al., demonstrating an increase in resisting moment and range of motion for large diameter heads. Additionally, surface stresses at both the impingement site and the head egress site were shown to decrease with increased head sizes, owing to an increase in contact engagement area. Similar to the Scifert at al. study, while experimentally validated, the Kluess model did not include the effects of the capsule on construct stability. Additionally, the bearing geometry was developed from idealized analytical surfaces, and only a few separate orientations were investigated, thus making extrapolation to other head sizes and cup orientations difficult.

Methods for FE Metal-on-Metal Optimization

Given the limited, and often conflicting, data on the biomechanics of component orientation and size, a significant knowledge gap exists concerning how these factors influence outcomes in THA, specifically as regards MoM hip replacement. To take a substantial step forward towards significantly closing this gap, a novel FE study of considerable size and scope was endeavored. This study simultaneously addressed the influence of femoral and acetabular component orientation, as well as femoral head diameter, on both short- and long-term outcome predictions for MoM THA by considering both implant stability and bearing surface wear.

The MoM FE model consisted of CoCr bearings, with model specifics similar to those described previously in this chapter. Orientation effects on implant stability and bearing surface wear were addressed by considering thirty-six distinct cup orientations (anatomic definition), varying the cup inclination (25° to 75° in 10° increments) and acetabular anteversion (0° to 50° again in 10° increments) (Figure 99). These orientations were chosen to ensure that a state-space of 45° ± 20° of cup inclination and 20° ± 20° of acetabular anteversion could be represented in anatomic (Figure 99), operative (Figure 37) or radiographic (Figure 100) orientation.

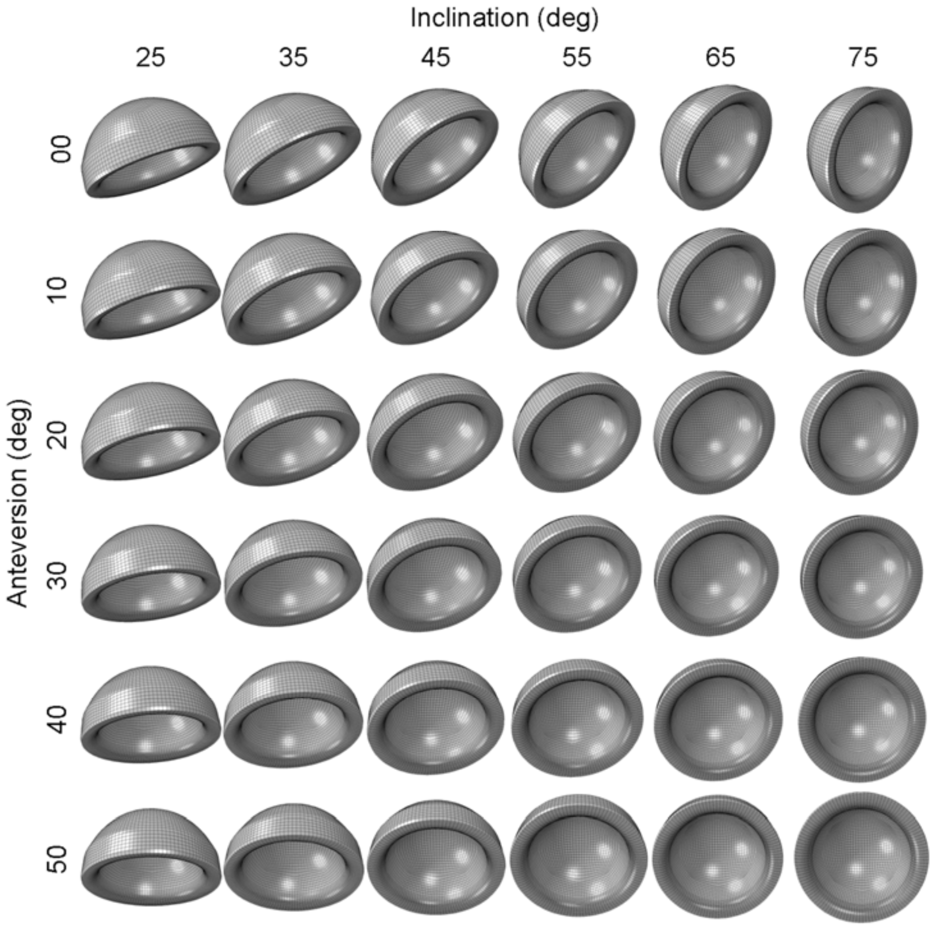

Figure 99: Thirty-six distinct cup orientations were investigated. These were determined using the anatomic reference frame.

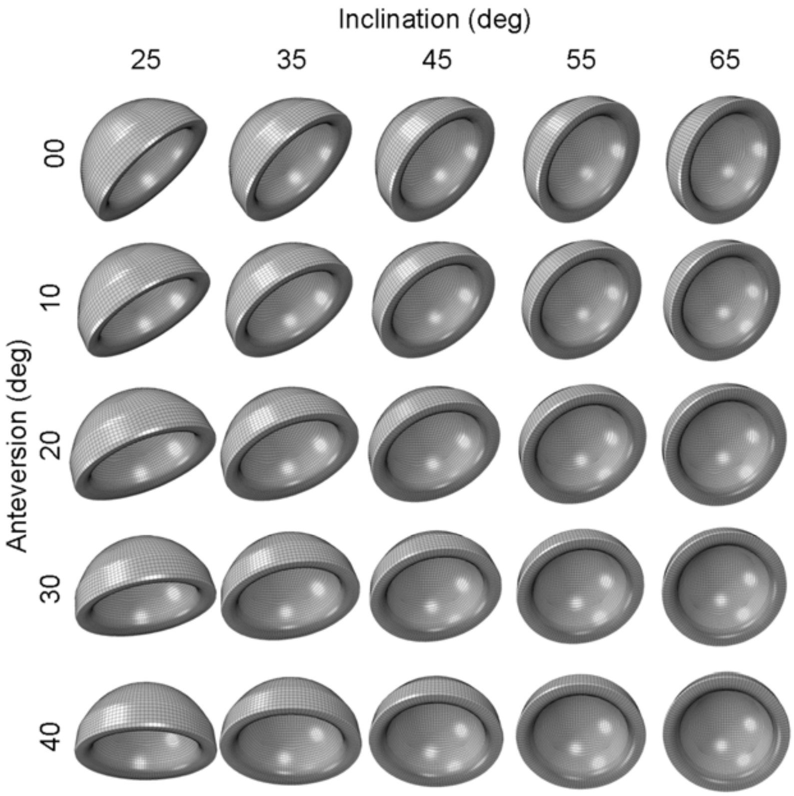

Figure 100: Interpolation of the anatomic cup orientations allows for representation of the FE state-space rendered in the more clinically useful radiographic orientation.

Femoral anteversion was investigated by considering four distinct orientations (0°, 10°, 20° and 30°) (Figure 101). The average femoral anteversion used in this study is similar to that observed radiographically for implanted stems (16.5°) [298, 299], as well as that identified cadaverically [300] (12°) and intraoperatively [294] (10°).

The effect of head size on stability and bearing surface wear was investigated by considering five distinct values of femoral head diameters (Figure 102) that are available for many contemporary modular MoM implants.

Six separate input motion challenges were considered: standard gait, and five dislocation challenges. These included four separate posterior-dislocation-prone challenges (stooping, squatting, sit-to-stand from a low chair, and sit-to-stand from a normal height) and one anterior-dislocation-prone maneuver (lateral foot pivoting).

Again, this ratio of posterior:anterior dislocation directions is similar to the relative incidence of dislocations observed clinically [252].

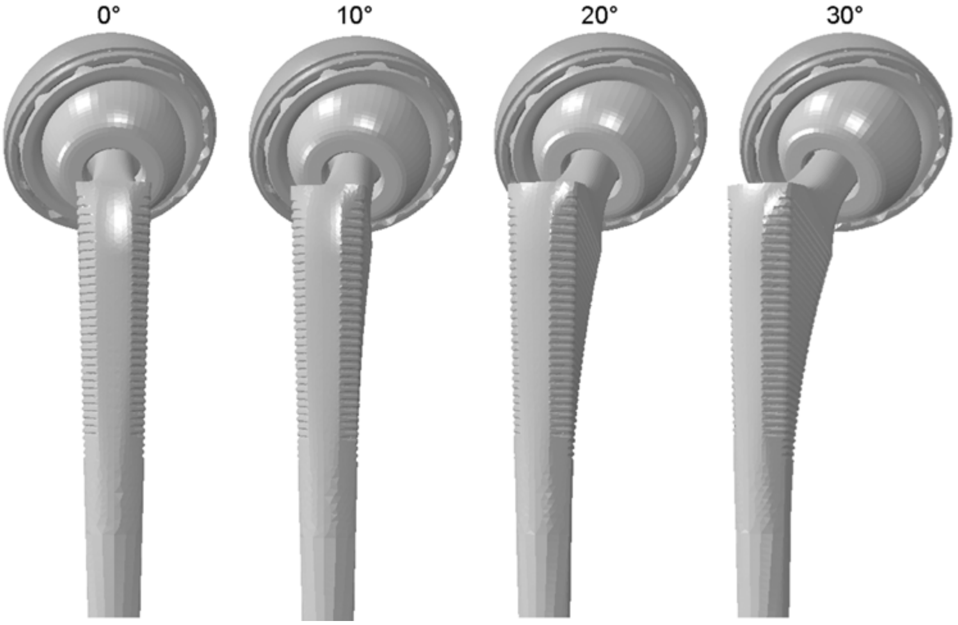

Figure 101: Four values of femoral anteversion were investigated (0°, 10°, 20°, 30°).

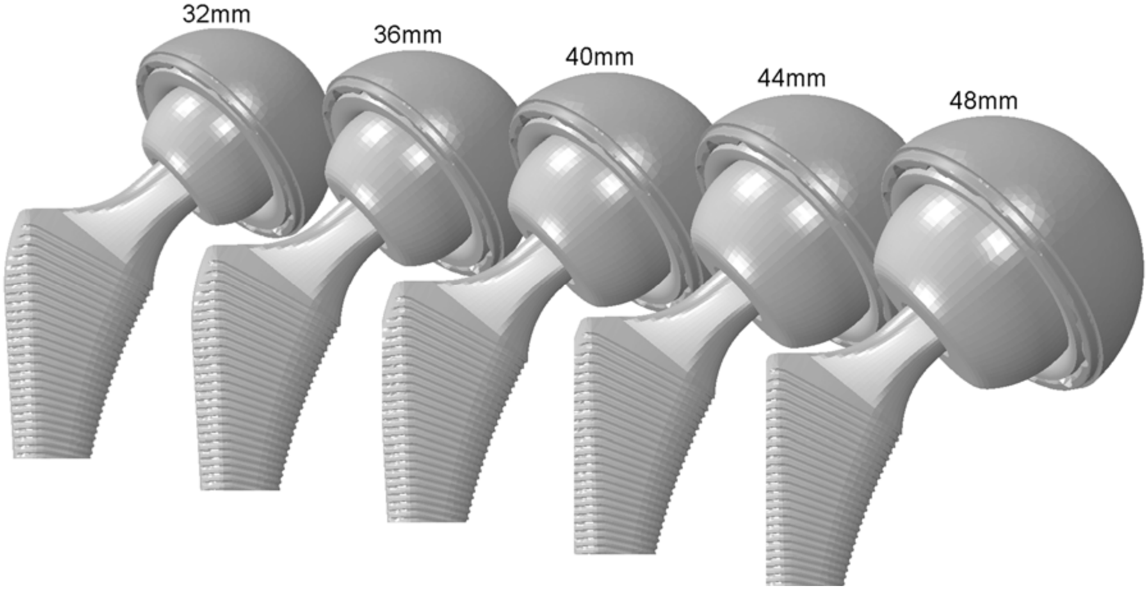

Figure 102: Five femoral head diameters were investigated (32, 36, 40, 44 and 48mm).

The process for identifying optimal conditions for MoM THA was rather involved (Figure 103). A total of 4,320 distinct FE simulations (36 cup orientations x 6 motion challenges x 4 femoral positions x 5 head diameters) were used in the optimization.

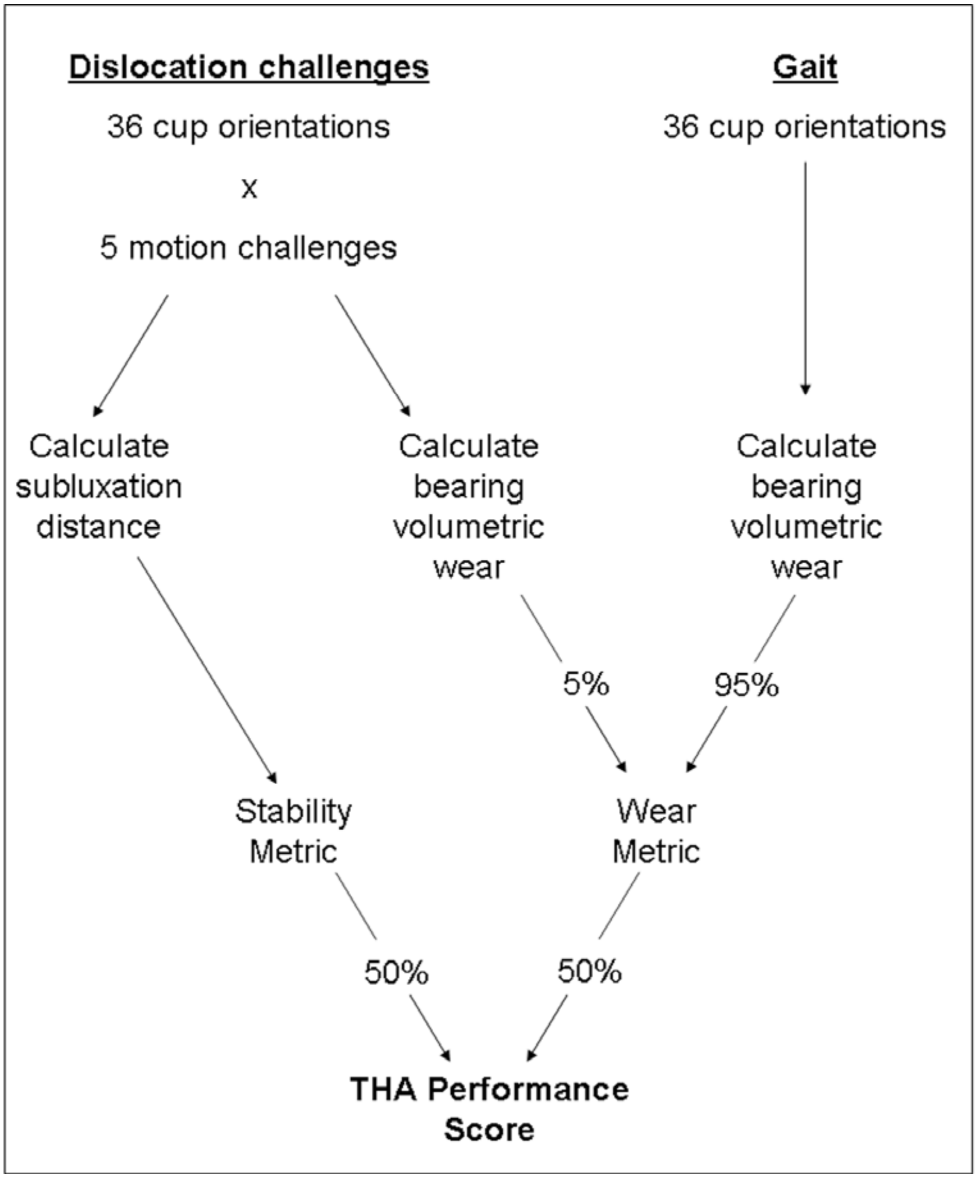

Figure 103: Optimization algorithm. Optimization of MoM THA considered both implant stability and bearing surface wear. The algorithm was applied to each combination of femoral head diameter and femoral anteversion (twenty such combinations). Using this methodology, final optimization determination was regressed for both femoral head diameter and femoral anteversion.

The final metric used to determine optimized conditions ("THA Performance Score") is a combination of implant stability and bearing surface wear. For any given combination of femoral head diameter and femoral anteversion, Stability (defined in terms of femoral head subluxation) was tracked for all five of the dislocation challenges. The magnitudes of femoral head subluxation were then averaged (Figure 104).

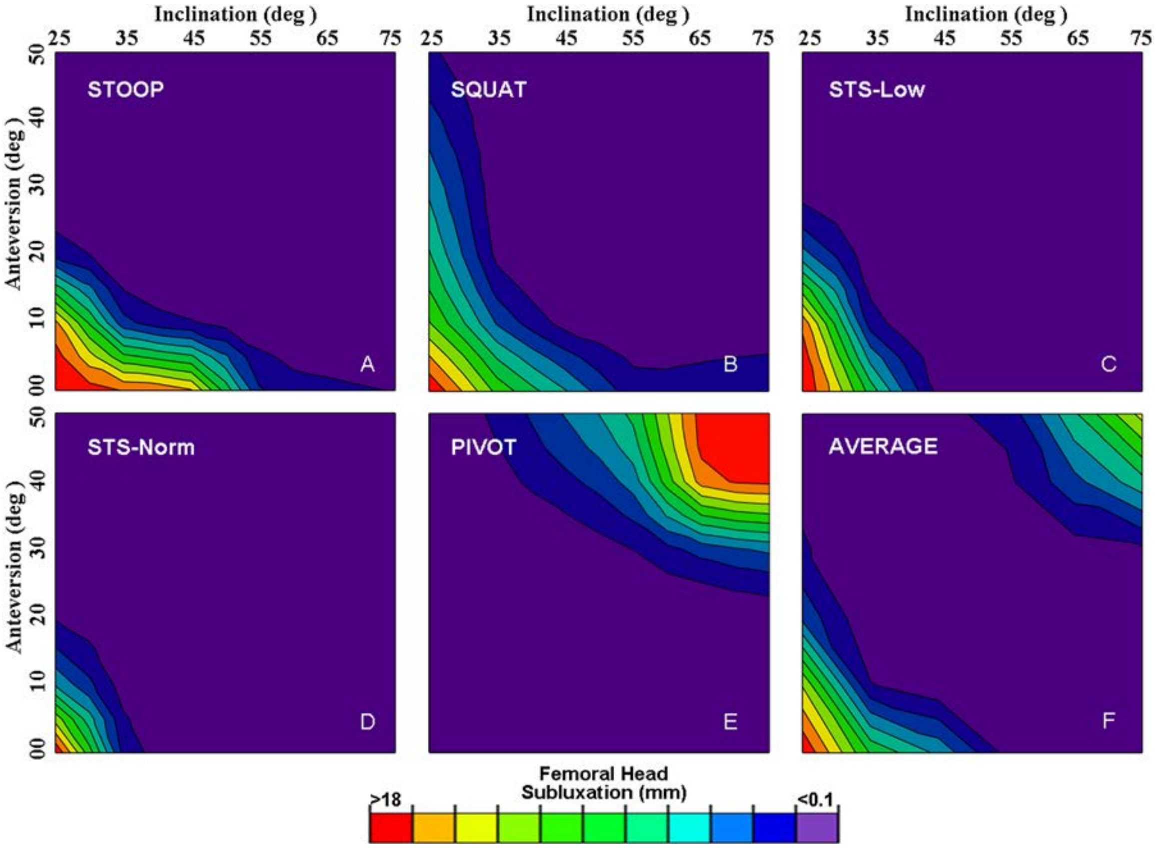

Figure 104: For every combination of head size and femoral anteversion, femoral head subluxation was assessed for each of the five dislocation challenges (A-E). The average subluxation (F) was then computed by taking the arithmetic mean at each of the thirty-six cup orientations for all five motion challenges. The illustration shown is for a 36mm femoral head with 20° femoral anteversion (anatomic reference frame).

For each instance of head size and femoral anteversion, a "Stability Metric" is computed from the averaged head subluxation (Figure 105). To generate the stability metric, each averaged (subluxation distance) data point is inverted. Then, this portion of the state-space is normalized on a scale of 1 to 100, with a value of 100 representing the most stable cup orientation.

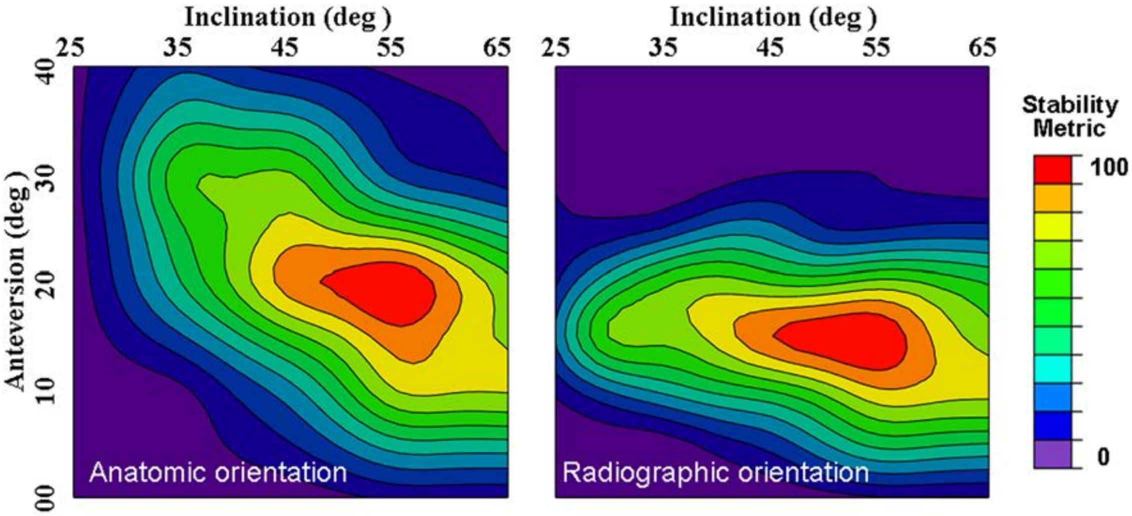

Figure 105: From the averaged head subluxation, a "stability metric" was computed in anatomic orientation (left), which was then interpolated into the radiographic reference frame (right). The stability metric is a normalized parameter (1-100). The instance shown is that for a 36mm femoral head with 20° femoral anteversion.

For each simulation, bearing surface wear was also computed using the Archard formulation. Using FE analysis to calculate bearing surface wear has a long precedent [301, 302]. However, conventional methodology used to calculate bearing wear is typically very computationally expensive. Therefore, to efficiently calculate wear from the 4,320 simulations, a slightly modified calculation routine was developed. The wear program efficiency is greatly improved by declaring several global variables prior to the calculation of wear. Input files for orphan meshes list nodal connectivities for each element in the model, i.e., what nodes are associated with each element. For linear hexahedral elements, each element has eight such connectivities. The first global variable is a list of connectivities for the contact surface elements. For these surface elements, only four (or rarely six) nodes are present on the surface (Figure 106). Conversely, each node on the surface is connected to two or four elements (Figure 106D). The second globally-declared variable is a list of "element connectivities" for each node in the surface face set, i.e., for each node on the surface, the elements it contacts. The last global variable deals with element normals. Linear wear (as calculated by the Archard formulation) is assumed to act in a direction normal to the contact pressure. Numerical determination of linear wear is performed at nodes. Nodes, however, do not have a normal direction, whereas element faces do. Therefore, volumetric wear needs to be calculated by displacing the node in an approximate face-normal direction. For such purpose, a list of nodal "normals" needs to be determined. This was done first by computing the normals of each face. Then, using the face connectivities (the first global variable described above), the normal direction for the face is passed to its four connected nodes. However, since each node on the surface (usually) contacts four elements, at the end of the computation, each node on the surface would have an approximate normal direction taken as the average of its four neighboring elements. Per the Archard calculation, instantaneous linear wear is the product of the k-factor, the contact pressure and instantaneous slipping rate. Rather than read in an output file of nodal slip quantities and performing numerical differentiation, the slipping rate was determined as the sum of the instantaneous translational and rotational velocities:

$$\mathrm{slip}(t) = dU(t) + V(t)\cdot\frac{\mathrm{head\_diameter}}{2}$$

where U is the femoral head subluxation, and V is the rotational velocity (specified as input boundary conditions) of the head. Functions for V(t) and dU(t) were determined by writing cubic splines. Instantaneous linear wear at every node for each time increment was then calculated as

$$\mathrm{linear\_wear}(t) = k_{\mathrm{wear}}\cdot \mathrm{CPRESS}(t)\cdot \mathrm{slip}(t)$$

where CPRESS was a node output file listing nodal contact pressures. At each time increment, instantaneous volumetric wear was computed by repositioning the nodes of each element at each time increment. As previously described, nodes were considered as being displaced along their “normal” direction. Instantaneous volumetric wear at t_i was then calculated as $[V(t_{i-1}) – V(t_i)]$. The initial and final elements volumes at each increment were determined using an efficient algorithm for the volume of hexahedral cells [303]. Total volumetric wear at t_i was then computed by the summation of V(t) from t=0 to $t=t_i$. To avoid confounding factors from adverse loading conditions, total volumetric wear for each FE simulation was truncated if the femoral head subluxates more than 4mm.

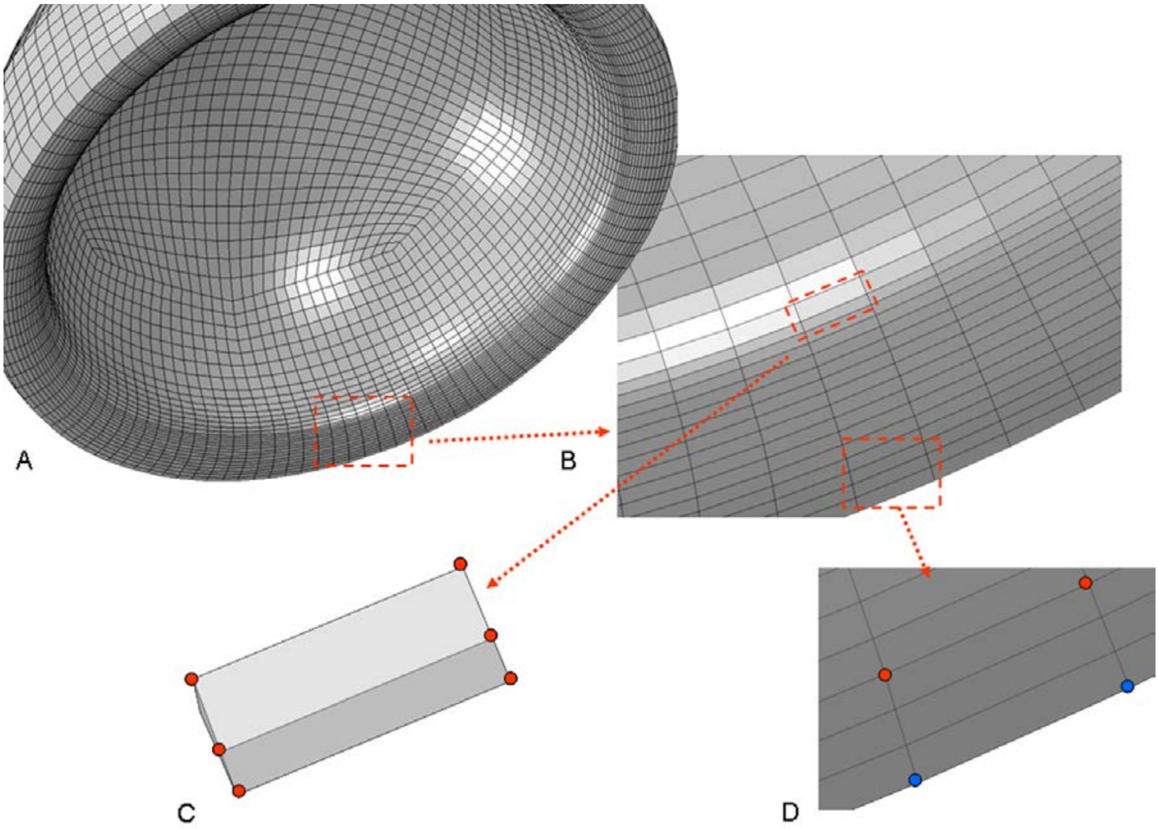

Figure 106: Surface element connectivities. (A) Ceramic liner. (B) High-resolution view of the cup edge. Whereas most surface elements had four nodes on the surface, a ring of elements forming the cup (radiused) edge contain six nodes (C). Additionally, most nodes on the cup surface were connected to four elements (red nodes, D), some nodes on the peripheral surface were associated with only two elements (blue nodes). Bookkeeping of these features were required to generate the declared global variables for the bearing surface wear calculations.

This modified wear algorithm featured several advantages over previously developed methods [304]. First, by direct computation of nodal slip rate (versus numerical differentiation of large output data files), the efficiency of the linear wear calculation was substantially improved. Second, computation of total volumetric wear by performing simple calculations on each element represented a significant reduction in computational time versus more complex surface integral calculations. These advantages resulted in at least a 50-fold reduction in computation time per simulation, a non-trivial savings in consideration of the thousands of FE simulations that required post-processing. In addition to improvements in time efficiency, the modified procedure was also advantageous in that the algorithm simultaneously repositioned nodal coordinates and calculated volumetric wear, rather than requiring separate custom written procedures. While not considered in the present study, this would allow for a highly efficient analysis of cumulated bearing surface wear over many (millions) of duty cycles. This would be especially beneficial to for explicit FE analyses, which currently do not support automatic remeshing subroutines. For each instance of femoral head diameter and femoral stem anteversion, volumetric wear was calculated for the 180 dislocation simulations (Figure 107A) and the 36 gait simulations (Figure 107B).

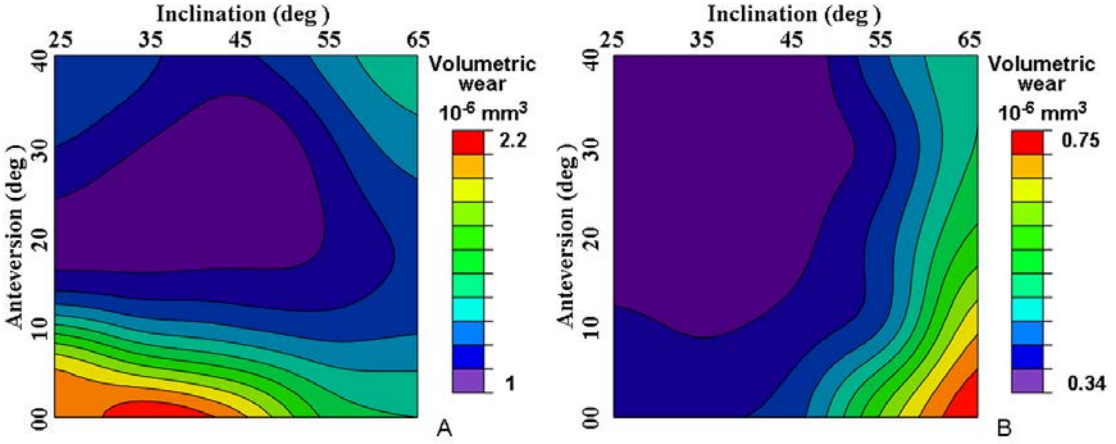

Figure 107: Volumetric wear for the five dislocation challenges (A) and gait (B). Illustration shown for a 36mm head diameter with 20° femoral anteversion.

To determine the “wear metric”, overall volumetric wear was weighted so that gait accounted for 95% of the total, while wear from the dislocation-challenge simulations accounted for 5% (i.e., for each combination of femoral anteversion and head diameter, the wear metric was the summation of 0.95 times the matrix illustrated in Figure 107A and 0.05 times the matrix illustrated in Figure 107B). These relative weighting ratios were determined from data from monitored THA patients performing activities of daily living [305]. The final wear metric was generated using the same normalization procedure for THA stability as described previously. The overall combined “THA performance score” was computed using equal weighting of both stability and volumetric bearing surface wear (Figure 108).

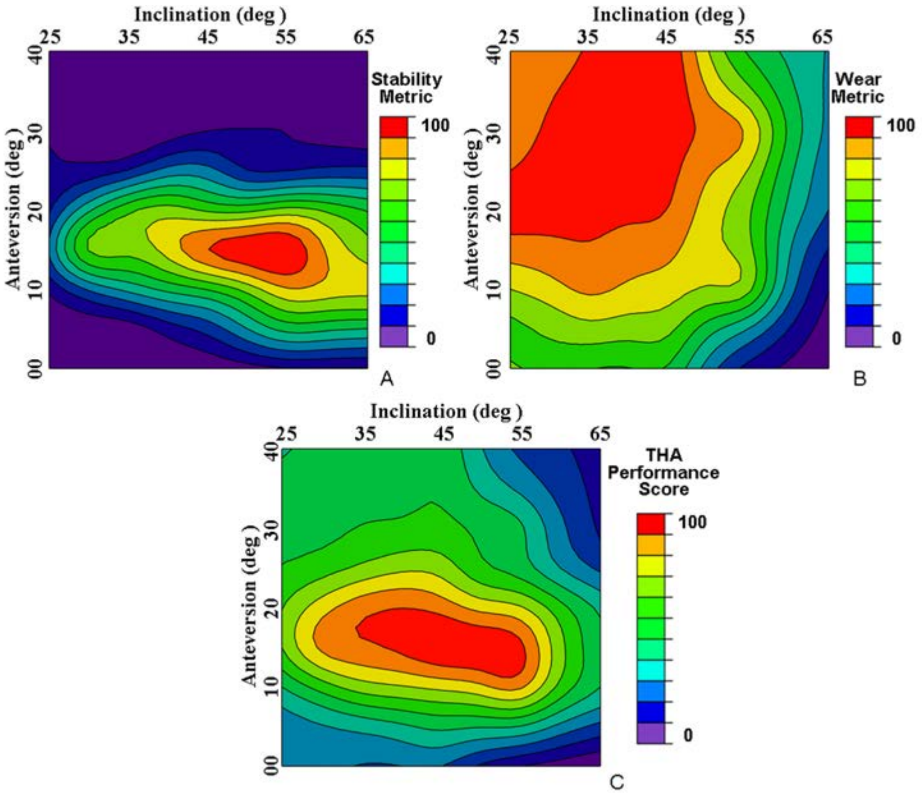

Figure 108: Equal contributions of stability (A) and volumetric wear (B) determined the overall THA performance score (C). For each instance of head diameter and femoral anteversion, a “landing zone” of optimal cup positioning was identified, which markedly was more sensitive to cup anteversion than for cup inclination. Instance shown is that for a 36mm femoral head with 20° femoral anteversion.

Results of Metal-on-Metal Optimization FE Series

The THA performance score for each series was combined to allow for optimal cup orientation to be regressed against femoral head diameter (Figures 109-113) or femoral stem anteversion. Optimal positioning was determined by computing an isosurface of the resulting THA scores above a value of 90. An ellipse was fit to this isosurface, and the optimized cup orientation was determined as the center of this ellipse (Figure 114).

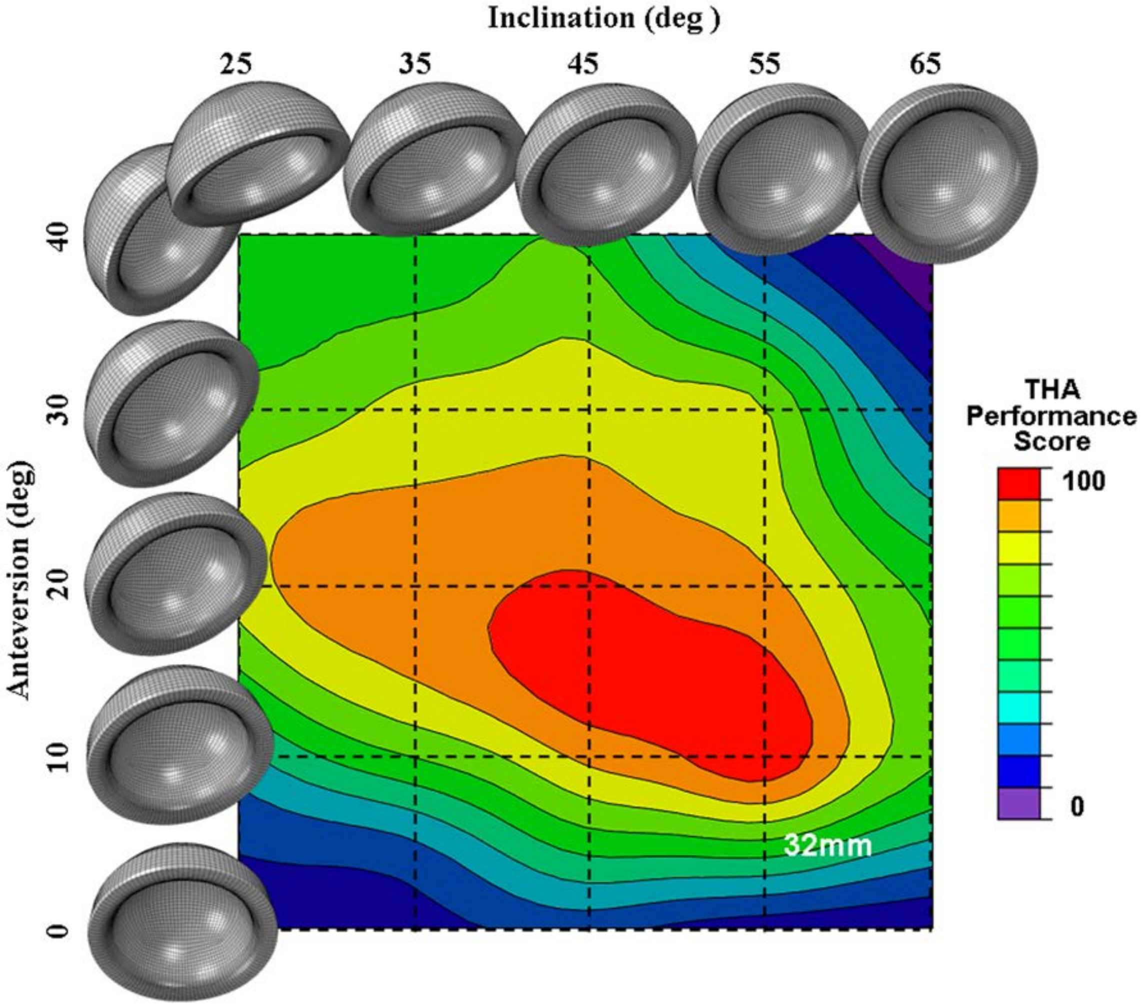

Figure 109: Combined THA performance scores from 864 distinct FE simulations with femoral head size of 32mm.

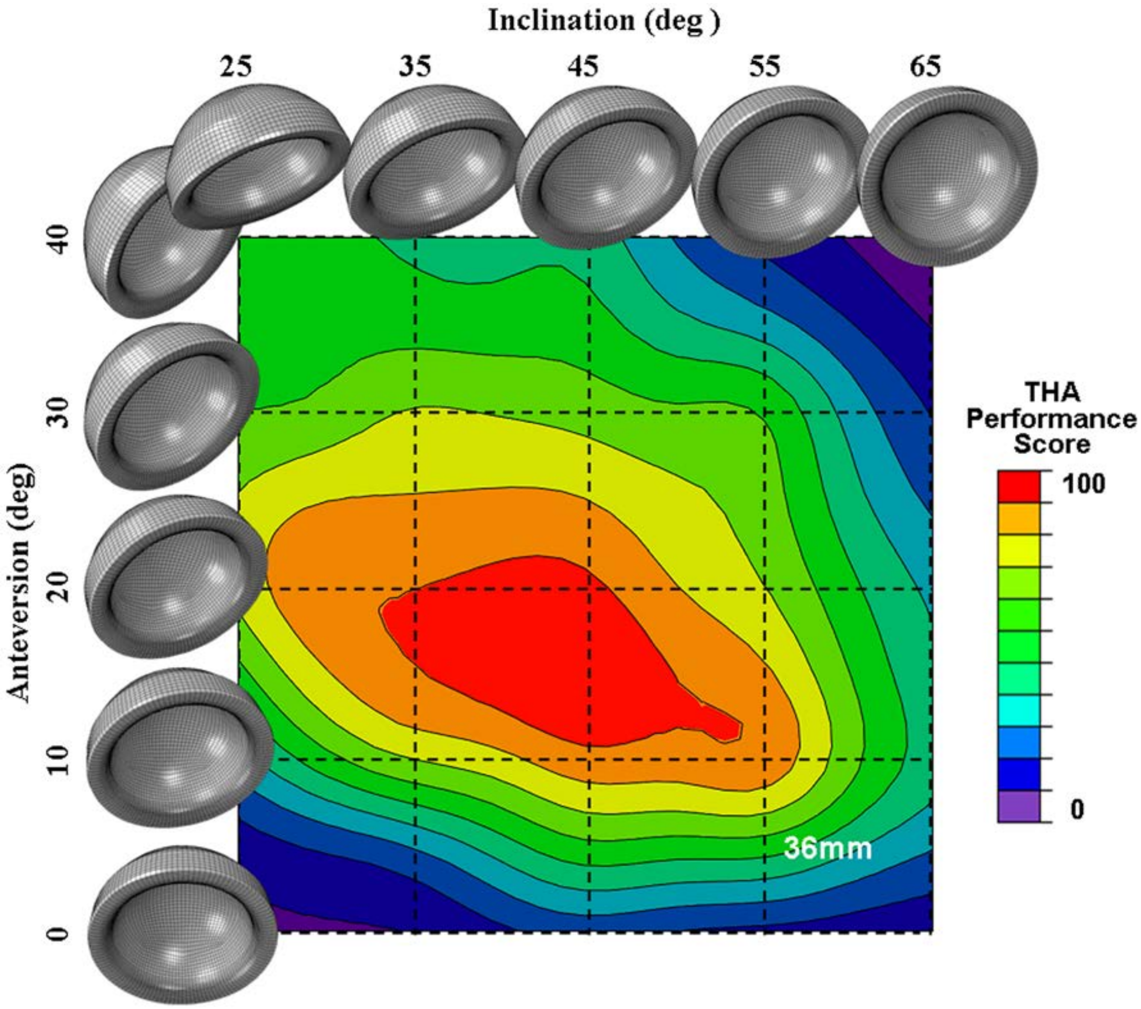

Figure 110: Combined THA performance scores from 864 distinct FE simulations with femoral head size of 36mm.

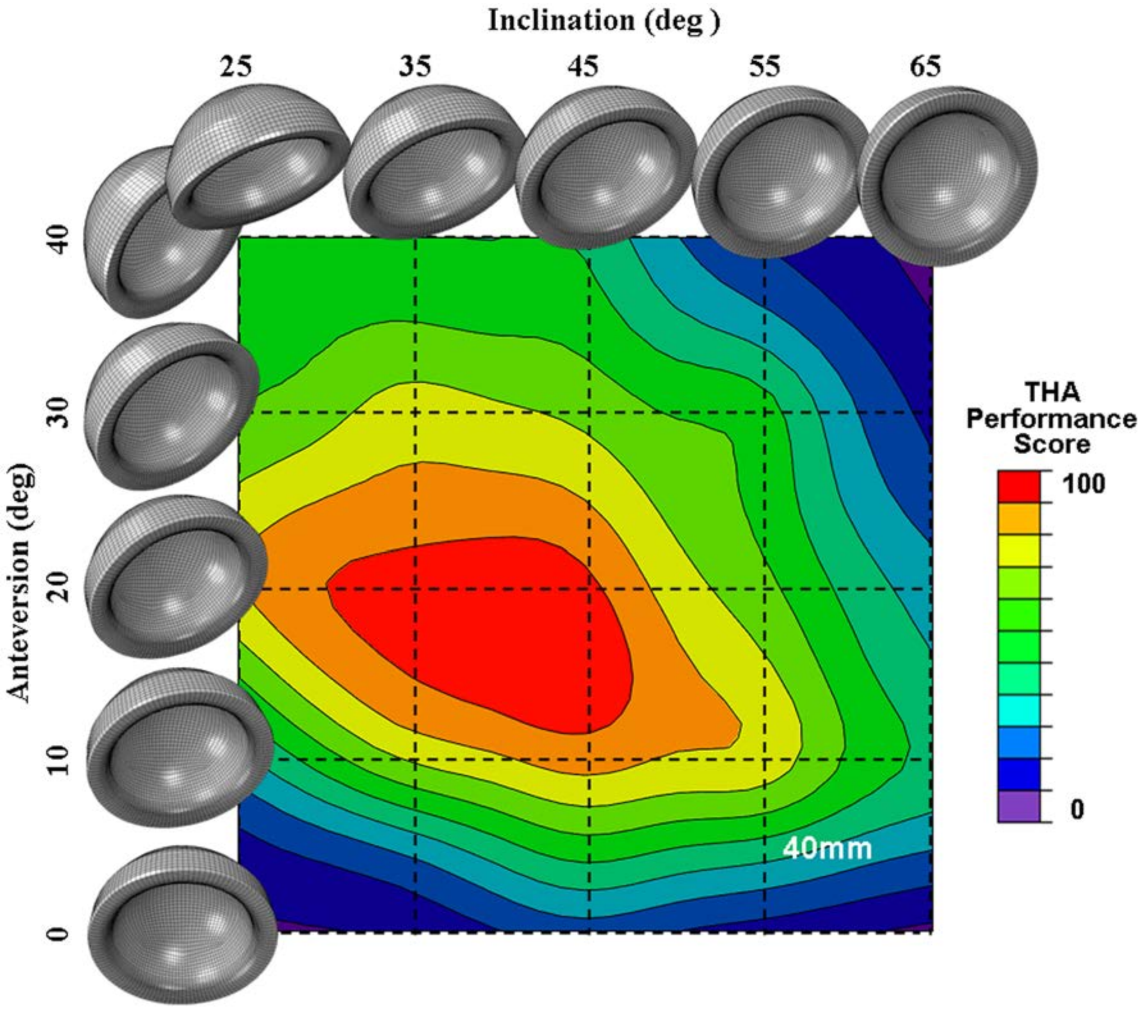

Figure 111: Combined THA performance scores from 864 distinct FE simulations with femoral head size of 40mm.

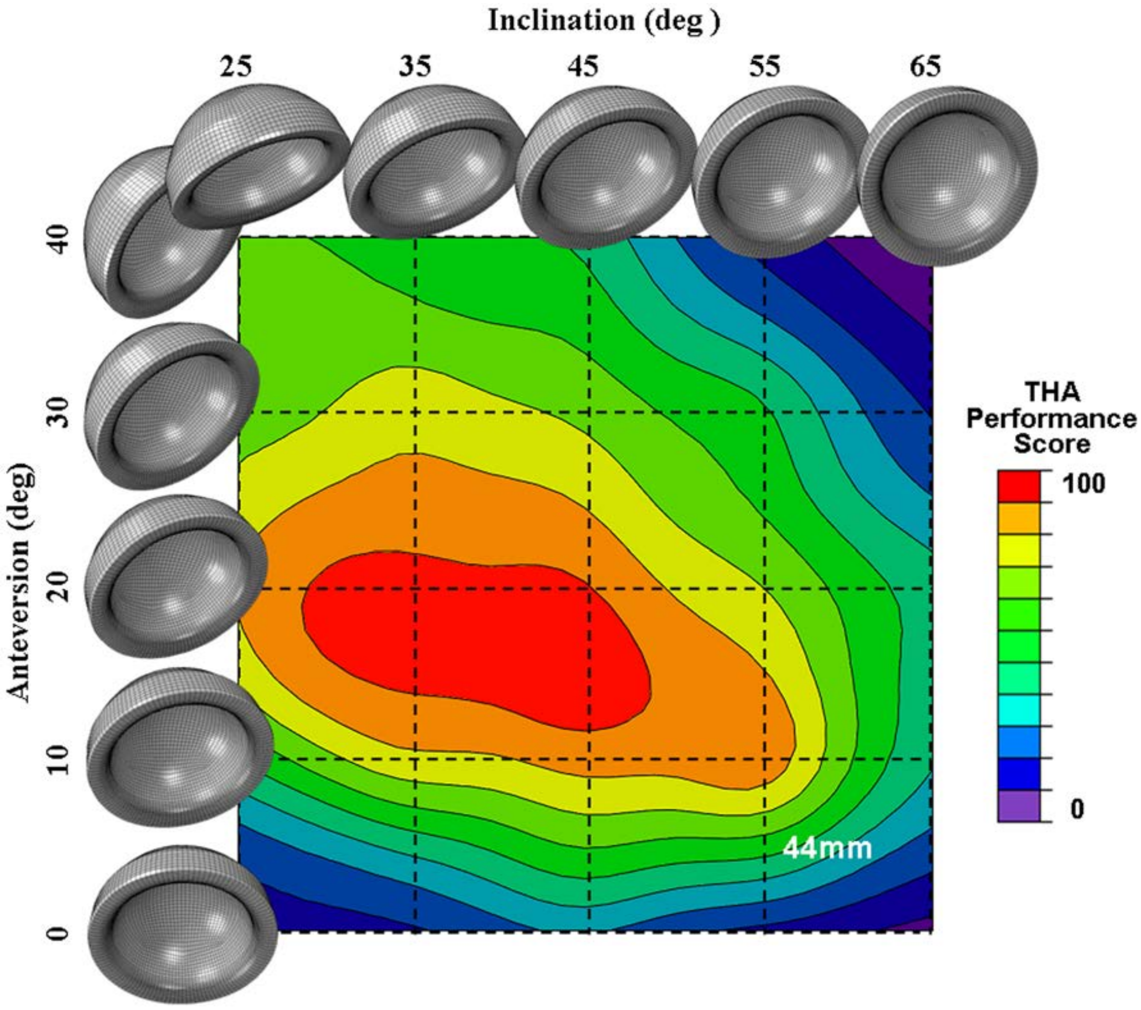

Figure 112: Combined THA performance scores from 864 distinct FE simulations with femoral head size of 44mm.

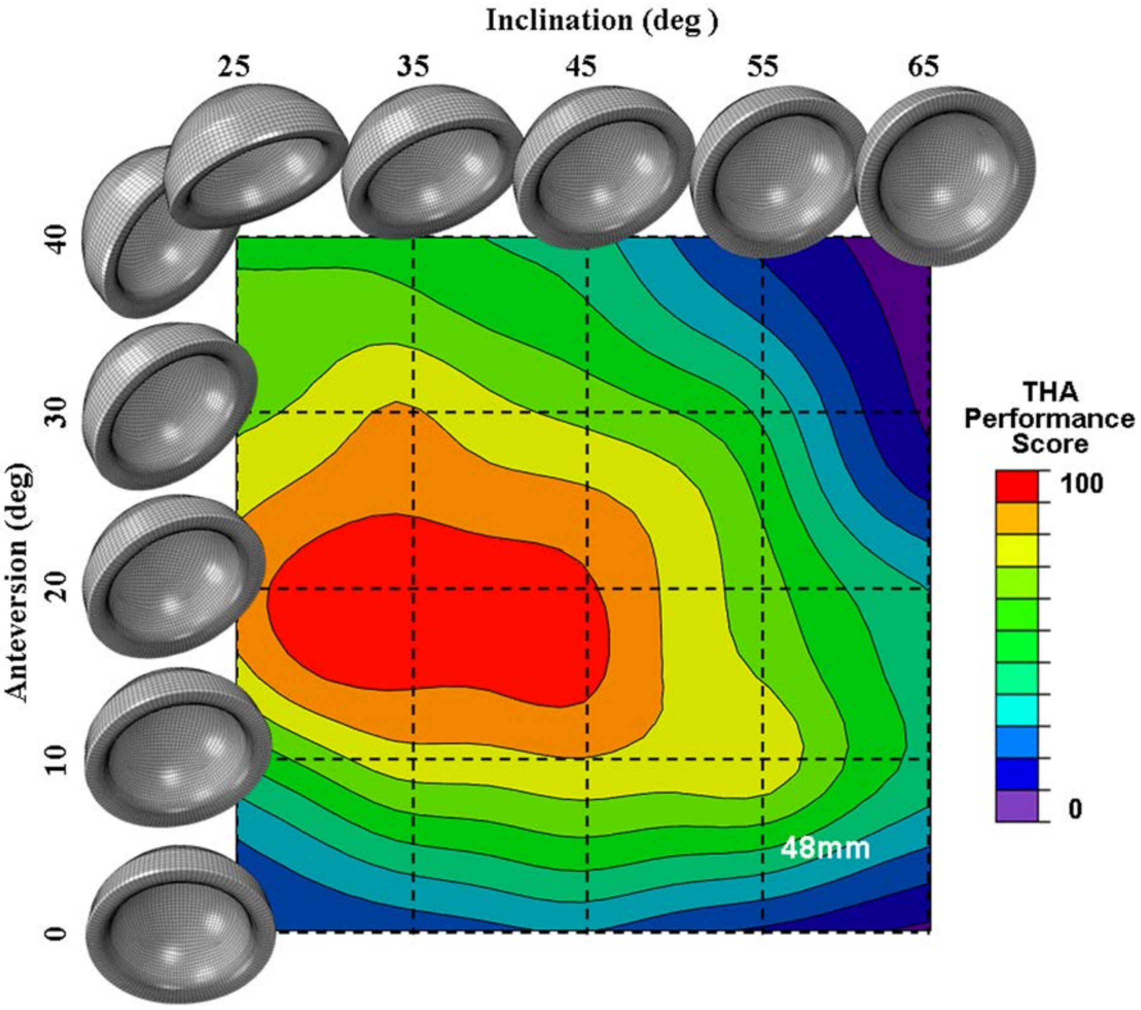

Figure 113: Combined THA performance scores from 864 distinct FE simulations with femoral head size of 48mm.

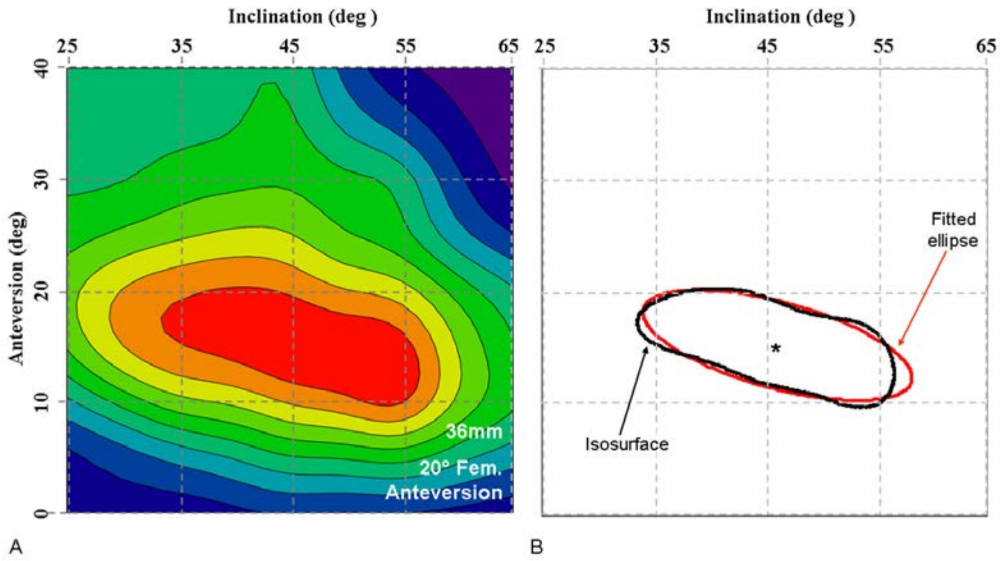

Figure 114: Optimal cup positioning. For THA performance scores from a single instance of femoral anteversion and head diameter (A) ideal cup orientation was determined by fitting an ellipse to an isosurface of the identified “safe zone”(B). The optimal cup positioning was considered as the center of the ellipse (*).

When regressions were performed, high correlations were found between optimal cup inclination (Figure 115) and anteversion (Figure 116) with femoral head diameter and femoral stem anteversion.

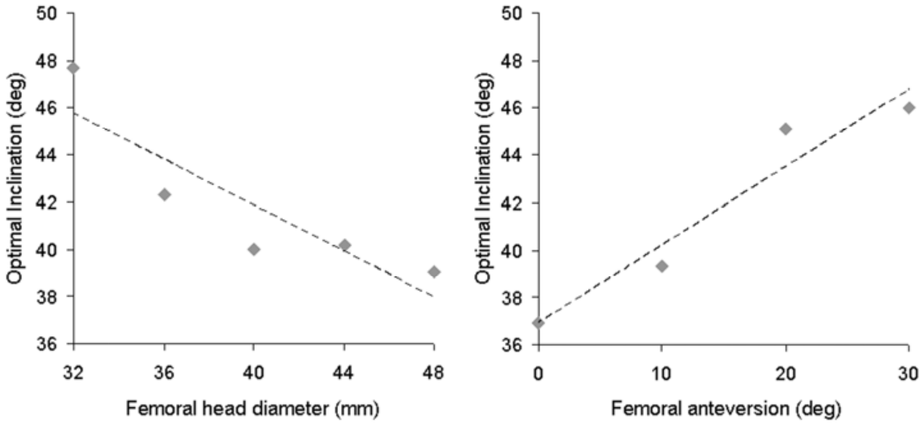

Figure 115: Regression for optimal cup inclination with head diameter (left) demonstrated a correlation coefficient of 0.882. Regression with respect to femoral anteversion (right) yielded a correlation coefficient of 0.965.

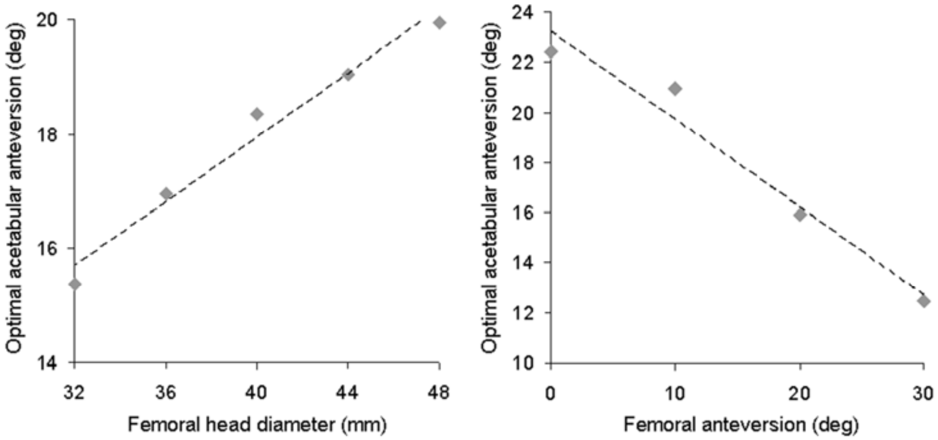

Figure 116: Regression for optimal cup anteversion with head diameter (left) demonstrated a correlation coefficient of 0.986. Regression with respect to femoral anteversion (right) yielded a correlation coefficient of 0.982.

Inclination is optimized when the following equation is met:

$$-0.33*\text{femoral}_{\text{anteversion}} + 0.48*\text{diameter} + \text{cup}_{\text{inclination}} = 56$$

Similarly, the equation for optimal cup anteversion is:

$$0.35*\text{femoral}_{\text{anteversion}} - 0.28*\text{diameter} + \text{cup}_{\text{anteversion}} = 12$$

Discussion of Optimizing Metal-on-Metal THA

The importance of implant positioning in THA has been long-recognized and extensively investigated. Yet, owing to a myriad of study limitations, uncertain, and often directly contradictory, conclusions have emerged. This present study was undertaken to overcome many of those prior limitations, and to provide definitive quantitative conclusions regarding the influence of specific factors upon THA outcomes. Besides representing the most comprehensive computational analysis to date of component optimization, it is notable in terms of being the first combined/concurrent balancing of considerations for preserving stability and minimizing wear. The weighting of these factors represent balancing considerations for both short-term (instability) and long-term (particulate wear burden) failure modalities in contemporary MoM arthroplasty. While the specific weighting factors used in this study were derived from clinical observations of failure modalities in contemporary MoM THA [213, 306], a significant attraction of the present formulation is that it can be straightforwardly modified to consider any specific set of weights for stability, wear, or other consideration (e.g. contact stress minimization).

Several important considerations regarding component orientation were identified. First, ideal cup anteversion and inclination were found to be strongly correlated to femoral stem anteversion. To the author's knowledge, only two previous studies [288, 292] of "combined anteversion" have observed a similar interaction of cup anteversion and femoral anteversion. However, this is the first investigation to observe a dependency of ideal cup inclination on femoral anteversion. Second, equally strong correlations were observed between ideal cup inclination and ideal cup anteversion versus femoral head size. This observation, that optimal cup positioning depends on head diameter (again to the author's knowledge) has never been suggested previously. And finally, this investigation has identified that the so called "landing zone" of ideal cup orientation (Figure 108C) is considerably more sensitive to cup anteversion than to cup inclination (Figure 114). Additionally, the size of the landing zone does not appreciably change with increased head diameter. These final observations are perhaps those with the most clinical importance. Despite extensive clinical investigation, the influence of cup anteversion on wear potential in MoM THA remains unclear. Wear has been shown to be both increased [212, 224] and decreased [222] with increased acetabular anteversion. Perhaps this is reflective of the smaller landing zone and/or higher sensitivity to cup anteversion identified with the present investigation. As regards sensitivity to cup anteversion, this study corroborates clinical observations of sensitivity of metallic ion release to cup anteversion [307]. The relative insensitivity to landing zone size with head size is perhaps of equal clinical significance. Assertions such as "larger acetabular components are more tolerant of the effects of malalignment in abduction and version" [308] are pervasive in the orthopaedic literature, yet lack sufficient biomechanical evidence.

This investigation of orientation optimization is subject to a number of limitations. First, while six distinct motion challenges were considered, a significant proportion of the final results depended upon wear computed from gait. While the dominance of gait compared to other activities of daily living used in this study (95%) was derived from observation studies of THA patients [305, 309], the reliance upon a singular gait motion could plausibly have biased the results towards the particular pattern of level-walking gait considered. However, compared to the variability seen with hip joint motion associated with other activities of daily living, variation among different gait patterns is probably only a small consideration. Second, only implant stability and bearing surface wear were considered when determining optimized component positioning, yet there are plausibly additional sources of deleterious effects associated with and influenced by component orientation. These include the potential for plastic deformation [165] and for third body debris ingress [310] associated with component impingement. Additionally, trunnion surface wear, as previously investigated, potentially contributes significantly to the metal ion/debris burden in MoM THA, especially with increased head size.

In summary, positioning MoM bearings involves balancing the competing considerations of joint stability and implant bearing surface wear, and that parity can be obtained through careful consideration of component orientation. Optimal acetabular cup orientation was found to strongly correlate to both femoral anteversion and femoral head size, challenging the notion of a 'one-size-fits-all' safe-zone to guide component positioning.

CHAPTER 5: PATH FORWARD

> “Would you tell me, please, which way I ought to go from here?”
> “That depends a good deal on where you want to get to,” said the Cat.
> “I don’t much care where -- ” said Alice
> “Then it doesn’t matter which way you go,” said the Cat.
> “-- so long as I get SOMEWHERE,” Alice added as an explanation.
> “Oh, you’re sure to do that,” said the Cat, “if you only walk long enough.”
>
> Charles Dodgson (Lewis Carroll) – Alice’s Adventures in Wonderland

A major theme of this body of work is to illustrate how improved understanding of biomechanics can quantify, reliably predict, and potentially mitigate failure in THA. The finite element model has proven to be sufficiently robust to investigate historical (dislocation), emerging (trunnionosis), novel (obesity), and complex (fracture) influences upon failure. Given this broad utility, it is quite conceivable that this general approach can, and will, continue to be used to analyze THA biomechanics for concerns that are presently unknown.

Several topics investigated with the FE formulation merit additional attention and future work. Perhaps the most inviting is the topic of adverse outcomes for obese patients. The FE model was used to identify a novel dislocation mechanism in morbidly obese patients. While increased dislocation risk was seen to be a mechanical response to obesity, this investigation largely ignored the numerous physiological effects of obesity. As described, there is some indication that obesity plays a detrimental role in terms of soft tissue integrity, yet the topic, in general, is grossly under-investigated. Soft tissue balance is an important consideration not just for dislocation propensity following THA, but also in several other areas of orthopaedics and medicine in general.

The assessment of fracture phenomena in ceramic bearings should be viewed as just initial groundwork for the topic. The ceramic liner linear elastic fracture mechanics investigation was the first study in the orthopaedic literature to attempt the address the (bio)mechanics of liner fracture. With mounting concerns regarding MoM implants, and with the increasing need to replace hips in younger, heavier and more active patients, the search continues to identify the ideal bearing couple, and ceramics may be a logical choice. Performance of ceramic bearings has drastically improved in recent years, and now represents the lowest intermediate-term revision rates of any bearing couple [264]. Owing to extensive mechanical investigation, the once common occurrence of femoral head fracture has now been effectively eliminated. However, fracture of the liner continues as a clinical concern. And, unlike many other failure modalities, ceramic fracture is of a “catastrophic” nature, one which involves substantially increased morbidity for the patient. Several nascent advances in FE technology hold promise for increased ability to address fracture in brittle materials. The XFEM study was the first application of this technology to an orthopaedic implant, but will likely not be the last. Additional techniques, such as co-simulation and stochastic modeling formulations may soon facilitate fracture modeling in complex systems (such as hip arthroplasty), further increasing the momentum of investigational efforts with fracture mechanics in orthopaedic research.

Appreciable effort was expended in assessing failure modes for CoC and MoM bearings. However, the third entity of the advanced bearing category, *viz*. highly crosslinked polyethylene (HXLPE), was not addressed. However, HXLPE shares many similarities with both ceramic and MoM implants. Being more brittle than conventional polyethylene, HXLPE is prone to fracture and chipping. But unlike the biologically inert particulate wear generated in ceramics [311-315], HXLPE wear debris is immunologically-reactive, with potential consequences for osteolysis and perhaps soft tissue reaction. Therefore, a logical extension of the current model would be to apply the CoC (XFEM) and MoM (FE) methodologies directly to HXLPE.

And finally, the idea of “choices and compromises” in implant design has been alluded to many times, and there is substantial room for additional optimization-type FE studies in the future. Examples include radiused edge profiles on ceramic bearings. While the initial XFEM study had indicated decreased fracture potential for increased edge radii, the results from the MoM edge radius study indicated that increased edge radius decreases stability and increases edge loading severity. An inviting topic for further investigation would be to attempt to optimize ceramic liner geometry to balance these considerations. And, as previously mentioned, an additional avenue for implant design optimization relates to the design of the trunnion with large diameter THA. The advantages of larger femoral heads are well recognized, and could be beneficial to many patients. Therefore, optimization of the trunnion/head interface is a well-deserving topic for further analysis.

APPENDIX

Scholarship Related to Failure Mechanisms in THA

Peer-Reviewed Manuscripts

1. Elkins JM, O'Brian MK, Stroud NJ, Pedersen DR, Callaghan JJ, Brown TD. Hard-on-hard total hip impingement causes extreme contact stress concentrations. *Clinical Orthopaedics and Related Research* 469(2) 454-463. 2011

2. Elkins JM, Stroud NJ, Rudert MJ, Tochigi Y, Pedersen DR, Ellis BJ, Callaghan JJ, Weiss JA, Brown TD. The Capsule's Contribution to Total Hip Construct Stability – A Finite Element Analysis. William H. Harris Award Paper, Orthopaedic Research Society. *Journal of Orthopaedic Research* 29(11) 1642-1648. 2011

3. Elkins JM, Pedersen DR, Callaghan JJ, Brown TD. Fracture Propagation Propensity of Ceramic Liners during Impingement – A Finite Element Analysis. *Journal of Arthroplasty* 2011 [Epub ahead of print] (PMID 21855277).

4. Elkins JM, Kruger KM, Pedersen DR, Callaghan JJ, Brown TD. Edge-Loading Severity as a Function of Cup Lip Radius in Metal-on-Metal Total Hips – A Finite Element Analysis. *Journal of Orthopaedic Research* 2012 30(2) 169-177

5. Elkins JM, Liu X, Qin X, Du Z, Brown TD. Ceramic total hip liner fracture modeling in Abaqus using co- simulation and extended finite element modeling. *SIMULIA Realistic Simulation News*. 2011 (Invited Manuscript)

6. Elkins JM, Pedersen DR, Callaghan JJ, Brown TD. Bone-on-Bone vs. Implant Impingement in Large Femoral Diameter Total Hips. *Iowa Orthopaedic Journal* 2012 (submitted)

7. Elkins JM, Pedersen DR, Yack HJ, Callaghan JJ, Brown TD. Total Hip Instability in the Morbidly Obese Patient – A Finite Element Investigation. *Clinical Orthopaedics and Related Research* 2012 (submitted)

8. Elkins JM, Callaghan JJ, Brown TD. Are Large Heads an Unqualified Benefit for Metal-on-Metal Total Hip Replacement? Stability vs. "Trunnionosis" Wear. *Journal of Arthroplasty* 2012 (submitted)

9. Elkins JM, Pedersen DR, Callaghan JJ, Brown TD. Relationships between Obesity, Fracture and Stripe Wear in Ceramic THA – An eXtended Finite Element (XFEM) Analysis. *Clinical Orthopaedics and Related Research*. 2012 (submitted)

10. Elkins JM, Callaghan JJ, Pedersen DR, Brown TD. Toward Optimization in Metal-on-Metal Total Hips – Balancing Competing Considerations of Wear and Stability. *Journal of Bone & Joint Surgery Am*. 2012 (in preparation)

11. Brown TD, Elkins JM, Pedersen DR, Callaghan JJ. Impingement in Total Hip Arthroplasty: Mechanisms and Consequences. The 2012 Orthopaedic Research Education Foundation OREF Clinical Research Award. *Journal of Bone & Joint Surgery Am*. 2012 (in preparation).

Conference Presentations

1. Elkins JM, Pedersen DR, Callaghan JJ, Brown TD. Orientation-dependent impingement contact mechanics for hard-on-hard total hip bearings. 33rd Annual Meeting of the American Society of Biomechanics, August 26–29, 2009, State College, Pennsylvania.

2. Pedersen, DR, Elkins JM, Callaghan JJ, Brown TD. Impingement contact mechanics of total hip bearings. Closed Scientific Meeting of the Hip Society, September 24–26, 2009, Palo Alto, California

3. Elkins JM, Pedersen DR, Tochigi Y, Rudert MJ, Ellis BJ, Callaghan JJ, Weiss JA, Brown TD. Implementing a fiber-directed anisotropic capsule in a total hip arthroplasty dislocation finite element model. 56th Annual Meeting of the Orthopaedic Research Society, March 6–9, 2010, New Orleans, Louisiana.

4. Elkins JM, Pedersen DR, Tochigi Y, Rudert MJ, Ellis BJ, Callaghan JJ, Weiss JA, Brown TD. Effect of cup orientation on resistance to hip dislocation during flexion/exorotation- dominated kinetic challenge. 56th Annual Meeting of the Orthopaedic Research Society, March 6–9, 2010, New Orleans, Louisiana.

5. Elkins JM, Pedersen DR, Callaghan JJ, Brown TD. Impingement contact mechanics for hard-on-hard total hip bearings. 56th Annual Meeting of the Orthopaedic Research Society, March 6–9, 2010, New Orleans, Louisiana.

6. Elkins JM, Pedersen DR, Callaghan JJ, Brown TD. The capsule's contribution to total hip construct stability—A finite element analysis. 34th Annual Meeting of the American Society of Biomechanics, August 18–21, 2010, Providence, Rhode Island.

7. Elkins JM, Pedersen DR, Callaghan JJ, Brown TD. Three dimensional fracture mechanics of ceramic total hip bearings. 34th Annual Meeting of the American Society of Biomechanics, August 18–21, 2010, Providence, Rhode Island.

8. Stroud NJ, Elkins JM, Tochigi Y, Rudert MJ, Brown TD. Cadaveric Transpelvic Implantation of THA Hardware for Physically Testing an Intact Hip Capsule with a Dislocation Challenge. 57th Annual Meeting of the Orthopaedic Research Society, January 13-16, 2011. Long Beach, California.

9. Elkins JM, Stroud NJ, Pedersen DR, Tochigi Y, Rudert MJ, Callaghan JJ, Weiss JA, Brown TD. The effect of regional hip capsule defects on total hip dislocation stability — A finite element analysis. 57th Annual Meeting of the Orthopaedic Research Society, January 13-16, 2011. Long Beach, California.

10. Elkins JM, Pedersen DR, Callaghan JJ, Brown TD. Total hip instability in the morbidly obese patient – A finite element exploration. 57th Annual Meeting of the Orthopaedic Research Society, January 13-16, 2011. Long Beach, California.

11. Elkins JM, Stroud NJ, Pedersen DR, Tochigi Y, Rudert MJ, Callaghan JJ, Weiss JA, Brown TD. The effect of regional hip capsule defects on total hip dislocation stability — A finite element analysis. 57th Annual Meeting of the Orthopaedic Research Society, January 13-16, 2011. Long Beach, California. ORS Awards Presentation, January 15, 2011.

12. Elkins JM, Liu C, Qin X, Du Z, Brown TD. Ceramic total hip bearing fracture modeling in Abaqus using co- simulation and extended finite element modeling. 2011 SIMULIA Customer Conference. May 17–19, 2011, Barcelona, Spain.

13. Elkins JM, Pedersen DR, Singh B, Yack HJ, Callaghan JJ, Brown TD. Dislocation in the Morbidly Obese Total Hip Patient. 35th Annual Meeting of the American Society of Biomechanics, August 18–21, 2011, Long Beach, California.

14. Elkins JM, Brown TD, Pedersen DR, Callaghan JJ. Advanced Fracture Analysis of 36-mm Alumina Total Hip Bearings. Closed 2011 Scientific Meeting of the Hip Society. September 22-24, 2011. New Albany, Ohio

15. Callaghan JJ, Elkins JM, Brown TD. Metal-on-Metal: Finite Element modeling. Harvard Hip Advances in Arthroplasty Course. October 2011, Boston, Massachusetts.

16. Elkins JM, Pedersen DR, Callaghan JJ, Brown TD. Bone-on-Bone vs. Implant Impingement in Large Diameter Total Hips. 58th Annual Meeting of the Orthopaedic Research Society, February 4-7, 2012. San Francisco, California.

17. Elkins JM, Pedersen DR, Callaghan JJ, Brown TD. Toward Optimizing Orientation in Metal-on-Metal Total Hips: Balancing Competing Considerations. 58th Annual Meeting of the Orthopaedic Research Society, February 4-7, 2012. San Francisco, California.

18. Elkins JM, Pedersen DR, Callaghan JJ, Brown TD. Edge-Scraping Wear in Metal-on-Metal Total Hips. 58th Annual Meeting of the Orthopaedic Research Society, February 4-7, 2012. San Francisco, California.

19. Elkins JM, Liu X, Pedersen DR, Callaghan JJ, Brown TD. Computational Fracture Analysis of Ceramic-on-Ceramic Total Hip Liners. 58th Annual Meeting of the Orthopaedic Research Society, February 4-7, 2012. San Francisco, California.

20. Elkins JM, Pedersen DR, Callaghan JJ, Brown TD. Balancing Competing Considerations for Optimal Orientation in 36-mm Metal-on-Metal Total Hips. The 2012 American Academy of Orthopaedic Surgeons (AAOS) Annual Meeting. February 7-11, 2012, San Francisco, California. Paper #311

21. Elkins JM, Pedersen DR, Callaghan JJ, Brown TD. Dislocation Risk in Morbidly Obese Total Hip Patients. 30th Annual Meeting of Mid-America Orthopaedic Association. April 18-22, 2012. Bonita Springs, Florida

REFERENCES

1. McKeever D. Biomechanics of hip prostheses. *Clin Orthop Relat Res* 1961. 19: 187-199.

2. Learmonth ID, Young C, Rorabeck C. The operation of the century: Total hip replacement. *Lancet* 2007. 370: 1508-1519.

3. Kurtz S, Ong K, Lau E, Mowat F, Halpern M. Projections of primary and revision hip and knee arthroplasty in the united states from 2005 to 2030. *J Bone Joint Surg Am* 2007. 89: 780-785.

4. Ong K, Mowat F, Chan N, Lau E, Halpern M, Kurtz S. Economic burden of revision hip and knee arthroplasty in Medicare enrollees. *Clin Orthop Relat Res* 2006. 446: 22-28.

5. Obituary. *The Lancet* 1849. 53: 324-325.

6. Thompson FR. An essay on the development of arthroplasty of the hip. *Clin Orthop Relat Res* 1966. 44: 73-82.

7. Glück T. Referat über die durch das moderne chirurgische experiment GewonnenenPositiven resultaten, betreffende die naht und den ersatz von defekten HöhererGewebe, sowie über die verwerthung resorbirbarer und lebendiger tampons in der chirurgie. *Arch Klin Chir* 1891. 41: 186-239.

8. Eynon-Lewis N, Ferry D, Pearse M. Themistocles Glück: An unrecognised genius. *Br Med J* 1992. 305: 1534-1536.

9. Glück T. 2011. The Classic: Report on the positive results obtained by the modern surgical experiment regarding the suture and replacement of defects of superior tissue, as well as the utilization of re-absorbable and living tamponade in surgery. *Clin Orthop Relat Res* 2011. 469: 1528-1535

10. Groves EWH. Some contributions to the reconstructive surgery of the hip. *Br J Surg* 1927. 14: 486-517.

11. Scales J. Arthroplasty of the hip using foreign materials: A history. *Proc Inst Mech Eng H* 1966. 181: 63-84.

12. Smith-Petersen MN. Arthroplasty of the hip a new method. *J Bone Joint Surg Am* 1939. 21: 269-288.

13. Aufranc OE. Constructive hip surgery with the Vitallium mold A report on 1,000 cases of arthroplasty of the hip over a fifteen-year period. *J Bone Joint Surg Am* 1957. 39: 237-316.

14. Bohlman HR. Replacement reconstruction of the hip. *Am J Surg* 1952. 84: 268-278.

15. Wiles P. The surgery of the osteo‐arthritic hip. *Br J Surg* 1958. 45: 488-497.

16. Judet J, Judet R. The use of an artificial femoral head for arthroplasty of the hip joint. *J Bone Joint Surg Br* 1950. 32: 166-173.

17. Moore AT. The self-locking metal hip prosthesis. *J Bone Joint Surg Am* 1957. 39: 811-827.

18. Thompson FR. Two and a half years' experience with a Vitallium intramedullary hip prosthesis. *J Bone Joint Surg Am* 1954. 36: 489-500.

19. McKee G. Developments in total hip joint replacement. *Proc Inst Mech Eng H* 1966. 181: 85-89.

20. Straub LR, King DE, Lambert CN. Symposium on femoral-head replacement prostheses based on the report of the committee for the study of femoral-head replacement prostheses as printed in the October (1954) issue of the bulletin. *J Bone Joint Surg Am* 1956. 38: 407-420.

21. Newman P, Scales J. The unsuitability of polythene for movable weight-bearing prostheses. *J Bone Joint Surg Br* 1951. 33: 392-398.

22. Scales JT. The unsuitability of nylon weight bearing prostheses articulating with bone or cartilage. *Acta Orthop Scand* 1957. 27: 13-39.

23. Charnley J. Arthroplasty of the hip. A new operation. *Lancet* 1961. 1: 1129-1132.

24. Charnley J. Factors in the design of an artificial hip joint. *Proc Inst Mech Eng H* 1966. 181: 104-111.

25. Wiltse L, Hall R, Stenehjem J. Experimental studies regarding the possible use of self-curing acrylic in orthopaedic surgery. *J Bone Joint Surg Am* 1957. 39: 961-972.

26. Henrichsen E, Jansen K, Krough-Poulsen W. Experimental investigation of the tissue reaction to acrylic plastics. *Acta Orthop Scand* 1952. 22: 141-146.

27. Spence WT. Form-fitting plastic cranioplasty. *J Neurosurg* 1954. 11: 219-225.

28. Amstutz HC, Grigoris P. Metal on metal bearings in hip arthroplasty. *Clin Orthop Relat Res* 1996. (329 Suppl): S11-34.

29. Georgiades G, Babis GC, Hartofilakidis G. Charnley low-friction arthroplasty in young patients with Osteoarthritis. Outcomes at a minimum of twenty-two years. *J Bone Joint Surg Am* 2009. 91: 2846-2851.

30. Berry DJ, von Knoch M, Schleck CD, Harmsen WS. The cumulative long-term risk of dislocation after primary Charnley total hip arthroplasty. *J Bone Joint Surg Am* 2004. 86: 9-14.

31. Schmalzried TP, Szuszczewicz ES, Akizuki KH, Petersen TD, Amstutz HC. Factors correlating with long term survival of McKee-farrar total hip prostheses. *Clin Orthop Relat Res* 1996. 329: S48-S59.

32. Campbell P, Urban RM, Catelas I, Skipor AK, Schmalzried TP. Autopsy analysis thirty years after metal-on-metal total hip replacement. A case report. *J Bone Joint Surg Am* 2003. 85: 2218-2222.

33. Müller ME. The benefits of metal-on-metal total hip replacements. *Clin Orthop Relat Res* 1995. 311: 54-59.

34. Boutin P. Arthroplastie totale de hanche par prothese en alumine frittee. *Rev Chir Orthop* 1972. 58: 229-246.

35. Bozic KJ, Kurtz S, Lau E, Ong K, Chiu V, Vail TP, Rubash HE, Berry DJ. The epidemiology of bearing surface usage in total hip arthroplasty in the united states. *J Bone Joint Surg Am* 2009. 91: 1614-1620.

36. Harris WH. Conquest of a worldwide human disease: Particle-induced periprosthetic osteolysis. *Clin Orthop Relat Res* 2004. 429: 39-42.

37. Brown TD, Callaghan JJ. Impingement in total hip replacement: Mechanisms and consequences. *Curr Orthop* 2008. 22: 376-391.

38. Courant R. Variational methods for the solutions of problems of equilibrium and vibrations. *Bull Am Math Soc* 1943. 49: 1-23.

39. Clough RW. The finite element method in plane stress analysis. *Proceedings of 2nd ASCE Conference on Electronic Computatation, Pittsburgh, PA, September 8-9, 1960.*

40. Yerry MA, Shephard MS. Automatic three‐dimensional mesh generation by the modified‐octree technique. *Int J Numer Methods Eng* 1984. 20: 1965-1990.

41. Bozic KJ, Kurtz SM, Lau E, Ong K, Vail TP, Berry DJ. The epidemiology of revision total hip arthroplasty in the United States. *J Bone Joint Surg Am* 2009. 91: 128-133.

42. Meek R, Allan D, McPhillips G, Kerr L, Howie C. Late dislocation after total hip arthroplasty. *Clin Med Res* 2008. 6: 17-23.

43. Patel PD, Potts A, Froimson MI. The dislocating hip arthroplasty: Prevention and treatment. *J Arthroplasty* 2007. 22: 86-90.

44. Alberton GM, High WA, Morrey BF. Dislocation after revision total hip arthroplasty: An analysis of risk factors and treatment options. *J Bone Joint Surg Am* 2002. 84: 1788-1792.

45. Colwell CW, Colwell. Instability after total hip arthroplasty. *Curr Orthop Prac* 2009. 20: 8-14.

46. Lewinnek GE, Lewis JL, Tarr R, Compere CL, Zimmerman JR. Dislocations after total hip-replacement arthroplasties. *J Bone Joint Surg Am* 1978. 60: 217-220.

47. Woo R, Morrey B. Dislocations after total hip arthroplasty. *J Bone Joint Surg Am* 1982. 64: 1295-1306.

48. Yuan L, Shih C. Dislocation after total hip arthroplasty. *Arch Orthop Trauma Surg* 1999. 119: 263-266.

49. Woolson ST, Rahimtoola ZO. Risk factors for dislocation during the first 3 months after primary total hip replacement. *J Arthroplasty* 1999. 14: 662-668.

50. White RE,Jr, Forness TJ, Allman JK, Junick DW. Effect of posterior capsular repair on early dislocation in primary total hip replacement. *Clin Orthop Relat Res* 2001. 393: 163-167.

51. Sanchez-Sotelo J, Berry DJ. Epidemiology of instability after total hip replacement. *Orthop Clin North Am* 2001. 32: 543-52, vii.

52. Goldstein WM, Gleason TF, Kopplin M, Branson JJ. Prevalence of dislocation after total hip arthroplasty through a posterolateral approach with partial capsulotomy and capsulorrhaphy. *J Bone Joint Surg Am* 2001. 83-A Suppl 2: 2-7.

53. Barrack RL, Butler RA, Laster DR, Andrews P. Stem design and dislocation after revision total hip arthroplasty: Clinical results and computer modeling. *J Arthroplasty* 2001. 16: 8-12.

54. Weeden SH, Paprosky WG, Bowling JW. The early dislocation rate in primary total hip arthroplasty following the posterior approach with posterior soft-tissue repair. *J Arthroplasty* 2003. 18: 709-713.

55. van Stralen G, Struben P, van Loon C. The incidence of dislocation after primary total hip arthroplasty using posterior approach with posterior soft-tissue repair. *Arch Orthop Trauma Surg* 2003. 123: 219-222.

56. Nadzadi ME, Pedersen DR, Yack HJ, Callaghan JJ, Brown TD. Kinematics, kinetics, and finite element analysis of commonplace maneuvers at risk for total hip dislocation. *J Biomech* 2003. 36: 577-591.

57. Barrack RL. Dislocation after total hip arthroplasty: Implant design and orientation. *J Am Acad Orthop Surg* 2003. 11: 89-99.

58. Nadzadi ME, Pedersen DR, Callaghan JJ, Brown TD. Effects of acetabular component orientation on dislocation propensity for small-head-size total hip arthroplasty. *Clin Biomech* 2002. 17: 32-40.

59. Soong M, Rubash HE, Macaulay W. Dislocation after total hip arthroplasty. *J Am Acad Orthop Surg* 2004. 12: 314-321.

60. Padgett DE, Lipman J, Robie B, Nestor BJ. Influence of total hip design on dislocation: A computer model and clinical analysis. *Clin Orthop Relat Res* 2006. 447: 48-52.

61. Kwon MS, Kuskowski M, Mulhall KJ, Macaulay W, Brown TE, Saleh KJ. Does surgical approach affect total hip arthroplasty dislocation rates? *Clin Orthop Relat Res* 2006. 447: 34-38.

62. Shon WY, Baldini T, Peterson MG, Wright TM, Salvati EA. Impingement in total hip arthroplasty a study of retrieved acetabular components. *J Arthroplasty* 2005. 20: 427-435.

63. Usrey MM, Noble PC, Rudner LJ, Conditt MA, Birman MV, Santore RF, Mathis KB. Does neck/liner impingement increase wear of ultrahigh-molecular-weight polyethylene liners? *J Arthroplasty* 2006. 21: 65-71.

64. Bader R, Steinhauser E, Gradinger R, Willmann G, Mittelmeier W. Computer-based motion simulation of total hip prostheses with ceramic-on-ceramic wear couple. analysis of implant design and orientation as influence parameters. *Z Orthop Ihre Grenzgeb.* 2002. 140: 310-316.

65. Kluess D, Martin H, Mittelmeier W, Schmitz KP, Bader R. Influence of femoral head size on impingement, dislocation and stress distribution in total hip replacement. *Med Eng Phys* 2007. 29: 465-471.

66. Barsoum WK, Patterson RW, Higuera C, Klika AK, Krebs VE, Molloy R. A computer model of the position of the combined component in the prevention of impingement in total hip replacement. *J Bone Joint Surg Br* 2007. 89: 839-845.

67. Pedersen DR, Callaghan JJ, Brown TD. Activity-dependence of the "safe zone" for impingement versus dislocation avoidance. *Med Eng Phys* 2005. 27: 323-328.

68. Fuss FK, Bacher A. New aspects of the morphology and function of the human hip joint ligaments. *Am J Anat* 1991. 192: 1-13.

69. Agur AMR, Dalley AF. 2009. Grant's atlas of anatomy, Eleventh Edition ed. Baltimore, Maryland: Lippincott Williams & Wilkins.

70. Kim YS, Kwon SY, Sun DH, Han SK, Maloney WJ. Modified posterior approach to total hip arthroplasty to enhance joint stability. *Clin Orthop Relat Res* 2008. 466: 294-299.

71. Suh KT, Park BG, Choi YJ. A posterior approach to primary total hip arthroplasty with soft tissue repair. *Clin Orthop Relat Res* 2004. 418: 162-167.

72. Pellicci PM, Bostrom M, Poss R. Posterior approach to total hip replacement using enhanced posterior soft tissue repair. *Clin Orthop Relat Res* 1998. 355: 224-228.

73. Yamaguchi T, Naito M, Asayama I, Kambe T, Fujisawa M, Ishiko T. The effect of posterolateral reconstruction on range of motion and muscle strength in total hip arthroplasty. *J Arthroplasty* 2003. 18: 347-351.

74. Stähelin T, Vienne P, Hersche O. Failure of reinserted short external rotator muscles after total hip arthroplasty. *J Arthroplasty* 2002. 17: 604-607.

75. Stähelin T, Drittenbass L, Hersche O, Miehlke W, Munzinger U. Failure of capsular enhanced short external rotator repair after total hip replacement. *Clin Orthop Relat Res* 2004. 420: 199-204.

76. Kao JT, Woolson ST. Piriformis tendon repair failure after total hip replacement. *Orthop Rev* 1992. 21: 171-174.

77. Robinson PS, Placide R, Soslowsky LJ, Born CT. Mechanical strength of repairs of the hip piriformis tendon. *J Arthroplasty* 2004. 19: 204-210.

78. Vicar AJ, Coleman CR. A comparison of the anterolateral, transtrochanteric, and posterior surgical approaches in primary total hip arthroplasty. *Clin Orthop Relat Res* 1984. 188: 152-159.

79. Masonis JL, Bourne RB. Surgical approach, abductor function, and total hip arthroplasty dislocation. *Clin Orthop Relat Res* 2002. 405: 46-53.

80. Berend KR, Sporer SM, Sierra RJ, Glassman AH, Morris MJ. Achieving stability and lower-limb length in total hip arthroplasty. *J Bone Joint Surg Am* 2010. 92: 2737-2752.

81. Elkins JM, Stroud NJ, Rudert MJ, Tochigi Y, Pedersen DR, Ellis BJ, Callaghan JJ, Weiss JA, Brown TD. The capsule's contribution to total hip construct stability--a finite element analysis. *J Orthop Res* 2011. 29: 1642-1648.

82. Stewart KJ, Pedersen DR, Callaghan JJ, Brown TD. Implementing capsule representation in a total hip dislocation finite element model. *Iowa Orthop J* 2004. 24: 1-8.

83. Gasser TC, Ogden RW, Holzapfel GA. Hyperelastic modeling of arterial layers with distributed collagen fibre orientations. *J R Soc Interface* 2006. 3: 15-35.

84. Stewart KJ, Edmonds-Wilson RH, Brand RA, Brown TD. Spatial distribution of hip capsule structural and material properties. *J Biomech* 2002. 35: 1491-1498.

85. Stroud NJ, Elkins JM, Tochigi Y, Rudert MJ, Brown TD. Cadaveric transpelvic implantation of THA hardware for physically testing an intact hip capsule with a dislocation challenge. *Transactions of the 57th Annual Meeting of the Orthopaedic Research Society. January 13-16, Long Beach, California.* 2011.

86. Stroud NJ. Advancements of a servohydraulic human hip joint motion simulator for experimental investigation of hip joint impingement/dislocation. M.S. Thesis, The University of Iowa, 2010.

87. Dihlmann W, Nebel G. Computed tomography of the hip joint capsule. *J Comput Assist Tomogr* 1983. 7: 278-285.

88. Gerber C, Schneeberger AG, Beck M, Schlegel U. Mechanical strength of repairs of the rotator cuff. *J Bone Joint Surg Br* 1994. 76: 371-380.

89. Carpenter NH, Gates DJ, Williams HT. Normal processes and restraints in wound healing. *Can J Surg* 1977. 20: 314-323.

90. Dovan TT, Ritty T, Ditsios K, Silva MJ, Kusano N, Gelberman RH. Flexor digitorum profundus tendon to bone tunnel repair: A vascularization and histologic study in canines. *J Hand Surg Am* 2005. 30: 246-257.

91. Flegal KM, Carroll MD, Kuczmarski RJ, Johnson CL. Overweight and obesity in the united states: Prevalence and trends, 1960-1994. Int J Obes Relat Metab Disord 1998. 22: 39-47.

92. Ogden CL, Carroll MD, Curtin LR, McDowell MA, Tabak CJ, Flegal KM. Prevalence of overweight and obesity in the united states, 1999-2004. *JAMA* 2006. 295: 1549-1555.

93. Flegal KM, Carroll MD, Ogden CL, Curtin LR. Prevalence and trends in obesity among US adults, 1999-2008. *JAMA* 2010. 303: 235-241.

94. Flegal KM, Graubard BI. Estimates of excess deaths associated with body mass index and other anthropometric variables. *Am J Clin Nutr* 2009. 89: 1213-1219.

95. Flegal KM, Graubard BI, Williamson DF, Gail MH. Excess deaths associated with underweight, overweight, and obesity. *JAMA* 2005. 293: 1861-1867.

96. Sturm R. Increases in morbid obesity in the USA: 2000-2005. *Public Health* 2007. 121: 492-496.

97. Das SR, Kinsinger LS, Yancy WS, Wang A, Ciesco E, Burdick M, Yevich SJ. Obesity prevalence among veterans at veterans affairs medical facilities. *Am J Prev Med* 2005. 28: 291-294.

98. Thompson D, Edelsberg J, Colditz GA, Bird AP, Oster G. Lifetime health and economic consequences of obesity. *Arch Intern Med* 1999. 159: 2177-2183.

99. Anandacoomarasamy A, Caterson I, Sambrook P, Fransen M, March L. The impact of obesity on the musculoskeletal system. *Int J Obes* 2008. 32: 211-222.

100. Sharma L, Lou C, Cahue S, Dunlop DD. The mechanism of the effect of obesity in knee osteoarthritis: The mediating role of malalignment. *Arthritis Rheumatism* 2001. 43: 568-575.

101. Sharma L, Chang A. Overweight: Advancing our understanding of its impact on the knee and the hip. *Ann Rheum Dis* 2007. 66: 141-142.

102. Lohmander L, Gerhardsson de Verdier M, Rollof J, Nilsson P, Engström G. Incidence of severe knee and hip osteoarthritis in relation to different measures of body mass: A population-based prospective cohort study. *Ann Rheum Dis* 2009. 68: 490-496.

103. Liu B, Balkwill A, Banks E, Cooper C, Green J, Beral V. Relationship of height, weight and body mass index to the risk of hip and knee replacements in middle-aged women. *Rheumatology* 2007. 46: 861-867.

104. Bourne R, Mukhi S, Zhu N, Keresteci M, Marin M. Role of obesity on the risk for total hip or knee arthroplasty. *Clin Orthop Relat Res* 2007. 465: 185-188.

105. Changulani M, Kalairajah Y, Peel T, Field RE. The relationship between obesity and the age at which hip and knee replacement is undertaken. *J Bone Joint Surg Br* 2008. 90: 360-363.

106. Fehring TK, Odum SM, Griffin WL, Mason JB, McCoy TH. The obesity epidemic: Its effect on total joint arthroplasty. *J Arthroplasty* 2007. 22: 71-76.

107. Turgeon T, Santore R, Coutts R. Influence of obesity on outcome following primary hip replacement. *AAOS 73rd Annual Meeting, Chicago* 2006. 15.

108. Pulido L, Ghanem E, Joshi A, Purtill JJ, Parvizi J. Periprosthetic joint infection: The incidence, timing, and predisposing factors. *Clin Orthop Relat Res* 2008. 466: 1710-1715.

109. Malinzak RA, Ritter MA, Berend ME, Meding JB, Olberding EM, Davis KE. Morbidly obese, diabetic, younger, and unilateral joint arthroplasty patients have elevated total joint arthroplasty infection rates. *J Arthroplasty* 2009. 24: 84-88.

110. Dowsey MM, Choong PF. Early outcomes and complications following joint arthroplasty in obese patients: A review of the published reports. *ANZ J Surg* 2008. 78: 439-444.

111. Dowsey MM, Choong PF. Obesity is a major risk factor for prosthetic infection after primary hip arthroplasty. *Clin Orthop Relat Res* 2008. 466: 153-158.

112. Grant JA, Viens N, Bolognesi MP, Olson SA, Cook CE. Two-year outcomes in primary THA in obese male veterans administration medical center patients. *Rheumatol Int* 2008. 28: 1105-1109.

113. Lubbeke A, Moons KG, Garavaglia G, Hoffmeyer P. Outcomes of obese and nonobese patients undergoing revision total hip arthroplasty. *Arthritis Rheum* 2008. 59: 738-745.

114. Lubbeke A, Stern R, Garavaglia G, Zurcher L, Hoffmeyer P. Differences in outcomes of obese women and men undergoing primary total hip arthroplasty. *Arthritis Rheum* 2007. 57: 327-334.

115. Andrew JG, Palan J, Kurup HV, Gibson P, Murray DW, Beard DJ. Obesity in total hip replacement. *J Bone Joint Surg Br* 2008. 90: 424-429.

116. Stickles B, Phillips L, Brox WT, Owens B, Lanzer WL. Defining the relationship between obesity and total joint arthroplasty. *Obes Res* 2001. 9: 219-223.

117. Busato A, Roder C, Herren S, Eggli S. Influence of high BMI on functional outcome after total hip arthroplasty. *Obes Surg* 2008. 18: 595-600.

118. Jackson MP, Sexton SA, Yeung E, Walter WL, Walter WK, Zicat BA. The effect of obesity on the mid-term survival and clinical outcome of cementless total hip replacement. *J Bone Joint Surg Br* 2009. 91: 1296-1300.

119. Singh JA, Lewallen D. Age, gender, obesity, and depression are associated with patient-related pain and function outcome after revision total hip arthroplasty. *Clin Rheumatol* 2009. 28: 1419-1430.

120. Kim SH. Morbid obesity and excessive hospital resource consumption for unilateral primary hip and knee arthroplasty. *J Arthroplasty* 2009.

121. Brown TD, Callaghan JJ. Impingement in total hip replacement: Mechanisms and consequences. *Curr Orthop* 2008. 22: 376-391.

122. McLaughlin JR, Lee KR. The outcome of total hip replacement in obese and non-obese patients at 10- to 18-years. *J Bone Joint Surg Br* 2006. 88: 1286-1292.

123. Paterno SA, Lachiewicz PF, Kelley SS. The influence of patient-related factors and the position of the acetabular component on the rate of dislocation after total hip replacement. *J Bone Joint Surg Am* 1997. 79: 1202-1210.

124. Azodi OS, Bellocco R, Eriksson K, Adami J. The impact of tobacco use and body mass index on the length of stay in hospital and the risk of post-operative complications among patients undergoing total hip replacement. *J Bone Joint Surg Br* 2006. 88: 1316-1320.

125. Kim Y, Morshed S, Joseph T, Bozic K, Ries MD. Clinical impact of obesity on stability following revision total hip arthroplasty. *Clin Orthop Relat Res* 2006. 453: 142-146.

126. Tilg H, Moschen AR. Adipocytokines: Mediators linking adipose tissue, inflammation and immunity. *Nature Reviews Immunology* 2006. 6: 772-783.

127. Anandacoomarasamy A, Fransen M, March L. Obesity and the musculoskeletal system. *Curr Opin Rheumatol* 2009. 21: 71-77.

128. Simopoulou T, Malizos K, Iliopoulos D, Stefanou N, Papatheodorou L, Ioannou M, Tsezou A. Differential expression of leptin and leptin's receptor isoform (ob-rb) mRNA between advanced and minimally affected osteoarthritic cartilage; effect on cartilage metabolism. *Osteoarthritis Cartilage* 2007. 15: 872-883.

129. Otero M, Lago R, Gomez R, Lago F, Dieguez C, Gomez-Reino J, Gualillo O. Changes in plasma levels of fat-derived hormones adiponectin, leptin, resistin and visfatin in patients with rheumatoid arthritis. *Ann Rheum Dis* 2006. 65: 1198-1201.

130. Wendelboe AM, Hegmann KT, Gren LH, Alder SC, White Jr GL, Lyon JL. Associations between body-mass index and surgery for rotator cuff tendinitis. *J Bone Joint Surg Am* 2004. 86: 743-747.

131. Werner RA, Franzblau A, Gell N, Ulin SS, Armstrong TJ. A longitudinal study of industrial and clerical workers: Predictors of upper extremity tendonitis. *J Occup Rehabil* 2005. 15: 37-46.

132. Shah MK. Simultaneous bilateral rupture of quadriceps tendons: Analysis of risk factors and associations. *South Med J* 2002. 95: 860-866.

133. Kelley DE, Slasky BS, Janosky J. Skeletal muscle density: Effects of obesity and non-insulin-dependent diabetes mellitus. *Am J Clin Nutr* 1991. 54: 509-515.

134. Dalferes ER,Jr, Radhakrishnamurthy B, Crouch MS, Berenson GS. A study of connective tissue macromolecules in skin of mice with goldthioglucose-induced obesity. *Proc Soc Exp Biol Med* 1975. 148: 918-924.

135. de Jongh RT, Serne EH, IJzerman RG, de Vries G, Stehouwer CDA. Impaired microvascular function in obesity: Implications for obesity-associated microangiopathy, hypertension, and insulin resistance. *Circulation* 2004. 109: 2529-2535.

136. Light D, Arvanitis GM, Abramson D, Glasberg SB. Effect of weight loss after bariatric surgery on skin and the extracellular matrix. *Plast Reconstr Surg* 2010. 125: 343-351.

137. Enser M, Avery N. Mechanical and chemical properties of the skin and its collagen from lean and obese-hyperglycaemic (ob/ob) mice. *Diabetologia* 1984. 27: 44-49.

138. Wilson JA, Clark JJ. Obesity: Impediment to postsurgical wound healing. *Adv Skin Wound Care* 2004. 17: 426-435.

139. Groszek DM. Promoting wound healing in the obese patient. *AORN* 1982. 35: 1132-1135.

140. Werner S, Grose R. Regulation of wound healing by growth factors and cytokines. *Physiol Rev* 2003. 83: 835-870.

141. Suter PM, Tremblay A. Is alcohol consumption a risk factor for weight gain and obesity? *Crit Rev Clin Lab Sci* 2005. 42: 197-227.

142. Colne P, Frelut ML, Peres G, Thoumie P. Postural control in obese adolescents assessed by limits of stability and gait initiation. *Gait Posture* 2008. 28: 164-169.

143. Menegoni F, Galli M, Tacchini E, Vismara L, Cavigioli M, Capodaglio P. Gender-specific effect of obesity on balance. *Obesity* 2009. 17: 1951-1956.

144. Singh D, Park W, Levy MS, Jung ES. The effects of obesity and standing time on postural sway during prolonged quiet standing. *Ergonomics* 2009. 52: 977-986.

145. Teasdale N, Hue O, Marcotte J, Berrigan F, Simoneau M, Dore J, Marceau P, Marceau S, Tremblay A. Reducing weight increases postural stability in obese and morbid obese men. *Int J Obes* 2007. 31: 153-160.

146. Hulens M, Vansant G, Lysens R, Claessens AL, Muls E, Brumagne S. Study of differences in peripheral muscle strength of lean versus obese women: An allometric approach. *Int J Obes Relat Metab Disord* 2001. 25: 676-681.

147. Maffiuletti NA, Jubeau M, Munzinger U, Bizzini M, Agosti F, De Col A, Lafortuna CL, Sartorio A. Differences in quadriceps muscle strength and fatigue between lean and obese subjects. *Eur J Appl Physiol* 2007. 101: 51-59.

148. Singh B, Brown TD, Callaghan JJ, Yack HJ. Abdomen-thigh contact forces during functional reaching tasks in obese individuals. *The 34th Annual Meeting of the American Society of Biomechanics, Providence, RI. August 18-21* 2010.

149. Ley C, Lees B, Stevenson J. Sex-and menopause-associated changes in body-fat distribution. *Am J Clin Nutr* 1992. 55: 950-954.

150. Hills AP, Hennig EM, Byrne NM, Steele JR. The biomechanics of adiposity--structural and functional limitations of obesity and implications for movement. *Obes Rev* 2002. 3: 35-43.

151. Lai PP, Leung AK, Li AN, Zhang M. Three-dimensional gait analysis of obese adults. *Clin Biomech* 2008. 23 Suppl 1: S2-6.

152. Nantel J, Brochu M, Prince F. Locomotor strategies in obese and non-obese children. *Obesity* 2006. 14: 1789-1794.

153. Berrigan F, Simoneau M, Tremblay A, Hue O, Teasdale N. Influence of obesity on accurate and rapid arm movement performed from a standing posture. *Int J Obes* 2006. 30: 1750-1757.

154. Lafortuna CL, Maffiuletti NA, Agosti F, Sartorio A. Gender variations of body composition, muscle strength and power output in morbid obesity. *Int J Obes* 2005. 29: 833-841.

155. Achard de Leluardiere F, Hajri LN, Lacouture P, Duboy J, Frelut ML, Peres G. Validation and influence of anthropometric and kinematic models of obese teenagers in vertical jump performance and mechanical internal energy expenditure. *Gait Posture* 2006. 23: 149-158.

156. Galli M, Crivellini M, Sibella F, Montesano A, Bertocco P, Parisio C. Sit-to-stand movement analysis in obese subjects. Int J Obes Relat Metab Disord 2000. 24: 1488-1492.

157. Sibella F, Galli M, Romei M, Montesano A, Crivellini M. Biomechanical analysis of sit-to-stand movement in normal and obese subjects. *Clin Biomech* 2003. 18: 745-750.

158. Samani A, Bishop J, Yaffe M, Plewes D. Biomechanical 3-D finite element modeling of the human breast using MRI data. *IEEE Trans Med Imaging* 2001. 20: 271-279.

159. Aritan S, Oyadiji SO, Bartlett RM. The in vivo mechanical properties of muscular bulk tissue. *Conf Proc IEEE Eng Med Biol Soc* 2009. 5259-5262.

160. McDowell MA, Fryar CD, Hirsch R, Ogden CL. Anthropometric reference data for children and adults: US population, 1999–2002. *Adv Data* 2005. 361: 1-5.

161. Bartz RL, Noble PC, Kadakia NR, Tullos HS. The effect of femoral component head size on posterior dislocation of the artificial hip joint. *J Bone Joint Surg Am* 2000. 82: 1300-1307.

162. Rittmeister M, Callitsis C. Factors influencing cup orientation in 500 consecutive total hip replacements. *Clin Orthop Relat Res* 2006. 445: 192-196.

163. Murray D. The definition and measurement of acetabular orientation. *J Bone Joint Surg Br* 1993. 75: 228-232.

164. Jaramaz B, DiGioia III AM, Blackwell M, Nikou C. Computer assisted measurement of cup placement in total hip replacement. *Clin Orthop Relat Res* 1998. 354: 70-81.

165. Elkins JM, O'Brien MK, Stroud NJ, Pedersen DR, Callaghan JJ, Brown TD. Hard-on-hard total hip impingement causes extreme contact stress concentrations. *Clin Orthop Relat Res* 2011. 469: 454-463.

166. Tanino H, Harman MK, Banks SA, Hodge WA. Association between dislocation, impingement, and articular geometry in retrieved acetabular polyethylene cups. *J Orthop Res* 2007. 25: 1401-1407.

167. Barrack RL, Schmalzried TP. Impingement and rim wear associated with early osteolysis after a total hip replacement : A case report. *J Bone Joint Surg Am* 2002. 84-A: 1218-1220.

168. Scifert CF, Noble PC, Brown TD, Bartz RL, Kadakia N, Sugano N, Johnston RC, Pedersen DR, Callaghan JJ. Experimental and computational simulation of total hip arthroplasty dislocation. *Orthop Clin North Am* 2001. 32: 553-567.

169. Sanders AP, Brannon RM. Assessment of the applicability of the Hertzian contact theory to edge-loaded prosthetic hip bearings. *J Biomech* 2011. 44: 2802-2808.

170. Brockett C, Williams S, Jin Z, Isaac G, Fisher J. Friction of total hip replacements with different bearings and loading conditions. *J Biomed Mater Res B Appl Biomater* 2007. 81: 508-515.

171. Archard J. Contact and rubbing of flat surfaces. *J Appl Phys* 1953. 24: 981-988.

172. Liu F, Leslie I, Williams S, Fisher J, Jin Z. Development of computational wear simulation of metal-on-metal hip resurfacing replacements. *J Biomech* 2008. 41: 686-694.

173. Chandler DR, Glousman R, Hull D, McGuire PJ, Kim IS, Clarke IC, Sarmiento A. Prosthetic hip range of motion and impingement: The effects of head and neck geometry. *Clin Orthop Relat Res* 1982. 166: 284-291.

174. Cinotti G, Lucioli N, Malagoli A, Calderoli C, Cassese F. Do large femoral heads reduce the risks of impingement in total hip arthroplasty with optimal and non-optimal cup positioning? *Int Orthop* 2011. 35:317-323.

175. Elkins JM, Pedersen DR, Callaghan JJ, Brown TD. Fracture propagation propensity of ceramic liners during impingement-subluxation. *J Arthroplasty* 2011. PMID 21855277 [Epub ahead of print].

176. Sedel L. Evolution of alumina-on-alumina implants: A review. *Clin Orthop Relat Res* 2000. (379): 48-54.

177. Irwin GR. *Analysis of stresses and strains near the end of a crack traversing a plate. J. Appl. Mech* 1957. 24: 361-364.

178. Willmann G. Ceramic femoral heads for total hip arthroplasty. *Adv Engineer Mater* 2000. 2: 114-122.

179. Hannouche D, Hamadouche M, Nizard R, Bizot P, Meunier A, Sedel L. Ceramics in total hip replacement. *Clin Orthop Relat Res* 2005. (430): 62-71.

180. Heimke G. The safety of ceramic balls on metal stems in hip arthroplasty. *Adv Mater* 2004. 6: 165-170.

181. Andrisano AO, Dragoni E, Strozzi A. Axisymmetric mechanical analysis of ceramic heads for total hip replacement. *Proc Inst Mech Eng H* 1990. 204: 157-167.

182. Dorre E, Richter HG, Willmann G. Fracture load of ceramic ball heads of hip joint prostheses. *Biomed Tech (Berl)* 1991. 36: 305-307.

183. Anderson I, Bowden M, Wyatt T. Stress analysis of hemispherical ceramic hip prosthesis bearings. *Med Eng Phys* 2005. 27: 115-122.

184. Weisse B, Zahner M, Weber W, Rieger W. Improvement of the reliability of ceramic hip joint implants. *J Biomech* 2003. 36: 1633-1639.

185. Drouin J, Cales B, Chevalier J, Fantozzi G. Fatigue behavior of zirconia hip joint heads: Experimental results and finite element analysis. *J Biomed Mater Res A* 1997. 34: 149-155.

186. Knahr K, Böhler M, Frank P, Plenk H, Salzer M. Survival analysis of an uncemented ceramic acetabular component in total hip replacement. *Arch Orthop Trauma Surg* 1987. 106: 297-300.

187. Willmann G. Ceramic femoral head retrieval data. *Clin Orthop Relat Res* 2000. (379): 22-28.

188. Ha YC, Kim SY, Kim HJ, Yoo JJ, Koo KH. Ceramic liner fracture after cementless alumina-on-alumina total hip arthroplasty. *Clin Orthop Relat Res* 2007. 458: 106-110.

189. Park YS, Hwang SK, Choy WS, Kim YS, Moon YW, Lim SJ. Ceramic failure after total hip arthroplasty with an alumina-on-alumina bearing. *J Bone Joint Surg Am* 2006. 88: 780-787.

190. Toni A, Traina F, Stea S, Sudanese A, Visentin M, Bordini B, Squarzoni S. Early diagnosis of ceramic liner fracture. guidelines based on a twelve-year clinical experience. *J Bone Joint Surg Am* 2006. 88 Suppl 4: 55-63.

191. Sariali E, Stewart T, Mamoudy P, Jin Z, Fisher J. Undetected fracture of an alumina ceramic on ceramic hip prosthesis. *J Arthroplasty* 2010. 658 e1-5.

192. Hannouche D, Nich C, Bizot P, Meunier A, Nizard R, Sedel L. Fractures of ceramic bearings: History and present status. *Clin Orthop Relat Res* 2003. 417: 19-26.

193. Poggie RA, Turgeon TR, Coutts RD. Failure analysis of a ceramic bearing acetabular component. *J Bone Joint Surg Am* 2007. 89: 367-375.

194. Hasegawa M, Sudo A, Hirata H, Uchida A. Ceramic acetabular liner fracture in total hip arthroplasty with a ceramic sandwich cup. *J Arthroplasty* 2003. 18: 658-661.

195. Min BW, Song KS, Kang CH, Bae KC, Won YY, Lee KY. Delayed fracture of a ceramic insert with modern ceramic total hip replacement. *J Arthroplasty* 2007. 22: 136-139.

196. Barrack RL, Burak C, Skinner HB. Concerns about ceramics in THA. *Clin Orthop Relat Res* 2004. 429: 73-79.

197. Maher SA, Lipman JD, Curley LJ, Gilchrist M, Wright TM. Mechanical performance of ceramic acetabular liners under impact conditions. *J Arthroplasty* 2003. 18: 936-941.

198. Bierbaum BE, Nairus J, Kuesis D, Morrison JC, Ward D. Ceramic-on-ceramic bearings in total hip arthroplasty. *Clin Orthop Relat Res* 2002. 405: 158-163.

199. Diwanji SR, Seon JK, Song EK, Yoon TR. Fracture of the ABC ceramic liner: A report of three cases. *Clin Orthop Relat Res* 2007. 464: 242-246.

200. Elkins JM, Liu C, Qin X, Du Z, Brown TD. Ceramic total hip bearing fracture modeling in abaqus using co-simulation and extended finite element modeling. *Proceedings of the 2011 SIMULIA Customer Conference* 2011. 670-679.

201. Amanatullah DF, Landa J, Strauss EJ, Garino JP, Kim SH, Di Cesare PE. Comparison of surgical outcomes and implant wear between ceramic-ceramic and ceramic-polyethylene articulations in total hip arthroplasty. *J Arthroplasty* 2011. 26: 72-77.

202. Lee YK, Yoo JJ, Koo KH, Yoon KS, Kim HJ. Metal neck and liner impingement in ceramic bearing total hip arthroplasty. *J Orthop Res* 2011. 29: 218-222.

203. Moes N, Dolbow J, Belytschko T. A finite element method for crack growth without remeshing. *Int J Numer Meth Engng* 1999. 46: 131-150.

204. CeramTec AG. Scientific information and performance data, Biolox Delta - nanocomposites for arthroplasty. the fourth generation of ceramics, medical product division, CeramTec AG, p.11. 2008.

205. Nevelos J, Ingham E, Doyle C, Fisher J, Nevelos A. Analysis of retrieved alumina ceramic components from Mittelmeier total hip prostheses. *Biomaterials* 1999. 20: 1833-1840.

206. Global Business Intelligence Research. The future of orthopedic implants, analysis and forecasts to 2016 - joint reconstruction and spinal implants creating growth opportunities. May 2010.

207. Girard J, Bocquet D, Autissier G, Fouilleron N, Fron D, Migaud H. Metal-on-metal hip arthroplasty in patients thirty years of age or younger. *J Bone Joint Surg Am* 2010. 92: 2419.

208. Zywiel MG, Sayeed SA, Johnson AJ, Schmalzried TP, Mont MA. Survival of hard-on-hard bearings in total hip arthroplasty: A systematic review. *Clin Orthop Relat Res* 2011. 469:1536-1546

209. Dobbs H, Minski M. Metal ion release after total hip replacement. *Biomaterials* 1980. 1: 193-198.

210. Willert HG, Buchhorn GH, Fayyazi A, Flury R, Windler M, Koster G, Lohmann CH. Metal-on-metal bearings and hypersensitivity in patients with artificial hip joints. A clinical and histomorphological study. *J Bone Joint Surg Am* 2005. 87: 28-36.

211. Pandit H, Glyn-Jones S, McLardy-Smith P, Gundle R, Whitwell D, Gibbons CL, Ostlere S, Athanasou N, Gill HS, Murray DW. Pseudotumours associated with metal-on-metal hip resurfacings. *J Bone Joint Surg Br* 2008. 90: 847-851.

212. Langton D, Jameson S, Joyce T, Hallab N, Natu S, Nargol A. Early failure of metal-on-metal bearings in hip resurfacing and large-diameter total hip replacement: A consequence of excess wear. *J Bone Joint Surg Br* 2010. 92: 38-46.

213. Browne JA, Bechtold CD, Berry DJ, Hanssen AD, Lewallen DG. Failed metal-on-metal hip arthroplasties: A spectrum of clinical presentations and operative findings. *Clin Orthop Relat Res* 2010. 468: 2313-2320.

214. Donell S, Darrah C, Nolan J, Wimhurst J, Toms A, Barker T, Case C, Tucker J. Early failure of the Ultima metal-on-metal total hip replacement in the presence of normal plain radiographs. *J Bone Joint Surg Br* 2010. 92: 1501-1508.

215. Bolland B, Culliford D, Langton D, Millington J, Arden N, Latham J. High failure rates with a large-diameter hybrid metal-on-metal total hip replacement: Clinical, radiological and retrieval analysis. *J Bone Joint Surg Br* 2011. 93: 608-615.

216. Langton D, Jameson S, Joyce T, Gandhi J, Sidaginamale R, Mereddy P, Lord J, Nargol A. Accelerating failure rate of the ASR total hip replacement. *J Bone Joint Surg Br* 2011. 93: 1011-1016.

217. Williams S, Leslie I, Isaac G, Jin Z, Ingham E, Fisher J. Tribology and wear of metal-on-metal hip prostheses: Influence of cup angle and head position. *J Bone Joint Am* 2008. 90: 111-117.

218. Khan M, Kuiper JH, Richardson J. The exercise-related rise in plasma cobalt levels after metal-on-metal hip resurfacing arthroplasty. *J Bone Joint Surg Br* 2008. 90: 1152-1157.

219. De Haan R, Pattyn C, Gill HS, Murray DW, Campbell PA, De Smet K. Correlation between inclination of the acetabular component and metal ion levels in metal-on-metal hip resurfacing replacement. *J Bone Joint Surg Br* 2008. 90: 1291-1297.

220. Elkins JM, Kruger KM, Pedersen DR, Callaghan JJ, Brown TD. Edge-loading severity as a function of cup lip radius in metal-on-metal total hips - A finite element analysis. *J Orthop Res* 2012. 2012. 30: 169-177.

221. Udofia IJ, Yew A, Jin ZM. Contact mechanics analysis of metal-on-metal hip resurfacing prostheses. *Proc Inst Mech Eng H* 2004. 218: 293-305.

222. Lusty PJ, Watson A, Tuke MA, Walter WL, Walter WK, Zicat B. Wear and acetabular component orientation in third generation alumina-on-alumina ceramic bearings: An analysis of 33 retrievals. *J Bone Joint Surg Br* 2007. 89: 1158-1164.

223. Brodner W, Grübl A, Jankovsky R, Meisinger V, Lehr S, Gottsauner-Wolf F. Cup inclination and serum concentration of cobalt and chromium after metal-on-metal total hip arthroplasty. *J Arthroplasty* 2004. 19: 66-70.

224. Bernstein M, Walsh A, Petit A, Zukor DJ, Antoniou J. Femoral head size does not affect ion values in metal-on-metal total hips. *Clin Orthop Relat Res* 1-1650.

225. Leslie I, Williams S, Brown C, Isaac G, Jin Z, Ingham E, Fisher J. Effect of bearing size on the long-term wear, wear debris, and ion levels of large diameter metal-on-metal hip replacements? an in vitro study. *J Biomed Mater Res B Appl Biomater* 2008. 87B: 163-172.

226. Leslie IJ, Williams S, Isaac G, Ingham E, Fisher J. High cup angle and microseparation increase the wear of hip surface replacements. *Clin Orthop Relat Res* 2009. 467: 2259-2265.

227. Al-Hajjar M, Leslie IJ, Tipper J, Williams S, Fisher J, Jennings LM. Effect of cup inclination angle during microseparation and rim loading on the wear of biolox delta ceramic-on-ceramic total hip replacement. *J Biomed Mater Res B Appl Biomater* 2010. 95: 263-268.

228. Mak MM, Besong AA, Jin ZM, Fisher J. Effect of microseparation on contact mechanics in ceramic-on-ceramic hip joint replacements. *Proc Inst Mech Eng H* 2002. 216: 403-408.

229. Griffin WL, Nanson CJ, Springer BD, Davies MA, Fehring TK. Reduced articular surface of one-piece cups: A cause of runaway wear and early failure. *Clin Orthop Relat Res* 2010. 468: 2328-2332.

230. Mak M, Jin Z, Fisher J, Stewart TD. Influence of acetabular cup rim design on the contact stress during edge loading in ceramic-on-ceramic hip prostheses. *J Arthroplasty* 2011. 26: 131-136.

231. ASTM F-799-95. Standard specification for cobalt-28 chromium-6 molybdenum alloy forgings for surgical implants. *American Society for Testing and Materials.* 1995. 13.01: 230-232.

232. Johansson HR, Johnson AJ, Zywiel MG, Naughton M, Mont MA, Bonutti PM. Does acetabular inclination angle affect survivorship of alumina-ceramic articulations? *Clin Orthop Relat Res* 469: 1560-1566.

233. Walter WL, Insley GM, Walter WK, Tuke MA. Edge loading in third generation alumina ceramic-on-ceramic bearings: Stripe wear. *J Arthroplasty* 2004. 19: 402-413.

234. Antoine J, Visa C, Sauvey C, Abba G. Approximate analytical model for Hertzian elliptical contact problems. *J Tribol* 2006. 128: 660-664.

235. Sariali E, Lazennec JY, Khiami F, Catonne Y. Mathematical evaluation of jumping distance in total hip arthroplasty: Influence of abduction angle, femoral head offset, and head diameter. *Acta Orthop* 2009. 80: 277-282.

236. Berry DJ, von Knoch M, Schleck CD, Harmsen WS. Effect of femoral head diameter and operative approach on risk of dislocation after primary total hip arthroplasty. *J Bone Joint Surg Am* 2005. 87: 2456-2463.

237. Berton C, Girard J, Krantz N, Migaud H. The Durom large diameter head acetabular component: Early results with a large-diameter metal-on-metal bearing. *J Bone Joint Surg Br* 2010. 92: 202-208.

238. Garbuz DS, Tanzer M, Greidanus NV, Masri BA, Duncan CP. The John Charnley award: Metal-on-metal hip resurfacing versus large-diameter head metal-on-metal total hip arthroplasty: A randomized clinical trial. *Clin Orthop Relat Res* 2010. 468: 318-325.

239. Silva M, Heisel C, Schmalzried TP. Metal-on-metal total hip replacement. *Clin Orthop Relat Res* 2005. 430: 53-61.

240. Dowson D, Hardaker C, Flett M, Isaac GH. A hip joint simulator study of the performance of metal-on-metal joints: Part II: Design. *J Arthroplasty* 2004. 19: 124-130.

241. Howie DW, McCalden RW, Nawana NS, Costi K, Pearcy MJ, Subramanian C. The long-term wear of retrieved McKee-farrar metal-on-metal total hip prostheses. *J Arthroplasty* 2005. 20: 350-357.

242. Cuckler JM, Moore KD, Lombardi AV, McPherson E, Emerson R. Large versus small femoral heads in metal-on-metal total hip arthroplasty. *J Arthroplasty* 2004. 19: 41-44.

243. Stuchin SA. Anatomic diameter femoral heads in total hip arthroplasty: A preliminary report. *J Bone Joint Surg Am* 2008. 90 Suppl 3: 52-56.

244. Lombardi AV, Skeels MD, Berend KR, Adams JB, Franchi OJ. Do large heads enhance stability and restore native anatomy in primary total hip arthroplasty? *Clin Orthop Relat Res* 2010. 1-1553.

245. Burroughs BR, Hallstrom B, Golladay GJ, Hoeffel D, Harris WH. Range of motion and stability in total hip arthroplasty with 28-, 32-, 38-, and 44-mm femoral head sizes: An in vitro study. *J Arthroplasty* 2005. 20: 11-19.

246. D'Lima DD, Urquhart AG, Buehler KO, Walker RH, COLWELL CW. The effect of the orientation of the acetabular and femoral components on the range of motion of the hip at different head-neck ratios. *J Bone Joint Surg Am* 2000. 82: 315-321.

247. Scifert CF, Brown TD, Pedersen DR, Callaghan JJ. A finite element analysis of factors influencing total hip dislocation. *Clin Orthop Relat Res* 1998. 355: 152-162.

248. Crowninshield RD, Maloney WJ, Wentz DH, Humphrey SM, Blanchard CR. Biomechanics of large femoral heads: What they do and don't do. *Clin Orthop Relat Res* 2004. 429: 102-107.

249. Fessler H, Fricker D. Friction in femoral prosthesis and photoelastic model cone taper joints. *Proc Inst Mech Eng H* 1989. 203: 1-14.

250. Heiney JP, Battula S, Vrabec GA, Parikh A, Blice R, Schoenfeld AJ, Njus GO. Impact magnitudes applied by surgeons and their importance when applying the femoral head onto the Morse taper for total hip arthroplasty. *Arch Orthop Trauma Surg* 2009. 129: 793-796.

251. Elias JJ, Nagao M, Chu YH, Carbone JJ, Lennox DW, Chao E. Medial cortex strain distribution during noncemented total hip arthroplasty. *Clin Orthop Relat Res* 2000. 370: 250-258.

252. Dorr LD, Wolf AW, Chandler R, Conaty JP. Classification and treatment of dislocations of total hip arthroplasty. *Clin Orthop Relat Res* 1983. 173: 151-158.

253. Svensson O, Mathiesen EB, Reinholt F, Blomgren G. Formation of a fulminant soft-tissue pseudotumor after uncemented hip arthroplasty: A case report. *J Bone Joint Surg Am* 1988. 70: 1238-1242.

254. McKellop HA, Sarmiento A, Brien W, Park SH. Interface corrosion of a modular head total hip prosthesis. *J Arthroplasty* 1992. 7: 291-294.

255. Gilbert JL, Buckley CA, Jacobs JJ. In vivo corrosion of modular hip prosthesis components in mixed and similar metal combinations. the effect of crevice, stress, motion, and alloy coupling. *J Biomed Mater Res* 1993. 27: 1533-1544.

256. Goldberg JR, Gilbert JL, Jacobs JJ, Bauer TW, Paprosky W, Leurgans S. A multicenter retrieval study of the taper interfaces of modular hip prostheses. *Clin Orthop Relat Res* 2002. 401: 149-161.

257. Collier JP, Mayor MB, Williams IR, Surprenant VA, Surprenant HP, Currier BH. The tradeoffs associated with modular hip prostheses. *Clin Orthop Relat Res* 1995. 311: 91-101.

258. Cook SD, Barrack RL, Clemow A. Corrosion and wear at the modular interface of uncemented femoral stems. *J Bone Joint Surg Br* 1994. 76: 68-72.

259. Goldberg JR, Gilbert JL. In vitro corrosion testing of modular hip tapers. *J Biomed Mater Res B Appl Biomater* 2003. 64: 78-93.

260. Brown S, Flemming C, Kawalec J, Placko H, Vassaux C, Merritt K, Payer J, Kraay M. Fretting corrosion accelerates crevice corrosion of modular hip tapers. *J Appl Biomater* 1995. 6: 19-26.

261. Fisher J. Bioengineering reasons for the failure of metal-on-metal hip prostheses: An engineer's perspective. *J Bone Joint Surg Br* 2011. 93: 1001-1004.

262. Jacobs JJ, Gilbert JL, Urban RM. Current concepts review. corrosion of metal orthopaedic implants. *J Bone Joint Surg Am* 1998. 80: 268-282.

263. Kop AM, Swarts E. Corrosion of a hip stem with a modular neck taper junction: A retrieval study of 16 cases. *J Arthroplasty* 2009. 24: 1019-1023.

264. Annual report of the Australian orthopaedic association national joint registry. http://www.dmac.adelaide.edu.au/aoanjrr/documents/aoanjrrreport_2010.pdf. accessed Nov, 2011.

265. Insall JN. Presidential address to the knee society: Choices and compromises in total knee arthroplasty. *Clin Orthop Relat Res* 1988. 226: 43-48.

266. Annual report of the U.K. national joint registry. http://www.njrcentre.org.uk/NjrCentre/Portals/0/Documents/NJR%208th%20Annual%20Report%202011.pdf accessed Nov. 2011.

267. Dastane MR, Long WT, Wan Z, Chao L, Dorr LD. Metal-on-metal hip arthroplasty does equally well in osteonecrosis and osteoarthritis. *Clin Orthop Relat Res* 2008. 466: 1148-1153.

268. Delaunay CP, Bonnomet F, Clavert P, Laffargue P, Migaud H. THA using metal-on-metal articulation in active patients younger than 50 years. *Clin Orthop Relat Res* 2008. 466: 340-346.

269. Dorr LD, Wan Z, Longjohn DB, Dubois B, Murken R. Total hip arthroplasty with use of the Metasul metal-on-metal articulation. four to seven-year results. *J Bone Joint Surg Am* 2000. 82: 789-798.

270. Eswaramoorthy V, Moonot P, Kalairajah Y, Biant L, Field R. The Metasul metal-on-metal articulation in primary total hip replacement: Clinical and radiological results at ten years. *J Bone Joint Surg Br* 2008. 90: 1278-1283.

271. Grübl A, Marker M, Brodner W, Giurea A, Heinze G, Meisinger V, Zehetgruber H, Kotz R. Long-term follow-up of metal-on-metal total hip replacement. *J Orthop Res* 2007. 25: 841-848.

272. Jacobs M, Gorab R, Mattingly D, Trick L, Southworth C. Three-to six-year results with the Ultima metal-on-metal hip articulation for primary total hip arthroplasty. *J Arthroplasty* 2004. 19: 48-53.

273. Lombardi AV, Mallory TH, Alexiades MM, Cuckler JM, Faris PM, Jaffe KA, Keating EM, Nelson CL, Ranawat CS, Williams J. Short-term results of the M2a-taper metal-on-metal articulation. *J Arthroplasty* 2001. 16: 122-128.

274. Long WT, Dorr LD, Gendelman V. An American experience with metal-on-metal total hip arthroplasties: A 7-year follow-up study. *J Arthroplasty* 2004. 19: 29-34.

275. MacDonald SJ, McCalden R, Chess D, Bourne R, Rorabeck C, Cleland D, Leung F. Metal-on-metal versus polyethylene in hip arthroplasty: A randomized clinical trial. *Clin Orthop Relat Res* 2003. 406: 282-296.

276. Neumann DRP, Thaler C, Hitzl W, Huber M, Hofstädter T, Dorn U. Long-term results of a contemporary metal-on-metal total hip arthroplasty: A 10-year follow-up study. *J Arthroplasty* 2010. 25: 700-708.

277. Paleochorlidis IS, Badras LS, Skretas EF, Georgaklis VA, Karachalios TS, Malizos KN. Clinical outcome study and radiological findings of Zweymuller metal on metal total hip arthroplasty. a follow-up of 6 to 15 years. *Hip Int.* 2009. 19: 301-308.

278. Saito S, Ryu J, Watanabe M, Ishii T, Saigo K. Midterm results of Metasul metal-on-metal total hip arthroplasty. *J Arthroplasty* 2006. 21: 1105-1110.

279. Sharma S, Vassan U, Bhamra MS. Metal-on-metal total hip joint replacement: A minimum follow-up of five years. *Hip Int.* 2007. 17: 70-77.

280. Wagner M, Wagner H. Medium-term results of a modern metal-on-metal system in total hip replacement. *Clin Orthop Relat Res* 2000. 379: 123-133.

281. Weber BG. Experience with the Metasul total hip bearing system. *Clin Orthop Relat Res* 1996. 329: S69-S77.

282. Zijlstra WP, Van Raay JJ, Bulstra SK, Deutman R. No superiority of cemented metal-on-metal over metal-on-polyethylene THA in a randomized controlled trial at 10-year follow-up. *Orthopedics* 2010. 154-161.

283. Biedermann R, Tonin A, Krismer M, Rachbauer F, Eibl G, Stöckl B. Reducing the risk of dislocation after total hip arthroplasty: The effect of orientation of the acetabular component. *J Bone Joint Surg Br.* 2005. 87: 762-769.

284. Morrey B. Instability after total hip arthroplasty. *Orthop Clin North Am* 1992. 23: 237-248.

285. McCollum DE, Gray WJ. Dislocation after total hip arthroplasty. causes and prevention. *Clin Orthop Relat Res* 1990. 261: 159-170.

286. Charnley J. 1979. Low friction arthroplasty of the hip: Theory and practice. Berlin: Springer-Verlag.

287. Barrack RL, Lavernia C, Ries M, Thornberry R, Tozakoglou E. Virtual reality computer animation of the effect of component position and design on stability after total hip arthroplasty. *Orthop Clin North Am* 2001. 32: 569-77, vii.

288. Widmer KH, Zurfluh B. Compliant positioning of total hip components for optimal range of motion. *J Orthop Res* 2004. 22: 815-821.

289. Yoshimine F. The safe-zones for combined cup and neck anteversions that fulfill the essential range of motion and their optimum combination in total hip replacements. *J Biomech* 2006. 39: 1315-1323.

290. Ranawat CS, Maynard MJ. Modern technique of cemented total hip arthroplasty. *Tech Orthop* 1991. 6: 17-25.

291. Jolles BM, Zangger P, Leyvraz PF. Factors predisposing to dislocation after primary total hip arthroplasty. *J Arthroplasty* 2002. 17: 282-288.

292. Hisatome T, Doi H. Theoretically optimum position of the prosthesis in total hip arthroplasty to fulfill the severe range of motion criteria due to neck impingement. *Journal of Orthopaedic Science* 2011. 16: 229-237.

293. Fackler CD, Poss R. Dislocation in total hip arthroplasties. *Clin Orthop Relat Res* 1980. 151: 169-178.

294. Dorr LD, Malik A, Dastane M, Wan Z. Combined anteversion technique for total hip arthroplasty. *Clin Orthop Relat Res* 2009. 467: 119-127.

295. Kelley SS, Lachiewicz PF, Hickman JM, Paterno SM. Relationship of femoral head and acetabular size to the prevalence of dislocation. *Clin Orthop Relat Res* 1998. 355: 163-170.

296. Amlie E, Hovik O, Reikeras O. Dislocation after total hip arthroplasty with 28 and 32-mm femoral head. *J Orthop Traumatol.* 2010. 11: 111-115.

297. Hedlundh U, Ahnfelt L, Hybbinette CH, Wallinder L, Weckström J, Fredin H. Dislocations and the femoral head size in primary total hip arthroplasty. *Clin Orthop Relat Res* 1996. 333: 226-233.

298. Pierchon F, Pasquier G, Cotten A, Fontaine C, Clarisse J, Duquennoy A. Causes of dislocation of total hip arthroplasty. CT study of component alignment. *J Bone Joint Surg Br* 1994. 76: 45-48.

299. Wines AP, McNicol D. Computed tomography measurement of the accuracy of component version in total hip arthroplasty. *J Arthroplasty* 2006. 21: 696-701.

300. Maruyama M, Feinberg JR, Capello WN, D'Antonio JA. Morphologic features of the acetabulum and femur: Anteversion angle and implant positioning. *Clin Orthop Relat Res* 2001. 393: 52-65.

301. Maxian TA, Brown TD, Pedersen DR, Callaghan JJ. Adaptive finite element modeling of long-term polyethylene wear in total hip arthroplasty. *J Orthop Res* 1996. 14: 668-675.

302. Maxian TA, Brown TD, Pedersen DR, Callaghan JJ. A sliding-distance-coupled finite element formulation for polyethylene wear in total hip arthroplasty. *J Biomech* 1996. 29: 687-692.

303. Grandy J. Efficient computation of volume of hexahedral cells. *Lawrence Livermore National Laboratory, Livermore, CA* 1997.

304. Lundberg HJ. Third body acceleration of THA wear. Ph.D. Thesis, the University of Iowa, 2006.

305. Morlock M, Schneider E, Bluhm A, Vollmer M, Bergmann G, Muller V, Honl M. Duration and frequency of every day activities in total hip patients. *J Biomech* 2001. 34: 873-881.

306. Ebramzadeh E, Campbell PA, Takamura KM, Lu Z, Sangiorgio SN, Kalma JJ, De Smet KA, Amstutz HC. Failure modes of 433 metal-on-metal hip implants: How, why, and wear. *Orthop Clin North Am* 2011. 42: 241-250.

307. Haddad F, Thakrar R, Hart A, Skinner J, Nargol A, Nolan J, Gill H, Murray D, Blom A, Case C. Metal-on-metal bearings: The evidence so far. *J Bone Joint Surg Br* 2011. 93: 572-579.

308. Shimmin A, Walter W, Esposito C. The influence of the size of the component on the outcome of resurfacing arthroplasty of the hip: A review of the literature. *J Bone Joint Surg Br* 2010. 92: 469-476.

309. Vissers M, Bussmann J, de Groot I, Verhaar J, Reijman M. Walking and chair rising performed in the daily life situation before and after total hip arthroplasty. *Osteoarthritis Cartilage* 2011. 1102-1107.

310. Lundberg HJ, Pedersen DR, Baer TE, Muste M, Callaghan JJ, Brown TD. Effects of implant design parameters on fluid convection, potentiating third-body debris ingress into the bearing surface during THA impingement/subluxation. *J Biomech* 2007. 40: 1676-1685.

311. Harms J, Mäusle E. Tissue reaction to ceramic implant material. *J Biomed Mater Res* 1979. 13: 67-87.

312. Christel P. Biocompatibility of surgical-grade dense polycrystalline alumina. *Clin Orthop Relat Res* 1992. 282: 10-18.

313. Catelas I, Huk OL, Petit A, Zukor DJ, Marchand R, Yahia LH. Flow cytometric analysis of macrophage response to ceramic and polyethylene particles: Effects of size, concentration, and composition. *J Biomed Mater Res* 1998. 41: 600-607.

314. Catelas I, Petit A, Marchand R, Zukor DJ, Yahia LH, Huk OL. Cytotoxicity and macrophage cytokine release induced by ceramic and polyethylene particles in vitro. *J Bone Joint Surg Br* 1999. 81: 516-521.

315. Lerouge S, Huk O, Yahia LH, Witvoet J, Sedel L. Ceramic-ceramic and metal-polyethylene total hip replacements: Comparison of pseudomembranes after loosening. *J Bone Joint Surg Br* 1997. 79: 135-139.